CREEP PERFORMANCE AND ANALYSIS OF BUFFER MATERIAL IN A NUCLEAR WASTE DISPOSAL VAULT

by

Demosthenes Yiotis

A thesis submitted to the Faculty of Graduate Studies and Research in partial fulfillment of the requirements of the Degree of Master of Engineering

Department of Civil Engineering and Applied Mechanics
McGill University
Montreal

August 1984

TO: ERIPHILI

CREEP PERFORMANCE AND ANALYSIS OF BUFFER MATERIAL IN A NUCLEAR WASTE DISPOSAL VAULT

by

Demosthenes Yiotis

Dept. of Civil Engineering
and Applied Mechanics

M.Eng.
August 1984

ABSTRACT

The purpose of this study is to analyze and/or predict the long-term creep characteristics of the buffer material placed around the nuclear waste container in the disposal vault. The analytical techniques examined have the objectives of deriving statically possible stresses compatible with kinematically possible strains while satisfying the boundary conditions. In order to detect any creep in the buffer material under actual boundary conditions a scale-model testing procedure is adopted, called the glass-box technique, which enables the visual observation of the buffer movement by scaling down half of the in-hole disposal system through its longitudinal axis. The experimental results are then analyzed by the Finite Element method and the visioplasticity approach. The major considerations of this study include the following requirements:

1. Development of the finite element solution technique to take into account the boundary

conditions of the problem

2. Study the effect of the boundary conditions on the buffer response
3. Verification of the analytical/predictive model established by comparing the predicted results with those measured experimentally.

The application of the predictive procedure developed provides satisfactory information regarding the long-term buffer response in the nuclear waste disposal system under a variety of complex boundary conditions imposed, and calls for simple data acquisition without sacrificing the accuracy of the prediction.

PERFORMANCE DE FLUAGE ET ANALYSE DES MATERIEL TAMPON DANS UN PUITS DE DECHETS RADIOACTIFS

par

Demosthenes Yiotis

Département de Génie Civil
et Méchaniques Appliquées

M.Eng.
août 1984

RESUME

Le but de cette étude est d'analyser et/ou prédire les caractéristiques de fluage à longue échéance du matériel tampon situé autour du réservoir de déchets nucléaires dans le puits.

Les méthodes analytiques examinées ont comme objectif de dériver des forces statiques compatibles avec des déformations possibles cinématiques tout en satisfaisant les conditions limites.

Pour détecter tout fluage dans le matériel tampon sous des conditions limites actuelles, un procédé expérimental appelé technique de "boîte-vitrée" a été adopté. Ceci permet l'observation visuelle du mouvement du matériel tampon. Le modèle fût crée en reduisant les dimensions du prototype original et en utilisant la moitié de celui-ci limité par son axe longitudinal. Les résultats expérimentaux furent ensuite analysés par la méthode d'éléments finis et la méthode de la plasticité visuelle. Les considérations majeures de cette étude comprenent les exigences suivantes:

1. Le dévelopement de la téchnique de la solution d'éléments finis pour prendre en considération les conditions limites du problème.
2. Etude de l'effet des conditions limites sur la performance du matériel tampon.
3. Vérification du modèle analytique/et de prédiction établi en comparant les résultats prédits avec les résultats expérimentaux.

L'application de la méthode de prédiction developpée offre une information satisfaisante sur la performance du matériel tampon à longue échéance dans le puits sous une variété des conditions limites complèxes imposées, et ne demande que des données simples à acqueir sans pour cela sacrifier l'éxactitude des prédictions.

ACKNOWLEDGEMENTS

The author expresses his sincere appreciation to:

1. Dr. R.N. Yong, William Scott Professor of Civil Engineering and Applied Mechanics, for his sustained guidance and inspiration so readily extended throughout this investigation.
2. Dr. P. Boonsinsuk, for his constant encouragement and invaluable suggestions during the course of this study.
3. Mr. F. Caporuscio and Mr. K. Shikatani for their technical help in developing the test facility.
4. Mr. N. Sciadas for his assistance during the Finite Element analysis.
5. The Atomic Energy Canada Ltd. and Mr. R. Lopez for the research assistantship provided.
6. Miss J. Armour for typing this thesis.

TABLE OF CONTENTS

LIST OF FIGURES

LIST OF TABLES

NOTATION

The symbols used in this thesis are defined at their first appearance. The major ones are listed below.

A_i	area of i^{th} quadrilateral of inscribed grid
C	soil cohesion
D_i (i-1,2,3)	displacements
E	elastic modulus
E_o	initial elastic modulus
E_T	slope of the deviator stress ($\sigma_1 - \sigma_3$), versus principal strain, ε_1, curve
f	lumped force field
F_i	body force field
I	strain rate invariant
K	element stiffness matrix
K_n	element stiffness per unit length in the normal direction
K_s	element stiffness per unit length in the tangential direction
U,V	velocity components
U	velocity field
u,v	displacement of velocity components
w	work done
Y	strain energy

γ soil density

γ_{xy} shear strain

$\varepsilon_i (i=1,2,3)$ major, intermediate and minor principal strains, respectively

$\varepsilon_x, \varepsilon_y$ normal strains

ν Poisson's ratio

σ normal stresses on failure plane

$\bar{\sigma}$ effective stress

$\sigma_i (i=1,2,3)$ major, intermediate and minor principal stresses, respectively

σ_x, σ_y normal stresses

τ shear stress

τ_i stress tensor

τ_{xy} shear stress component

ϕ friction angle

ϕ coordinate matrix of the nodal points

$\{\ \}$ column vector

$[\ ]$ matrix form

ABBREVIATIONS

mm	millimeter
m	meter
kPa	kilopascal
sec	second
min	minute
F.E.	finite element
C.S.T.(element)	constant strain triangular (element)
AECL	Atomic Energy Canada Limited
GRC	Geotechnical Research Centre
CBR	California Bearing Ratio test
CU	Consolidated Undrained test

CHAPTER 1

INTRODUCTION

1.1 Summary of the General Problem

Nuclear energy has become a valuable contributor to the supply of electricity. It supplements coal, replaces oil and does not pollute the air or water. Countries all over the world recognize this contribution and are moving ahead with their nuclear energy programs. Three hundred nuclear-electricity generating stations are in operation worldwide, and 200 more are being built.

Only one category of waste from nuclear-electric power plants is highly radioactive. After three to four years of use, the uranium fuel pellets used to generate energy contain a small percentage of radioactive byproducts called high-level waste. These byproducts must be carefully isolated from our environment.

The volume of this waste is very small, compared to the waste from other industrial processes. Therefore, it is thus much easier to control, contain and dispose of.

The National Academy of Sciences of the United States has reaffirmed that high-level nuclear waste can be disposed of thousands of feet underground, in geologic formations that have been stable for millions of years. Laboratory analyses performed and practical experience have led to a strong scientific consensus: The many natural and engineering barriers of a deep geologic repository will keep nuclear waste safely isolated from our environement and our descendants.

Here is the Department of Energy's (U.S.) preliminary design for the planned geologic disposal:

1) the waste, in a glass or ceramic-like form, will be sealed within metal canisters;
2) the canisters will be lowered 2,500 feet below the ground to repositories mined within stable geologic formations, such as granite, basalt or salt;
3) the canisters will be placed in holes that are then filled and plugged with a material like bentonite clay.

All these barriers are designed with one purpose: to keep the waste safely isolated from our environment for many thousands of years. Eventually, the waste hazard decreases to the level of natural uranium ore.

Until the nuclear waste in-hole disposal system is constructed the waste will remain stored in steel-lined pools inside the nuclear plants themselves.

Many countries are pursuing the geologic disposal method. West Germany has been drilling to test the suitability of a deep salt formation. Switzerland favours disposal in rock far beneath the Swiss lowlands. Canada's research and development is focusing on the ancient granite formations of the Canadian Shield area.

The theme of this study concentrates on the long-term creep characteristics of the buffer material placed around the nuclear waste container in the disposal vault.

Creep is defined herein as long-term soil movement under constant applied loading.

One of the requirements of the buffer material is to be capable of withstanding the applied pressure generated by:

(a) the self-weight of the container

(b) surrounding rock

(c) overburden pressure (from the buffer and backfill material)

(d) and other unaccountables.

The deformation of the buffer material under operating loading conditions should be negligible, particularly in the long-term, so that any possible movement of the container is restricted. This is to ensure that sufficient buffer material will always be in close contact with the container at all times to perform its function as designed.

1.2 Statement of the Problem

Based on the latest developments in the design concept of the immobilized waste vault (according to AECL) the layout of the in-hole disposal system is illustrated in Fig. 1.1. The total weight of each container (0.60 m in diameter) is 78.4 kN which will result in a pressure of 277.4 kPa acting on the underlying buffer material. Obviously the buffer material has to be able to sustain this loading without any detrimental deformation.

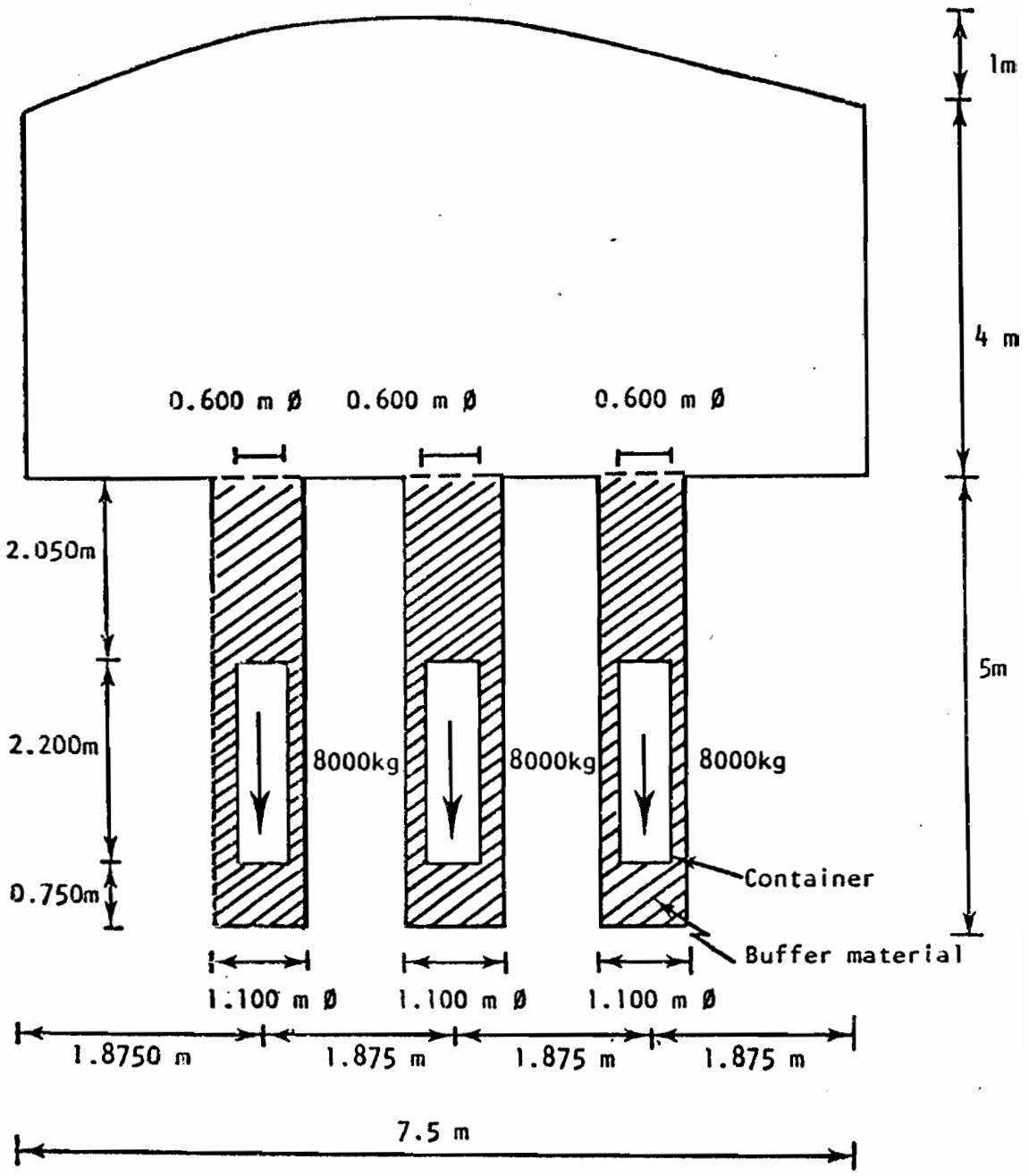

Fig 1.1 Details of Trench Emplacement Concept

(after AECL)

It is possible that once the nuclear waste container is installed in the disposal hole and surrounded with the buffer material, there will be a considerable period prior to backfilling of the disposal vault. Any water intake during this time will lead to the situation shown in Fig. 1.2. Of particular concern is the case of water uptake around the bottom part of the container, which may cause accelerating deformation of the buffer material, provided that the amount of heave due to water uptake is successfully suppressed by the overburden pressure. In essence, the increase in moisture content of the buffer material which should be placed at relatively low moisture content (around its optimum) may give rise to the undesirable long-term creep.

If the water uptake of the buffer material occurs only after the vault is fully backfilled, increasing the moisture content around the lower part of the buffer material should still be one of the main mechanisms responsible for inducing long-term creep. The overburden pressure acting on the buffer due to the backfill material is increased by approximately 100 kPa, resulting in a total pressure of about 400 kPa at the bottom of the container. It should be noted that water uptake above the top of the container alone (possible through local unfavourable rock joint system) may further increase the pressure acting on the container, depending on the interaction between the buffer and the backfill materials together with the configuration

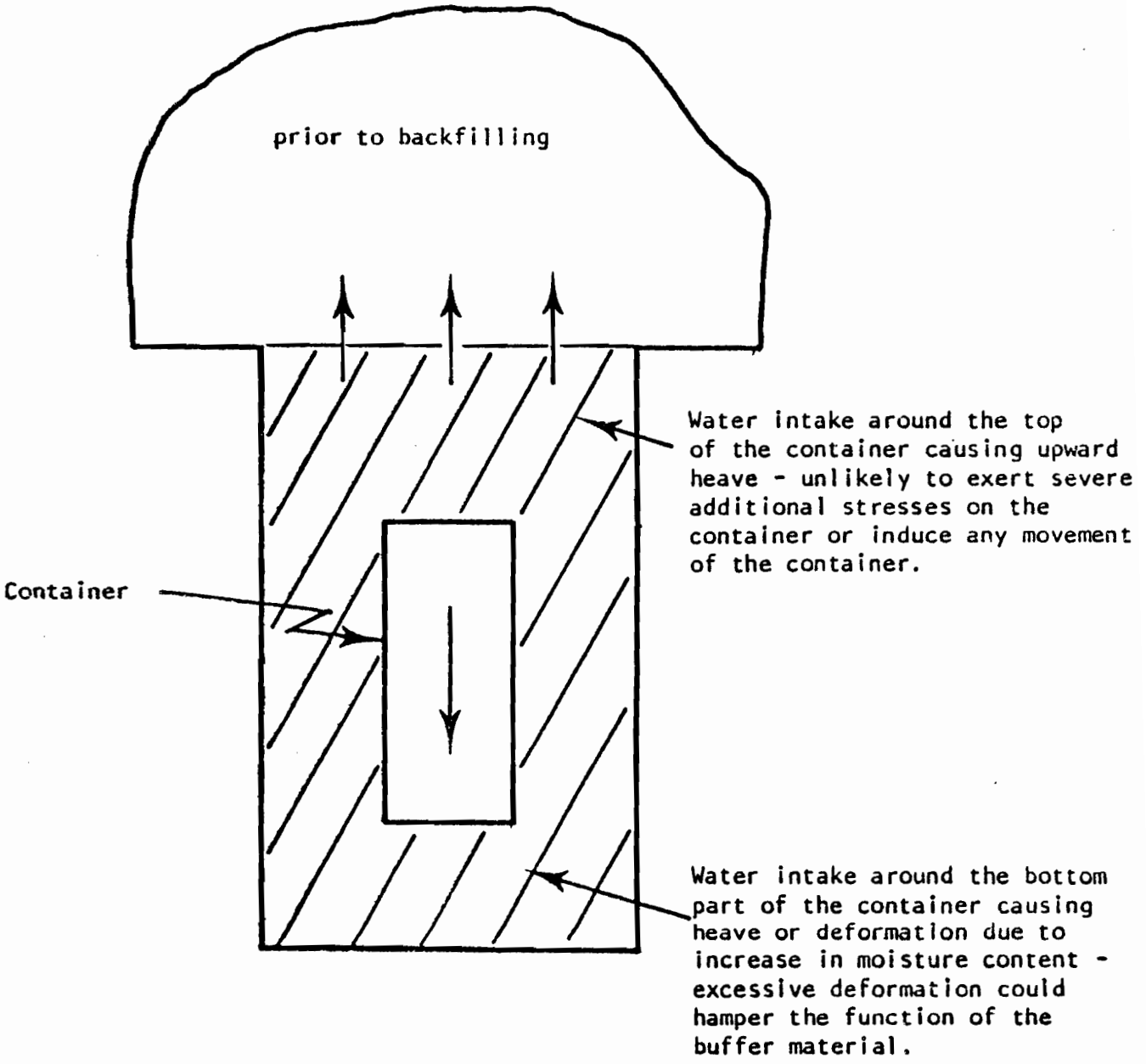

Fig 1.2 Possible situation leading to creep of the container

(after Yong, 1982)

of the in-hole disposal vault. Nevertheless, the pressure exerted on the buffer material at the bottom level of the container is at a minimum value of about 320 kPa while the maximum value can be higher than 400 kPa.

In the case of constant moisture content in the buffer material (i.e. no water uptake), long-term creep is still possible, depending on the density, compaction effort, placement technique etc.

It should be pointed out that the above situations could actually degrade the function of the buffer material by inducing a system of cracks or excessive movement of the buffer material (which would reduce its thickness around the container or would lose the tight contact with the container).

Other possible loadings include rock stresses, thermal stresses, interaction between the buffer/backfill material - container - rock system etc. Once cracks occur within the buffer layer, access to water must be available for the buffer material to swell and seal the cracks. Otherwise, these cracks might prevail or propagate following the drying cycle after being wetted.

All the above-mentioned possibilities necessitate the evaluation, in terms of long-term performance, of the buffer material with respect to its creep behaviour.

1.3 Purpose of Study

The purpose of this study is to investigate the long-term creep characteristics of the buffer material in the in-hole disposal system under different loading and water intake conditions. In addition, an analytical model will be provided which would allow for the derivation of the necessary time dependent stress and strain parameters within the deforming buffer, compatible with the observed buffer deformations, while satisfying the actual boundary conditions.

1.4 Scope of Study

The scope of this study is to examine experimental techniques such as model testing when applied in order to obtain a satisfactory simulation of the actual boundary conditions of the problem.

In addition, the validity of the application of empirical semi-analytical techniques - visioplasiticty - and numerical techniques - finite element method - to the analysis of the problem will be verified.

1.5 Thesis Organization

The thesis consists of seven main chapters and three appendices. The main body of the thesis may be sub-divided as follows:

Chapter 1, of which this section forms a part, is an introductory chapter which presents the statement

and the nature of the problem as well as the aim and the scope of the present study.

Chapter 2, provides a brief review on model testing in soil mechanics, on soil creep theories and associated rheological models and on the development of the visioplasticity approach.

Chapter 3, describes the experimental facilities used, together with the proposed test program and the additional tests performed by the Geotechnical Research Centre staff for the investigation of the buffer material properties.

Chapter 4, presents the experimental results together with the related discussions and comments.

Chapter 5, provides the developed predictive model for the overall buffer performance. Comparisons of the predicted results and both the experimentally measured ones and the results obtained using other existing approaches are all included.

Chapter 6, contains the concluding remarks.

Chapter 7, provides some recommentations for further study.

The second part of the thesis consists of three appendices which provide a theoretical approach to the finite element technique as applied to the present problem, additional information on the experimentation and the computer programs which were used for the analysis of the experimental results.

APPENDIX A, presents a theoretical approach to the finite element technique and deals with subjects such as idealization, formulation of the problem, boundary conditions, constitutive relationships and method of analysis.

APPENDIX B, provides additional information on the sample preparation and experimental set-up used by GRC staff in order to investigate the buffer characteristics.

APPENDIX C, lists the computer programs used in this thesis, together with a brief analysis of their structure and their advantages.

CHAPTER 2

LITERATURE REVIEW

2.1 Model Testing in Soil Mechanics

Scale-model tests based on similitude principles have played a major role in the development of aerodynamics and hydrodynamics. From this work has stemmed the capability to design and analyse systems involving fluid flows that are too complex for purely analytical techniques. Aerodynamics in particular has benefitted from wind-tunnel studies based on similitude. The benefit not only been in the immediate practical sense of providing detailed information about a particular component or a proposed design, but also, in a more fundamental way, in support of the evolution of a comprehensive aerodynamic theory.

Scale model tests usually are conducted for one of two reasons:

a) to gain understanding of the nature, magnitude and effect of the physical parameters that are present in the system whether defined or not.

b) to predict prototype performance from values measured on a relatively small and inexpensive system (Freitag, Schafer, Wismer, 1970).

Instead of having a test of differential equations to be solved in closed form, the model is looked upon as the statement or formulation of the problem in the associated boundary values. The test medium then is complete definition of the constitutive properties of the actual medium

and the conduct of the test is an analog solution of the differential equations of the system.

Application of the principles of similitude involves the concept of similar systems - a prototype and a model. Two systems which will exhibit similar behaviour if geometric, kinematic and dynamic similarity are achieved. Geometric similarity is attained if the two systems are geometrically proportionate. Dynamic similarity is attained if the ratios of all forces are the same in the two systems. Kinematic similarity usually follows if geometric and dynamic similarity are present (Freitag, Schaffer, Wismer, 1970).

According to Roscoe (1968) in soil mechanics there are two main uses of model tests. The first is where principles of similarity are not of first importance and tests are made at model scale to examine, usually on a non-quantitative basis, the assumptions that have been adopted in theoretical analyses of prototype problems. The second use is to determine and satisfy, the principles of similitude so that the behaviour of a prototype may be correctly predicted from the observation of a model. For this to be achieved, it is necessary for the investigator to assess not only the physical quantities that are relevant to the problem, but also to use judgement to reduce them to a working minimum by selecting the most significant parameters. This second approach has not been more widely adopted in soil mechanics since there is no general agreement among engineers concerning the mechanical behaviour of soils.

Clough and Pirtz (1958) developed conditions of similitude for the construction and testing of models to investigate the effects of earthquakes on rock-fill dams with earth cores. Their work was extended by Seed and Clough (1963) but they claimed only to have obtained semi-quantitative results.

Kondner and Green (1962) developed functional relations for the load-deflection characteristics of vertical piles subjected to horizontal loads when embedded in sand.

Schuring and Emori (1964) attempted to develop, by dimensional analysis, a general formula to cover many soil-deforming processes such as vertical penetration, bulldozing and land locomotion.

However, the most important contribution to the study of the applications of the principles of similarity to soil mechanics model studies has been made by Rocha (1953, 1957). He established in 1957 the similarity conditions which should be fulfilled by models to be used in studying the engineering problems of soil masses. He generally considered the soil as a two phase material and he first gave the similarity conditions when the liquid phase can be ignored, then he took into account the liquid phase and he finally offered the conditions for the general case of any deformation including rupture.

In their effort to reduce the necessary parameters to a minimum and hence facilitate theoretical work and the possibility of obtaining repeatable results in tests under controlled laboratory conditions, Roscoe and Poorooshasb (1963) produced experimental evidence which showed that to a close degree of approximation the strain behaviours of two elements of soil will only be identical when the elements are subjected to geometrical similar stress paths and their initial states on an e-lnσ' plot are equidistant from the critical-state line. With the aid of this principle it is possible to conduct tests using the same soil, but at different initial states, in both the prototype and the model. According to Roscoe (1968) this principle is appropriate for remoulded soils, and may prove useful for undisturbed, recently consolidated clays and for over-consolidated clays that do not alter their behaviour when subjected to remoulding. It is not appropriate for the modelling of over-consolidated soils that are sensitive to remoulding. As Roscoe (1968) states, if self-weight is not significant, the prototype material must be used in the same initial state in the model and the same stresses must be imposed on the model as on the prototype. Under these conditions the identity of stress-strain curves in model and prototype is ensured. When these conditions are fulfilled all time effects will then be proportional to h^2, where h is the linear scale ratio between the prototype and the model.

The ultimate goal of research on similitude in soil mechanics is to refine the ability to predict soil performance to the point that it is adequate for all applications. Further research should be directed toward conducting analyses of full-sized prototype performance to reflect the degree to which the model is accurate and thereby highlight areas needing more study.

2.2 Soil Creep Theories

In the development of creep theories for soils, two different paths have been taken over the years (Ladanyi 1972); one aiming at an engineering theory of creep to be used in design work; the other aiming at a physical theory capable of describing the creep phenomena in terms of already established concepts of physics.

The engineering or macro-analytical theory of creep can be considered as a collection of laws that are found by experience to adequately describe the observed macroscopic manifestations of creep. Typical examples of such theories are that of viscoelasticity (Gross, 1953) and creep of frozen soils (Haefeli, 1953; Vyalov, 1957, 1961, 1965; Vyalov and Meschyan, 1969).

On the other hand, the aim of a physical or micro-mechanistic theory of creep is to establish a set of laws that would be able to describe the observed phenomena of creep in terms of previously established quantities and laws of physics. An example is the theory of creep which

is based on the concept of rate processes developed in statistical mechanics.

In more general terms, as stated by Scott (1969), "Each approach has advantages which depend on the problem to be studied: one may be of value in interpreting material properties from a test, another may be used in the calculation of a time-dependent stress or displacement field in the same material".

Many theories developed from the micromechanistic view point are based on the rate process theory, also called absolute reaction rate theory. This theory was developed by Eyring (1941) through statistical mechanics considerations of the Arrhenius equation. According to Eyring-Glasstone and Laidler (1941) the modern development of the theory of reaction rates may be said to have come from the proposal made by S. Arrhenius to account for the influence of temperature on the rate of inversion of sucrose. He suggested that an equilibrium existed between inert and active molecules if the reactant and that latter only were able to take part in the inversion process. Arrhenius derived the formula to express the variation of the specific rate at the reaction with temperature:

$$\ln k = \ln A - E/RT$$

where A is quantity known as "collision number" or more often "frequency factor"; E is termed the "heat of activation" or "energy of activation" of the reaction; it

represents the energy that the molecule in the initial state of the process must acquire before it can take part in the reaction, whether it be physical or chemical.

In its simplified form, the problem of making absolute calculations of reaction rates involves two independent aspects: these are the derivation of the energy of activation and the frequency factor, respectively. For the calculation of the frequency factor Eyring introduced the use of "partition functions" which for a given molecule, per unit volume, are measures of the probability of the occurrence of that molecule in the specified volume. Considerations of the partition functions for the various molecular species in the system, led to statistical calculations of reaction rates. This reaction rate is given by the velocity at which an activation complex, or flow unit, travels over the peak of an energy barrier.

The "absolute reaction rate" theory has had wide application to many processes involving a movement of particles such as the deformation of materials under stress (Abdel-Hady and Herrin, 1966). The theory has been applied in 1953 by Hogan at the University of Utah to the creep characteristics of several plastic laminates and it was found to be a highly satisfactory engineering hypothesis applicable to the particular material. Also, the same theory was used by Herrin (1963) to describe the rate of shear of a particular type of bituminous material as a function of the shear stress and temperature.

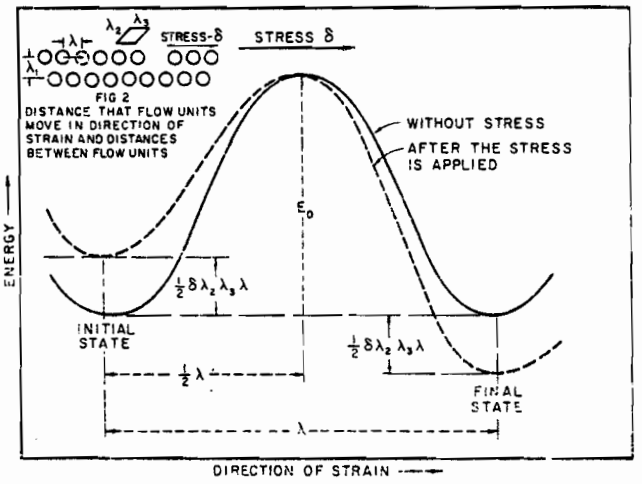

Fig 2.1

Potential energy barrier for strains with and without shearing stress

(after Hady and Herrin, 1966)

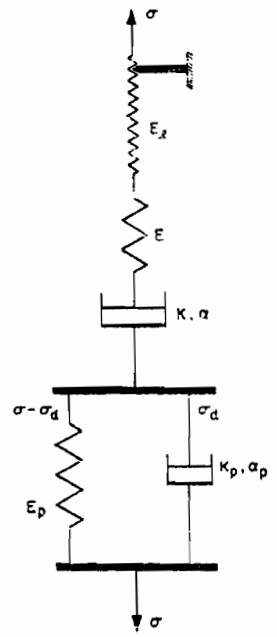

Fig 2.2

Picturization of the mechanical model used by Hady and Herrin (1966)

In the field of soil mechanics the concepts of this theory were used by Goldstein, Misumsky and Lapidys (1961), who determined a mathematical relationship between the long-term strength and time to failure of soil samples in a creep test.

Since this theory gives the functional relationship between rate of flow, frequency of mutual exchange of position between reaction elements, applied force, energy barrier to be overcome for a single jump of position, and temperature, it is potentially a powerful theory to describe the creep mechanism of clay soils (Chen, 1975).

Based on the theory of rate processes is the model derived by Murayama and Shibata (1961, 1964). They assumed that the structure of the clay skeleton is composed of a heap of micrometric clay segments (i.e. mineral particles which move as units) in a card-house structure and between the segments connecting in edge to face contacts there lies a thin layer of absorbed water which binds up the segments. The connecting joints are classified into elastic (no relative sliding between segments) and visco-elastic joints (do not slide simultaneously). Furthermore, they assumed that the frequency distribution of the applied force on a segment is expressed by a Gaussian distribution. By applying Eyring's theory they calculate the viscosity of absorbed water around clay segments. Assuming that the segments are independent of each other and that a displacement of a segment of any type is assumed to contribute an increment to

the overall shearing strain of clay skeleton, they derive the shear strain as a sum of all the strains of the elastic and visco-elastic joints. They analogize this behaviour with a mechanical model which consists of an independent Hookean spring G1 connected in series with a modified Kelvin or Voigt element.

Christensen and Wu (1964) also studied the soil creep from the viewpoint of rate process theory. The process of creep is considered to be the result of slip at the weakly bonded contacts followed by the transfer of load from these weakly bonded contacts to the strongly bonded contacts. The activation energy represents the bond strength of the contact that constitutes the shearing resistance of the soil. Their model is a Kelvin-Maxwell rheological model that is considered appropriate to describe the two possible conditions: flow and non-flow. The rheological parameters are calculated by combining the formulae of the rate process theory with those describing the behaviour of the mechanical model.

Abdel-Hady and Herrin (1966) sought a mechanical model representing the creep behaviour of soil-asphalt mixture material. In their attempt to include the main parts of the creep process in a mechanical model they devised another combination of Maxwell, Kelvin elementary models, thus taking into account the instantaneous plastic deformation, the transient creep and the secondary creep. The rheological parameters are calculated through the "rate process" equations, and creep test results.

According to Mitchell et al. (1968), since the theory of absolute reaction rates can be applied to any process involving the time-dependent rearrangement of matter, it has the potential for providing a powerful tool for the description and prediction of soil behaviour. However, little direct evidence has been presented which supports the application of this theory tosoils, since earlier studies have assumed it to be valid a priori. The fact that a number of characteristics of the shearing resistance of soils appear to conform to the theory does not provide proof of its validity. From the results of carefully controlled triaxial creep tests on undisturbed and remoulded clays over a range of temperature and stress conditions they concluded that:

1) Creep of soils can be treated as a thermally activated process.
2) The experimental activation energy decreases linearly with increase in creep shear stress, in accordance with the theory.
3) At stresses greater than about 20% to 30% of the shear strength, the logarithm of strain rate after any given period of creep is directly proportional to the creep stress.
4) The creep rate is time dependent, decreasing according to an inverse power funciton of the type:

$$\dot{\varepsilon} = A \left(\frac{t_1}{t}\right)^m \exp (aD)$$

Thus while their study has supported the validity of the temperature, activation energy

and stress terms of the rate process equation:

$$\dot{\varepsilon} = x \frac{k\,T}{h} \exp\left(-\frac{\Delta F}{RT}\right) \exp\left(\frac{f\lambda}{2kT}\right)$$

They consider necessary an interpretation of the physical factors controlling the variation of parameters, x, df with time.

5) The study of creep behaviour of soils provides a means for examination of mechanisms of deformation of soils, primarily through evaluation of the activation energy and the number of bonds per area under different conditions of consolidaiton, over-consolidation and disturbance.

6) Considerations of the activation energy for creep of clays suggests that interparticle bonding is probably of the primary valence type, and resistance to shear cannot be developed by viscous water films, i.e. interparticle contacts must be effectively solid to solid (Mitchell et al., 1968).

Although the functional relationship between parameters based on the rate process theory seem to be in conformity with experimental results, there are still some questions remaining unanswered (Chen, 1975). For example, there is not direct way by which the mechanism of creep soils as postulated in the rate process theory can be proven. Secondly, the unit of activation energy is expressed in Kcal/mole. Since no simple molecular formula can be written for clay soil, it becomes difficult to explain the physical

implications of the value of activation energy thus obtained.

Another approach to the modelling of creep behaviour of clay soils is proposed by Yong and Chen (1969). Here the important point becomes the relationship between micro-(fundamental unit) and macro-behaviour and the appropriate representation of the micro-behaviour in a macroscopic rheological model of clay soil. Means for that analysis were the retardation time distribution method introduced by Alfrey (1948). Studying the rheological behaviour of high polymers and rubber-like materials, Alfrey (1948) found that the time of retardation is a characteristic property of the molecule of high polymer and the spectrum of the retardation time distribution shows a characteristic distribution of the substance under investigation. Examining the continuous, uniformly increasing creep function represented by the integral:

$$C_r(t) = \int_0^t f(r)\ (1-e^{t/r})\ d\tau$$

in which f(r), the distribution function of retardation times of strain, may be graphically evaluated, providing the normalization factor is so determined that

$$\int_0^\infty f(r)\ d\tau = 1$$

The graphical solution as given by Alfrey, consists the following steps:

1) Plot the retarded portion of strain versus the logarithm of time, thus obtaining an "S" shaped curve.
2) Normalize the curve by dividing the vertical coordinates by the ultimate retarded strain, this gives the accumulative distribution function f(r).

For different materials tested, different characteristic distributions of retardation time may be obtained. For high polymers, the retardation time for each molecule is different from other molecules with different structural polymer molecules.

In their attempt to create a physical model of the clay soils in order to examine and analyse the demonstrated creep behaviour of such soils using retardation time distributions, Yong and Chen considered necessary some form of statistical treatment. They state that "in view of the physical make-up of the clay soil, where interparticle action occurs between elementary units which are not necessarily similar, some form of statistical treatment is necessary if one is to examine and analyse the demonstrated creep behaviour of such a soil". Their method of analysis is based on the postulate that the macroscopic body (clay soil) possesses a complex three-dimensional structure, consisting of a multiplicity of various elementary units. The experimentally obtained creep curve therefore represents an integral effect

encompasing all elementary unit behaviour, and the distribution of retardation times is a characteristic of the test sample. By using the retardation time method with statistical treatment they underline the influence of the micro-behaviour on the macro-behaviour of clay soil. The retardation time distribution is thus regarded as an indication of the distribution of the structural elements and microvolumes participating in the process of deformation. By representing the macroscopic straining as a continuous function in the following form:

$$e_T = A\,\sigma + \int_{-\infty}^{t} f(t-r)\,\sigma\, d\tau + B\,t\,\sigma$$

the three components of deformation, i.e. instantaneous retarded and constant rate are accounted for.

In order to obtain the coefficients for an appropriate rheological model they extended Alfrey's method. The new step consists of normalizing the distribution curve to obtain a probability density function g(r) from whence the fraction of compliance due to each elementary unit may be obtained. The importance of this result is that by this method it will enable one to obtain the probability weighing factor from series of experimental results.

The theories of creep previously described were developed from the micromechanistic viewpoint. They dealt with events occurring at the atomic level and provided knowledge of the processes that control creep (Ladanyi, 1972).

The model derived by Komamura and Huang (1974) to describe the soil-creep behaviour is the result of a macro-analytical theory. They state that soil conditions change gradually from solid state through plastic state to liquid state with increasing water content. Therefore, a new rheological model which will be sufficiently valid to describe mathematically the soil deformation under various conditions of stress and water content is needed. From creep tests and flow tests they concluded to a rheological model with parameters which are calculated from test results.

Mitchell and Singh (1968) derived a set of simple expressions for characterization of creep. These expressions were the result of the relationships between strain rate, stress and time. As they state "phenomenological relationships developed are empirical curve-fitting techniques that do not necessarily imply anything about the mechanisms underlying the deformation process". They obtained a general pattern of relationship between strain rate and time from tests in undisturbed and remoulded clay, wet clay and dry clay, normally consolidated and over-consolidated soil, and sand. The same pattern was observed by Bishop (1966) and Murayama and Shibata (1958). Another pattern of relationship was derived between strain rate and creep stress intensity, D. The relationship between strain rate and time was described by the formula:

$$\ln = \frac{\dot{\varepsilon}}{\dot{\varepsilon}(t_1, D)} = - m \ln \left(\frac{t}{t_1}\right)$$

and for the relationship between creep stress intensity and strain rate the formula:

$$\ln \left(\frac{\dot{\varepsilon}}{\dot{\varepsilon}(t, D_o)}\right) = a\ D$$

Their final phenomenological expression was of the type:

$$\dot{\varepsilon} = A\ e^{aD} \left(\frac{t_1}{t}\right)^m$$

The parameter A reflects an order of magnitude for the creep rate under a given set of conditions, it is in that sense a soil property (Mitchell). The parameter a has units of reciprocal stress. A minimum of two creep tests are needed to establish the values of A, a and m for a soil.

The criticism by Geuze (1964) against the mechanical models for the representation of the soil behaviour pointed out the serious disadvantages of the basis of the technique: the superposition of components representing the various mechanisms inherent to the deformation of clay systems. The system behaviour predicted by the model is based on the principle of superposition of stresses and strains, which is strictly valid only for small magnitudes. The problem of modelling the soil creep behaviour is just a part of the main engineering problem. Proper modelling of soil behaviour for accurate prediction of its behaviour. A sound engineering theory has to be based on an understanding of the physical make-up of the soil and realistic experiments in the field as well as in the laboratory.

2.3 Visioplasticity

The method of visioplasticity is an empirical-analytical method which requires the specification of the strain rate distribution throughout the deforming region. The strain rates are generally obtained from experimentally measured time-displacement patterns.

This method is apparently due to Yang and Thomsen (1953). They used this analysis in their attempt to determine metal flow directions and plastic strains during a small stepwise deformation process from distorted, originally square, grid-line network scribed on a meridian plane. They determined the strain fields throughout that deformed plane and then they obtained the stress distribution using the known strains, principal stress trajectories and known boundary conditions.

The visioplasticity method presents a powerful empirical experimental-analytical tool for use with problems involving plastic deformation in plane strain or under conditions of axial symmetry.

The accuracy of the method is only as good as the accuracy of the experimentation, and the measurements obtained therefrom. With this provision, it undoubtedly remains one of the more rigorous of the experimental-analytical tools available for the solution of problems of plastic deformation.

Examples of this kind of solution technique and its successful application in soil mechanics has been reported

by Yong and Webb (1969), by Chen (1972) and by Sylvestre-Williams (1973).

The method assumes that the velocity field may be measured visually. This is usually achieved by inscribing a network of grid lines on the surface of the workpiece and recording the distorted grid at successive times after the start of the deformation process. With the knowledge of the deformation patterns, obtained from the records of the distorted grid, velocity distribution within the failed mass may be specified.

For the specific case of a plane-strain problem, once the velocity field is known, the velocity vector components V_x and V_y, in the x and y coordinate directions respectively, may be plotted as functions of x and y. It is then possible to obtain the strain rate distribution within the sample from the following relations:

$$\dot{\varepsilon}_{xx} = \frac{V_x}{x}$$

$$\dot{\varepsilon}_{yy} = \frac{V_y}{y}$$

$$\dot{\gamma}_{xy} = \frac{1}{2} \left(\frac{V_x}{y} + \frac{V_y}{x} \right)$$

Unlike problems in metal processing, the method of visioplasticity cannot be readily applied to problems in soil mechanics since valid constitutive equations which describe the stress-deformation behaviour of soils are not immediately available.

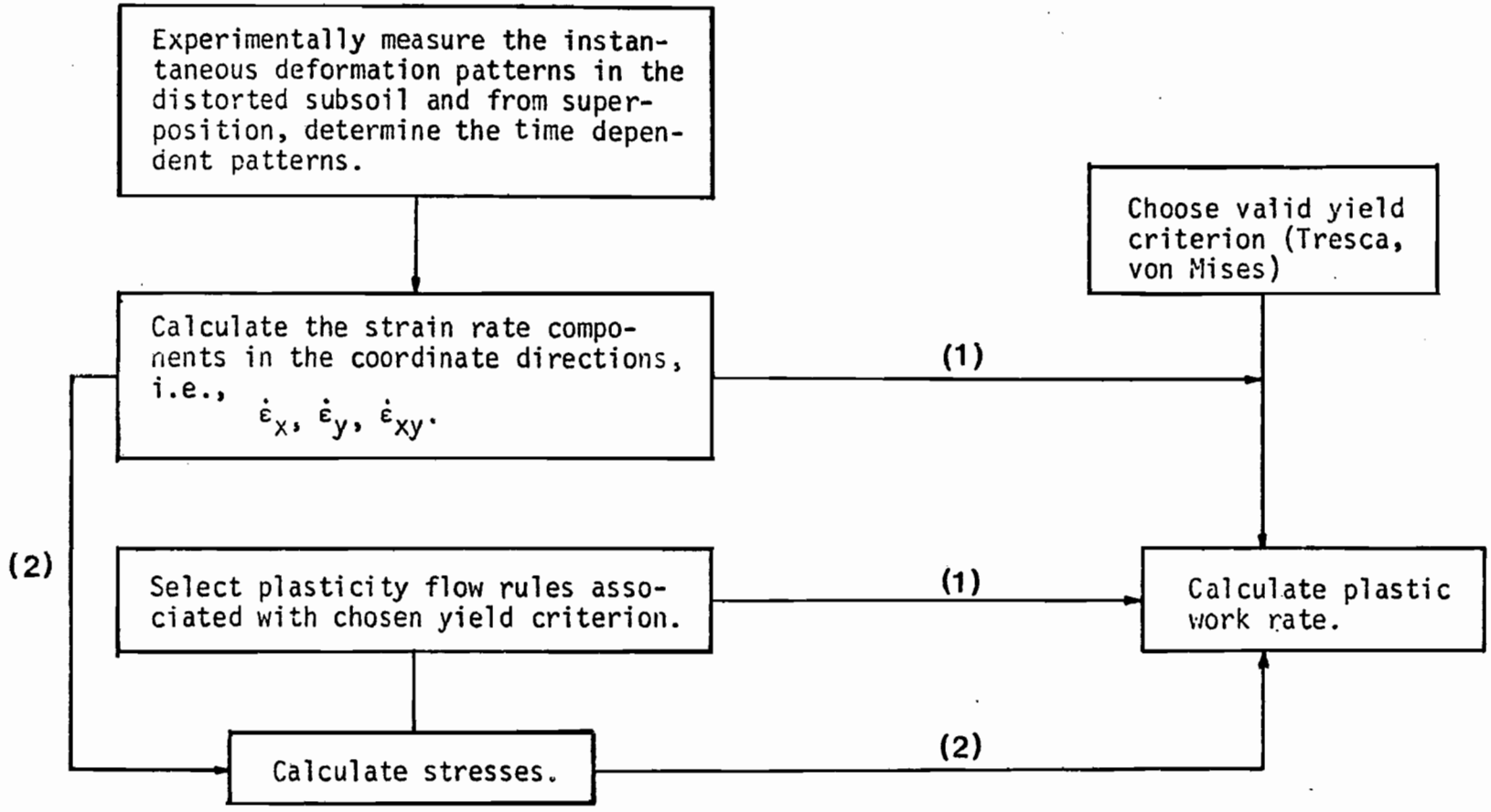

Fig. 2.3 Flow diagram of the method of visioplasticity.

McKyes (1969) has shown that the Levy-Mises equations of perfect plasticity viz:

$$\dot{\varepsilon}_x = \lambda \frac{f}{\sigma'_{xx}}$$

$$\dot{\varepsilon}_y = \lambda \frac{f}{\sigma'_{yy}}$$

$$\dot{\gamma}_{xy} = \lambda \frac{f}{\tau_{xy}}$$

or in summation convention

$$\dot{\varepsilon}_{ij} = \lambda \frac{f}{\sigma'_{ij}}$$

are valid over a limited range of application to the deformation behaviour of a clay soil. The expression f/σ'_{ij} may be regarded as being the gradient of the loading surface given by the equation $f = f(\sigma'_{ij})$

As a consequence of McKyes' results, the required constitutive equations were derived by Webb (1969) and are given as:

$$\dot{\varepsilon}_{xx} = \frac{\sqrt{I_2}}{K} \sigma'_{xx}$$

$$\dot{\varepsilon}_{yy} = \frac{\sqrt{I_2}}{K} \sigma'_{yy}$$

$$\dot{\gamma}_{xy} = \frac{\sqrt{I_2}}{K} \tau_{xy}$$

where

I_2 = second invariant of the strain-rate tensor

$$= \frac{1}{6} [(\varepsilon_1-\varepsilon_2)^2 + (\varepsilon_2-\varepsilon_3)^2 + (\varepsilon_3-\varepsilon_1)^2]$$

$K^2 = J_2$ = second invariant of the stress tensor

$$= \frac{1}{6}\left[(\sigma_1-\sigma_2)^2 + (\sigma_2-\sigma_3)^2 + (\sigma_3-\sigma_1)^2\right]$$

σ'_{xx} = deviatoric stress component in the x-direction

$= \sigma_{xx}-\sigma_m$ where σ_m is the mean stress

$= \frac{1}{3}(\sigma_1+\sigma_2+\sigma_3)$

Similar definitions hold for σ'_{yy}.

$\sigma_1, \sigma_2, \sigma_3$ = principal stresses

$\varepsilon_1, \varepsilon_2, \varepsilon_3$ = principal strains

By setting $K^2 = J_2$, the above formulation utilizes the von Mises yield criterion.

The final equation necessary for a visioplastic solution is given by a general continuity equation of the form

$$\frac{(\rho V_x)}{x} + \frac{(\rho V_y)}{y} = 0$$

if the material is assumed to be incompressible, the equation reduces to the condition of incompressibility given by

$$\dot{\varepsilon}_{xx} + \dot{\varepsilon}_{yy} = 0$$

CHAPTER 3

EXPERIMENTATION

3.1 Material

The buffer material under investigation was a 50% Avonlea clay (sodium bentonite) and 50% graded sand (by weight) mixture.

The solution used in mixing clay and sand was the standard granitic groundwater as required by AECL. For the characterization of Avonlea clay, mineralogical properties and surface characteristics were determined at Geotechnical Research Centre and the results are given in Appendix B.2. The minerals present in the clay in decreasing order of abundance are shown in Table 3.1. Specific gravity for the buffer material was found to be 2.76. Atterberg limits tests were also conducted. The results are shown in Table 3.2.

The particle size analysis of the buffer material was determined by wet sieving on a No. 200 sieve. For the material passing the No. 200 sieve the sedimentation process was used, while the retained material was dry sieved. The results are shown in Table 3.3 and Fig. 3.1.

In order to determine the density-moisture relationships modified Proctor compaction tests have been conducted on the buffer material. Specimens for the tests were prepared at the optimum values obtained from the compaction results. The results of the modified Proctor compaction

TABLE 3.1 Minerals in Avonlea Clay
(in decreasing order of abundance)

Montmorillonite

Illite

Feldspar

Quartz

TABLE 3.2 Summary of Index Properties

Material	Specific Gravity	Atterberg Limits		
		L.L. (%)	P.L. (%)	P.I.
50% sand - 50% clay	2.76	98	19.2	78.8

L.L. = liquid limit; P.L. = plastic limit;
P.I. = plasticity index

TABLE 3.3 Grain Size Distribution Results

Material	Grain Size Distribution		
	Sand (%)	Silt (%)	Clay (%)
50% sand - 50% clay	45	6	49

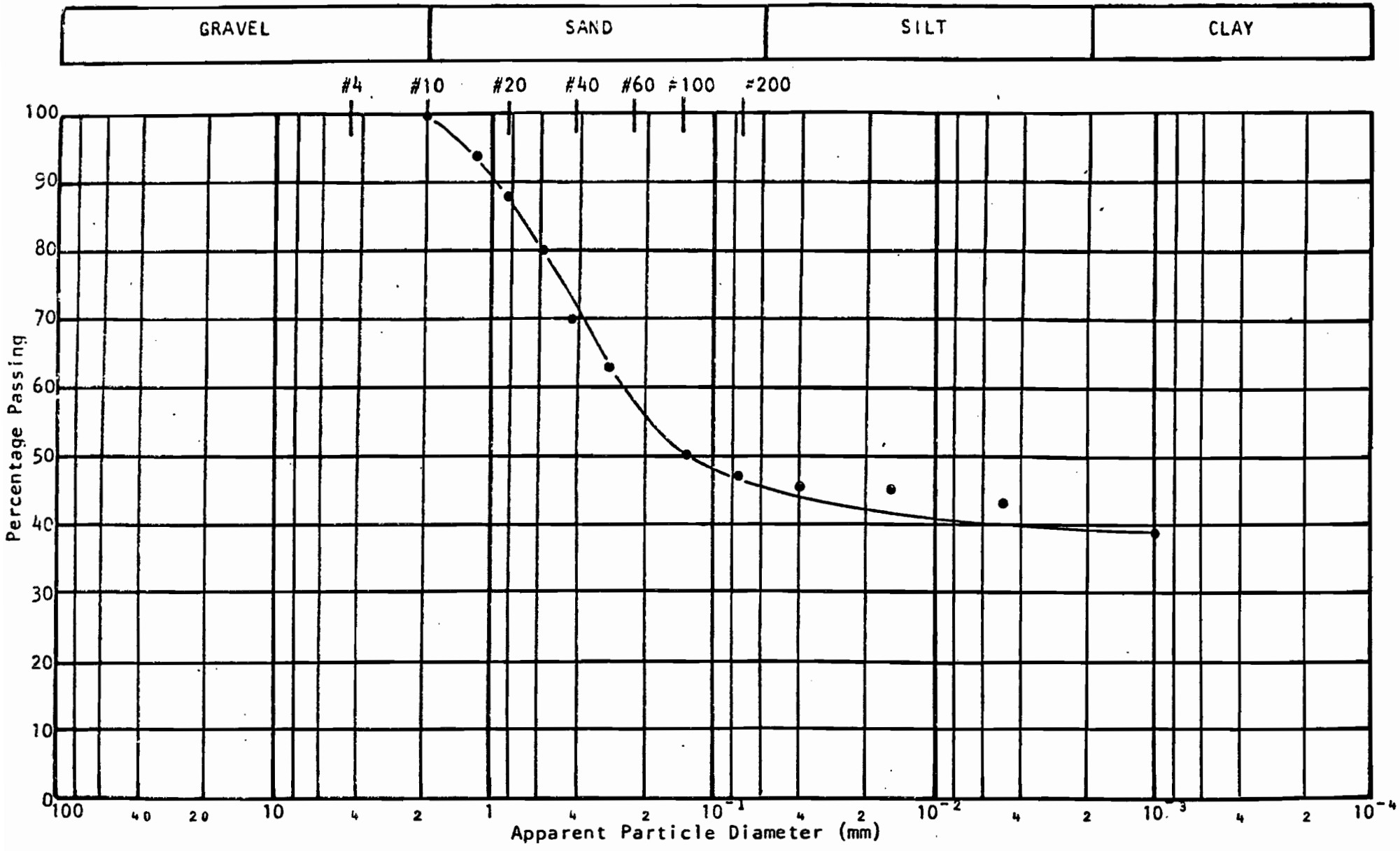
GRAVEL
SAND
SILT
CLAY
#4
#10
#20
#40
#60
#100
#200
100
90
80
70
60
50
40
30
20
10
0
Percentage Passing
100
40
20
10
4
2
1
4
2
10⁻¹
4
2
10⁻²
4
2
10⁻³
4
2
10⁻⁴
Apparent Particle Diameter (mm)

Fig. 3.1

tests are shown in Fig. 3.2. The dry unit weight attains a maximum value of 1.57 Mg/m^3, corresponding to an optimum moisture content of 23.5%. The swelling properties of the soil were evaluated in terms of swelling pressure and amount of free swell. Details of the sample preparation and apparatus are in given in Appendix B.2. The free swell results are given in Fig. 3.3. The soil shows a high swell potential (max. swell 11% at 5000 minutes). In order to establish the level of loading to be imposed on the buffer specimens, a series of CU tests were carried out at different confining pressures. Four confining pressures (i.e. 172.4, 344.8, 785.4, 3585 kPa) were used in the series. The curves obtained are shown in Figs. 3.4 and 3.5. Table 3.4 summarizes the results obtained.

The strength parameters in terms of total stresses are:

cohesion intercept = 40.5 kPa

angle of friction ϕ = 8.6 degrees.

Details on sample preparation and test procedure are given in Appendix B.2. Load-deformation tests were also performed in a similar manner as the one-dimensional consolidation test, but without allowing the soil sample to absorb water prior to loading. Figure 3.6 shows the stress-settlement curve obtained and Fig. 3.7 the void ratio-stress relationship. CBR tests were also performed in both soaked and non-soaked samples. Results are shown in Fig. 3.8.

Density-Moisture Relationship for the 50/50 (Sand/Clay) Mixture 50%/50%

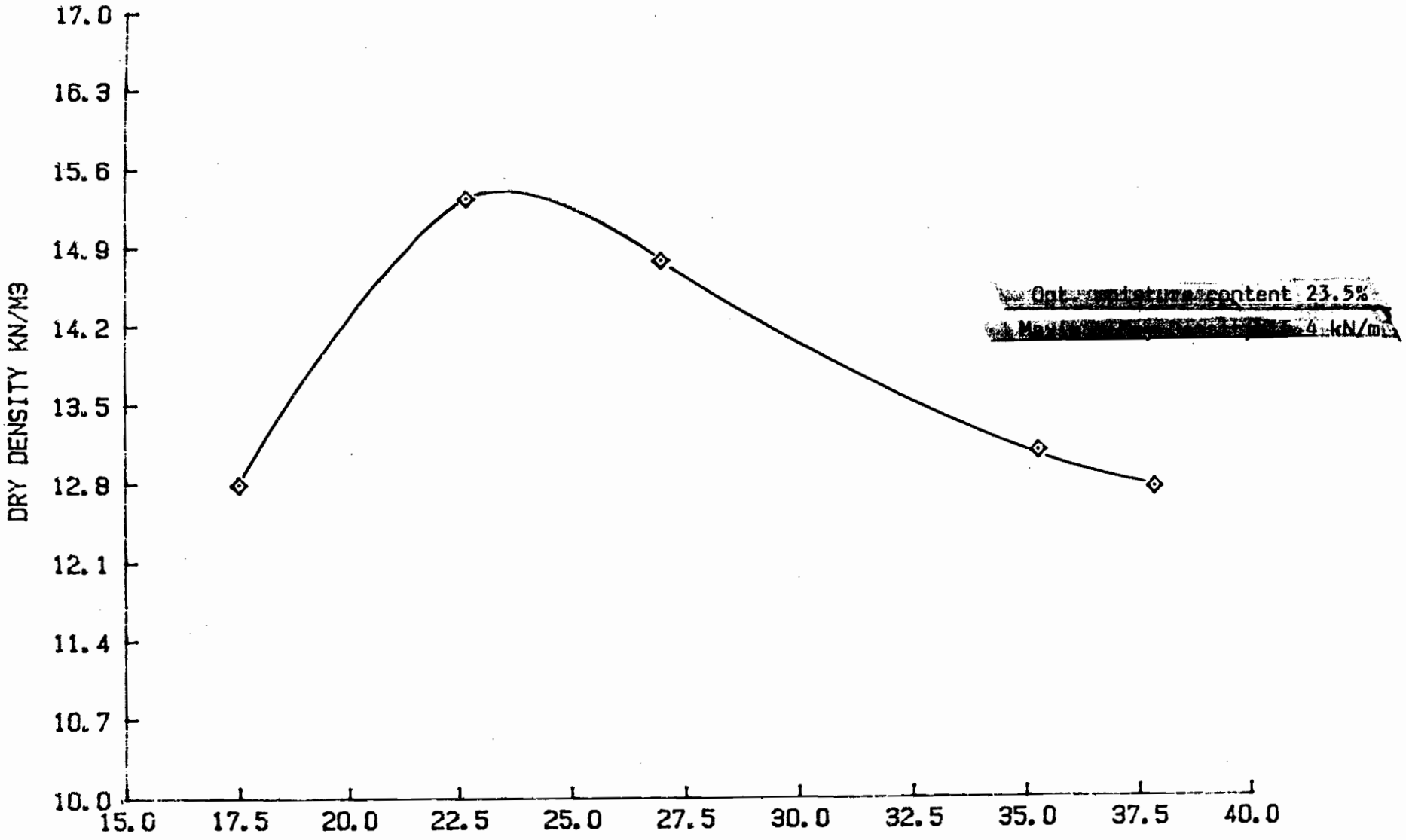

Fig. 3.2

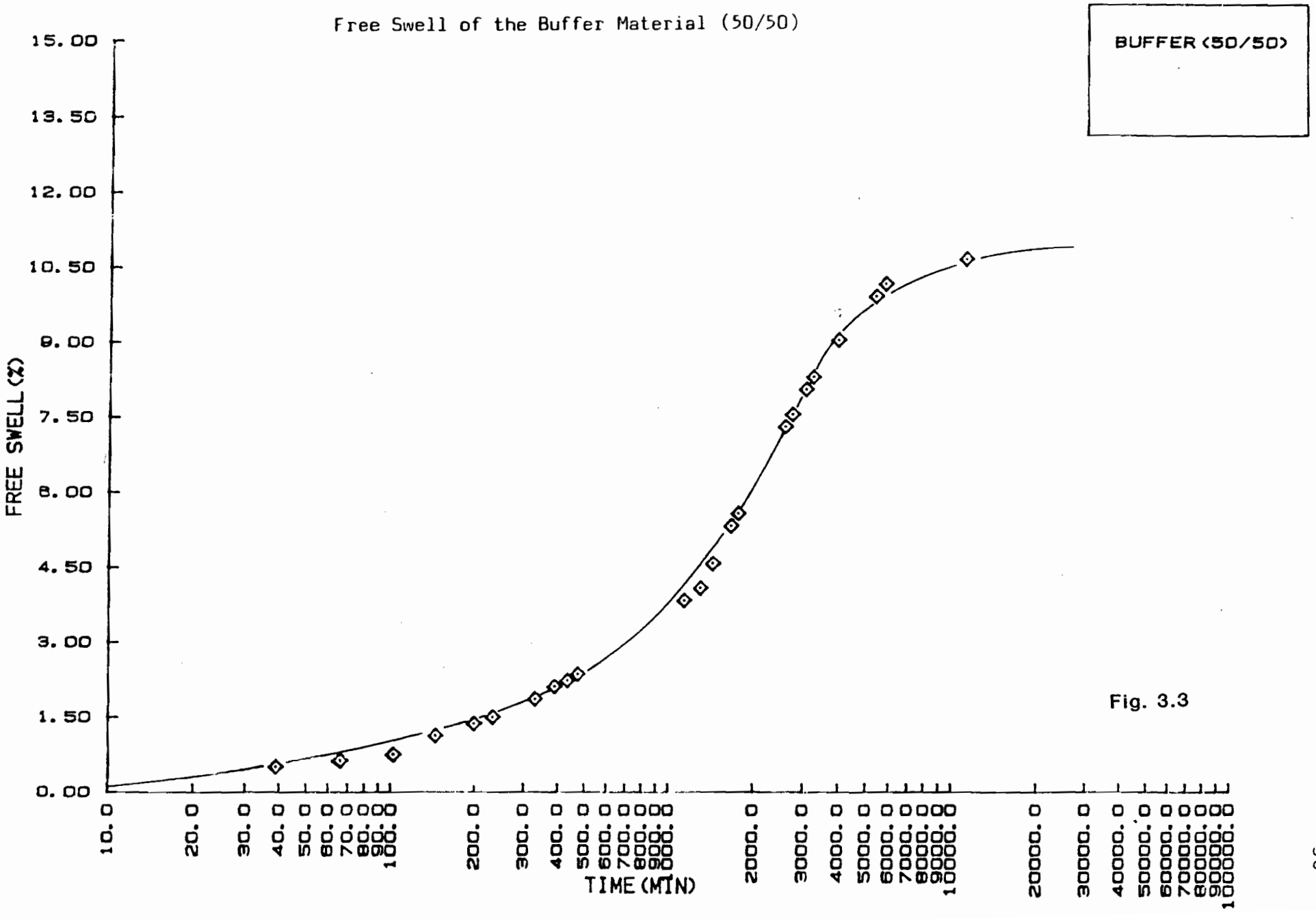
Free Swell of the Buffer Material (50/50)
BUFFER (50/50)
FREE SWELL (%)
15.00
13.50
12.00
10.50
9.00
7.50
6.00
4.50
3.00
1.50
0.00
TIME (MIN)
10.0
20.0
30.0
40.0
50.0
60.0
70.0
80.0
90.0
100.0
200.0
300.0
400.0
500.0
600.0
700.0
800.0
900.0
2000.0
3000.0
4000.0
5000.0
6000.0
7000.0
8000.0
9000.0
10000.0
20000.0
30000.0
40000.0
50000.0
60000.0
70000.0
80000.0
90000.0
100000.

Fig. 3.3

Table 3.4 Consolidated Undrained Triaxial Test Results for the Buffer Material

Test No.	Confining Pressure (kPa)	Initial Water Content (%)	Dry Density (Mg/m^3)	Deviator Stress at Failure (kPa)	Strain at Failure (%)	Strain Rate (mm/min)
1	172.4	27.0	1.46	127.4	10.5	6.35×10^{-3}
2	344.8	27.8	1.44	192.6	9.8	6.35×10^{-3}
3	785.3	26.2	1.50	260.0	9.0	6.35×10^{-3}
4	3585.0	24.3	1.5	785.2	12.0	6.35×10^{-3}

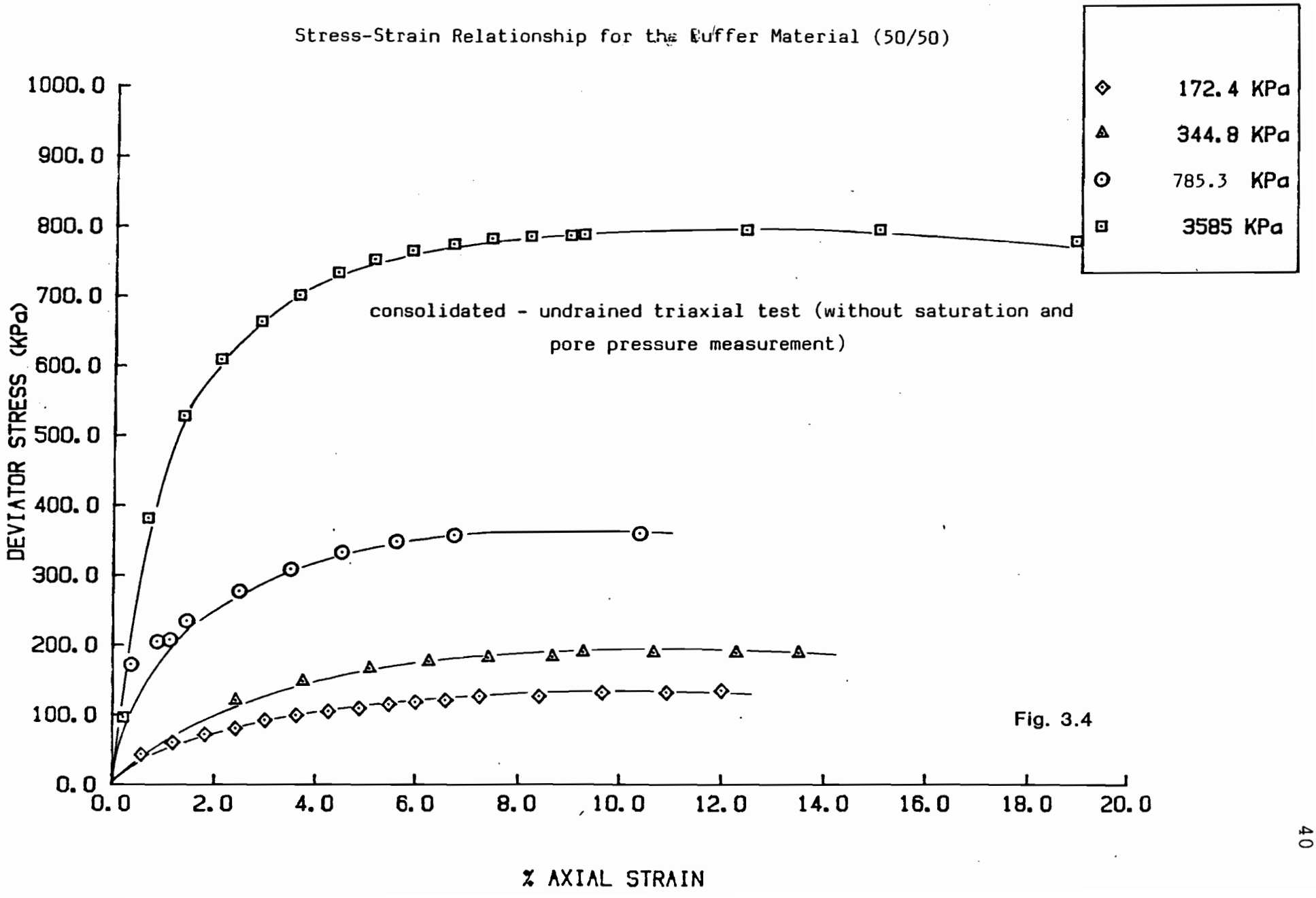
Stress-Strain Relationship for the Buffer Material (50/50)
172.4 KPa
344.8 KPa
785.3 KPa
3585 KPa
consolidated - undrained triaxial test (without saturation and pore pressure measurement)
DEVIATOR STRESS (KPa)
1000.0
900.0
800.0
700.0
600.0
500.0
400.0
300.0
200.0
100.0
0.0
0.0
2.0
4.0
6.0
8.0
10.0
12.0
14.0
16.0
18.0
20.0
% AXIAL STRAIN

Fig. 3.4

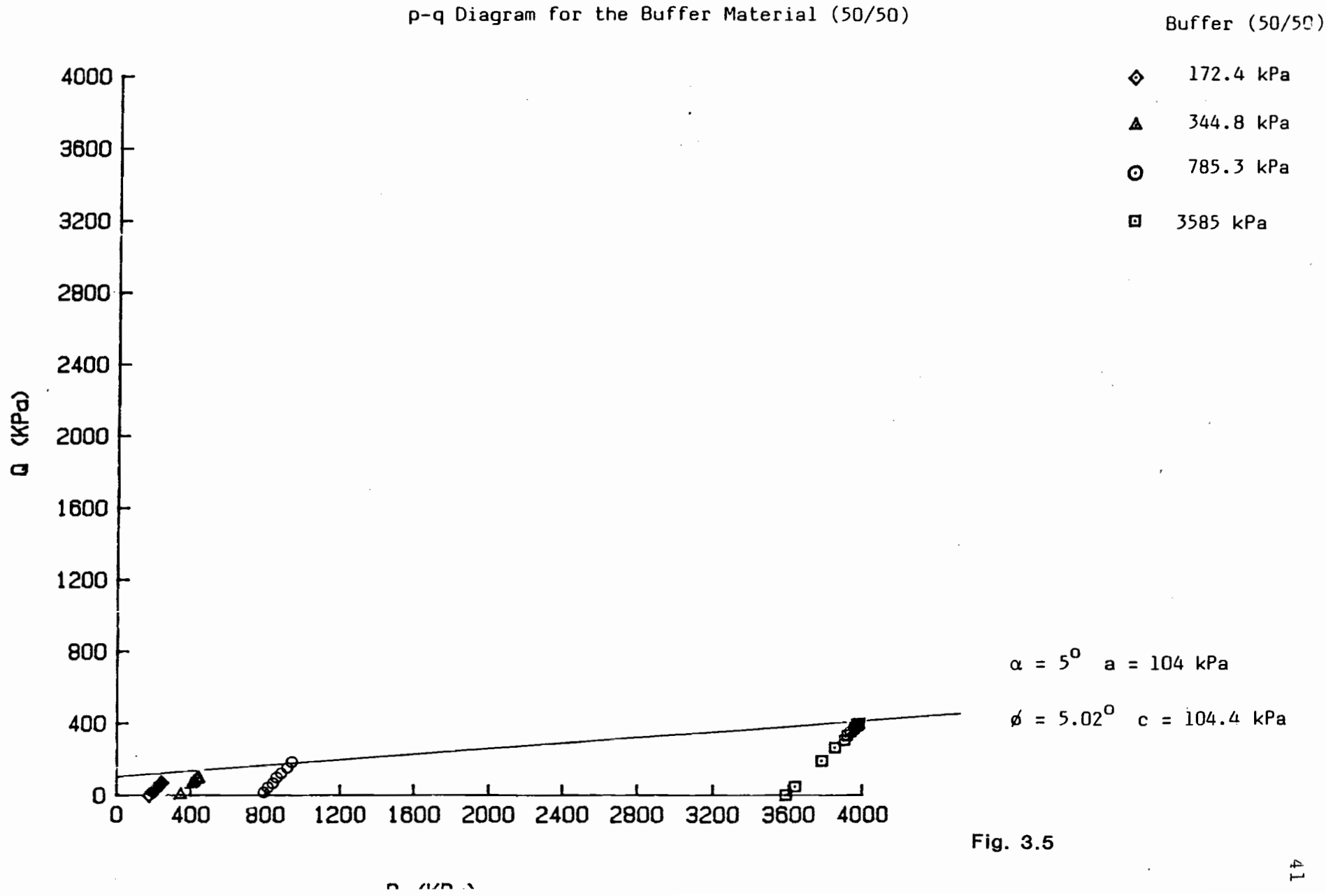
p-q Diagram for the Buffer Material (50/50)
Buffer (50/50)
172.4 kPa
344.8 kPa
785.3 kPa
3585 kPa
Q (KPa)
4000
3600
3200
2800
2400
2000
1600
1200
800
400
0
0
400
800
1200
1600
2000
2400
2800
3200
3600
4000
α = 5° a = 104 kPa
ø = 5.02° c = 104.4 kPa

Fig. 3.5

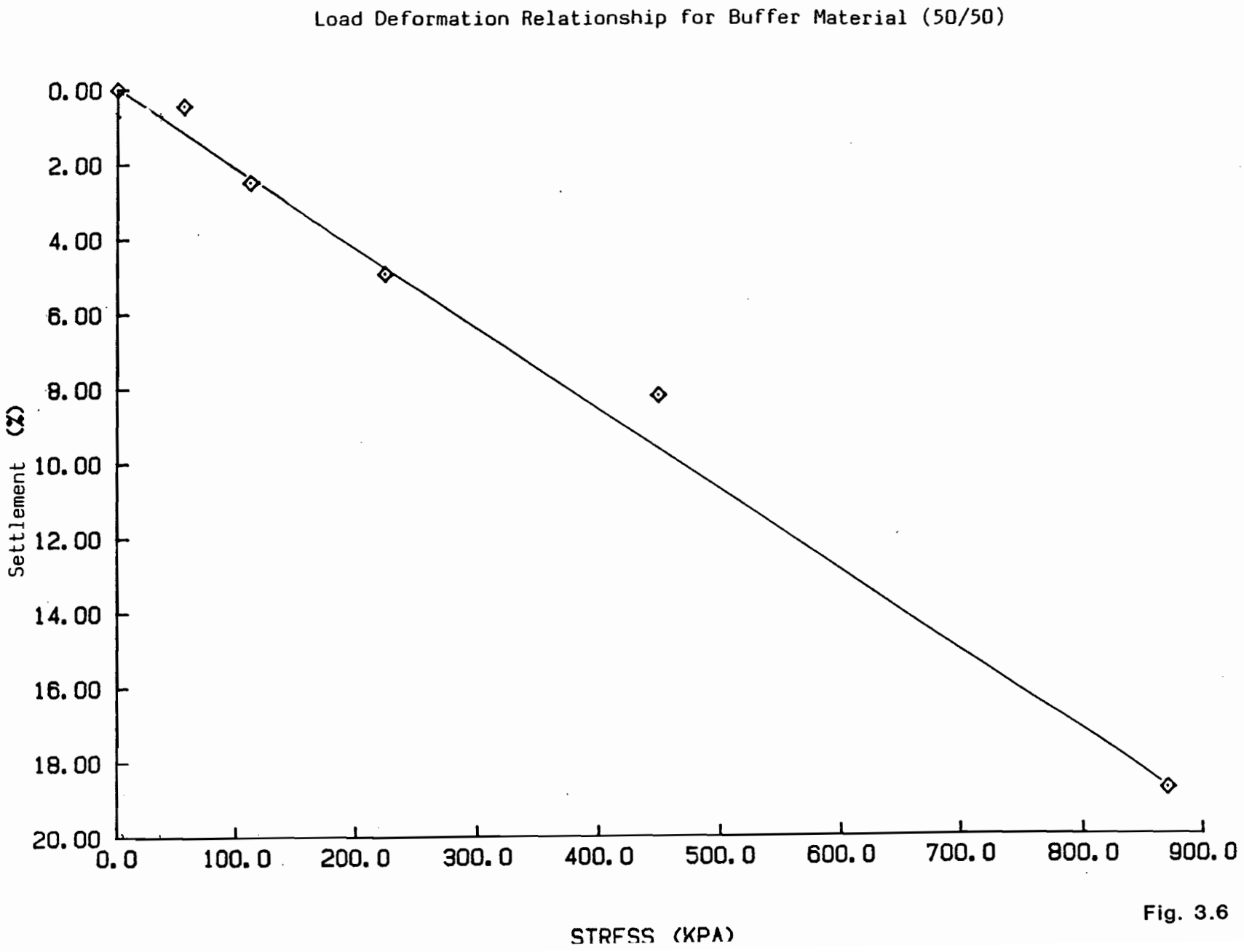
Load Deformation Relationship for Buffer Material (50/50)
Settlement (%)
0.00
2.00
4.00
6.00
8.00
10.00
12.00
14.00
16.00
18.00
20.00
0.0
100.0
200.0
300.0
400.0
500.0
600.0
700.0
800.0
900.0
STRESS (KPA)

Fig. 3.6

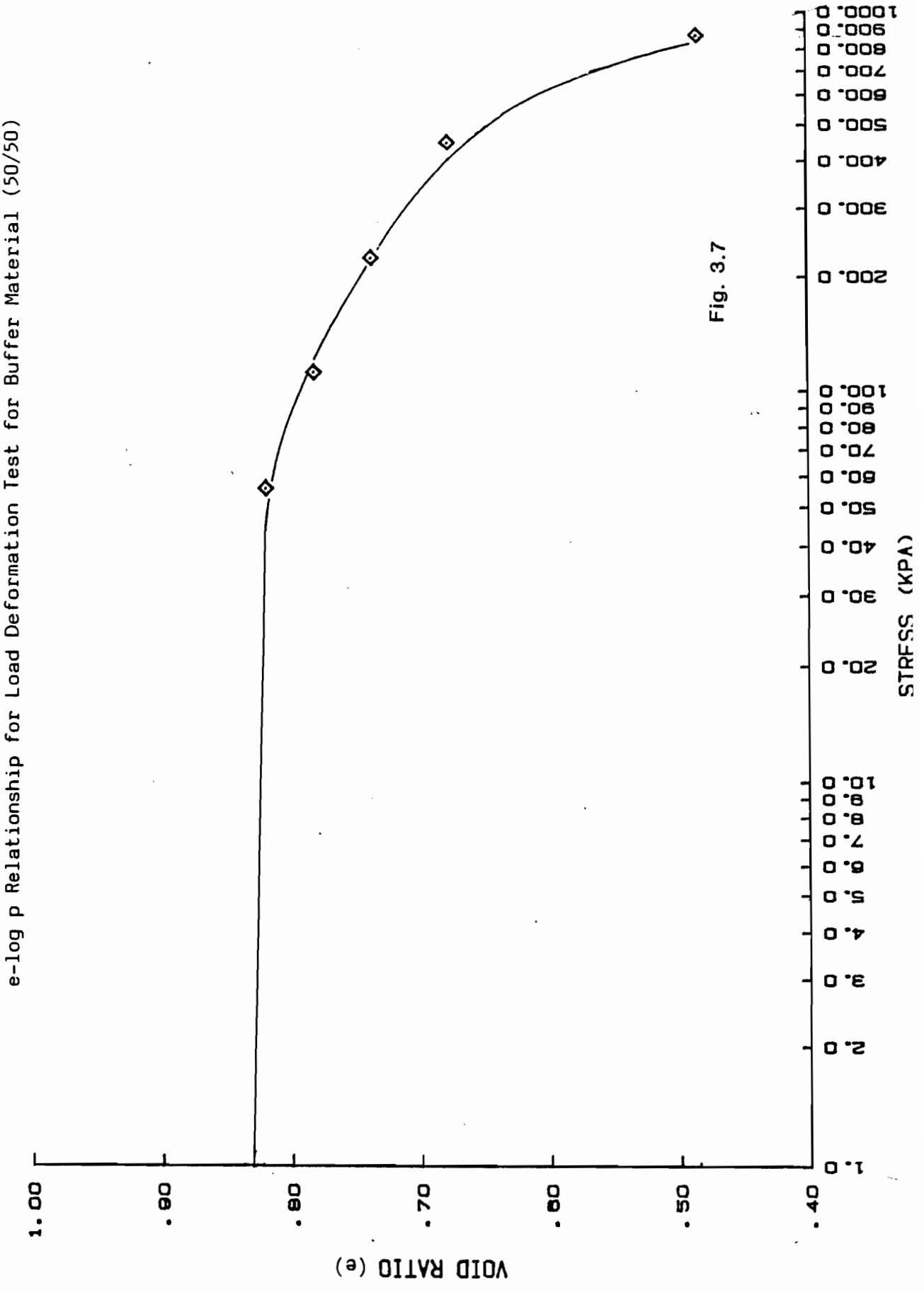
e-log p Relationship for Load Deformation Test for Buffer Material (50/50)
VOID RATIO (e)
1.00
.90
.80
.70
.60
.50
.40
STRESS (KPA)
1.0
2.0
3.0
4.0
5.0
6.0
7.0
8.0
9.0
10.0
20.0
30.0
40.0
50.0
60.0
70.0
80.0
90.0
100.0
200.0
300.0
400.0
500.0
600.0
700.0
800.0
900.0
1000.0

Fig. 3.7

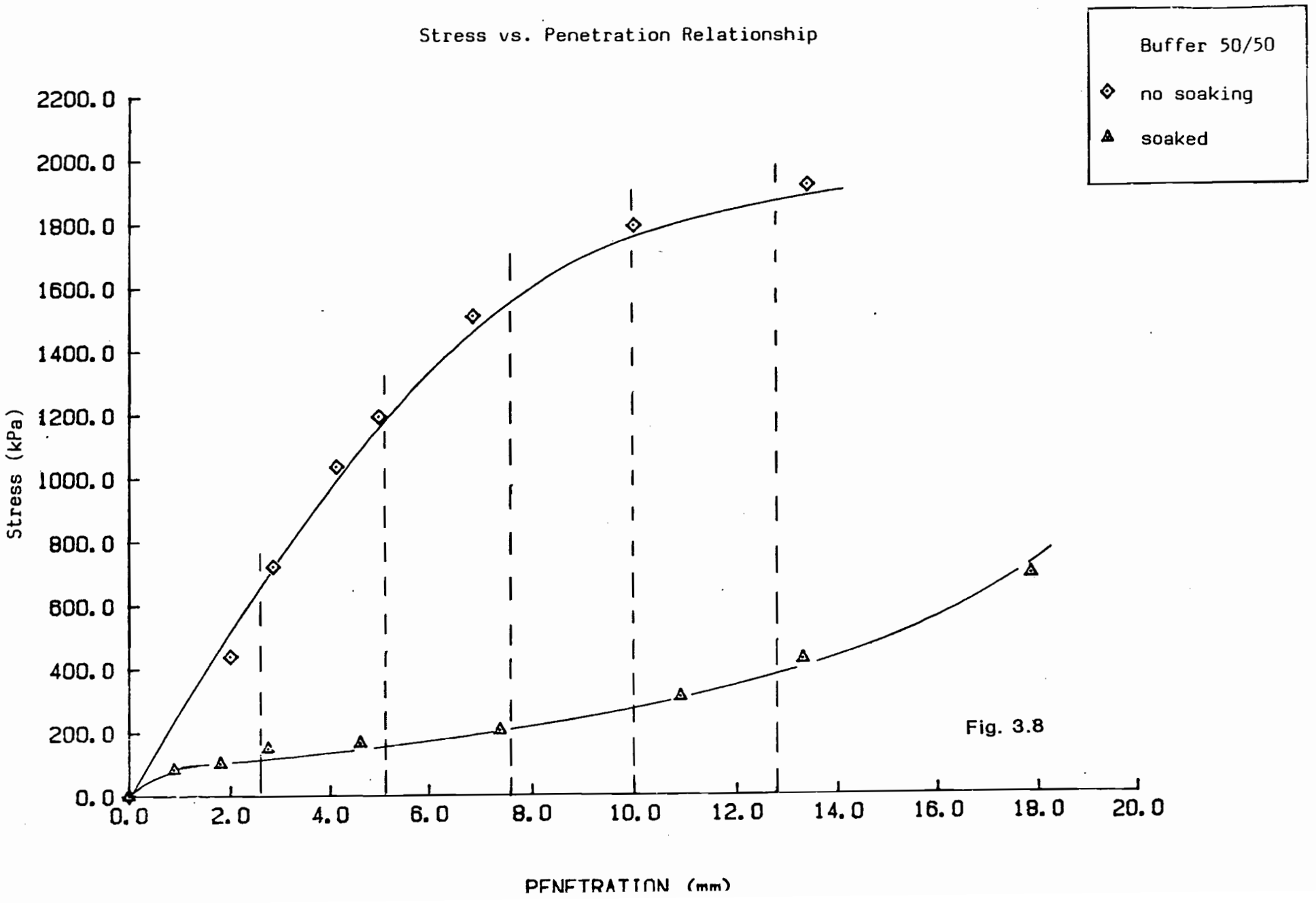
Stress vs. Penetration Relationship
Buffer 50/50
no soaking
soaked
Stress (kPa)
2200.0
2000.0
1800.0
1600.0
1400.0
1200.0
1000.0
800.0
600.0
400.0
200.0
0.0
0.0
2.0
4.0
6.0
8.0
10.0
12.0
14.0
16.0
18.0
20.0
PENETRATION (mm)

Fig. 3.8

The creep behaviour of the buffer material was investigated by subjecting the buffer to several deviator stresses under different confining pressures of 172.4, 344.8 and 689.5 kPa. The applied deviator stress was gradually imposed on the soil sample until the required level was reached, after which it was kept constant for a sufficiently long period of time so as to appreciate its creep characteristics (i.e. single level creep tests). The applied deviator stress was selected as a certain percentage of the maximum deviator stress (at failure) under the same confining pressure obtained from the triaxial test. Two series of tests were conducted with stress levels starting at 70% for the first series adn 90% for the second series. The stress level in each series was subsequently increased each time by 10% until failure was reached. The procedure for CU triaxial tests without saturation was adopted.

3.2 Test Equipment

In order to fully appreciate the creep characteristics of the buffer material as placed in the disposal hole, a special laboratory set-up, the "glass-box" technique, was adopted. Such a procedure enables the movement of the buffer material around the container to be observed visually by scaling down half of the in-hole disposal system through its longitudinal axis. Long-term movements of the buffer material are recorded by taking sequential photographs.

Strain and stress fields can then be analyzed using the visioplasticity approach. For a realistic simulation of the in-hole disposal system, a physical model was created using a scale of 1:8 approximately. The main parts of that model Figs. 3.9, 3.10 are:

1. Concrete block (half section) with a central semi-circular hole representing the surrounding host rock. Dimensions: 140 mm internal diameter, 750 mm total height.
2. Aluminum semi-cylinder representing the nuclear waste container. Dimensions: 76.4 mm diameter, 280 mm height.
3. Plexiglass plate to cover the exposed soil surface. Dimensions: 240 mm width, 750 mm length, 25.4 mm thickness.
4. Other parts of the model include a steel plate used as the base of the concrete tube and the top loading plate used to transfer the axial load simulating the overburden pressure induced by the tunnel backfill to the buffer material. The overburden pressure was produced by means of hydraulic pistons that pressed the top plate while calibrated through proving rings.

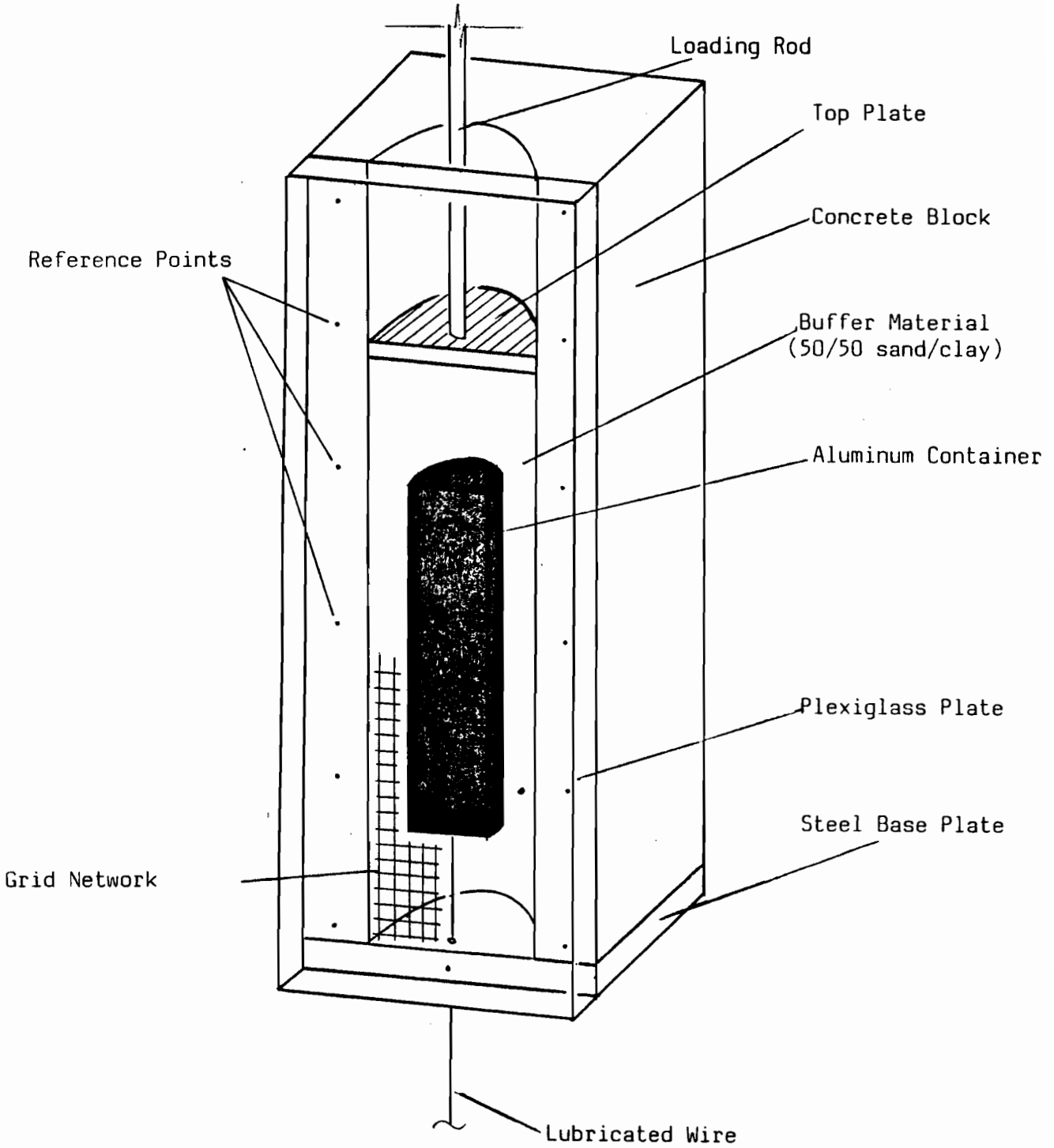

Schematic Diagram for the Physical Model of the Container-Buffer-Host Rock System

Fig. 3.9

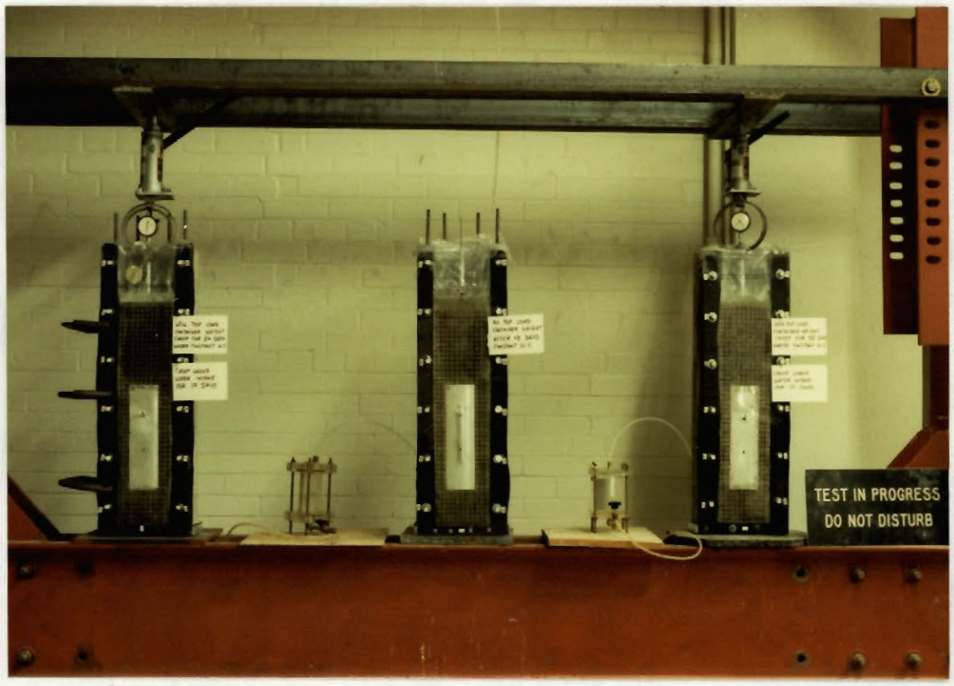

Model test set-up

Fig. 3.10

3.3 Test Procedure

The test procedures adopted were aimed at solving the numerous technical problems which arose, such as the nuclear waste container weight and special requirements, such as undrained condition and uniform density of the buffer material.

In order to obtain a uniform dry density of the buffer material around its optimal value, the in-hole system was divided into three areas - namely: below, around and above the waste container (Fig. 3.9). Each area was then subdivided into a number of layers to be subjected to the same amount of impact energy according to the modified Proctor test requirements. The necessary amount of soil was detemrined so that in each layer the required dry density was obtained. The waste container weight of the model, necessary to produce the actual amount of pressure on the buffer material similar to the prototype, was 636 N. This load was induced by pulling down the aluminum container with weights connected to the container through a thin lubricated wire that passed through the soil inside a short tube, so that friction between soil-wire was eliminated.

Leakage was prevented by using rubber sheets along the connection points of theconcrete block to the plexi-glass plate and the base plate. The concrete block interior was painted with sealing paint that prevented water absorption from the soil.

The procedures adopted for the test were as follows:

a) the soil was first placed and compacted in the area below the waste container

b) a hole of small diameter (6.5 mm) was drilled for a short tube to pass through the soil at a height of 40 mm.

c) the waste container was placed on the compacted soil while the lubricated wire connected to the container was passed through the short tube previously installed. In order to avoid any container misalignment during soil compaction around it, the container was belted temporarily but firmly onto a special compacting plate.

d) the buffer material was compacted around the container

e) compaction of the area above the container was then conducted, followed by levelling of the top of the buffer material.

After the compaction and placement part of the test preparation was finished, the plexiglass plate was bolted onto the concrete block, following the inscription of grid lines on the exposed soil surface. The next step was the loading of the system.

3.4 Loading Procedure

The axial load of 636 N, representing the waste container weight which produced the same pressure as the prototype, was applied by pulling the container down with standard weights. The load corresponding to the minimum load imposed on the soil at the top should produce the minimum overburden pressure of 36 kPa at the top of the container. All the axial loads were applied at the same time so as to monitor the immediate response of the container-buffer system.

3.5 Test Program

In assigning the test program to be followed certain considerations were included:

a) After the waste container is placed in the disposal hole and the buffer material is properly installed, there might be a waiting period before the room on top of the disposal hole is backfilled. This is simulated by restricting any overburden pressure on the model.

b) Once the backfill material is placed, the the verical pressure on the waste container should increase accordingly. The model is therefore loaded on top with various overburden pressures to account for the interaction between the disposal vault-host rock and the buffer material in the disposal hole.

c) Subsequent to installing the buffer material, it is likely that, in the long-term, groundwater will be absorbed by the buffer and/or backfill material through the network of rock joints/ cracks of the host rock formation. Since the buffer material is essentially capable of swelling upon water-intake, the resultant effect on the waste container movement need to be investigated. Such a possibility is simulated in the model study by allowing water intake and observing the container and soil particle movements. The test program followed is summarized in Table 3.5.

3.6 Test Results

The procedure for the test results acquisition consists of the following main steps:

1. Plotting of Grid Points
2. Transfer of nodal coordinates to computer memory.
3. Grid adjustments
4. Curve fitting of particle paths
5. Calculation of velocity components
6. Calculation of strain rates and effective strain rates.

This procedure was adopted for previous mobility (Windisch, 1969, El Mamlouk, 1980) and indentation studies (Chen, 1972; Sylvestre-Williams, 1973) at the Geotechnical Research Centre at McGill University.

TABLE 3.5 Summary of Test Conditions

Test No.	Overburden Pressure kPa	Water Intake	Initial Creep* (before Water Intake)	Creep Duration* Under Constant Water Intake Days	Creep Duration During Water Intake Days	Remarks
1	0	no	-	15	-	reference
2	0	yes, at bottom	yes	15	15	
3	36	no	-	18	-	
4	36	yes, at bottom	yes	24	24	
5	36	yes, at bottom	no	-	24	
6	120	no	-	18	-	about full backfill height
7	120	yes, at bottom	yes	24	24	" " "
8	120	top	yes	24	24	" " "
9	120	back	yes	24	24	" " "

* Prior to inducing water intake, the container-buffer system is allowed to reach its equilibrium state (i.e. no further creep after installation).

3.6.1 Plotting of Grid Nodes

A photographic record of the deforming grid was made during the tests. The initial, as well as the consequent images were obtained for each test. A slide projector was used to project the negative slide photographs onto a sheet of paper where the locations of horizontal and vertical grid line intersections (grid nodes) were plotted for the different subsequent images. The size of the plotted field for each image consisted of 11 vertical and 46 horizontal rows with spacing of 12.5 mm in between.

3.6.2 Transfer of Grid Nodes to Computer Output

The sheet of paper, with the grid points plotted on it, was then mounted on a digitizer which was connected to the IBM computer at McGill University. The recorder pen was placed at the locations of the grid points row by row and image by image. These locations were recorded and converted to voltages for each point. These output voltages through a GEPAC computer were in turn converted into x-y coordiantes, expressed in centimeters, relative to a chosen origin. These coordinates were finally transferred to the IBM computer memory ready for the subsequent computations.

3.6.3 Grid Adjustments

The undeformed grid was usually in a slightly distorted state. This distortion is due partly to the manual grid-making technique, and partly to soil heterogeneity. The method of approximate geometrical adjustments adopted by Windisch (1969) is described.

New underformed grid coordinates are arbitrarily defined to provide an "adjusted undeformed grid" of regular horizontal and vertical grid lines corresponding roughly to the original grid, Fig. 3.11. The respective displaced positions on the deformed grid are adjusted geometrically. The following symbols are used in the operations involved in these adjustments:

X1,Y1: original (distorted) undeformed grid coordinates
XIA,YlA: adjusted undeformed grid coordinates
XX,YY: original deformed grid coordinates
XXA,YYA: adjusted deformed grid coordinates

The adjustment in the abscissa of an undeformed grid point (I,J):

$$D1 = YIA(I,J) - YI(I,J)$$

and constitutes a first adjustment to the corresponding deformed grid point abscissa. The rate of adjusting along row J is:

$$(1 = \frac{YIA(J+1,J)-YI(I+1,J)-YIA(I,J)+YI(I,J)}{YI(I+1,J)-YI(I,J)}$$

resulting in a second adjustment to the abscissa of the deformed grid point:

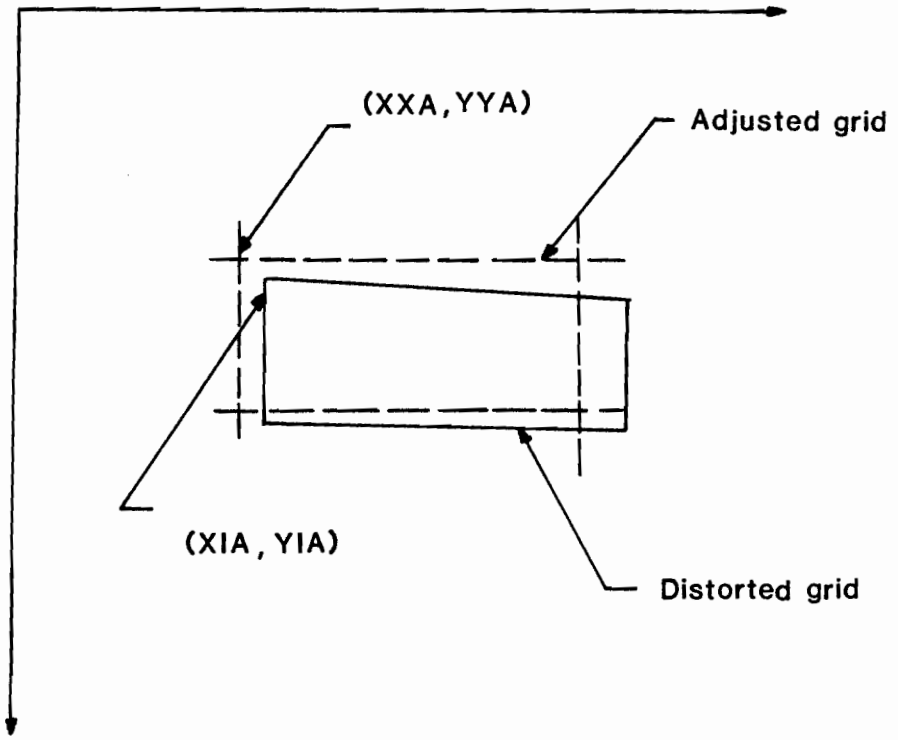

Fig. 3.11 Grid adjustment

D2 = (YY(I,J,JS) - Y1(I,J)) * C1

where JS represents the image after t_o, t_1, t_2, t_3 days and corresponds to the indices 2, 3, 4, 5. Similarly the rate of Y-adjusting along row J+1, is:

$$C2 = \frac{Y1A(I+1,J+1)-Y1(I+1,J+1)-Y1A(I,J+1)+Y1(I,J+1)}{Y1(I+1,J+1)-Y1(I,J+1)}$$

resulting in the adjustment:

D2' = (YY(I,J+1,JS) - Y1(I,J+1))*C2.

A third correction to the abscissa of the deformed grid point is due to vertical adjustments:

$$D3 = (D2'-D2)\ \frac{XX(I,J,JS)-XI(I,J)}{XI(I,J+1)-XI(I,J)}$$

The adjusted abscissa of the deformed grid point (I,J,JS) is finally given by the sum of the above adjustments:

YYS(I,J,JS) = YY(I,J,JS) + D1 + D2 + D3.

The ordinates of the deformed grid are similarly adjusted.

3.6.4 Curve Fitting of Particle Paths

The irregular shape of most of the particle paths opened the followoing options for consideration

(a) to ignore particle path irregularities and proceed with velocity calculations

(b) to perform visual smoothing of particle paths

(c) to fit a single equation to each of the y-components of a grid point in terms of its

x-components.

The adoption of (a) could lead to serious errors, while it was considered that visual smoothing would be impractical and too subjective. It was then decided to adopt the approach described in (c).

The method adopted consists of obtaining a single fit equation per particle path for each original grid point. The principle of least squares is applied to obtain the fit equations (Hildebrand, 1956).

The y-components $y_i = \phi(x_i)$ of the displacements are assumed to be approximated by a polynomial $f(x_i)$ in terms of the abscissae x_i of a given particle path of a grid point. Uniform weight is assumed for all data.

The polynomial used is as follows:

$$f(x_i) = \sum_{\ell=1}^{5} A_\ell f_\ell (x_i)$$

where A_ℓ = parameters

$f(x_i) = x_i^{-1}$

The sum of the errors squared:

$$u = \sum_{i=1}^{n} (\phi(x_i) - \sum_{\ell=1}^{n_o} A_\ell f_\ell (x_i))^2$$

where n = number of data points used = n_o.

This is minimized by setting its derivatives with respect to A equal to zero; hence

$$\frac{u}{A_k} = \sum_{i=1}^{n} (\phi(x_i) - \sum_{\ell=1}^{n_o} A_\ell f_\ell (x_i))\, f_k(x_i) = 0 \qquad (3.1)$$

$$k = 1 \ldots n_o$$

Equation (3.1) can be rearranged as:

$$\sum_{=1}^{n_o} \left(\sum_{i=1}^{n} f_k(x_i)\, f\,(x_i) \right) A = \sum_{i=1}^{n} f_k(x_i)\phi(x_i) \qquad (3.2)$$

$$k = 1,\ldots,n_o$$

The system of simultaneous equations (3.2) can be simply represented in matrix notation as:

$$(\psi)\ A = B$$

where

$$\psi_k = \sum_{i=1}^{n} (f_k(x_i) f\,(x_i))$$

$$B_k = \sum_{i=1}^{n} (f_k(x_i)\phi(x_i))$$

$$k = 1,\ldots.n_o$$

The required solution for the parameters A is then

$$A = (\psi)^{-1}\ B$$

3.6.5 Velocity Components

The fit parameters obtained in the preceding subseciton are used to approximate particle positions, herein referred to as XFIT, YFIT. The velocity components are then expressed as:

$$\dot{U}(I,J,JS) = (XFIT(I,J,JS1) - XFIT(I,J,JS))/\Delta t$$

$$\dot{V}(I,J,JS) = (YFIT(I,J,JS1) - YFIT(I,J,JS))/\Delta t$$

where I, J are column and row indices, respectively
JS, JS1 impage indices
$\dot{V}$, $\dot{U}$ particle velocity components

Δt time interval between images

XFIT,YFIT fitted coordinates as derived from subroutine CURVFT

3.6.6 Strain Rate Components

A Lagrangian space is selected in order to follow a given particle. Specifying rectangular Cartesian coordinates within this Lagrangian space, the relationship between the strain tensor E_{ij} and the displacement vector u is expressed as (Fung, 1965):

$$E_{ij} = \frac{1}{2} \left(\frac{u_j}{x_i} + \frac{u_i}{x_j} + \frac{u_a}{x_i} \frac{u_a}{x_j}\right)$$

or in unabridged notation:

$$E_{xx} = \frac{u}{x} + \frac{1}{2} \left(\left(\frac{u}{x}\right)^2 + \left(\frac{v}{x}\right)^2 + \left(\frac{w}{x}\right)^2\right)$$

$$E_{xy} = \frac{1}{2} \left(\frac{u}{y} + \frac{v}{x} + \left(\frac{u}{x} \frac{u}{y} + \frac{v}{x} \frac{v}{y} + \frac{w}{x} \frac{w}{y}\right)\right), \text{ etc.} \qquad (3.3)$$

u_j or u, v, w: components of the displacement vector.

The strain rate components are related to the components of the velocity vector by relations analogous to equation (3.3):

$$\dot{E}_{xx} = \frac{\dot{u}}{x} + \frac{1}{2} \left(\left(\frac{\dot{u}}{x}\right)^2 + \left(\frac{\dot{v}}{x}\right)^2 + \left(\frac{\dot{w}}{x}\right)^2\right)$$

$$\dot{E}_{xy} = \frac{1}{2} \left(\frac{\dot{u}}{y} + \frac{\dot{v}}{x} + \left(\frac{\dot{u}}{x} \frac{\dot{u}}{y} + \frac{\dot{v}}{x} \frac{\dot{v}}{y} + \frac{\dot{w}}{x} \frac{\dot{w}}{y}\right)\right), \text{ etc.}$$

$\dot{E}_{xx}$, $\dot{E}_{xy}$ ...: strain rate components

$\dot{u}$, $\dot{v}$, $\dot{w}$: velocity components

The error involved in neglecting the second order terms is often less than 1.5% and rarely greater than 20%. Since errors of this magnitude can be produced by lack of accuracy in the measurements of displacement, it seems justified to introduce an approximation to the strain rate components by Cauchy's infinitesimal strain rate tensor:

$$\dot{E}_{ij} = \frac{1}{2} \left(\frac{\dot{u}_j}{x_i} + \frac{\dot{u}_i}{x_j} \right)$$

or in unabridged notation:

$$\dot{E}_{xx} = \frac{\dot{u}}{x}$$

$$\dot{E}_{xy} = \frac{1}{2} \left(\frac{\dot{u}}{y} + \frac{\dot{v}}{x} \right), \text{ etc.}$$

Under plane starin conditions and in unabridged notation, the following equations are finally obtained:

$$\begin{aligned} \dot{E}_{xx} &= \frac{\dot{u}}{x} \\ \dot{E}_{xy} &= \frac{1}{2} \left(\frac{\dot{u}}{y} + \frac{\dot{v}}{x} \right) \\ \dot{E}_{yy} &= \frac{\dot{v}}{y} \end{aligned} \qquad (3.4)$$

The strain rate components obtained by equations (3.4) allow one to define the directions of the principal strain rates with the aid of the relations between the Mohr plane and the physical plane.

The effective strain rate $\dot{E}$ can be obtained from the strain rate components:

$$\dot{E}_{ij} = \frac{2}{3} \left((\dot{E}_x)^2_{ij} + (\dot{E}_y)^2_{ij} - (\dot{E}_x)_{ij} (\dot{E}_y)_{ij} + \frac{3}{4} (\dot{\gamma}_{xy})^2_{ij} \right)^{1/2}$$

CHAPTER 4

PRESENTATION OF RESULTS AND DISCUSSION

4.1 Introduction

Under the various boundary conditions imposed on the buffer material, time-dependent response characteristics are developed. The laboratory experiments performed in this study are directed towards the investigation of these response characteristics.

In this chapter, the time-history of the boundary condition-buffer material response is presented, through the experimental results obtained. Discussion of the effect of varying boundary conditions on the buffer response characteristics is included. In Fig. 4.1 the test program is presented in schematic form.

The overall experimental results presented in this chapter, together with the finite element analysis given in Chapter 5, are all incorporated in order to evaluate and predict the buffer performance under the different boundary conditions imposed.

4.2 Model Tests Under No Water Intake Conditions

The objectives of the tests performed under no water intake conditions, with the overburden pressure acting at the top of the buffer material the main variable, are to obtain information enabling prediction of the buffer behaviour prior to and after the tunnel backfilling,

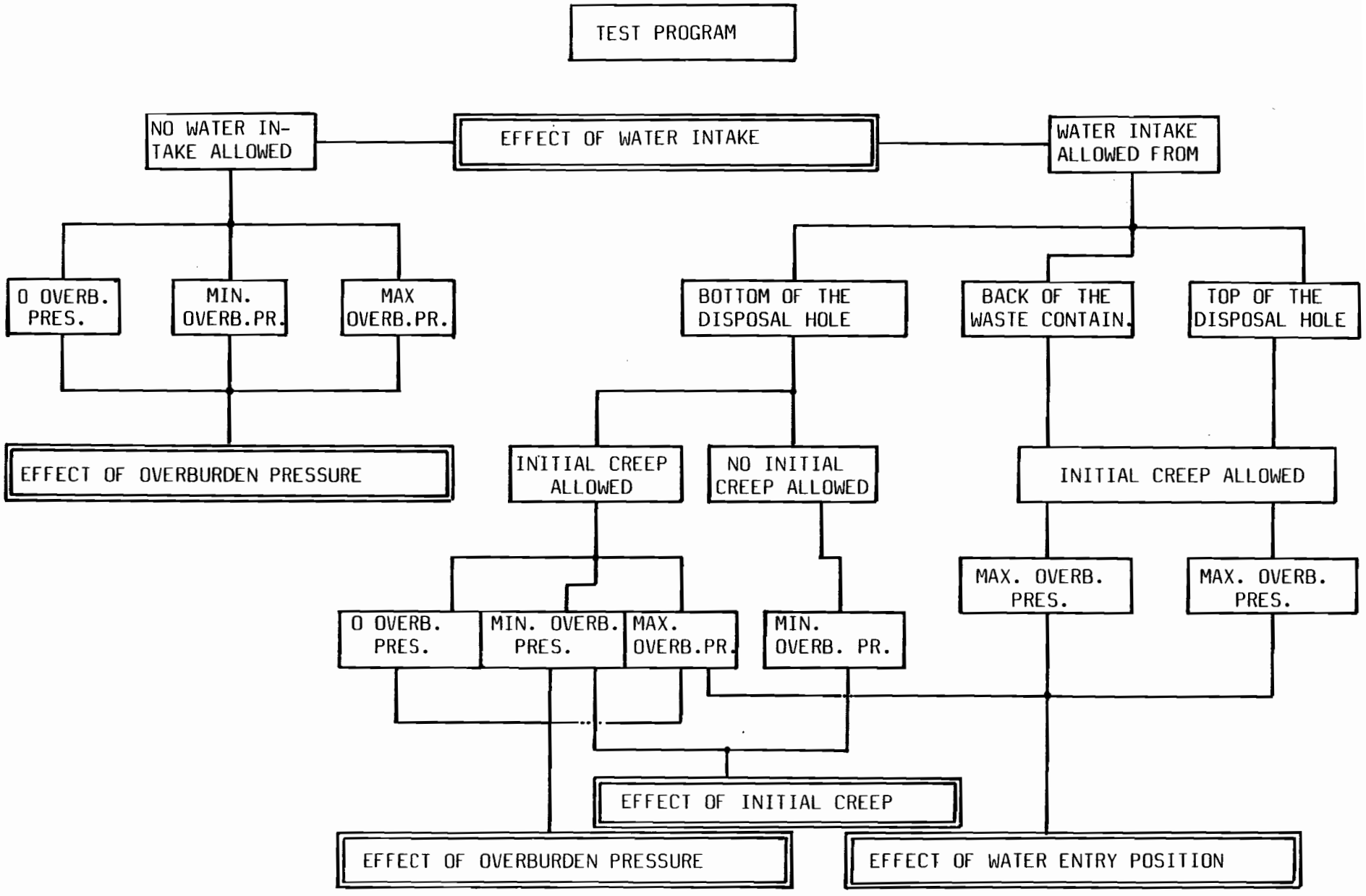

Flow diagram of the test program

Fig. 4.1

assuming no rock cracks nor subsequent water intake. This test series will be presented through: 1) soil particle movement characteristics which are the actual test results, 2) container movement-time histories, 3) compressibility characteristics which are derived from the actual test results, 4) friction estimates on buffer-container and buffer-host rock interface, and 5) correlation between the model test results and the tests performed at GRC.

4.2.1 Soil Particle Movements

For the appropriate observation of any general patterns of particle movement, the nodal displacement fields are plotted at an exaggerated scale in Figs. 4.2, 4.3 and 4.4. These fields describe the particle movements from the initial undeformed condition to the final deformed one, when no more additional displacement takes place.

In addition to the nodal displacement fields, vertical displacement-time histories for representative nodes are plotted at several cross-sections covering the disposal hole. These cross-sections are shown in Fig. 4.5 which will be used as a reference figure for the presentation of the test results.

The nodal displacement fields indicate that when overburden pressure increased from 0 kPa to 120 kPa the vertical nodal displacements above the waste container increased. From Figs. 4.6, and 4.7, where the displacement versus time relationship for points on the cross-section

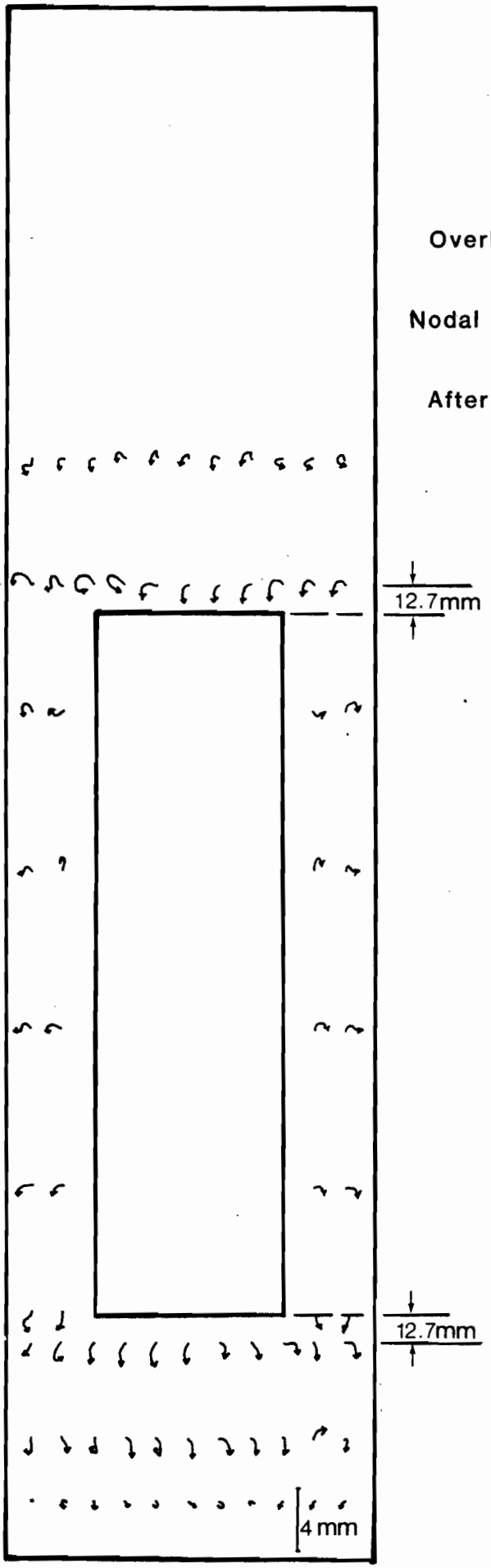
Overb.pr.: 0 kPa
Nodal displacement field
After 15 days
12.7mm
12.7mm
4 mm

Fig. 4.2

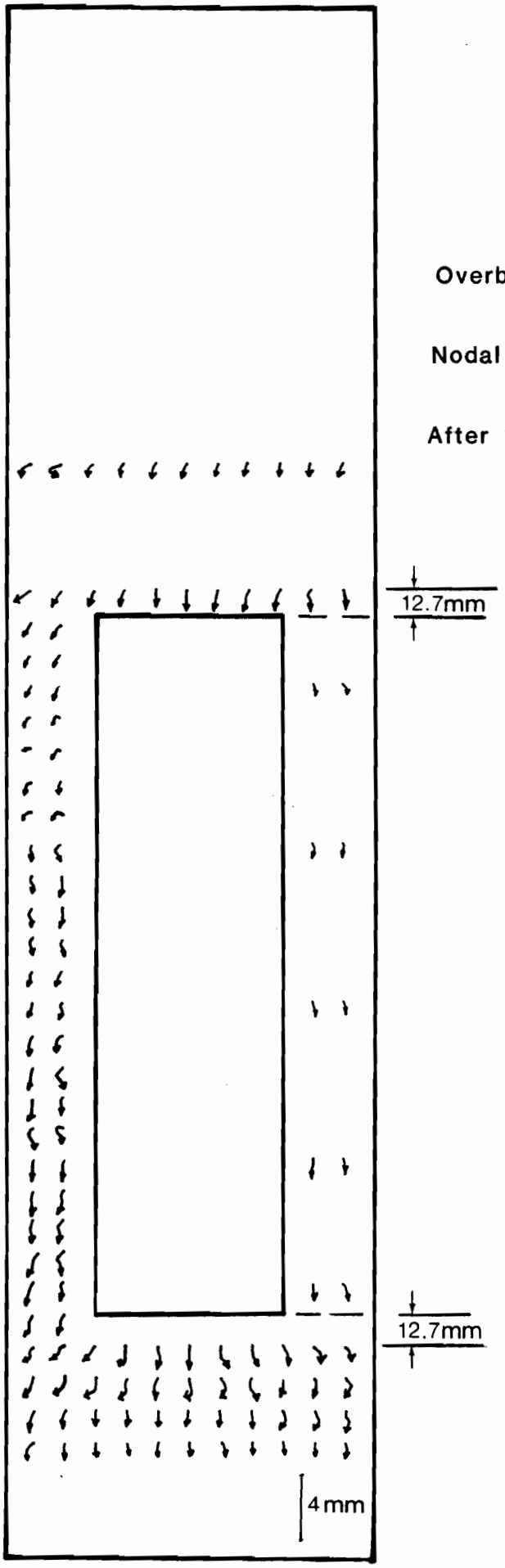

Overb.pr.: 36 kPa

Nodal displacement field

After 18 days

Fig. 4.3

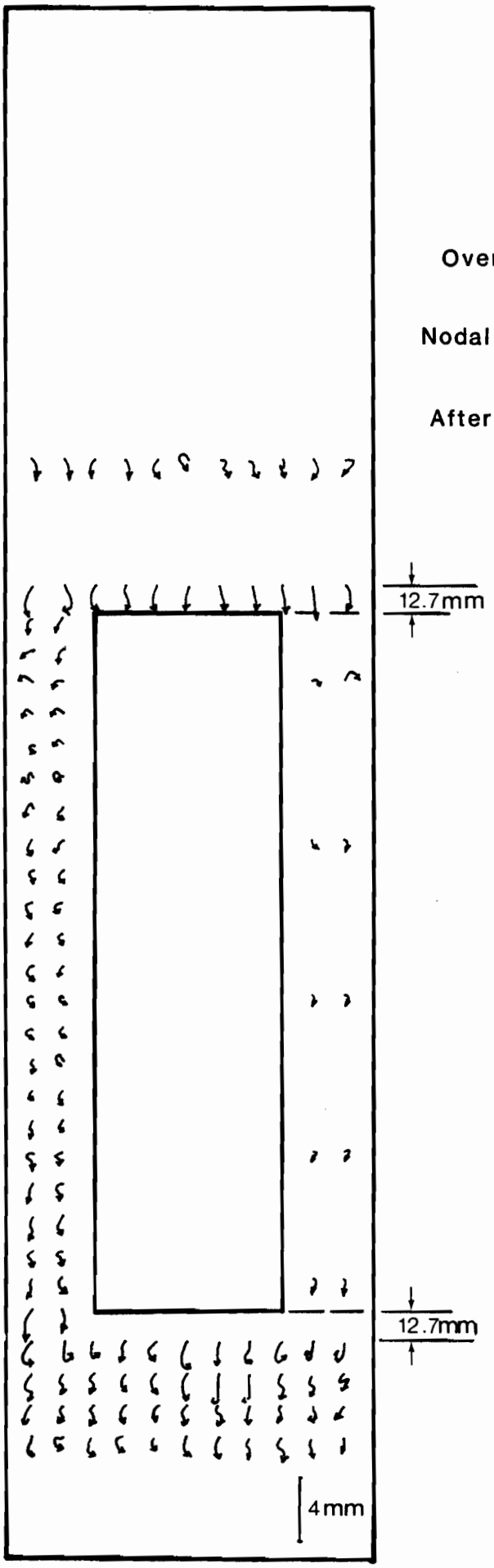

Overb.pr.: 120 kPa

Nodal displacement field

After 18 days

Fig. 4.4

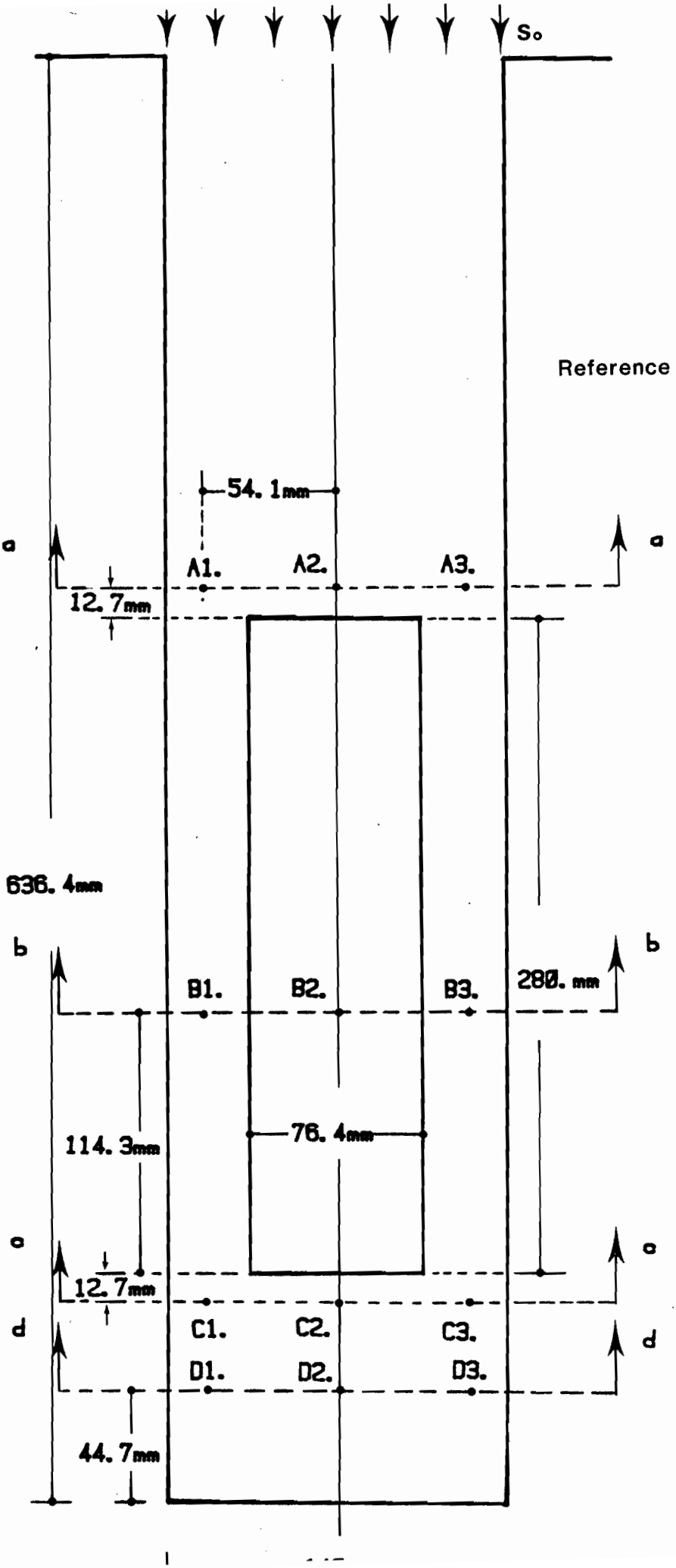
So
Reference figure
54. 1mm
a
A1.
A2.
A3.
a
12. 7mm
636. 4mm
b
B1.
B2.
B3.
280. mm
b
114. 3mm
76. 4mm
a
12. 7mm
a
d
C1.
C2.
C3.
d
D1.
D2.
D3.
44. 7mm

Fig. 4.5

A-A (see Reference Fig. 4.5) is plotted, the increase in displacement with overburden pressure is clearly illustrated. For the node A2, when pressure increased form 0 kPa to 36 kPa the corresponding vertical displacement increased froml.00 mm to 1.35 mm; Node A2 settled 1.70 mm when overburden pressure increased to 120 kPa. This increase in the displacement of node A2 reflects the overburden pressure effect in the area above the waste container. The highest vlaue of vertical displacement for node A2 was reached in 10 days when the overburden pressure was 0 kPa and at 18 days when the overburden pressure increased to 36 kPa and later to 120 kPa.

The same patterns of displacement are observed for other points on the same cross-section (Fig. 4.7). Vertical displacement increased with an increase in overburden pressures. The highest displacement vlaues were reached at 12-18 days for the cases of 36 kPa and 120 kPa of overburden pressure. When the overburden pressure was equal to 0 kPa (for the first 5 days of loading) upward displacements were observed up to 0.75 mm. This can be due to certain stress development and transfer mechanisms in the areas around the container.

For the area around the container the displacement fields indicate that the soil particles appear to move generally away from the container. Upward movements were again observed when overburden pressure was equal to 0 kPa, for the first 5 days after the container installation (Fig.

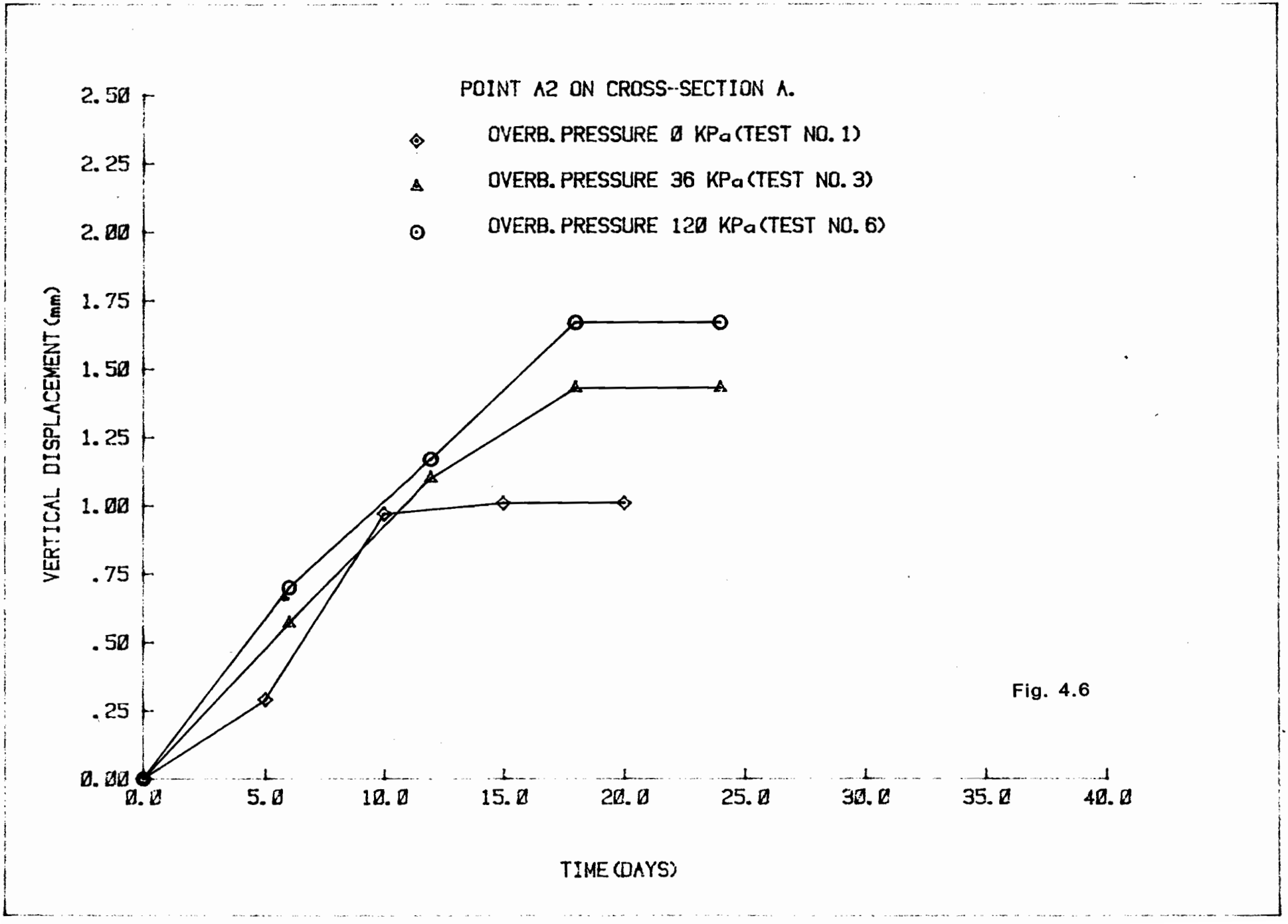
POINT A2 ON CROSS-SECTION A.
OVERB. PRESSURE Ø KPa (TEST NO. 1)
OVERB. PRESSURE 36 KPa (TEST NO. 3)
OVERB. PRESSURE 120 KPa (TEST NO. 6)
VERTICAL DISPLACEMENT (mm)
2.50
2.25
2.00
1.75
1.50
1.25
1.00
.75
.50
.25
0.00
0.0
5.0
10.0
15.0
20.0
25.0
30.0
35.0
40.0
TIME (DAYS)

Fig. 4.6

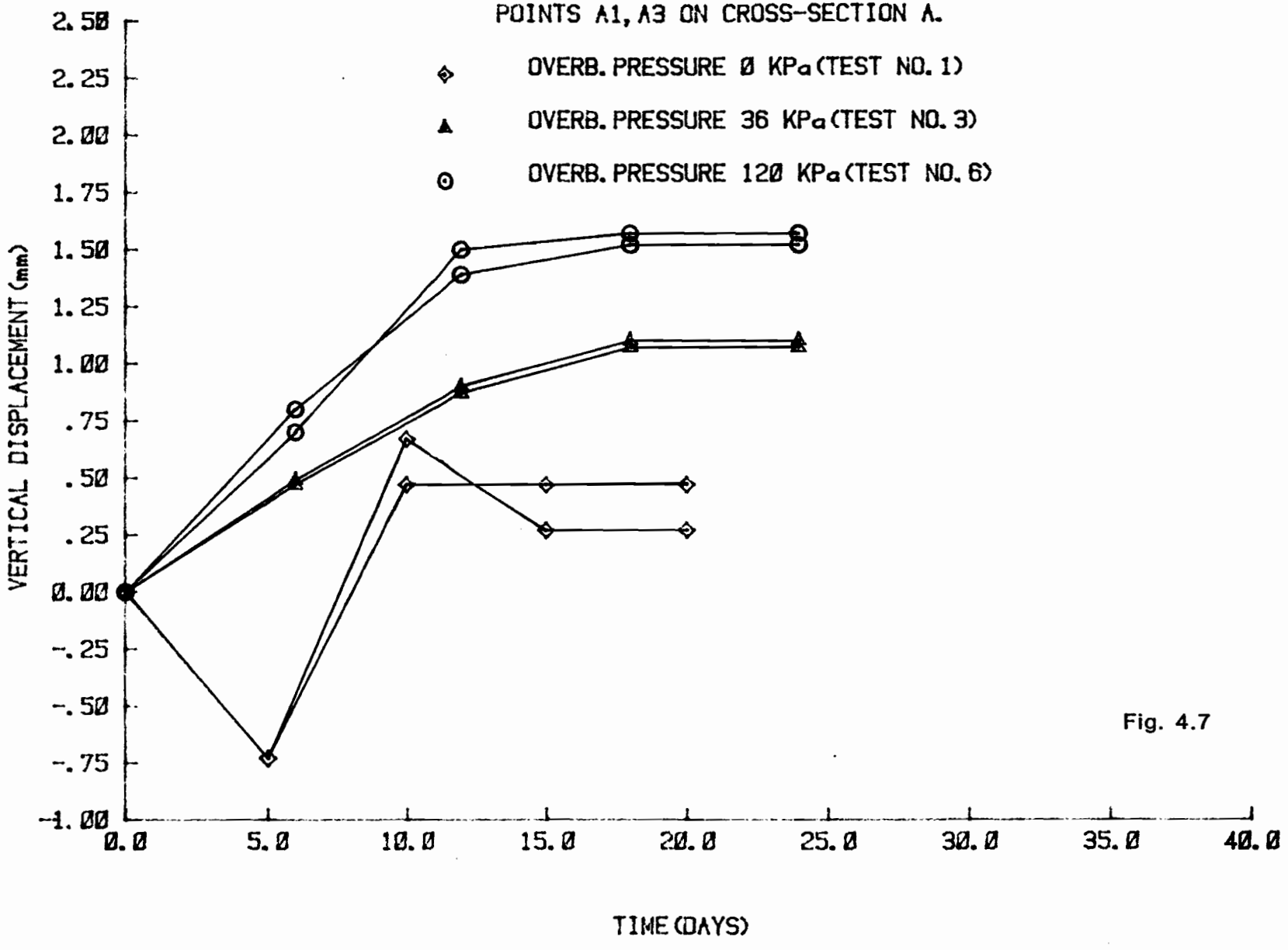
POINTS A1, A3 ON CROSS-SECTION A.
OVERB. PRESSURE Ø KPa (TEST NO. 1)
OVERB. PRESSURE 36 KPa (TEST NO. 3)
OVERB. PRESSURE 120 KPa (TEST NO. 6)
VERTICAL DISPLACEMENT (mm)
2.50
2.25
2.00
1.75
1.50
1.25
1.00
.75
.50
.25
0.00
-.25
-.50
-.75
-1.00
0.0
5.0
10.0
15.0
20.0
25.0
30.0
35.0
40.0
TIME (DAYS)

Fig. 4.7

4.8). The highest vertical displacement values were reached after 18 days of loading, when the overburden pressure was 36 kPa (displacement = 0.90 mm) and 120 kPa (displacement = 1.25 mm).

The most interesting phenomenon observed was the initial upwards movement of certain nodes when the overburden pressure was 0 kPa. These nodes were located between the waste container and the host rock surface. As already mentioned, stress development and transfer mechanisms are the main causes of this buffer response. After buffer compaction and container installation was finished, close contact between buffer and container was obtained. The container weight acted as a dead weight, pulling the waste container towards the bottom of the disposal system and the buffer underneath the container suffered a compressive load. This load resulted in volume change conditions in the zone below the waste container. Initial movement of the buffer below the container towards the edges (of the disposal system) and upwards was merely buffer readjustment towards areas of lower stress levels. These upward displacements were reduced with time due to factors such as buffer weight and friction generated along the buffer-container interfaces. It should be mentioned that when the overburden pressure was equal to 36 kPa these upward movements were no longer observed. The overburden pressure imposed on the buffer eliminated these movements by increasing the stress in the buffer. The upward movements observed when the overburden

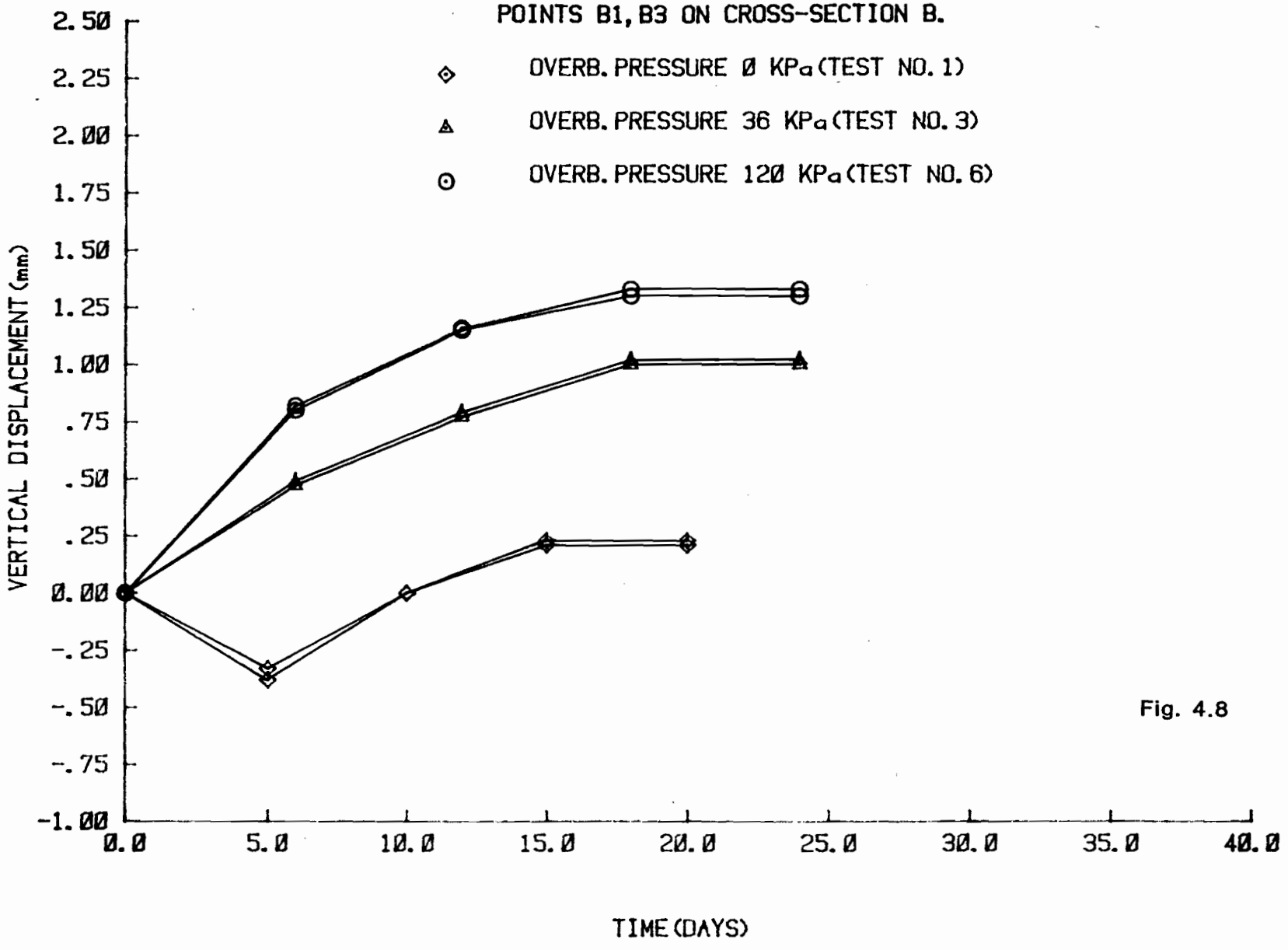
POINTS B1, B3 ON CROSS-SECTION B.
OVERB. PRESSURE Ø KPa (TEST NO. 1)
OVERB. PRESSURE 36 KPa (TEST NO. 3)
OVERB. PRESSURE 120 KPa (TEST NO. 6)
VERTICAL DISPLACEMENT (mm)
2.50
2.25
2.00
1.75
1.50
1.25
1.00
.75
.50
.25
Ø.ØØ
-.25
-.50
-.75
-1.00
Ø.Ø
5.Ø
10.Ø
15.Ø
20.Ø
25.Ø
30.Ø
35.Ø
40.Ø
TIME (DAYS)

Fig. 4.8

pressure was 0 kPa resulted in small cracks in certain areas around the waste container (see Fig. 4.9).

In Figs. 4.10 and 4.11, the vertical displacement-time relationships for the area below the waste container are described. From the figures it can be observed that the vertical displacements of node C2 - the node on the central line below the waste container - were higher than those of nodes C1 and C2 for every loading condition. The displacements of points C1 and C3 were 50% of those observed at point C2 when the overburden pressure was 0 kPa and 36 kPa and 70% when the pressure increased to 120 kPa. For small overburden pressure values the waste container seems to "penetrate" the buffer. Increased overburden pressure results in a more uniformly deformed cross-section pattern.

The largest displacements under the container were obtained after 15 days when the overburden pressure was 0 kPa (1.45 mm) and after 18 days when the pressure increased to 36 kPa (1.68 mm) and 120 kPa (1.72 mm). It should be noted that under the same loading conditions, the highest displacement values at the top of the waste container were reached after 10 days and 18 days respectively. These differences, especially for the low overburden pressure value of 0 kPa, reflect the different loading conditions which are experienced by the buffer along the disposal hole system. These response characteristics, which are boundary condition dependent, indicate that two zones of buffer

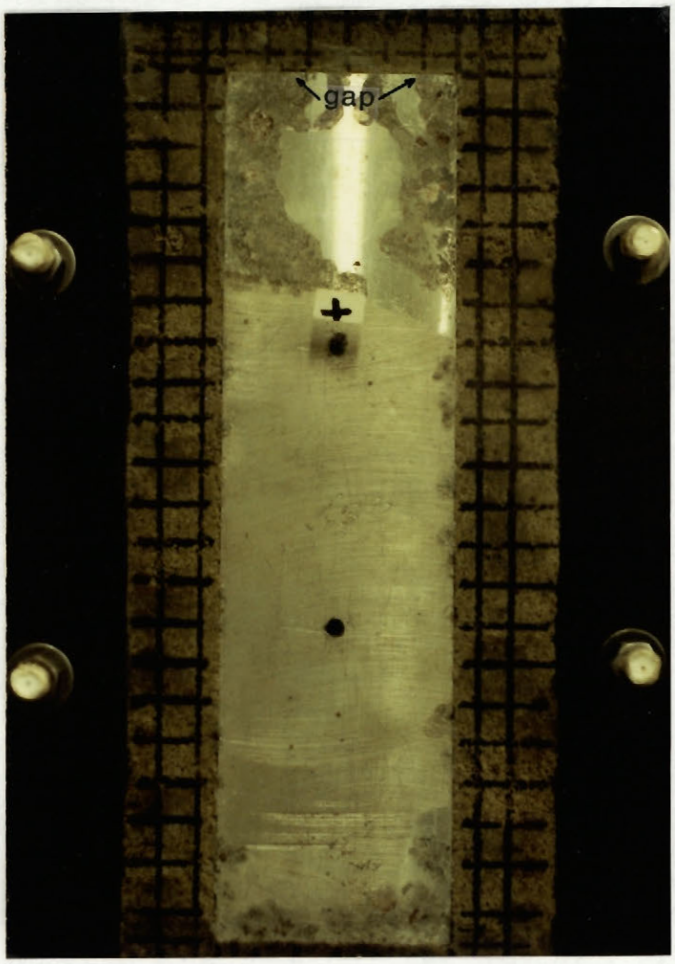

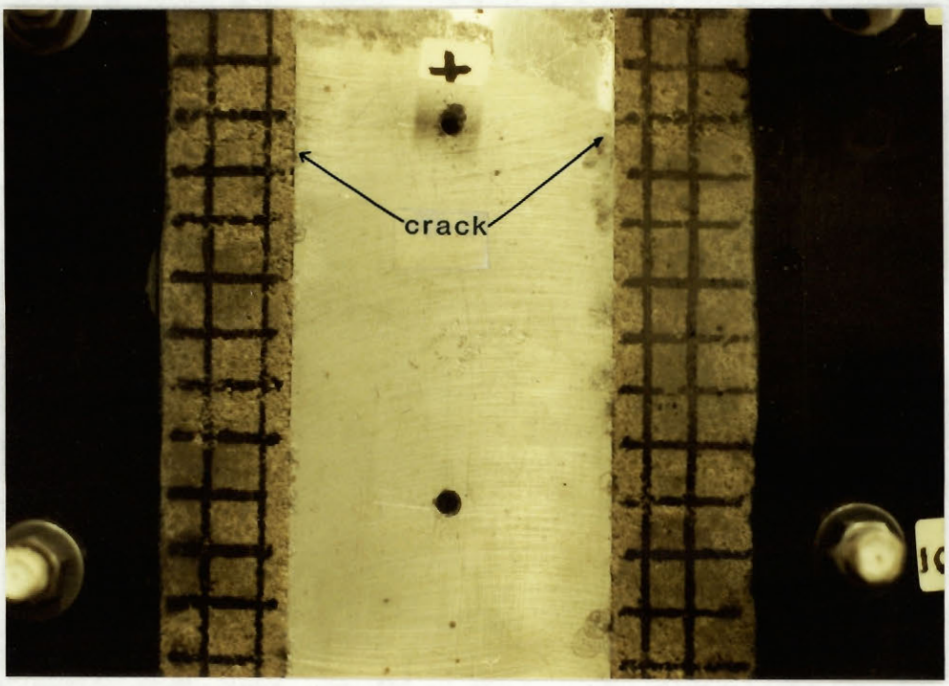

Pictures showing local cracks and separation at the top of the waste container Fig. 4.9

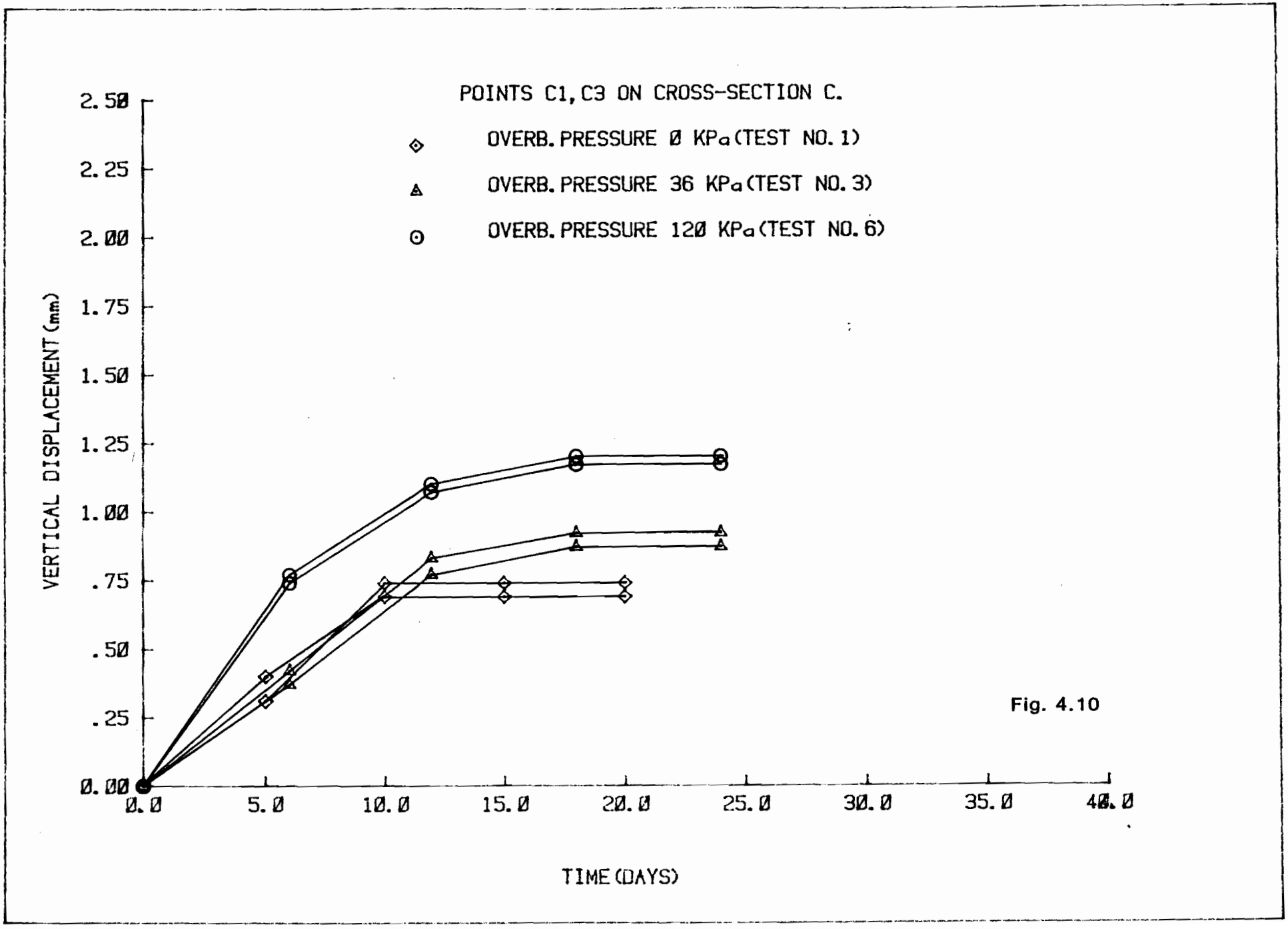
POINTS C1, C3 ON CROSS-SECTION C.
OVERB. PRESSURE Ø KPa (TEST NO. 1)
OVERB. PRESSURE 36 KPa (TEST NO. 3)
OVERB. PRESSURE 120 KPa (TEST NO. 6)
VERTICAL DISPLACEMENT (mm)
2.50
2.25
2.00
1.75
1.50
1.25
1.00
.75
.50
.25
0.00
0.0
5.0
10.0
15.0
20.0
25.0
30.0
35.0
40.0
TIME (DAYS)

Fig. 4.10

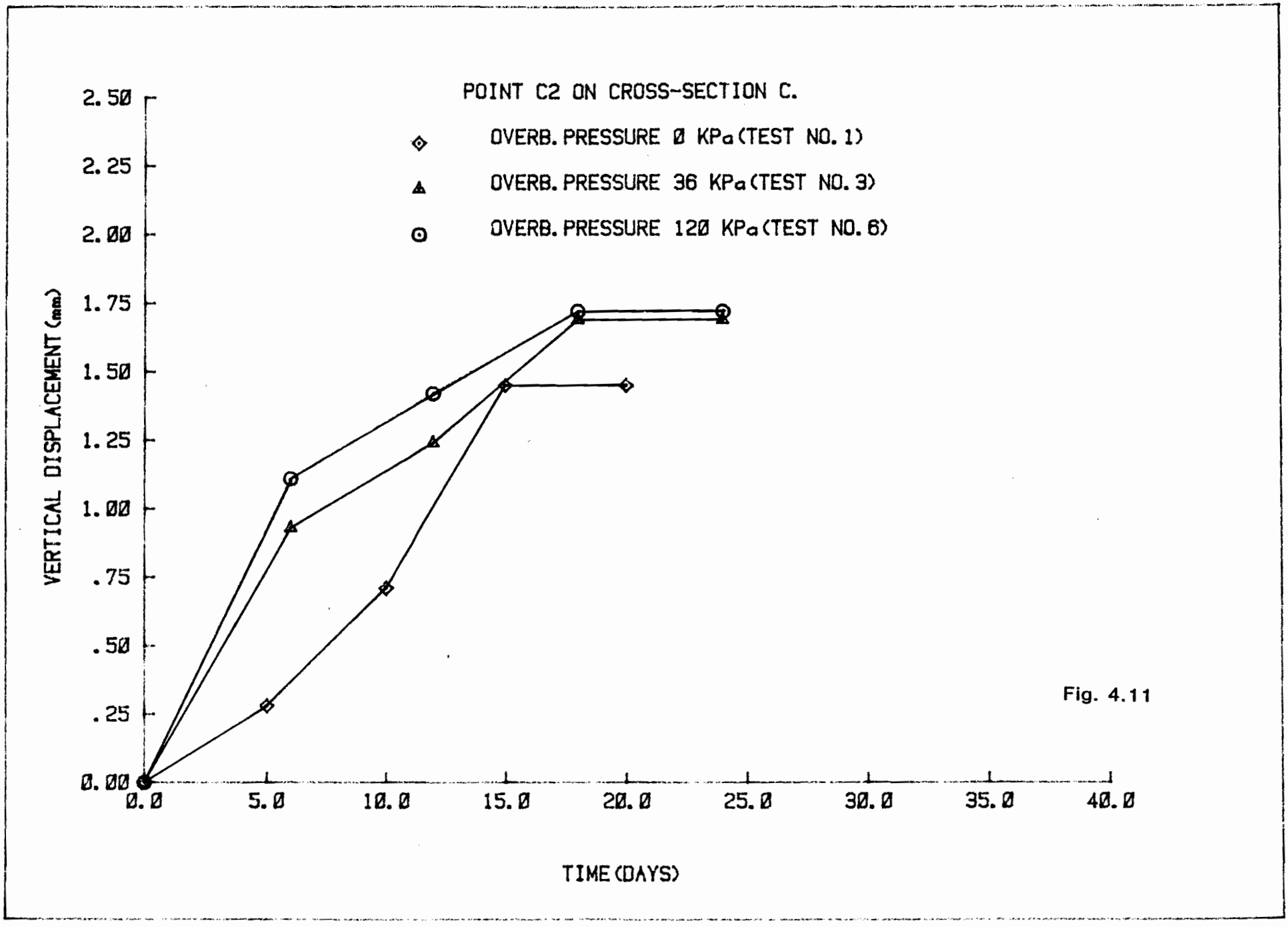
POINT C2 ON CROSS-SECTION C.
OVERB. PRESSURE Ø KPa (TEST NO. 1)
OVERB. PRESSURE 36 KPa (TEST NO. 3)
OVERB. PRESSURE 120 KPa (TEST NO. 6)
VERTICAL DISPLACEMENT (mm)
2.50
2.25
2.00
1.75
1.50
1.25
1.00
.75
.50
.25
0.00
0.0
5.0
10.0
15.0
20.0
25.0
30.0
35.0
40.0
TIME (DAYS)

Fig. 4.11

material should be taken into account in a simplified predictive model. One zone is above the waste container and experiences one-dimensional compression with yielding bottom support while the other zone, which surrounds the waste container, experiences triaxial stress conditions with no drainage allowed.

The observed vertical displacement-time histories lead to a few general additional comments about the overburden pressure effect on the overall buffer response. It can be concluded that the constant creep rate is reached after longer time periods for increased overburden pressures; the value of the constant creep rate increases with increasing overburden pressure. These experimental conclusions demonstrate the stress level effect on the creep response of the buffer. Yong and Chen (1969) analyzed the creep of clays using retardation time distribution and observed that the minimum creep rate increases nonlinearly as loading is increased. They also concluded that the instantaneous compliance becomes smaller as loading increases. This resulted from increased density due to structural rearrangement of the elementary units where a greater proportion of the load is now carried by the stronger units (Yong and Chen, 1969). Abdel Hady and Herrin (1966) showed that constant creep rate values increase nonlinearly with stress level and are obtained after larger time periods under higher loading. The same effect was also shown by Komamura and Huang (1974), by Prevost (1976) and other

researchers on the creep response of engineering materials.

Another interesting phenomenon observed during the experiment was the separation that occurred at the waste container top-buffer interface. When overburden pressure was 0 kPa, this separation was 0.5 mm, when the pressure increased to 36 kPa, the separation was 0.3 mm and when the overburden pressure reached 120 kPa no separation was observed. This separation is due to the boundary effects of the system and the buffer high cohesive characteristics, that produced, through the compaction process, a very rigid buffer structure. It should be noted that in CU tests performed at GRC for the buffer material, the cohesion intercept value derived was 40 kPa. In Fig. 4.12 the separation observed at the top of the waste container, when the overburden pressure was 36 kPa (after 18 days of loading) is shown.

In order to simulate the actual load-deformation relationship for the area below the waste container, CBR tests were performed under soaking and non-soaking conditions with a surcharge load of 8.8 kgr. The results from the CBR tests, relating penetration depths to the vertical displacements of the node on the centralline under the waste container are shown in Table 4.1.

TABLE 4.1

Stress (kPa)	CBR Penetration (mm)	Model Test Vertical Displacement (mm)
280	1.05	1.45
316	1.16	1.69
400	1.47	1.73

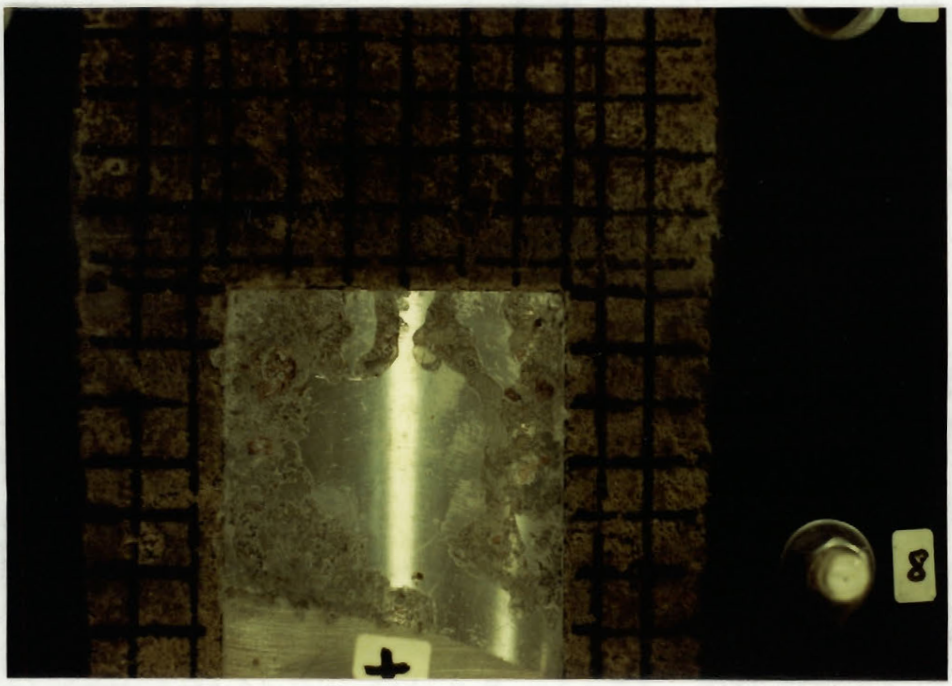

Separation at the top of the waste container

Fig. 4.12

The CBR results are lower than the model test results. This can be due to certain factors: technico-experimental (data acquisition techniques); friction generated along the penetrating device-soil interface; and compaction resulting in different buffer properties (homogeneity, density).

4.2.2 Container Movement

The container movement vs time relationship is plotted in Fig. 4.13. The vertical displacement time history of the container is identical to the one corresponding to point C2 (Ref. Fig. 4.5) underneath the container. Tilting of the container during the tests, due to soil heterogeneity resulting from the compaction technique and to container misalignment, was observed during the first experimental steps, but it was eliminated in the process. This improvement produced symmetrical nodal deformation patterns around the waste container.

4.2.3 Compressibility of Buffer

From the tests performed with varying overburden pressures, displacement patterns resulted, indicating certain compressibility characteristics for the buffer material. It should be mentioned that the initial average degree of saturation of the buffer was 86%. It should also be recalled that Poisson's ratio is 0.29, indicating a stiff soil. The general rating according to the CBR test is fair

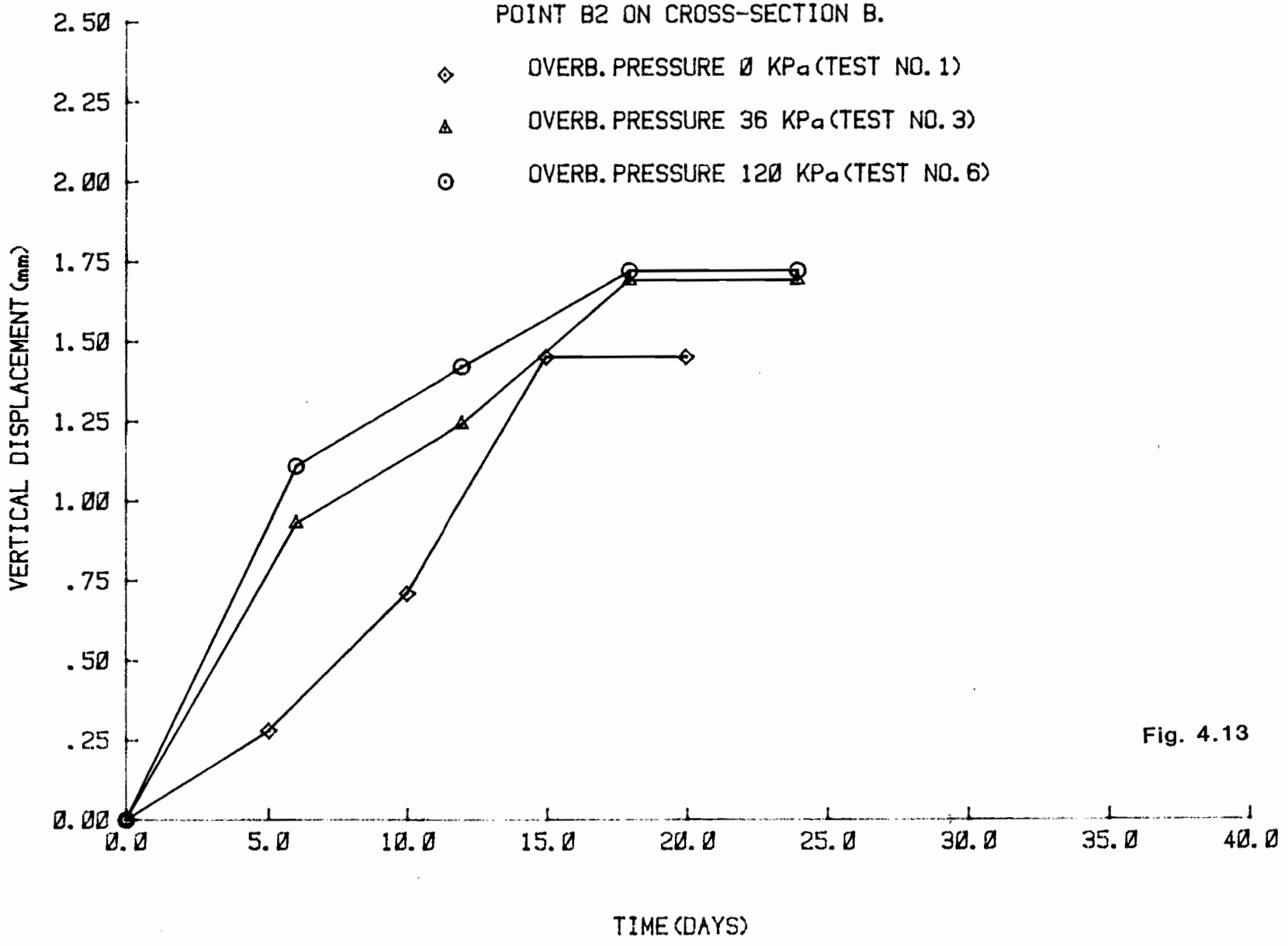
POINT B2 ON CROSS-SECTION B.
OVERB. PRESSURE Ø KPa (TEST NO. 1)
OVERB. PRESSURE 36 KPa (TEST NO. 3)
OVERB. PRESSURE 120 KPa (TEST NO. 6)
VERTICAL DISPLACEMENT (mm)
2.50
2.25
2.00
1.75
1.50
1.25
1.00
.75
.50
.25
0.00
0.0
5.0
10.0
15.0
20.0
25.0
30.0
35.0
40.0
TIME (DAYS)

Fig. 4.13

for non-soaking conditions and samples failed under different confining stresses at CU tests with 9 to 12% final strains.

In order to present and discuss the compressibility characteristics of the buffer material the displacement contours are plotted for the area below the waste container in Figs. 4.14 and 4.15. For easier comparison the same contours are plotted.

In Fig. 4.14 the contours plotted are for the case of overburden pressure equal to 36 kPa. In Fig. 4.15 the contours plotted resulted from the case of overburden pressure equal to 120 kPa. From Fig. 4.14 different creep rates are observed for certain depths below the container bottom. For a distance of 30 mm from the bottom of the container, the higher settlement values were reached only after 18 days. On the other hand, at greater depths the higher settlement values were reached after 12 days of loading. This is an indication of the "damping" of the settlement induced by the weight of the container with increasing depth. The same pattern is observed in Fig. 4.15. When Figs. 4.14 and 4.15 are compared, the increased settlement that is produced by the high overburden pressure value (120 kPa) is obvious, especially for the first 6 days under loading. For all the nodes of the area underneath the waste container for the zone of 20 mm, the settlements when overburden pressure is 36 kPa are equal to 90% of the corresponding settlements when pressure is 120 kPa. After

Settlement contours in (mm)

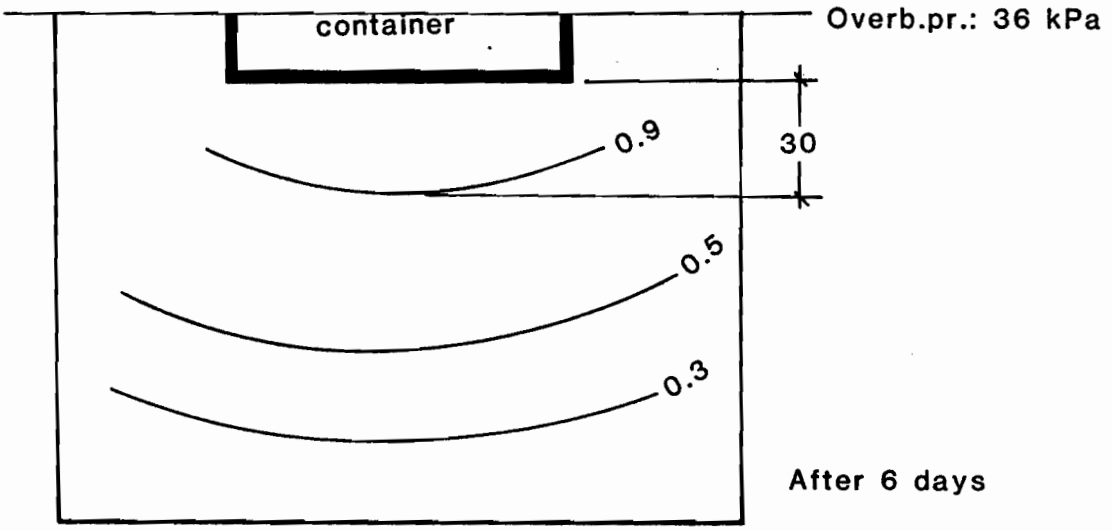

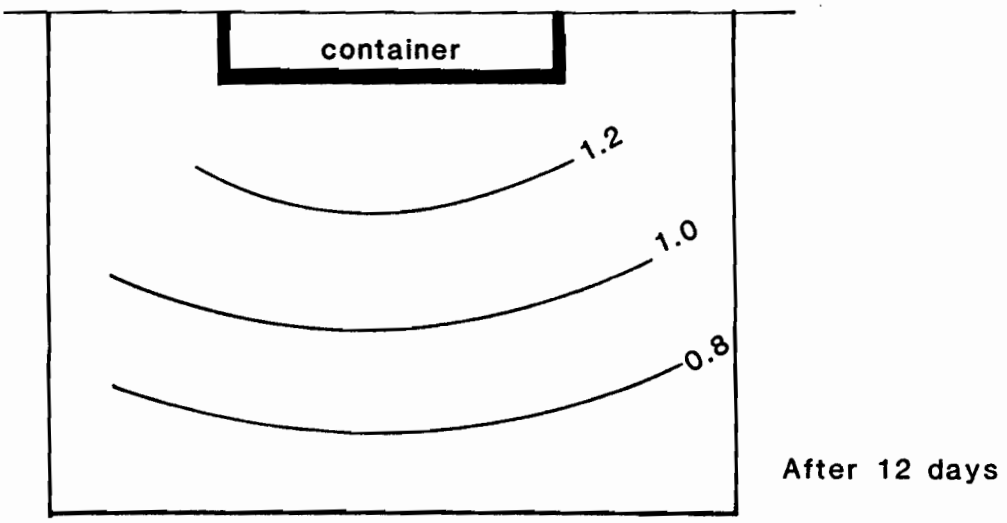

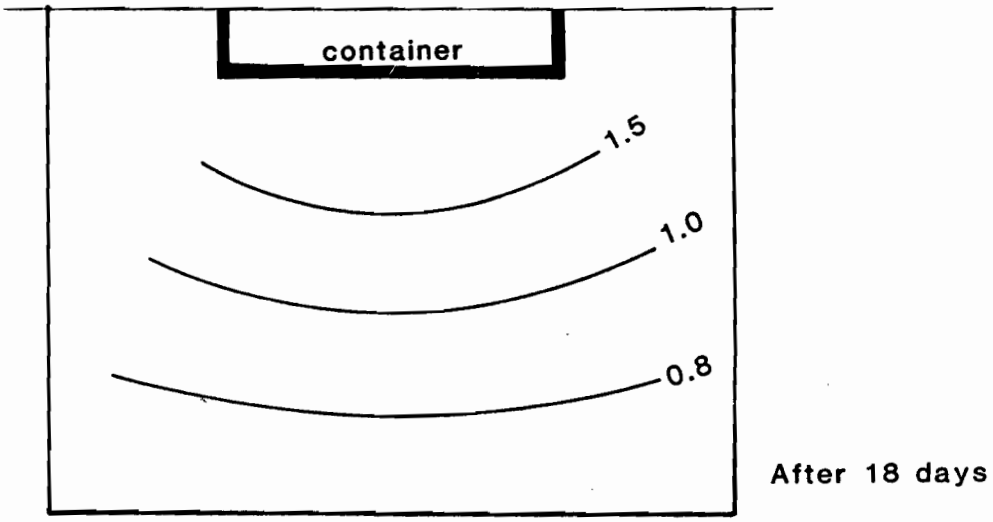

Fig. 4.14

Settlement contours in (mm)

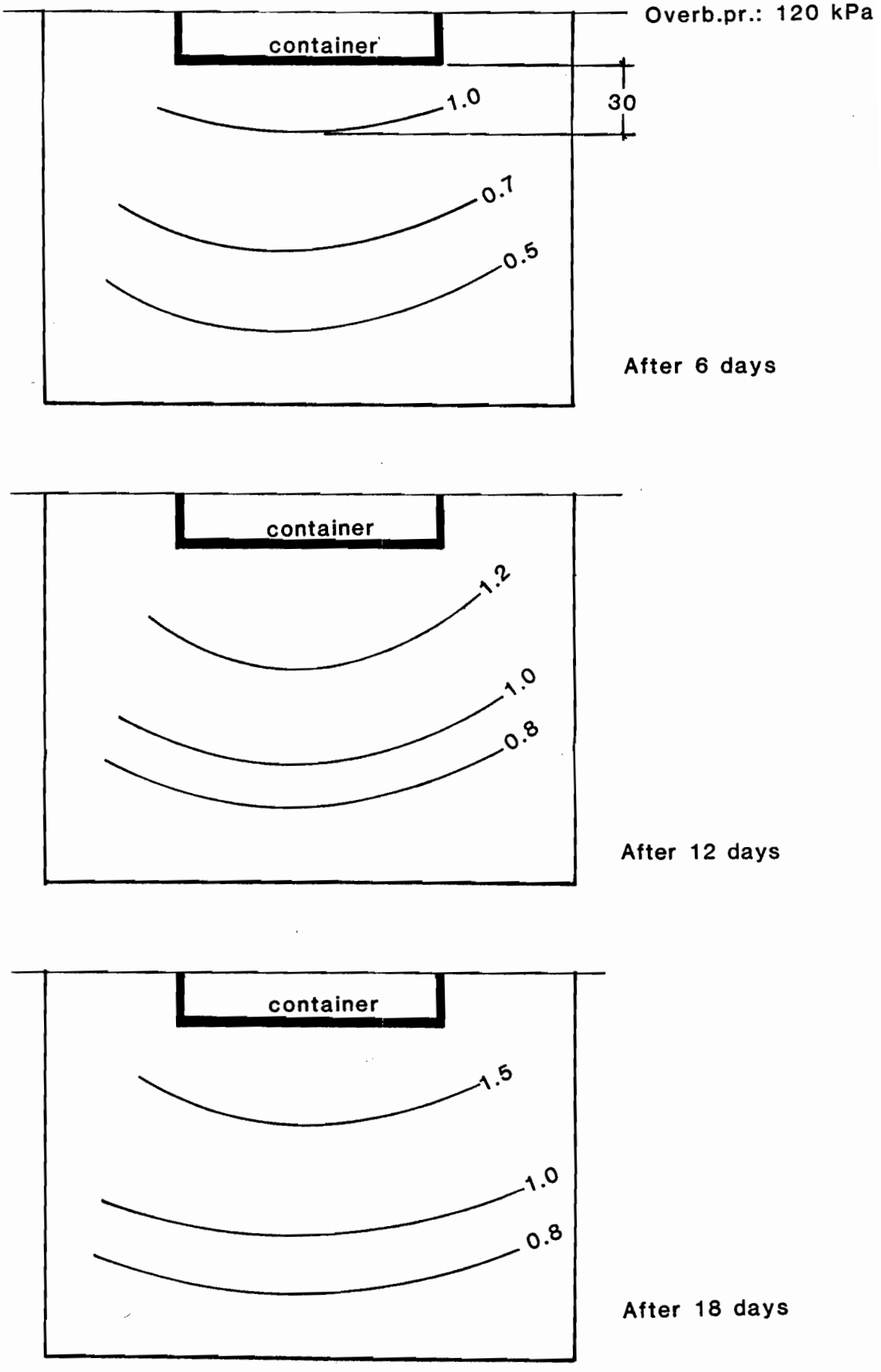

Fig.4.15

12 days the settlement bulbs tend to be identical. It is also very interesting to present the intensity and the extent of the settlement bulb as an overburden pressure function. This is done in Fig. 4.16. The final settlements are presented as percentages of the final settlements obtained at the point C2 underneath the container. In other words, they are the contours of the ratio $\Delta y_i/\Delta y_{C2}$, where:

Δy_i is the final settlement of node i, and

Δy_{C2} is the final settlment of the node C2

In Fig. 4.16 the intensity of the final settlement bulb for different overburden pressure values is shown. When the overburden pressure is 0 kPa the zone "1.00" extends to 45 mm below the container bottom. The same zone has a depth of 52 mm when the overburden pressure is 36 kPa and a depth of 85 mm when overburden pressure increases to 120 kPa. The distribution patterns, also shown in Fig. 4.16 in the form of longitudinal sections along the central line, indicate that when the overburden pressure increases, the overall confinement increases as well, producing a decrease in the settlements observed, especially for lower zones ("0.5 - 0.70"). In fact a cross-section could be observed (cross-section D-D Fig. 4.5) in the area below the waste container where the settlements would decrease with increasing overburden pressure (Fig. 4.17).

From the figures presented, the overburden pressure effect on the buffer compressibility is demonstrated. Increased overburden pressure causes increased settlements

Final settlement bulbs.

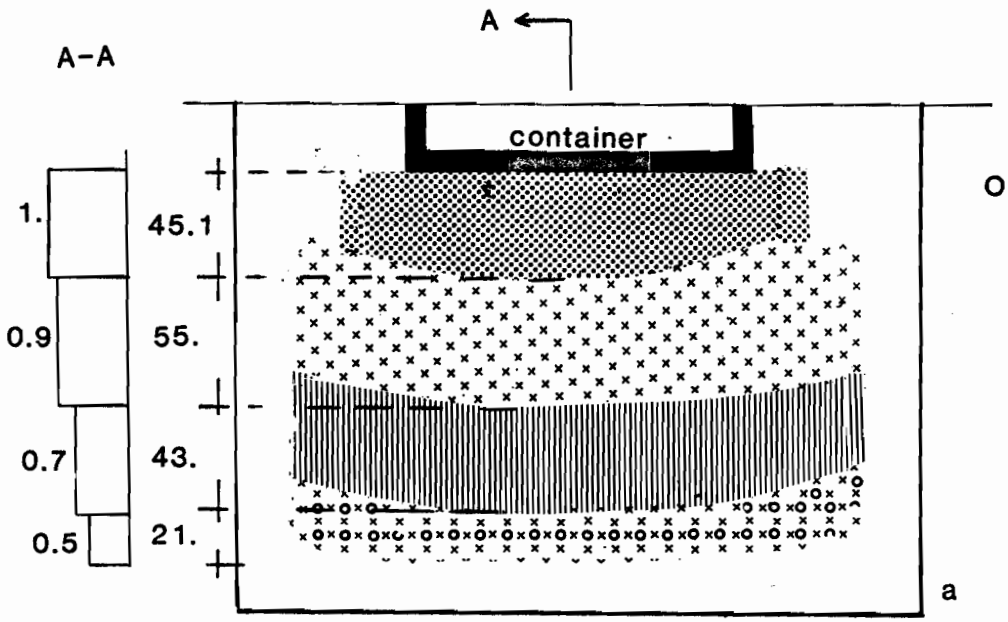

Overb. pr. : 0 kPa

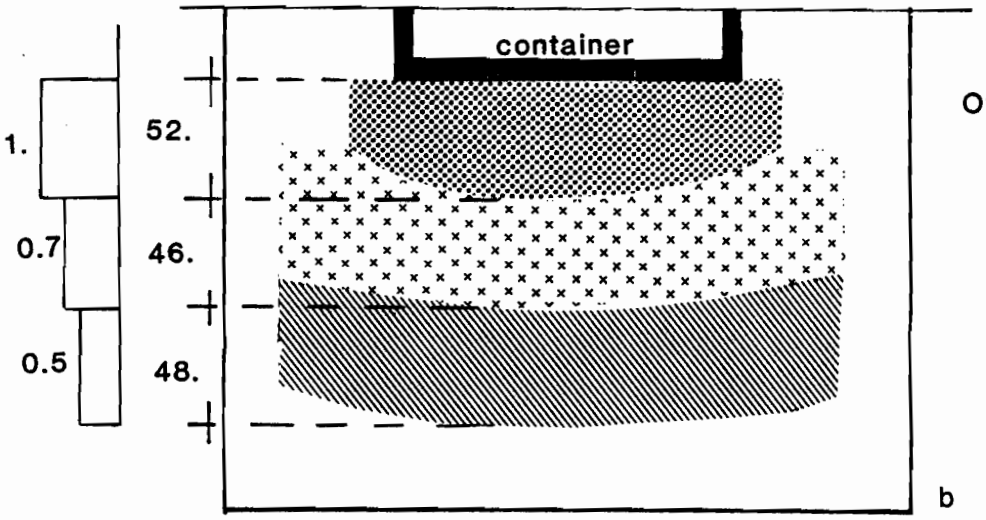

Overb. pr. : 36 kPa

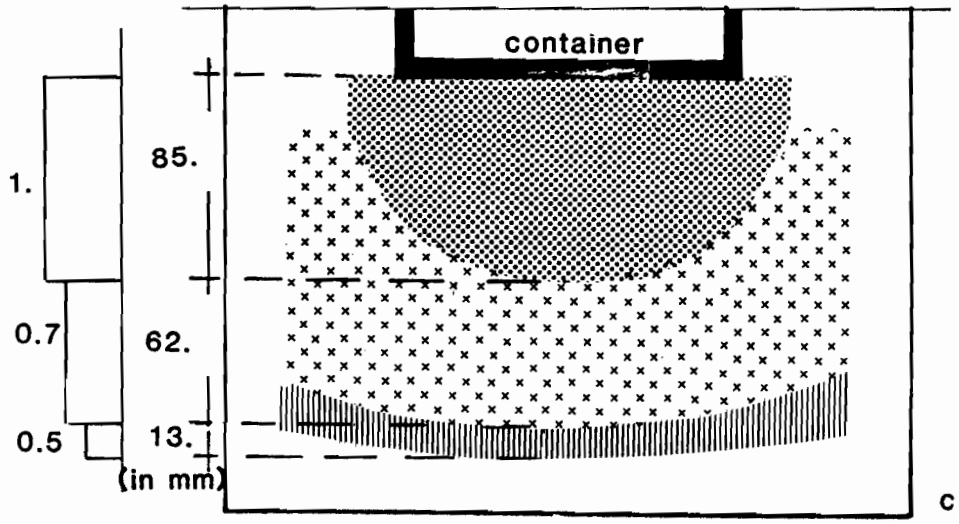

Overb. pr. : 120 kPa

Fig. 4.16

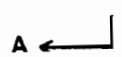

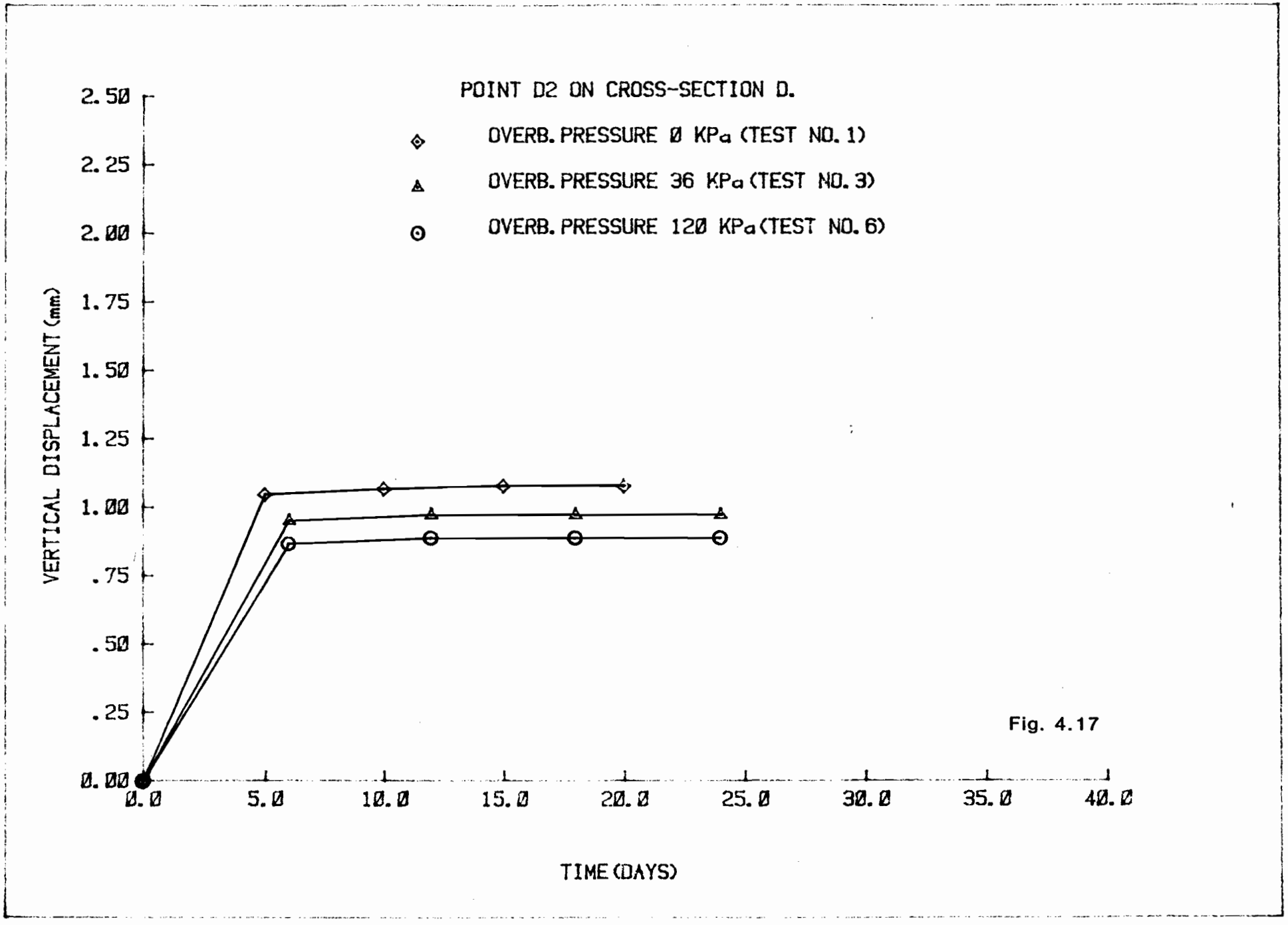
POINT D2 ON CROSS-SECTION D.
OVERB. PRESSURE Ø KPa (TEST NO. 1)
OVERB. PRESSURE 36 KPa (TEST NO. 3)
OVERB. PRESSURE 120 KPa (TEST NO. 6)
VERTICAL DISPLACEMENT (mm)
2.50
2.25
2.00
1.75
1.50
1.25
1.00
.75
.50
.25
0.00
0.0
5.0
10.0
15.0
20.0
25.0
30.0
35.0
40.0
TIME (DAYS)

Fig. 4.17

in the area underneath the waste container - a zone of depth equal to 50 mm - but for greater depths the increased confinement resulting from the high overburden pressure causes a "damped" settlement distribution pattern.

4.2.4 Friction Along the Interfaces

The areas of the disposal system where friction is developed are the rock-buffer interfaces and the contaier-buffer interfaces. In order to prevent any friction between the buffer and the waste container and between the buffer and the rock (concrete) semidylinder, the container and concrete surfaces which come in contact with the buffer were lubricated. But this did not eliminate the friction generated along the interfaces.

In order to obtain an estimate of the value of friction existing on the interfaces a simple test was performed. After the end of a 30 day period test, slices of buffer were kept in place in the disposal system and then pushed down by means of a calibrated hydraulic piston (Fig. 4.18). The loads necessary to induce sliding were recorded for slices of different thicknesses. The resulting stresses were considered as being the developed stresses at the moment that the friction between buffer and concrete was overcome. Any friction coefficient derived from using these stresses would correspond to a static friction coefficient μ. The results obtained are shown in Table 4.2.

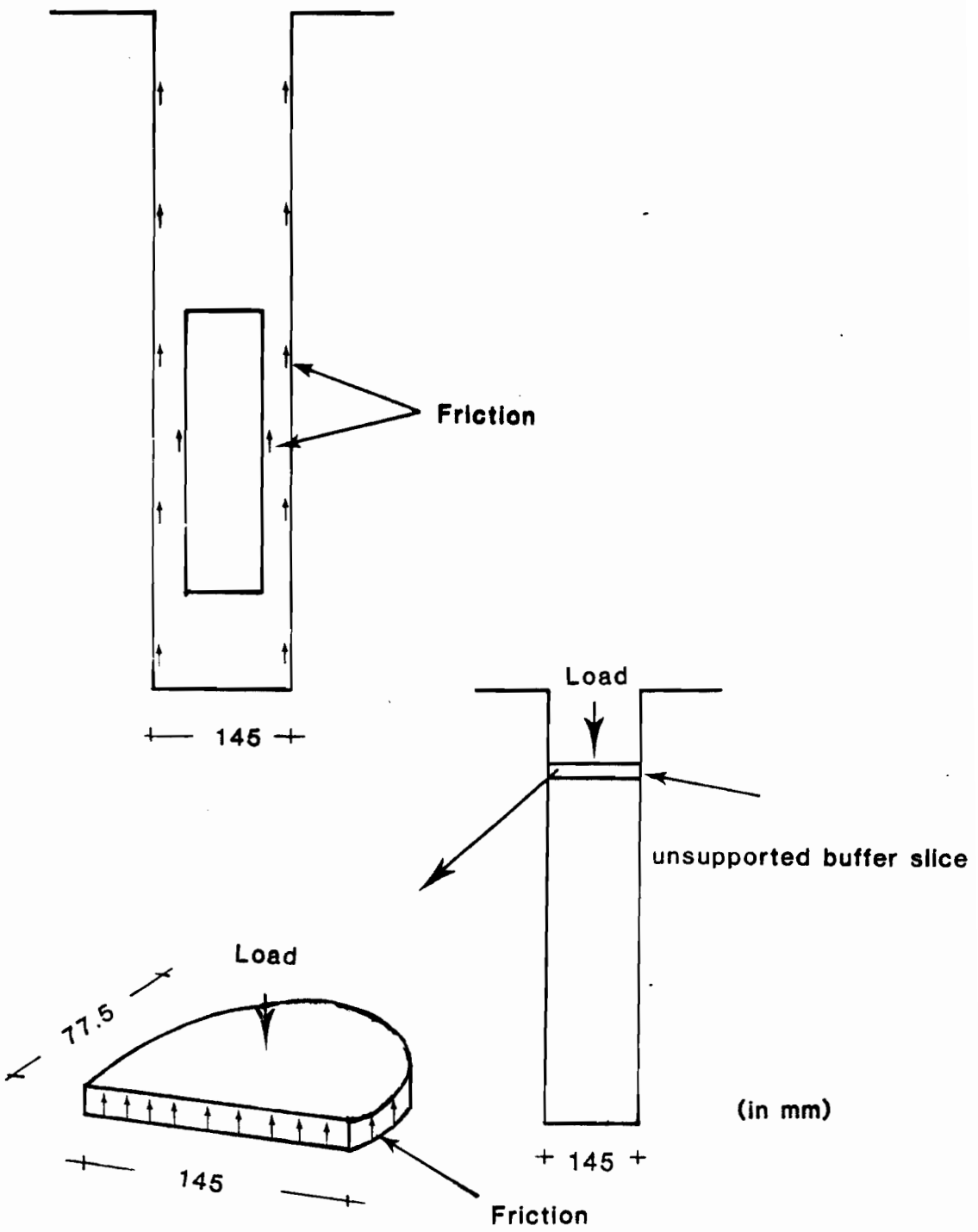
Friction
145
Load
unsupported buffer slice
Load
77.5
145
145
Friction
(in mm)

Fig. 4.18

TABLE 4.2

No.	Thickness (mm)	Normal Load (N_t)	τ (kPa)
1	25.4	91.00	9.00
2	38.1	142.40	9.5
3	40.0	147.00	9.20
4	23.8	45.00	7.80

Notes: 1. Slide No. 4 was tested without the plexiglass confinement. The stress, resulting from this test, compared with the other values obtained gives a rough estimate of the friction on the glass-buffer interface.

2. For the calculation of τ, the area used included the glass-buffer interface in addition to the concrete-buffer one, for slides No. 1, 2, 3. For slice No. 4 only the glass-buffer interface was taken into account.

3. The buffer self weight was included in the calculation of the stress τ.

4.3 Model Tests Under Water Intake Conditions

The major characteristic of these tests was that water intake was allowed under varying overburden pressure values. Water entry position was an additional variable in order to detect any possible zone of weakness in the buffer. For all tests, the buffer was allowed to creep and then water was allowed to flow in. In order to investigate the effect of the initial creep on the buffer response,

one test was performed where water intake was allowed from the beginning of the test without previous creep under no water intake conditions.

The objectives of these tests were to obtain information for the prediction of the buffer behaviour prior to and after the tunnel backfilling, considering rock cracks and subsequent water intake from different entry positions and at different time periods under loading. The same mode of presentation used in the previous subseciton (4.2) will be followed.

4.3.1 Soil Particle Movements

The additional nodal displacement fields for the tests under water intake conditions and the nodal displacement field for the test where no initial creep is allowed, are shown in Fig. 4.19, 4.20, 4.21 and 4.22. Reference Fig. 4.23 is used again for the proper presentation of the test results. In order to investigate the overburden pressure effect under water intake conditions, the results from three tests were compared. In these tests (Test No. 2, No. 4, and No. 7), water intake was allowed from the bottom of the disposal system with 105 kPa of back pressure, after the buffer was allowed to creep under no water intake conditions.

In Fig. 4.24 the nodal vertical displacement-time histories are shown for cross-section A-A. The node A2 suffers additional settlements for all three values of

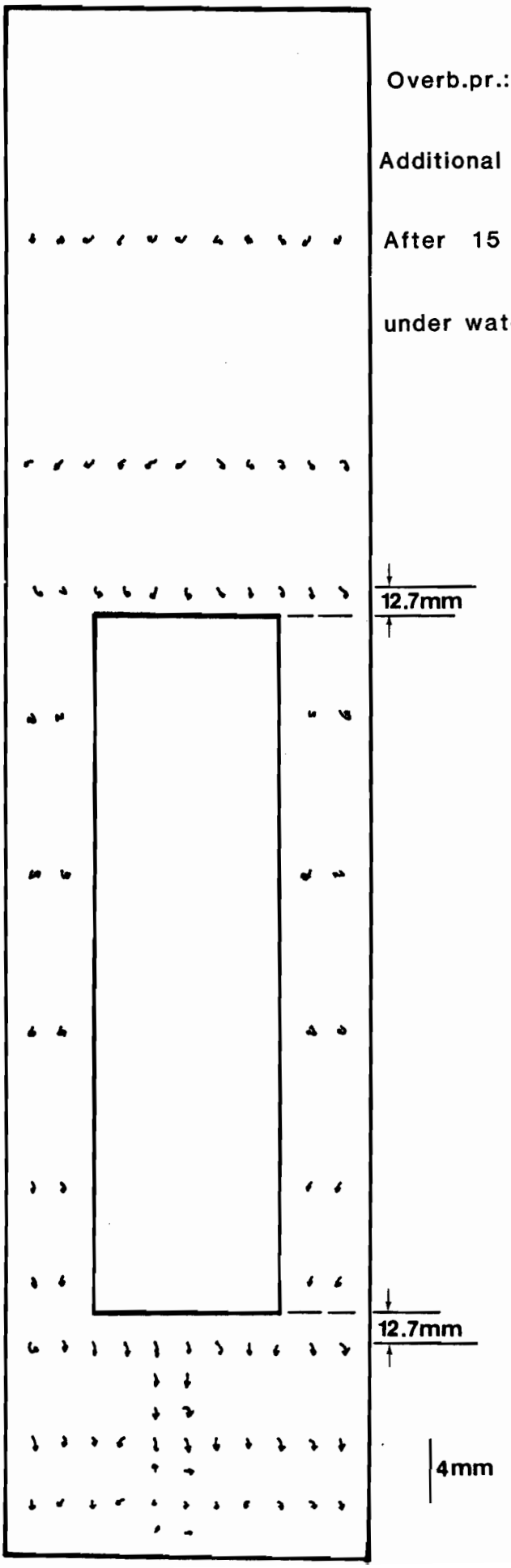
Overb.pr.: 0 kPa
Additional nodal displacement field
After 15 days
under water intake conditions
12.7mm
12.7mm
4mm

Fig. 4.19

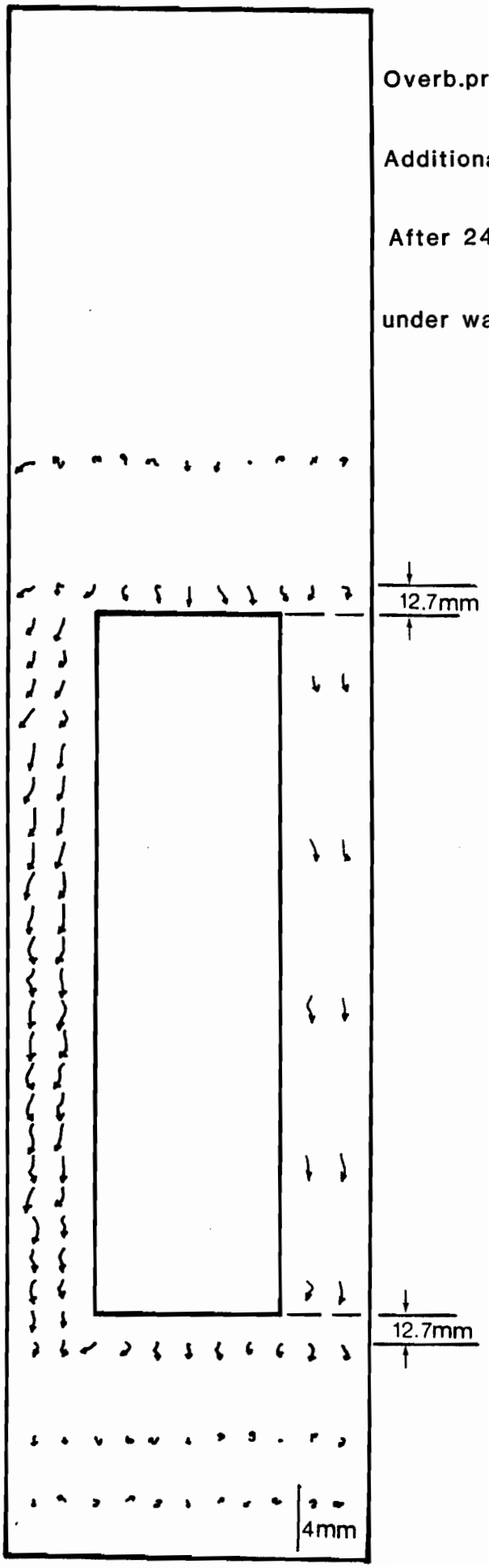
Overb.pr. 36 kPa
Additional nodal displacement fiel
After 24 days
under water intake conditions
12.7mm
12.7mm
4mm

Fig. 4.20

Overb.pr.: 120 kPa

Additional nodal displacement fiel

After 24 days

under water intake conditions

Fig. 4.21

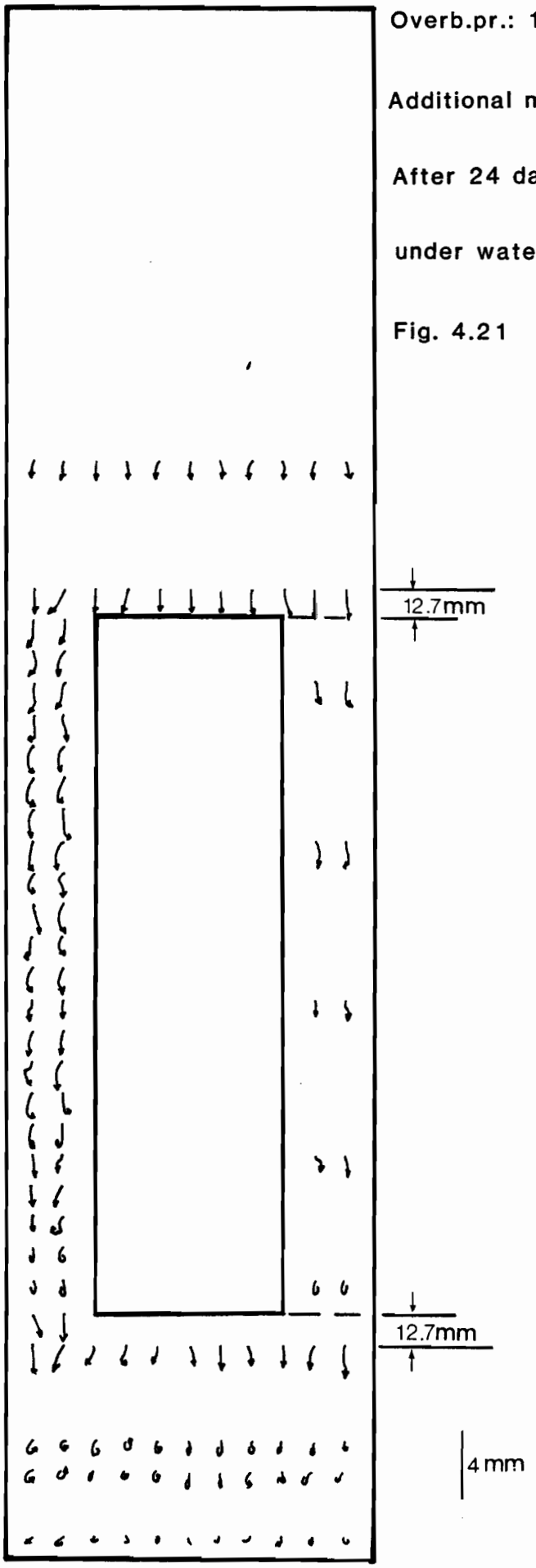

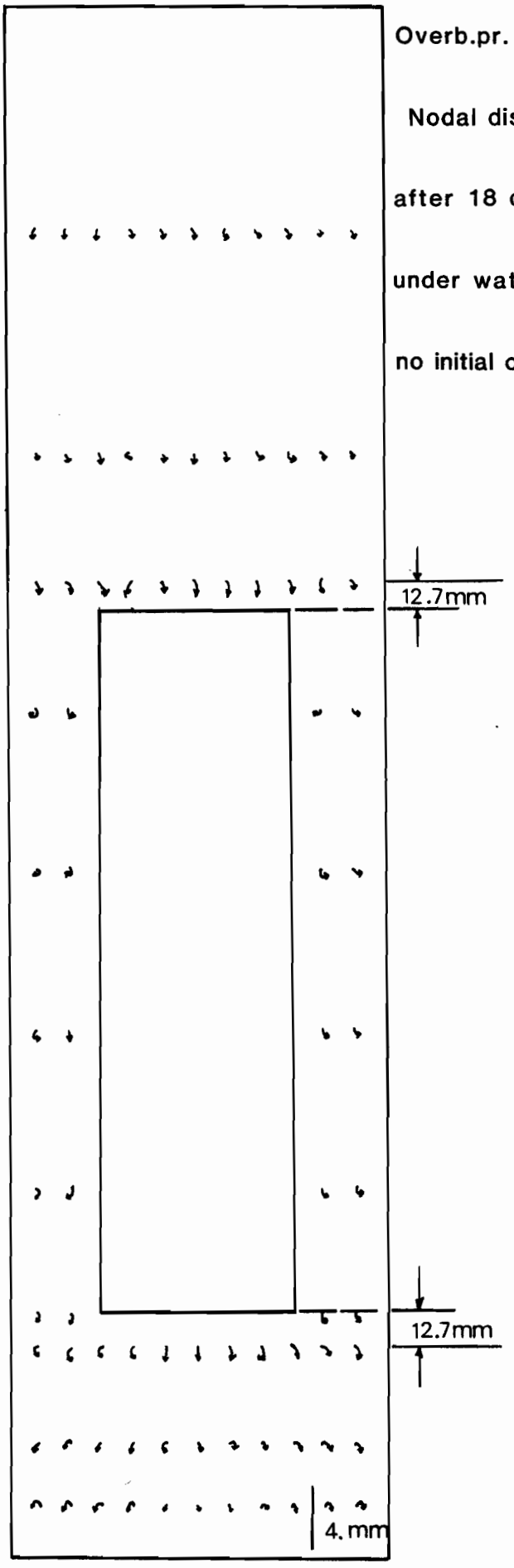
Overb.pr. : 36 kPa
Nodal displacement field
after 18 days
under water intake conditions
no initial creep
12.7mm
12.7mm
4.mm

Fig. 4.22

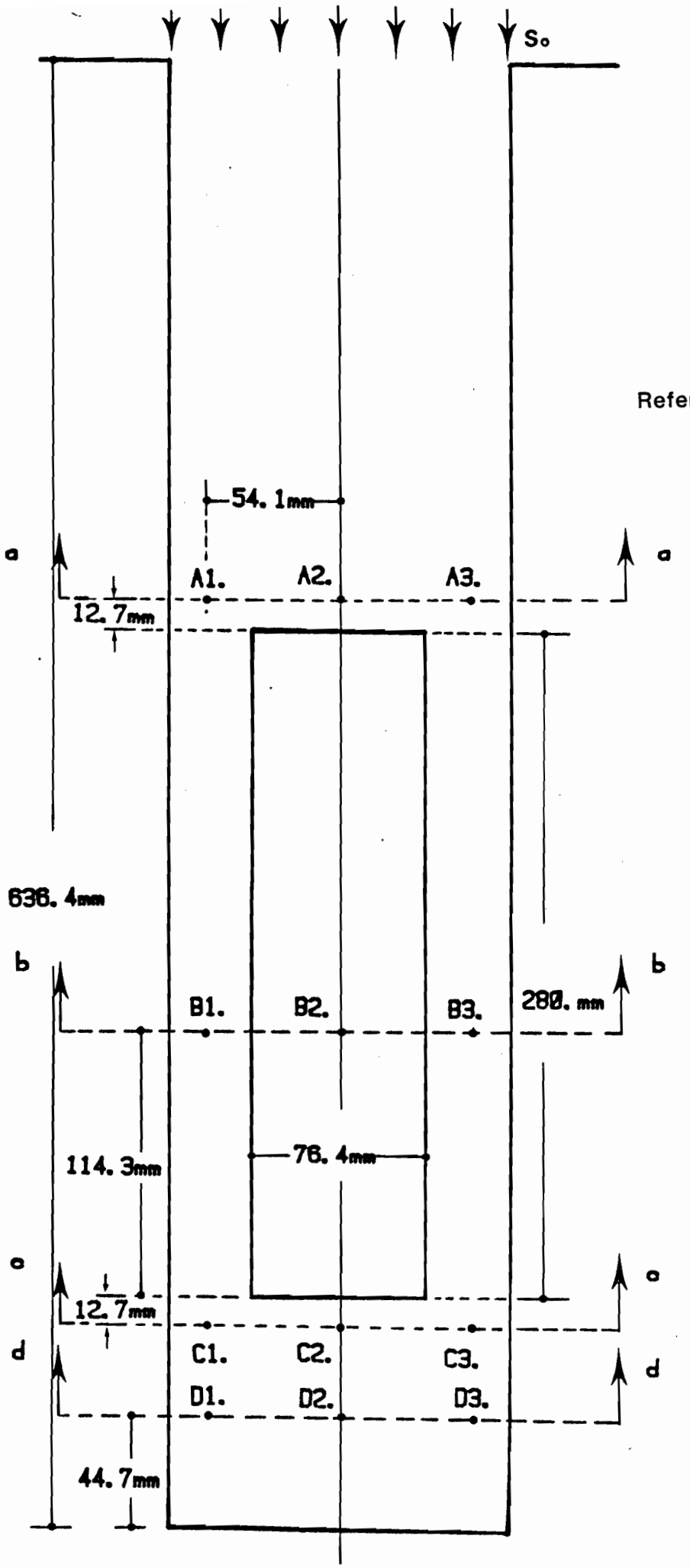

Reference figure

Fig. 4.23

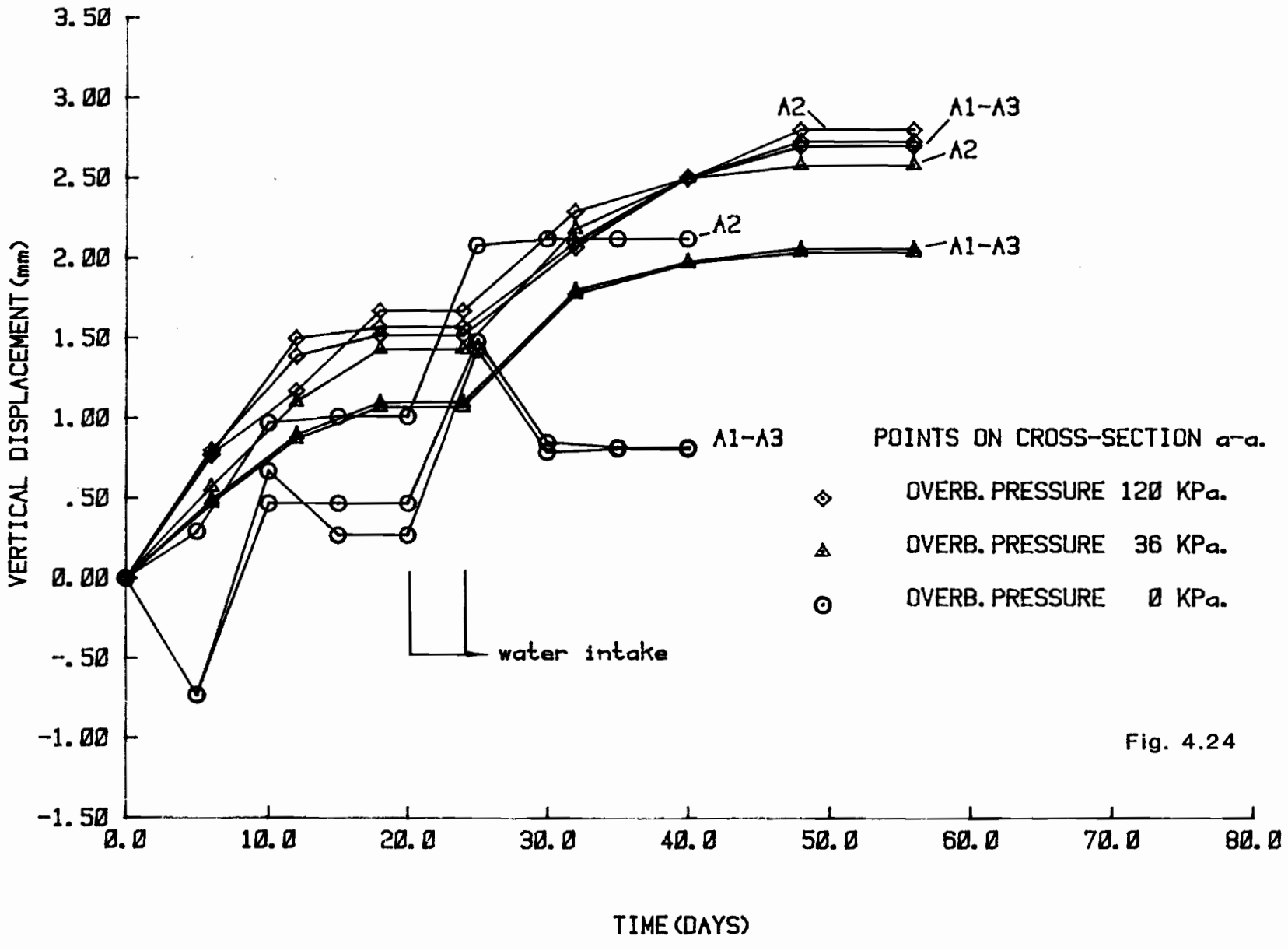
3.50
3.00
2.50
2.00
1.50
1.00
.50
0.00
-.50
-1.00
-1.50
VERTICAL DISPLACEMENT (mm)
0.0
10.0
20.0
30.0
40.0
50.0
60.0
70.0
80.0
TIME (DAYS)
A2
A1-A3
A2
A2
A1-A3
A1-A3
water intake
POINTS ON CROSS-SECTION a-a.
OVERB. PRESSURE 120 KPa.
OVERB. PRESSURE 36 KPa.
OVERB. PRESSURE 0 KPa.

Fig. 4.24

overburden pressure. When the overburden pressure is 0 kPa, the final total settlement was 2.12 mm translating to an additional settlement of 1.11 mm. When the overburden pressure was increased to 36 kPa, total settlement for the same point was 2.58 mm (additional settlement of 1.15 mm) and when the overburden pressure was 120 kPa, the total settlement was 2.8 mm (additional settlement of 1.13 mm). The additional settlements are approximately equal in size for the three cases of overburden pressure. But as a percentage of the final total additional settlements were 52% when the pressure was 0 kPa, 45% when the pressure was 36 kPa and 40% when the pressure was 120 kPa. This increase in settlement, which is almost independent of the overburden pressure, reflects the change in the buffer compressibility characteristics due to water intake conditions.

The other nodes on the same cross-section (Fig. 4.24) seem to follow the sample displacement patterns, especially when the overburden pressure was 36 kPa and 120 kPa. When the overburden pressure was 36 kPa for nodes A1 and A3, total settlement was 2.06 mm (additional settlement was 0.96 mm, or 47% of the total settlement). When the pressure was 120 kPa the total settlement was 2.73 mm (additional settlement was 1.16 mm or 42% of the total settlement). For the case of 0 kPa overburden pressure, initial additional settlement was observed equal to 1.16 mm after 5 days of water intake. It was then followed by an upward movement that resulted in a final total settlement of 0.81 mm

(additional settlement was 0.54 mm or 67% of the total).

These upward displacements were also observed for nodes around the waste container (Fig. 4.25) resulting from the interaction between the swelling characteristics of the buffer and the container weight. Where the container weight effect prevails, increased settlements were observed, and this mainly occurred in a zone underneath the waste container to a depth of 40 mm. Otherwise, the swelling characteristics of the buffer resulted in an upward displacement pattern that seems to prevail in areas of depth greater than 40 mm below the waste container and in some areas around the container. This interaction between swelling characteristics and container weight was observed for all three cases of overburden pressure. When the overburden pressure was increased to 36 kPa and 120 kPa, the additional settlement pattern was observed for the points above and around the container. Underneath the waste container (cross section C-C in Fig. 4.26) increased settlements were induced for all three cases of overburden pressure. When the overburden pressure was 0 kPa the additional displacement was higher. This can be attributed to the low confinement level experienced by the buffer. The buffer deformed symmetrically, especially for the high overburden pressure value. The lack of symmetry in deformation, often observed when the pressure was 0 kPa, was due to the buffer heterogeneity that resulted from the compaction and placement technique. The overburden pressure experienced by the buffer,

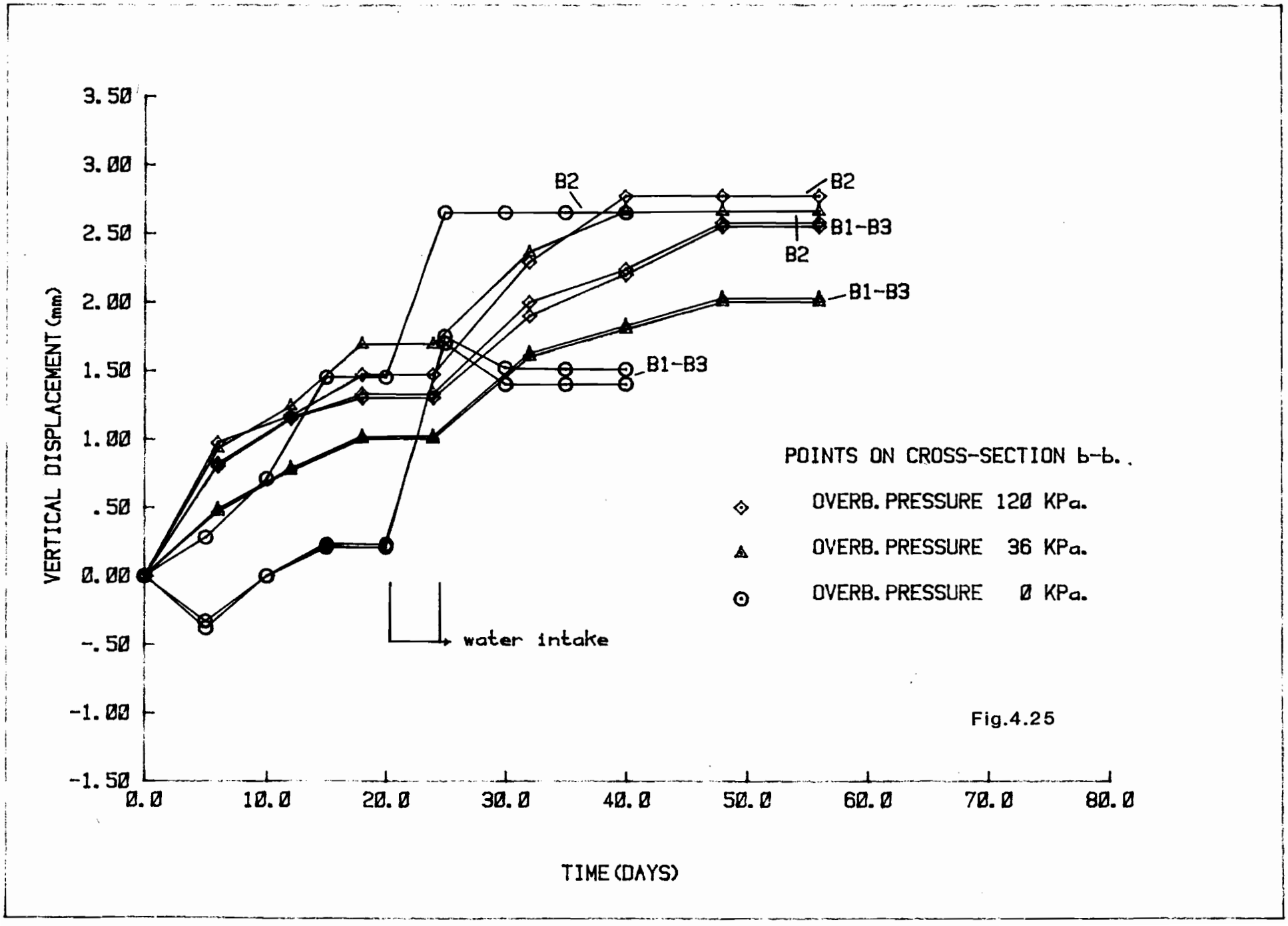
3.50
3.00
2.50
2.00
1.50
1.00
.50
0.00
-.50
-1.00
-1.50
VERTICAL DISPLACEMENT (mm)
0.0
10.0
20.0
30.0
40.0
50.0
60.0
70.0
80.0
TIME (DAYS)
B2
B2
B1-B3
B2
B1-B3
B1-B3
water intake
POINTS ON CROSS-SECTION b-b.
OVERB. PRESSURE 120 KPa.
OVERB. PRESSURE 36 KPa.
OVERB. PRESSURE 0 KPa.

Fig.4.25

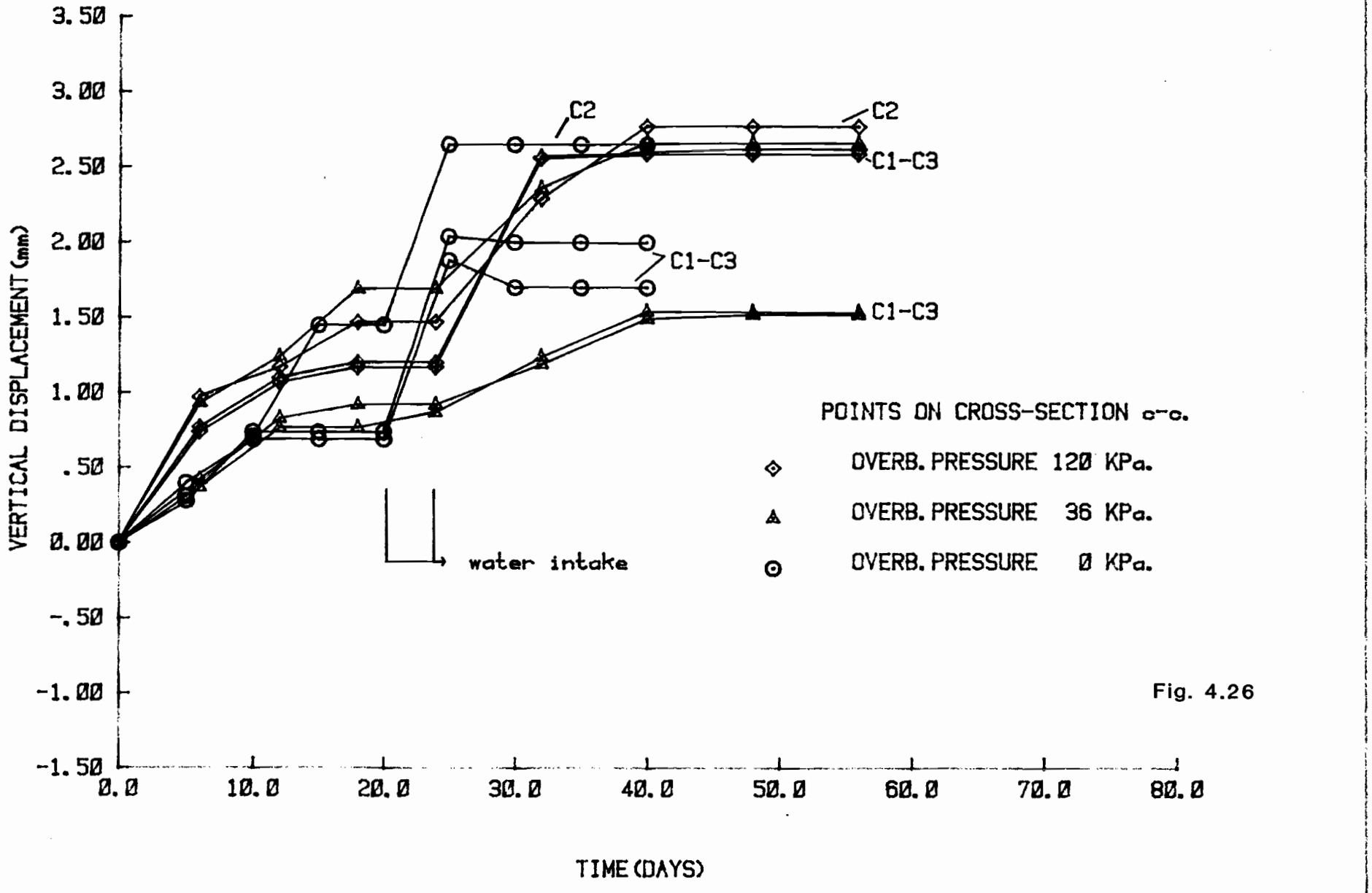
3.50
3.00
2.50
2.00
1.50
1.00
.50
0.00
-.50
-1.00
-1.50
VERTICAL DISPLACEMENT (mm)
0.0
10.0
20.0
30.0
40.0
50.0
60.0
70.0
80.0
TIME (DAYS)
C2
C2
C1-C3
C1-C3
C1-C3
water intake
POINTS ON CROSS-SECTION c-c.
OVERB. PRESSURE 120 KPa.
OVERB. PRESSURE 36 KPa.
OVERB. PRESSURE 0 KPa.

Fig. 4.26

resulted in an increased overall confinement thus improving the homogeneity of the buffer material. For higher depths below the waste container (Fig. 4.27), additional settlements were once again recorded. Especially when the overburden pressure was 0 kPa these additional settlements were higher than those for the other two overburden pressure values. An explanation for this could be that, due to the lack of overburden pressure, the resultant between the produced swelling and the container weight causes the soil displacement away from the area below the container and towards the areas around it, thus resulting in even higher additional settlements. The overburden pressure increases the confinement in this area, preventing upward soil displacement and additional settlement. In other words, it produces a more stable system below the container.

4.3.2 Compressibility of Buffer

The effect of the water intake on the compressibility characteristics of the buffer was also investigated. The pattern of presentation adopted in subsection 4.2.3 is followed. From Figs. 4.28, 4.29 and 4.30 the comments derived on the compressibility characteristics of the buffer are partly identical to those derived under no water intake conditions. The induced settlements were higher for increased overburden pressure, due to the increased stress level on the buffer material. But the most important characteristic shown using the settlement contours is the high swelling

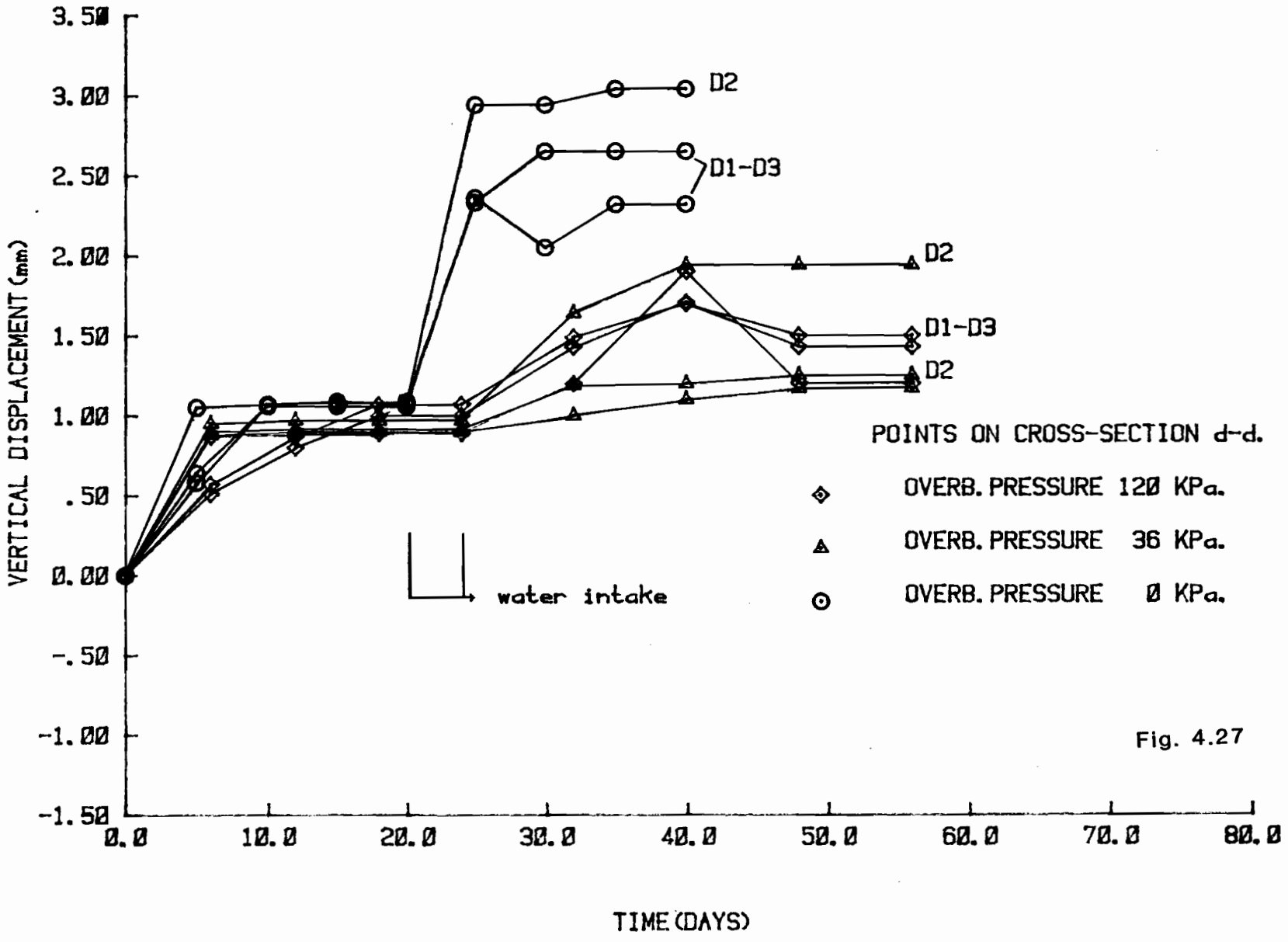
3.50
3.00
2.50
2.00
1.50
1.00
.50
0.00
-.50
-1.00
-1.50
VERTICAL DISPLACEMENT (mm)
0.0
10.0
20.0
30.0
40.0
50.0
60.0
70.0
80.0
TIME (DAYS)
D2
D1-D3
D2
D1-D3
D2
water intake
POINTS ON CROSS-SECTION d-d.
OVERB. PRESSURE 120 KPa.
OVERB. PRESSURE 36 KPa.
OVERB. PRESSURE 0 KPa.

Fig. 4.27

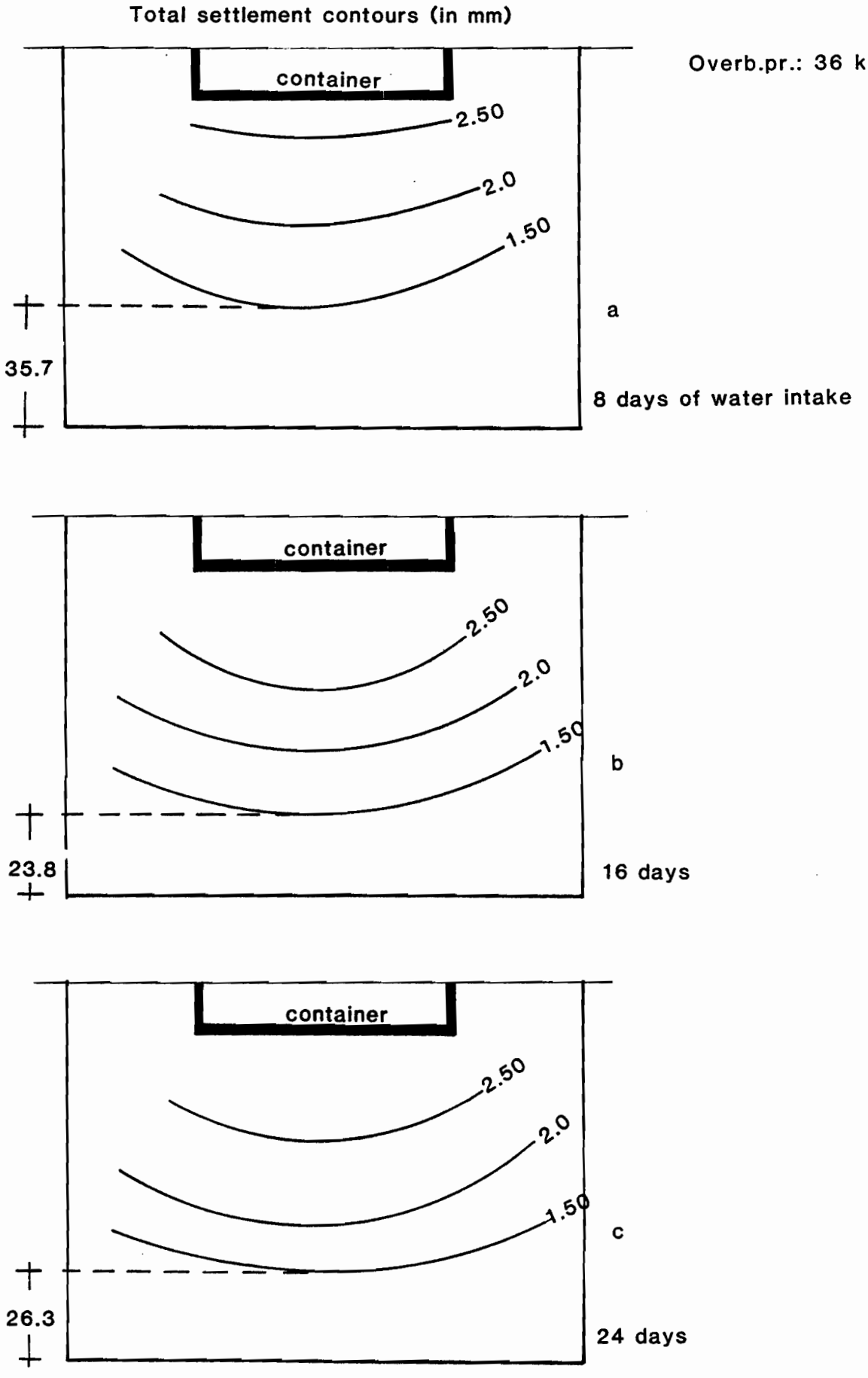
Total settlement contours (in mm)
Overb.pr.: 36 kPa
container
2.50
2.0
1.50
a
35.7
8 days of water intake
container
2.50
2.0
1.50
b
23.8
16 days
container
2.50
2.0
1.50
c
26.3
24 days

Fig. 4.28

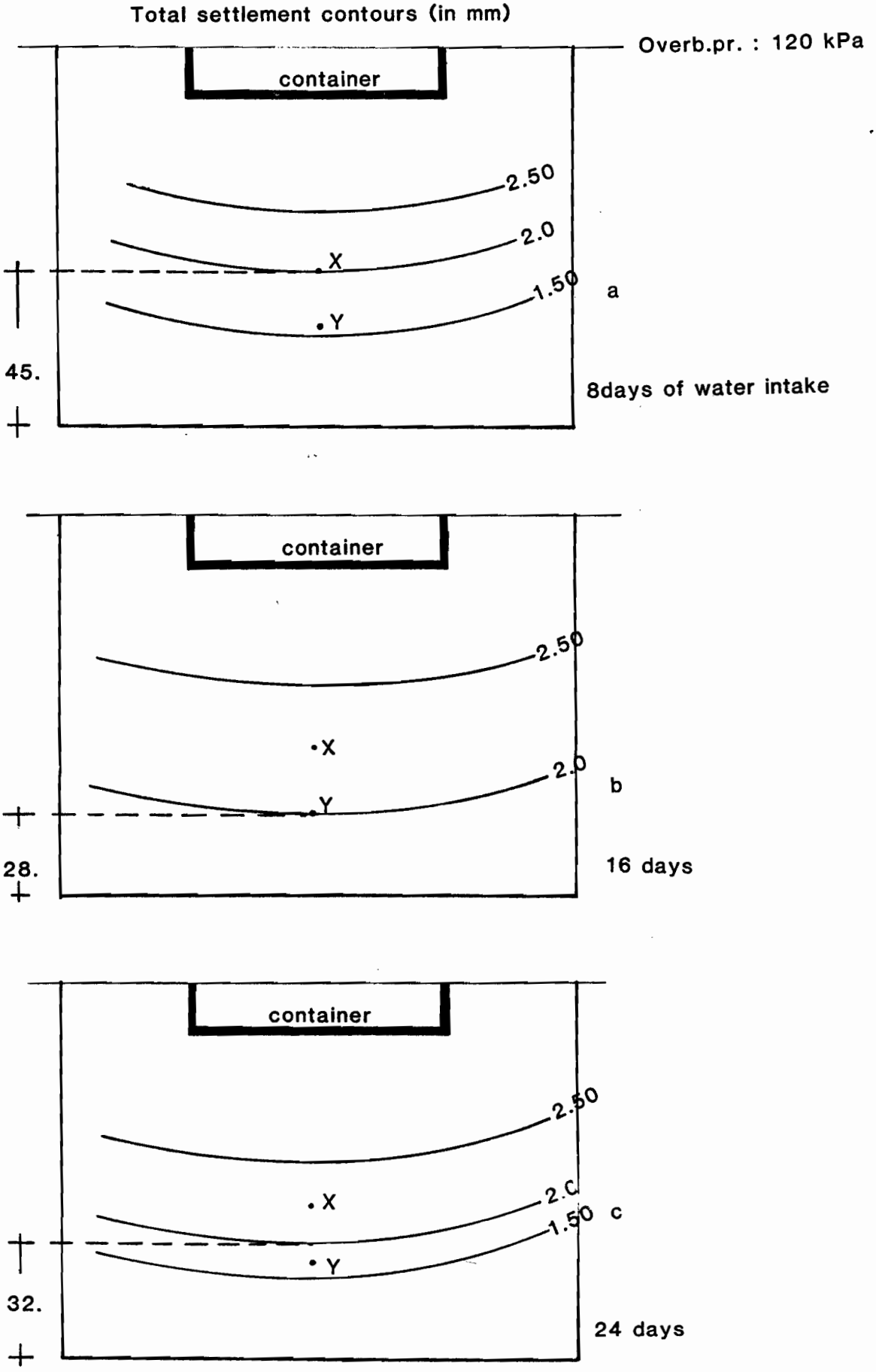
Total settlement contours (in mm)
Overb.pr. : 120 kPa
container
2.50
2.0
1.50
X
Y
a
45.
8days of water intake
container
2.50
2.0
X
Y
b
28.
16 days
container
2.50
2.0
1.50
X
Y
c
32.
24 days

Fig. 4.29

Total settlement contours (in mm)

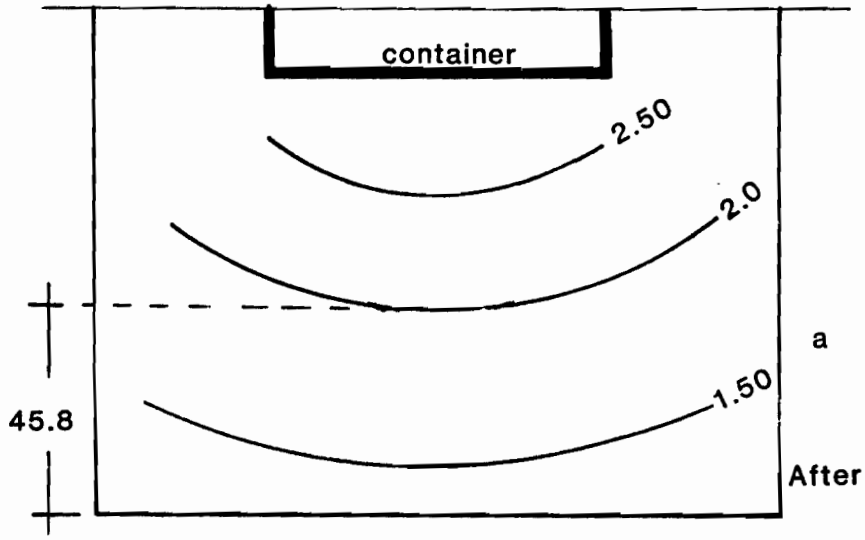

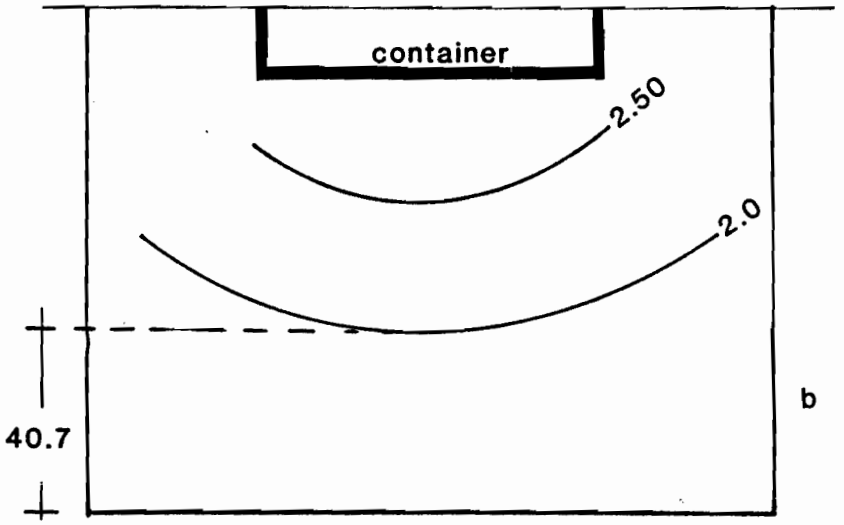

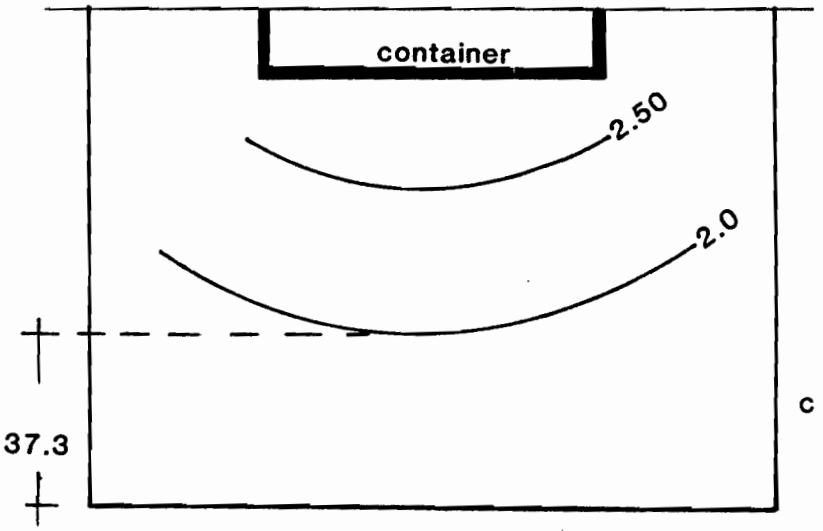

Fig. 4.30

potential of the buffer that was already demonstrated in the free swell tests performed at GRC. Even for the high overburden pressure value of 120 kPa, soil swelling was observed after the first 16 to 24 days with water intake conditions. This is indicated from the relative displacement of the settlement contours. In Fig. 4.28 the "1.50 mm" contour is displaced upwards for 2.5 mm. The same displacement movement pattern is shown in Fig. 4.29. For instance point x (Fig. 4.29) would reach a settlement equal to 2.00 mm after 8 days under water intake conditions and 2.30 mm after 16 days under the same conditions which was in fact, the final displacement value for this point. Point y (Fig. 4.29) would reach a settlement equal to 1.60 mm after the first 8 days under water intake conditions, 2.00 mm after 16 days under the same conditions, and 1.75 mm after 24 days which would be its final displacement value as well.

Although it is difficult to correlate directly the model test results with those obtained from the free swell and swelling pressure tests, the swelling potential of the buffer material, even under high load (conditions of high overburden pressure) is clearly indicated.

4.3.3 Effect of Initial Creep on Buffer Response

In order to investigate the effect of initial creep, under water intake conditions, on the response characteristics of the buffer, the displacement-time history of several

nodes, derived from the test where no initial creep was allowed, was superposed to the displacement-time history of the same nodes, when initial creep was allowed. In both tests overburden pressure was 36 kPa. The superposed figures are Fig. 4.31, 4.32, 4.33 and 4.34. The displacements which are compared are the additional settlements (right-hand part of the solid line plottings, after "water intake" label) which occurred when water intake was allowed after initial creep and the total displacements when water intake was allowed without previous creep of the buffer. From Figs. 4.31, 4.32, 4.33 and 4.34 it can be observed that the maximum displacement, under no initial creep conditions, was reached at shorter time periods (it was actually reached at 12-15 days). Whereas, for the test with initial creep allowed, the additional displacements reached their maximum values at 15-18 days. This difference is due to the compressibility characteristics of the buffer. The buffer, under conditions of no water intake, while experiencing the loading conditions imposed on it, becomes less compressible with time due to factors such as soil air-water redistribution because of the loads acting on the buffer three-phase system. It is interesting to note that under conditions of no water intake, the maximum displacements reached their highest values again in 12-15 days, demonstrating the initial creep effect on the buffer response. The different buffer response is also expected when observing Fig. 4.35, where the absorbed water-time

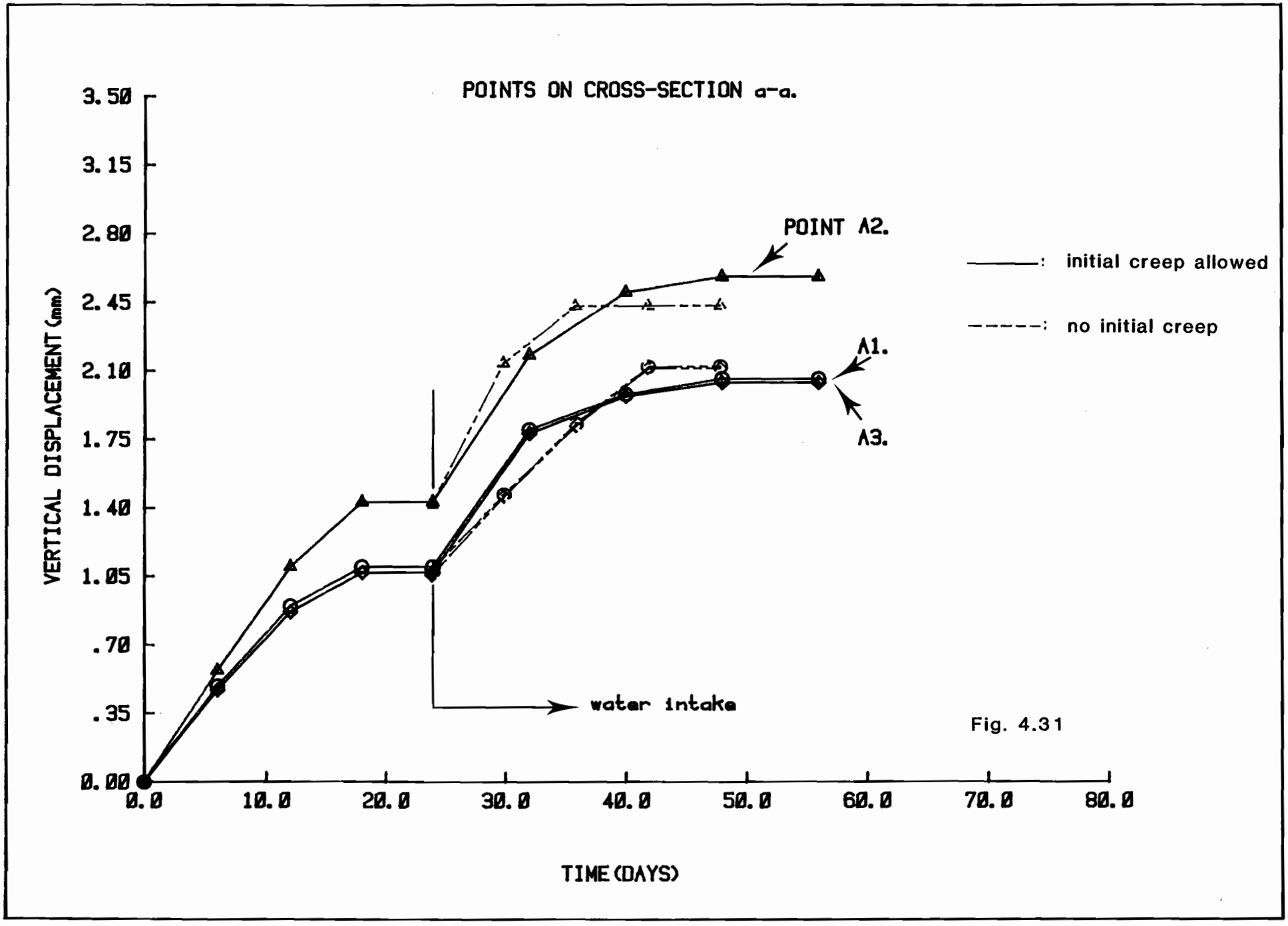
POINTS ON CROSS-SECTION a-a.
3.50
3.15
2.80
2.45
2.10
1.75
1.40
1.05
.70
.35
0.00
VERTICAL DISPLACEMENT (mm)
0.0
10.0
20.0
30.0
40.0
50.0
60.0
70.0
80.0
TIME (DAYS)
POINT A2.
A1.
A3.
water intake
: initial creep allowed
: no initial creep

Fig. 4.31

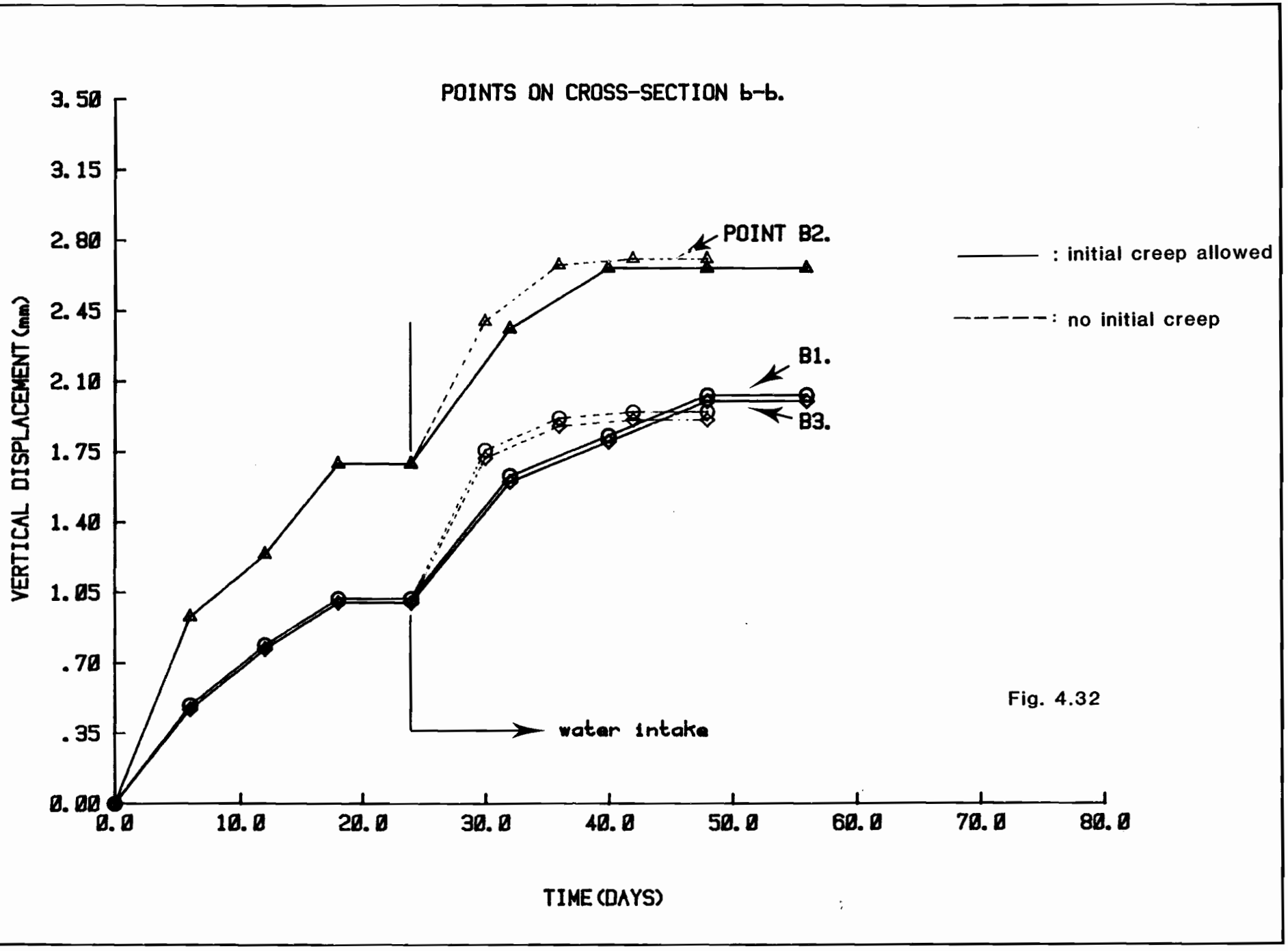
POINTS ON CROSS-SECTION b-b.
VERTICAL DISPLACEMENT (mm)
3.50
3.15
2.80
2.45
2.10
1.75
1.40
1.05
.70
.35
0.00
0.0
10.0
20.0
30.0
40.0
50.0
60.0
70.0
80.0
TIME (DAYS)
POINT B2.
B1.
B3.
water intake
: initial creep allowed
: no initial creep

Fig. 4.32

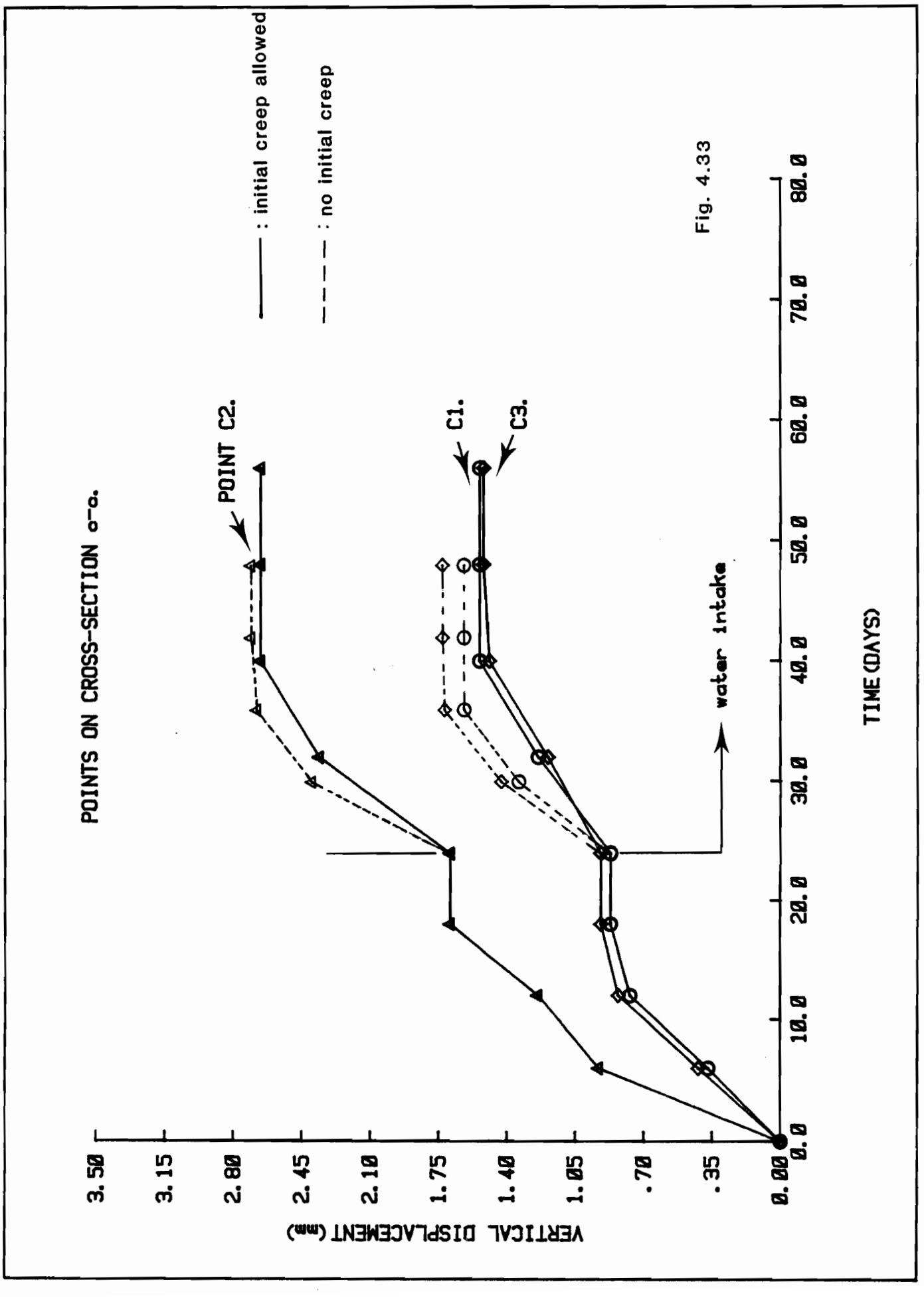
POINTS ON CROSS-SECTION a-a.
: initial creep allowed
: no initial creep
POINT C2.
C1.
C3.
water intake
VERTICAL DISPLACEMENT (mm)
TIME (DAYS)
0.00
.35
.70
1.05
1.40
1.75
2.10
2.45
2.80
3.15
3.50
0.0
10.0
20.0
30.0
40.0
50.0
60.0
70.0
80.0

Fig. 4.33

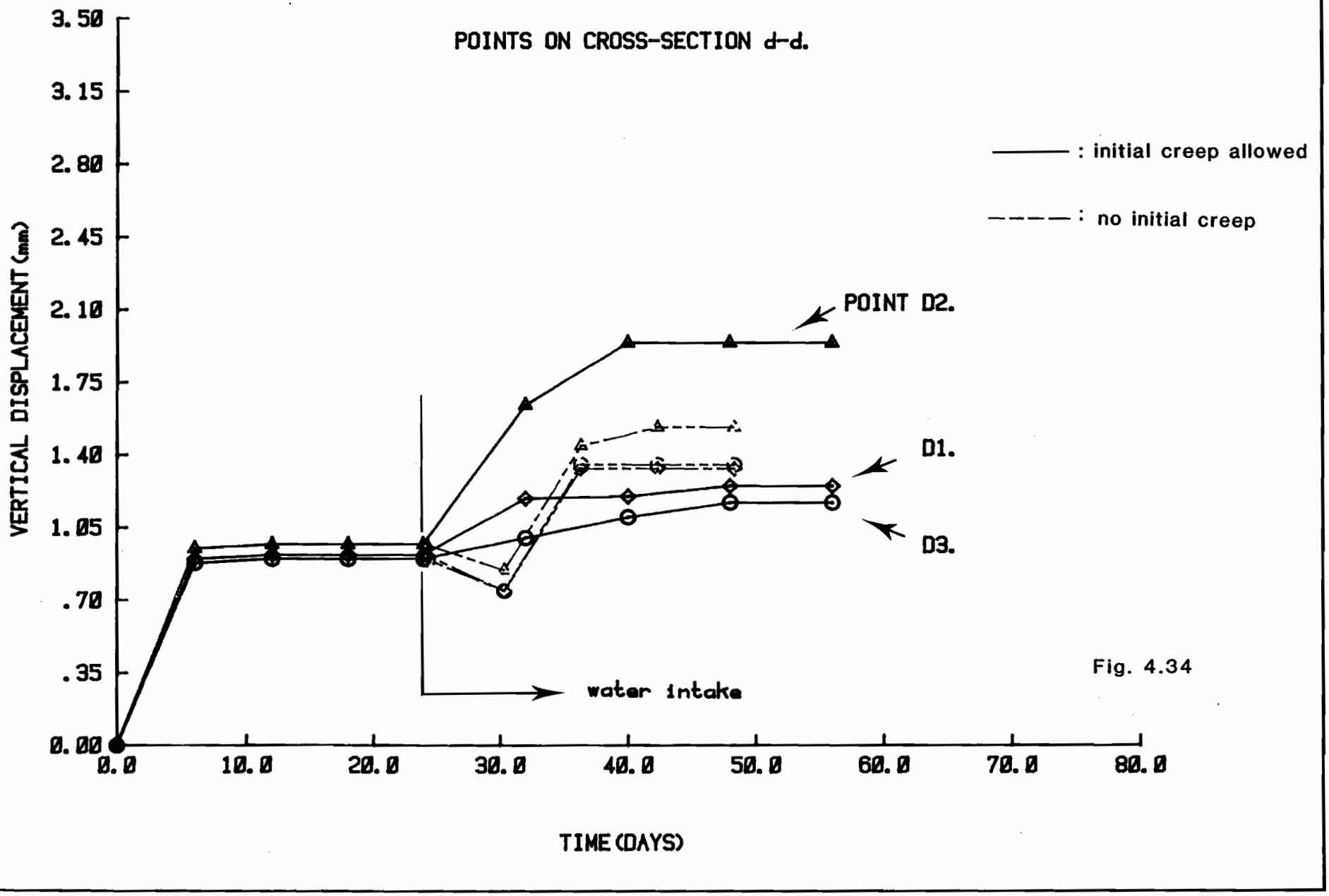
POINTS ON CROSS-SECTION d-d.
: initial creep allowed
: no initial creep
POINT D2.
D1.
D3.
water intake
VERTICAL DISPLACEMENT (mm)
TIME (DAYS)
3.50
3.15
2.80
2.45
2.10
1.75
1.40
1.05
.70
.35
0.00
0.0
10.0
20.0
30.0
40.0
50.0
60.0
70.0
80.0

Fig. 4.34

relationship is recorded for these two tests. More water is absorbed when no initial creep is allowed. Under no water intake conditions the buffer is compressed by the loads imposed on it, resulting in a decreased void space due to the air compressibility and soil water redistribution. The water is redistributed in the buffer, as shown in Fig. 4.36. When, later on, water is allowed to enter, the available void space is much smaller than the initially available one.

The maximum displacements obtained, with no initial creep, are approximately equal to the additional settlements that occur when initial creep is allowed, for almost all the areas. In Fig. 4.35, cross-section D-D, initial swelling is observed for the case of no initial creep. The resulting settlements are less or equal to the additional ones with initial creep. This resulting decreased settlement is due to the swelling occurring at the bottom area of the disposal system during water absorption. It seems reasonable to suggest that in order to predict the buffer response under variable conditions from the water intake point of view, two model tests can be performed: one under no water intake conditions and the other under water intake conditions without initial creep and these can be combined in order to take into account initial creep conditions followed by water intake conditions.

Any comment about the effect of initial creep on the buffer response under water intake conditions, must be

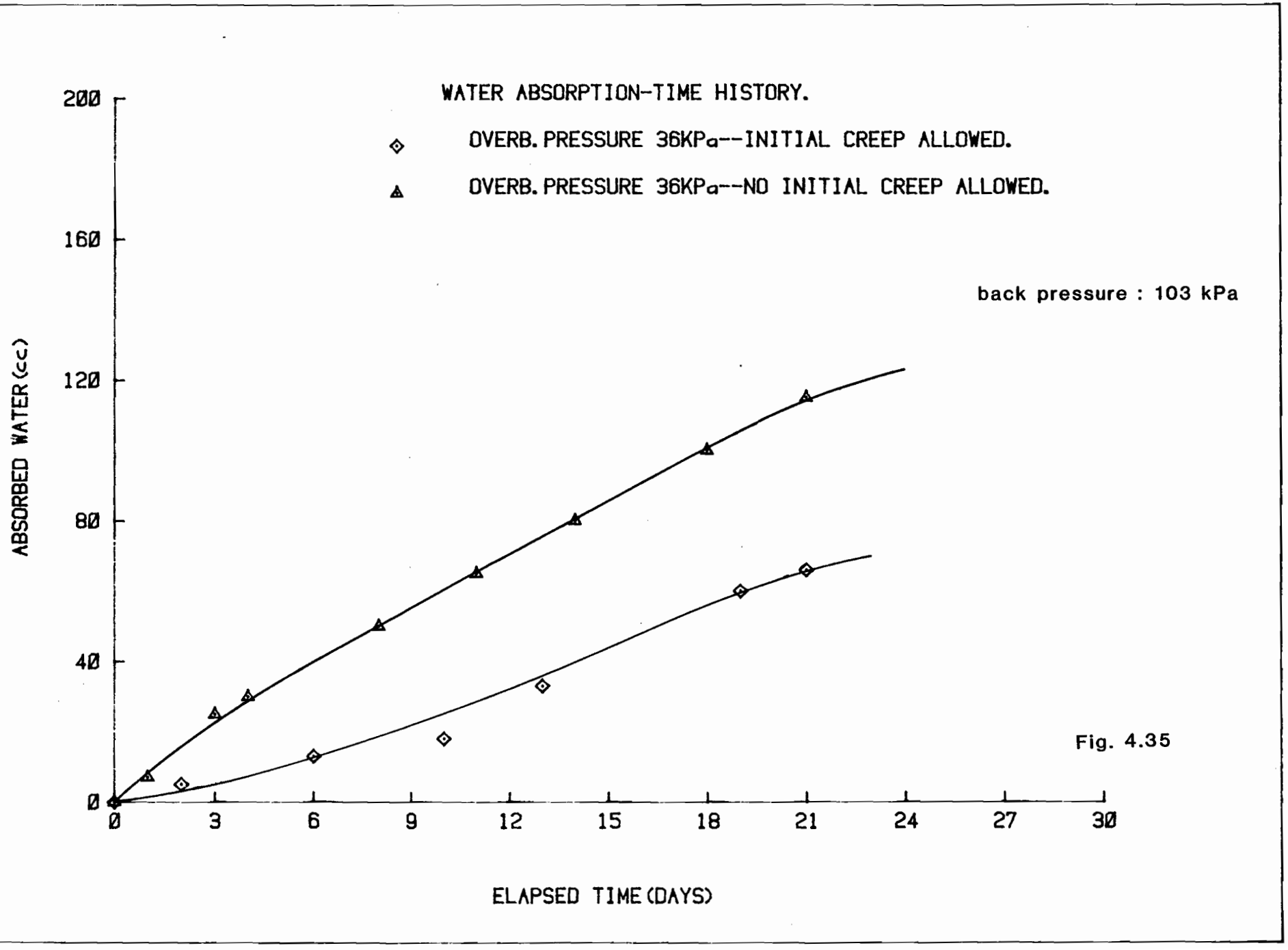
WATER ABSORPTION-TIME HISTORY.
OVERB. PRESSURE 36KPa--INITIAL CREEP ALLOWED.
OVERB. PRESSURE 36KPa--NO INITIAL CREEP ALLOWED.
back pressure : 103 kPa
ABSORBED WATER(cc)
200
160
120
80
40
0
0
3
6
9
12
15
18
21
24
27
30
ELAPSED TIME(DAYS)

Fig. 4.35

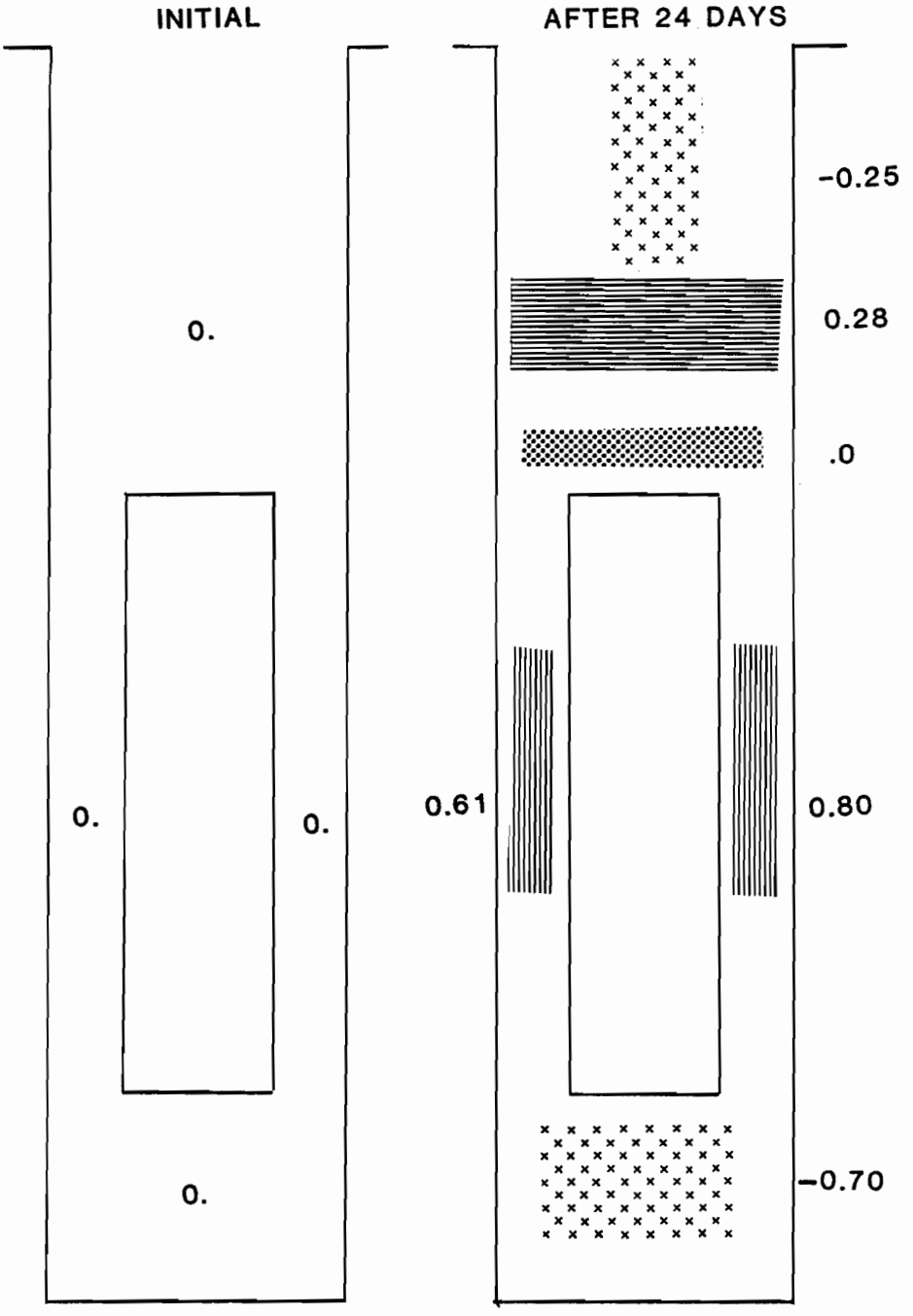

Changes in w.c. (in %) under no water intake conditions.

Fig. 4.36

the answer to one of the following questions:

1. How does the initial creep affect the unsaturated flow through a high swelling soil?
2. How are the boundary conditions that govern the flow characteristics affected by the initial creep?
3. What are the buffer characteristics which are affected by the initial creep?

Yong (1973) had suggested two types of flow in unsaturated soils with criteria being the swelling characteristics of the soil. Type 1 includes flow through non-swelling soils while Type 2 refers to flow through swelling soils under variable confinement conditions. Considering the buffer swelling properties, it is the second type of unsaturated flow that will be related to the specific case. The confinement condition pattern affects the buffer response under water intake conditions. Under initial creep conditions, the confinement is higher and the flow of fluid is confined. This results in a small volume change and increased swelling pressures, which in turn alter the flow characteristics. The confinement effect on the flow characteristics is generally shown through the wet front advance vs. $t^{1/2}$ relationship, which takes a non-linear geometrical shape under variable porosity conditions, and through wet front profile-time histories.

The initial creep causes, mainly in the zone underneath the waste container, an increase in the saturation

degree of the buffer due to the compressibility characteristics of the buffer and to soil fluid redistribution. An increased degree of saturation means decreased available void space and decreased soil suction values. The decrease in soil suction with increasing saturation is related to the physics of water absorption mechanisms. According to Yong (1973), the rate of decrease of the soil suction value is dependent on the degree of constraint applied against swelling, the osmotic potential, and other factors associated with the activity of the soil-water system which define the resulting rate of advance of the wet front.

Both conditions, decreased soil suction and decreased void space, result in a decreased time rate of wet front advance and a decreased absorbed water volume by the buffer. Initial creep increases the confinement of the buffer, restricts any additional volume change, increases the saturation degree in the zone underneath the waste container, decreases suction and results in reduced absorbed water volumes.

4.3.4 Effect of Water Intake Position on Buffer Response

In order to investigate the effect of the water intake position on the response characteristics of the buffer, two more tests were undertaken. The loading conditions included an overburden pressure equal to 120 kPa - simulating the backfilled tunnel conditions - and water intake was allowed from a point close to the top of the

disposal hole for the first test, while for the second one, water intake was allowed from a point at the back of the waste container. For the proper comparison of the test results for the time period examined, under different water intake positions, the displacement-time histories of several nodes are plotted. Reference Fig. 4.37 will be used again for the presentation of the results. The additional settlements indicated in cross-section A-A (Fig. 4.38), under water intake conditions, are (in percentage of the total settlement) 15% for the case of water intake from the back of the container, 32% when water intake is allowed from the top of the disposal hole, and 40% when water intake is allowed from the bottom of the disposal hole.

For cross-section B-B (Fig. 4.39), although additional settlement is indicated for the first 8 days with water intake from the container back, swelling reduces this additional settlement and the reduction (in percentage of the total) is 12%. Swelling was indicated after the first 10-14 days when 130 cc of water had already been absorbed. For the same cross-section B.B., when water intake is allowed from the top of the disposal hole, additional settlement is 31% of the total and 53% when water intake from the bottom of the disposal hole is allowed. While moving to cross-sections underneath the waste container bottom (Figs. 4.40, 4.41) the increasing effect of the water intake from the bottom of the disposal hole

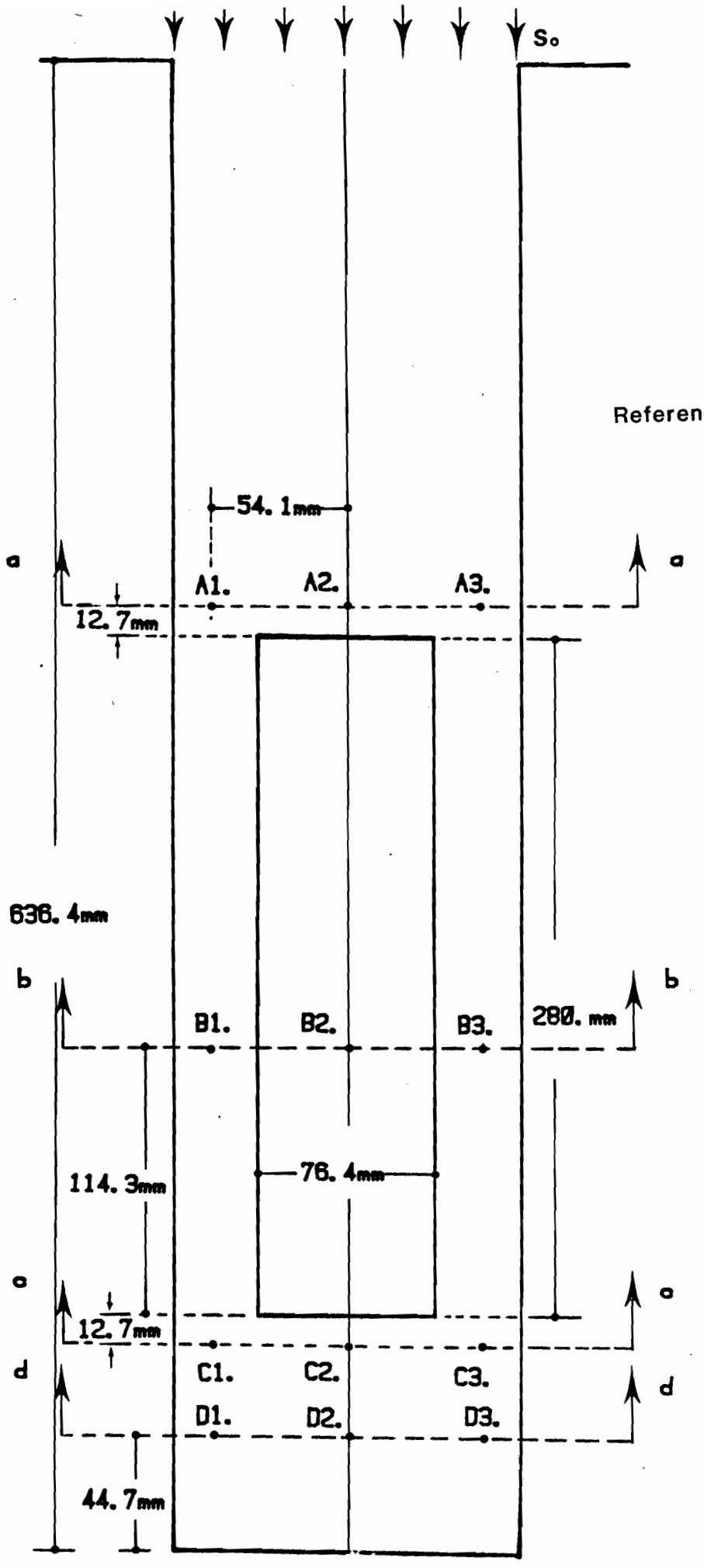
So
Reference figure
54. 1mm
a
a
A1.
A2.
A3.
12. 7mm
636. 4mm
b
b
B1.
B2.
B3.
280. mm
114. 3mm
76. 4mm
a
a
12. 7mm
d
C1.
C2.
C3.
d
D1.
D2.
D3.
44. 7mm

Fig. 4.37

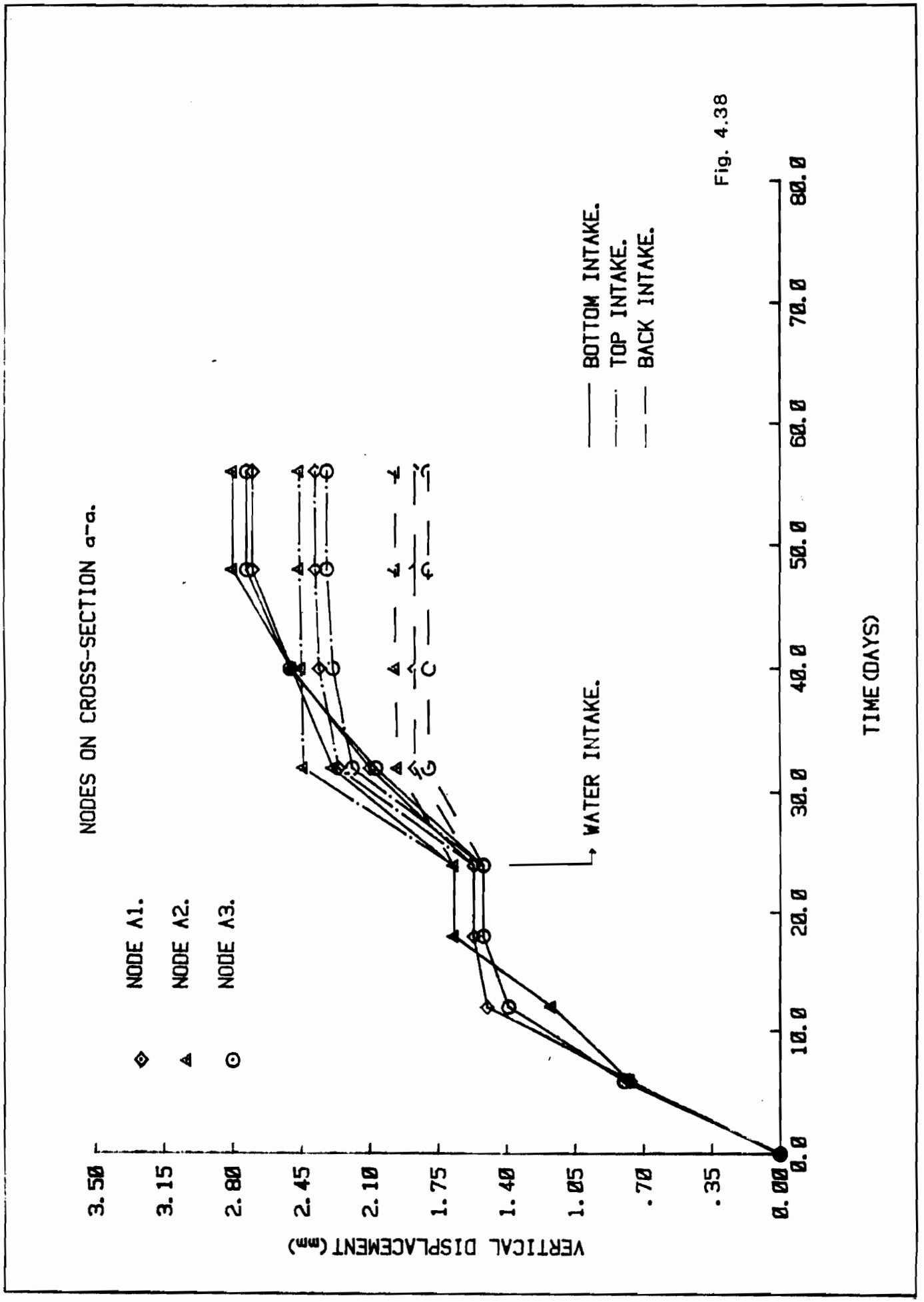
NODES ON CROSS-SECTION a-a.
NODE A1.
NODE A2.
NODE A3.
BOTTOM INTAKE.
TOP INTAKE.
BACK INTAKE.
WATER INTAKE.
VERTICAL DISPLACEMENT (mm)
TIME (DAYS)
3.50
3.15
2.80
2.45
2.10
1.75
1.40
1.05
.70
.35
0.00
0.0
10.0
20.0
30.0
40.0
50.0
60.0
70.0
80.0

Fig. 4.38

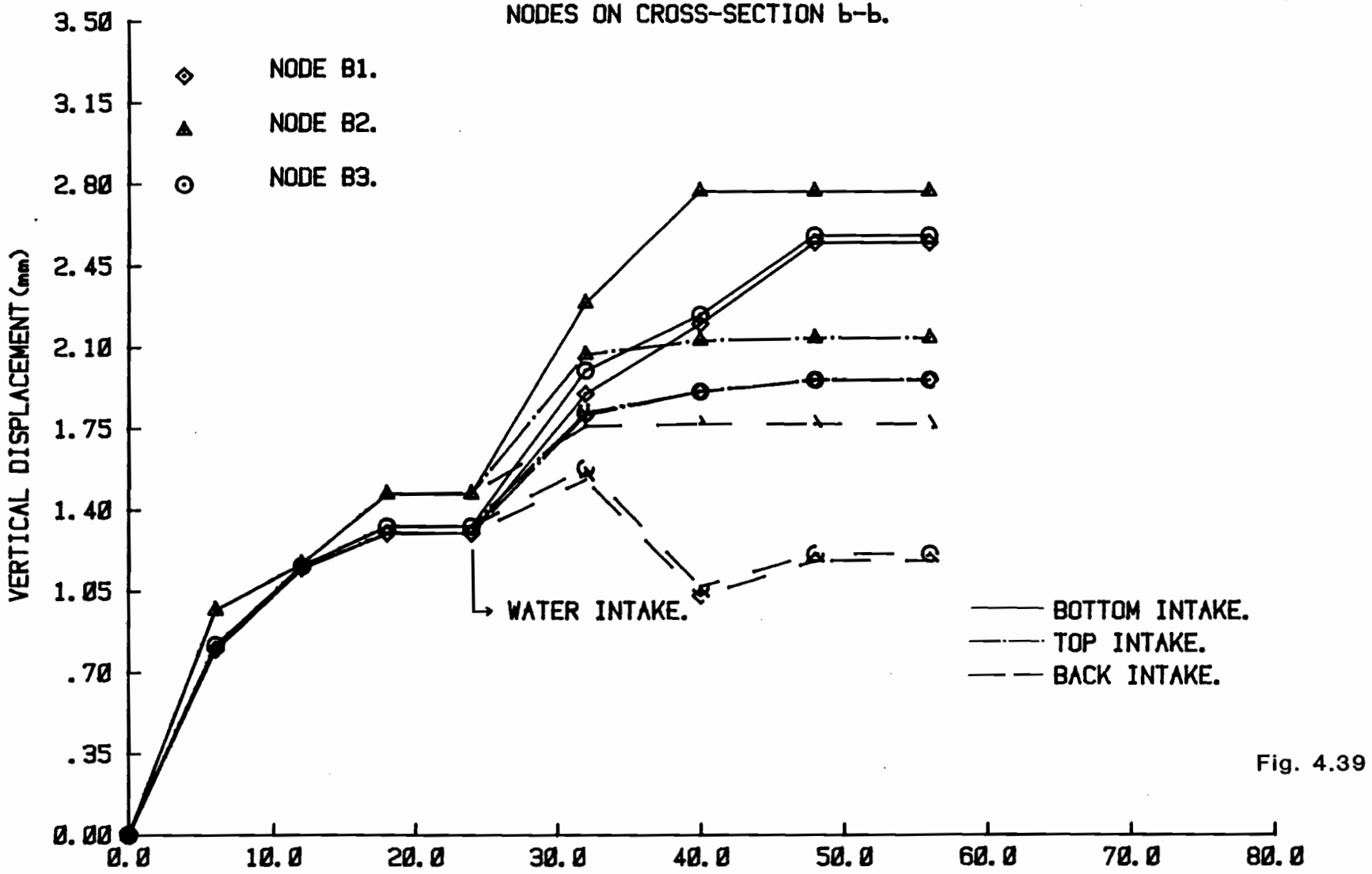
NODES ON CROSS-SECTION b-b.
NODE B1.
NODE B2.
NODE B3.
VERTICAL DISPLACEMENT (mm)
3.50
3.15
2.80
2.45
2.10
1.75
1.40
1.05
.70
.35
0.00
0.0
10.0
20.0
30.0
40.0
50.0
60.0
70.0
80.0
TIME (DAYS)
WATER INTAKE.
BOTTOM INTAKE.
TOP INTAKE.
BACK INTAKE.

Fig. 4.39

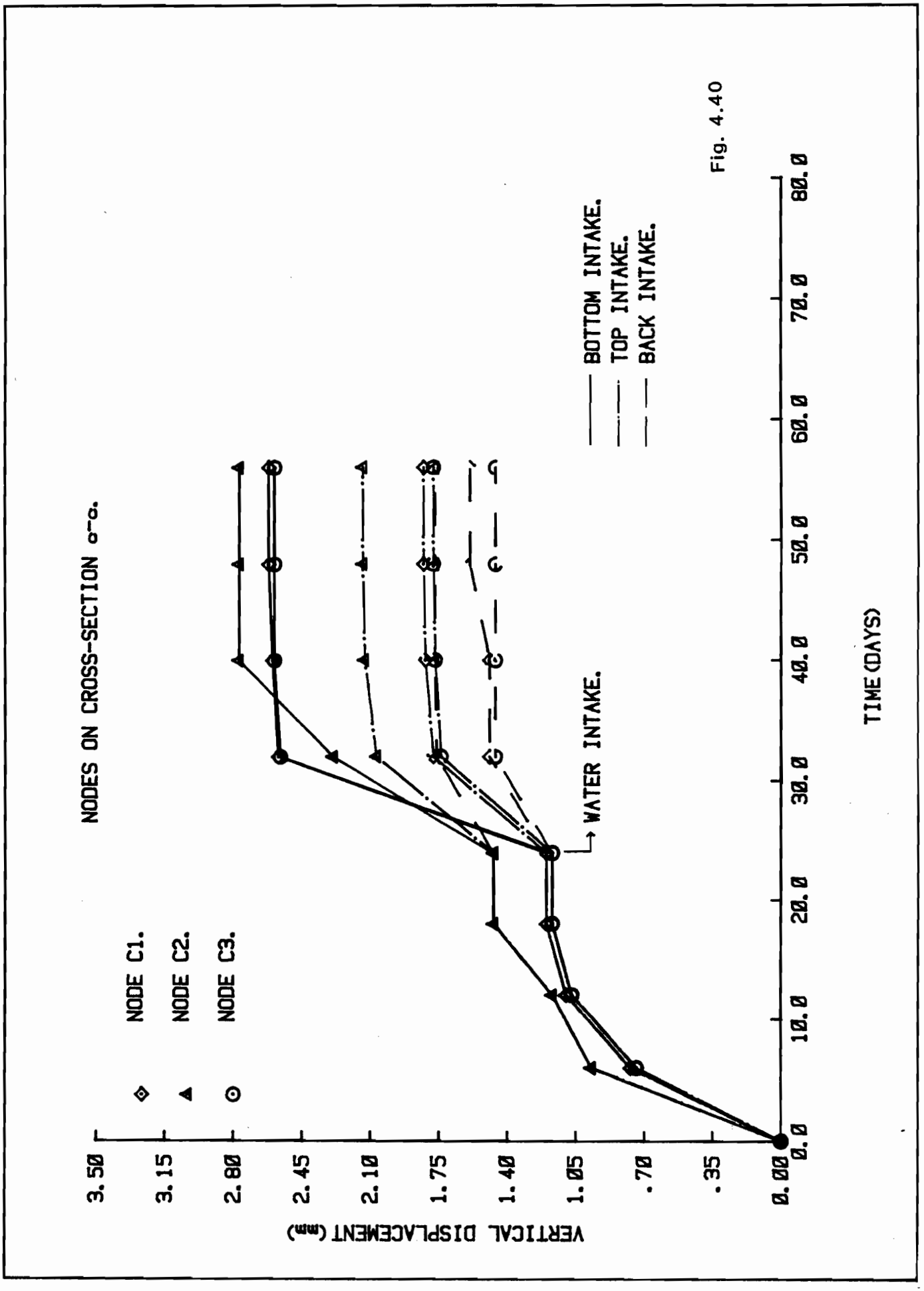
NODES ON CROSS-SECTION o-o.
NODE C1.
NODE C2.
NODE C3.
BOTTOM INTAKE.
TOP INTAKE.
BACK INTAKE.
WATER INTAKE.
VERTICAL DISPLACEMENT (mm)
TIME(DAYS)
3.50
3.15
2.80
2.45
2.10
1.75
1.40
1.05
.70
.35
0.00
0.0
10.0
20.0
30.0
40.0
50.0
60.0
70.0
80.0

Fig. 4.40

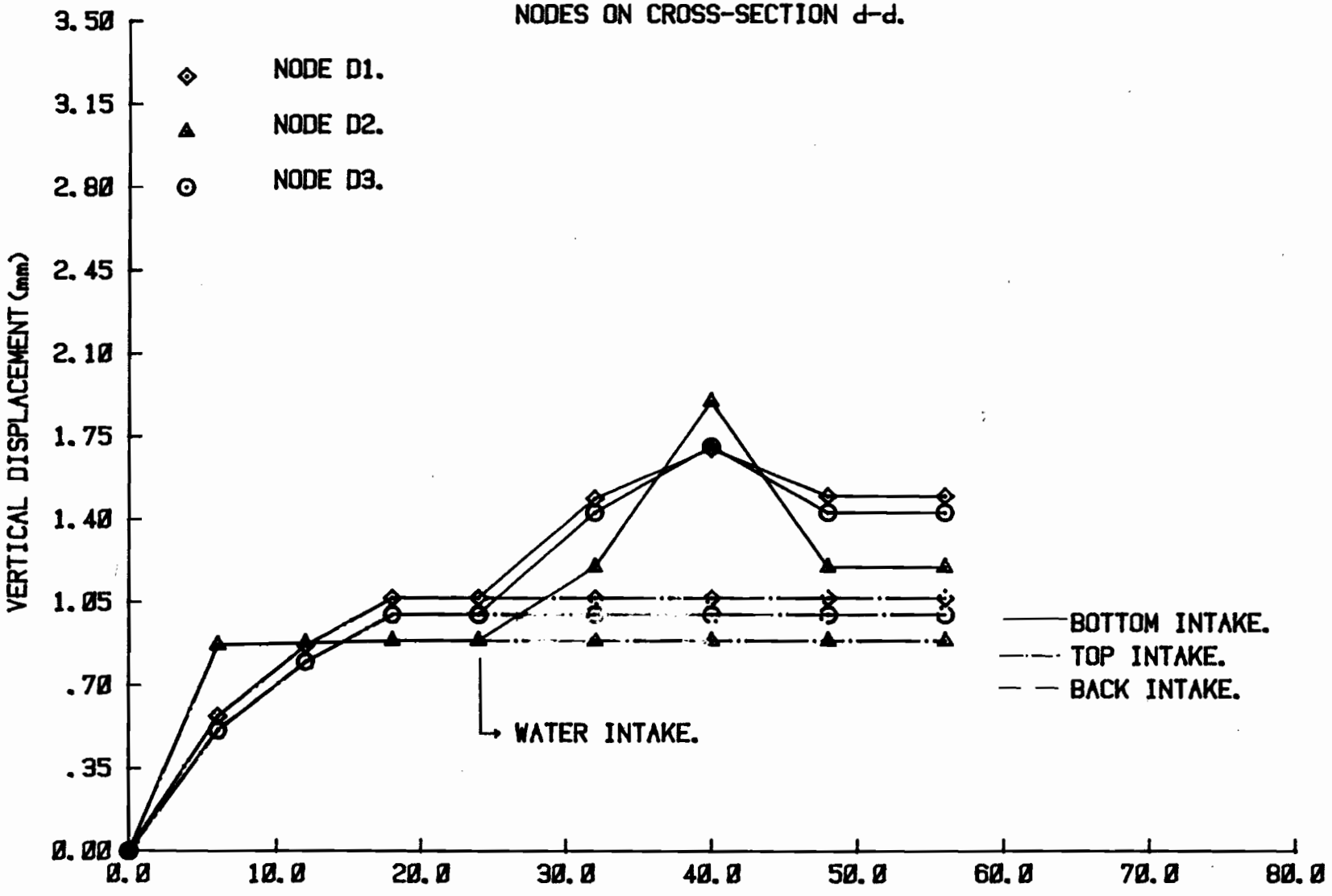
NODES ON CROSS-SECTION d-d.
NODE D1.
NODE D2.
NODE D3.
VERTICAL DISPLACEMENT (mm)
3.50
3.15
2.80
2.45
2.10
1.75
1.40
1.05
.70
.35
0.00
0.0
10.0
20.0
30.0
40.0
50.0
60.0
70.0
80.0
TIME (DAYS)
BOTTOM INTAKE.
TOP INTAKE.
BACK INTAKE.
WATER INTAKE.

Fig. 4.41

on the buffer response is expected. The additional settlements are 17% when water is absorbed from the back of the waste container, 31% when water is absorbed from the top of the disposal hole and 53% when water uptake (intake from the bottom of the disposal hole) is allowed (Fig. 4.40).

Throughout the buffer, water uptake conditions result in additional buffer settlements between 40-53%. When water intake is allowed from the back of the waste container, the increase is 15-18%, while, due to swelling close to the source of water intake, a decrease in the settlements is observed. The effect of water intake from the top of the disposal hole is kept almost constant at 31% for the whole buffer surface.

For the time period examined it is reasonable to conclude that the water uptake condition is the most crucial for the buffer-container system stability. This conclusion becomes more important when observing Fig. 4.42, where the absorbed water-time history is shown. The smallest quantity of water is absorbed when water intake is allowed from the bottom of the disposal system. The varying buffer-water absorption characteristics can be attributed to the different boundary conditions prevailing in every zone along the buffer which affect the flow characteristics. It is reasonable to conclude that the initial creep effect already described in Section 4.3.3 is not equally predominant

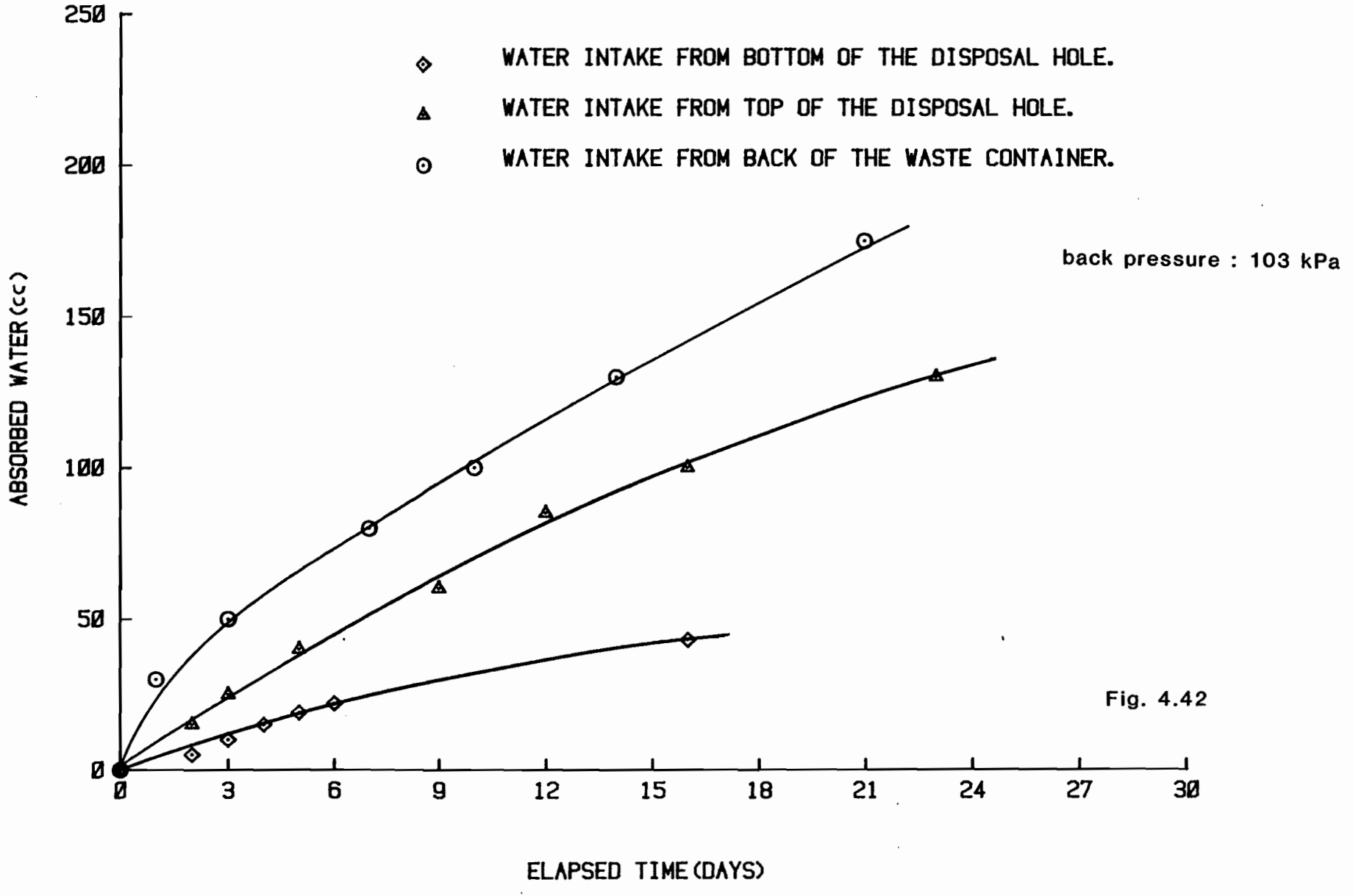
WATER INTAKE FROM BOTTOM OF THE DISPOSAL HOLE.
WATER INTAKE FROM TOP OF THE DISPOSAL HOLE.
WATER INTAKE FROM BACK OF THE WASTE CONTAINER.
back pressure : 103 kPa
ABSORBED WATER(cc)
250
200
150
100
50
0
0
3
6
9
12
15
18
21
24
27
30
ELAPSED TIME(DAYS)

Fig. 4.42

in all three zones. The effect of the initial creep, i.e. decreased suction due to a saturation increase and decreased void space, is not influential in the zone around the waste container where the overall stress levels, i.e. the buffer confinement, are lower and the unsaturated flow can be considered as unconfined or under small confinement conditions. This pattern of unconfined flow should be crucial at longer time periods, when adequate water quantities would be absorbed by the buffer. The reason higher additional settlements are observed for the case of water uptake, although smaller quantities of water are absorbed is as follows: When water is absorbed through the disposal vault bottom, the available void space is already decreased due to the previous creep under no water intake conditions. The available void space is filled completely in a zone of buffer that is now considered to respond like a saturated soil. Part of the stress imposed on the buffer is transferred to the water that is forced to redistribute. When this additional redistribution of water starts taking place, the additional settlements occur. When water intake is allowed from the container back, it is easily redistributed in that area because the stress levels there are lower and are not opposed to the water potential. This continuous redistribution increases, all around, the degree of saturation of the buffer but in a small and homogeneously distributed pattern that seems not to affect the system stability much, at least for the time

period examined. The soil water redistribution throughout the buffer is shown in Figs. 4.43 and 4.44.

It has already been concluded that water intake conditions affect the buffer response characteristics and demonstrate its swelling potential. From the tests performed under variable water intake positions, for the time period examined, water uptake is considered as the most crucial for the buffer-container system stability.

WATER INTAKE FROM TOP

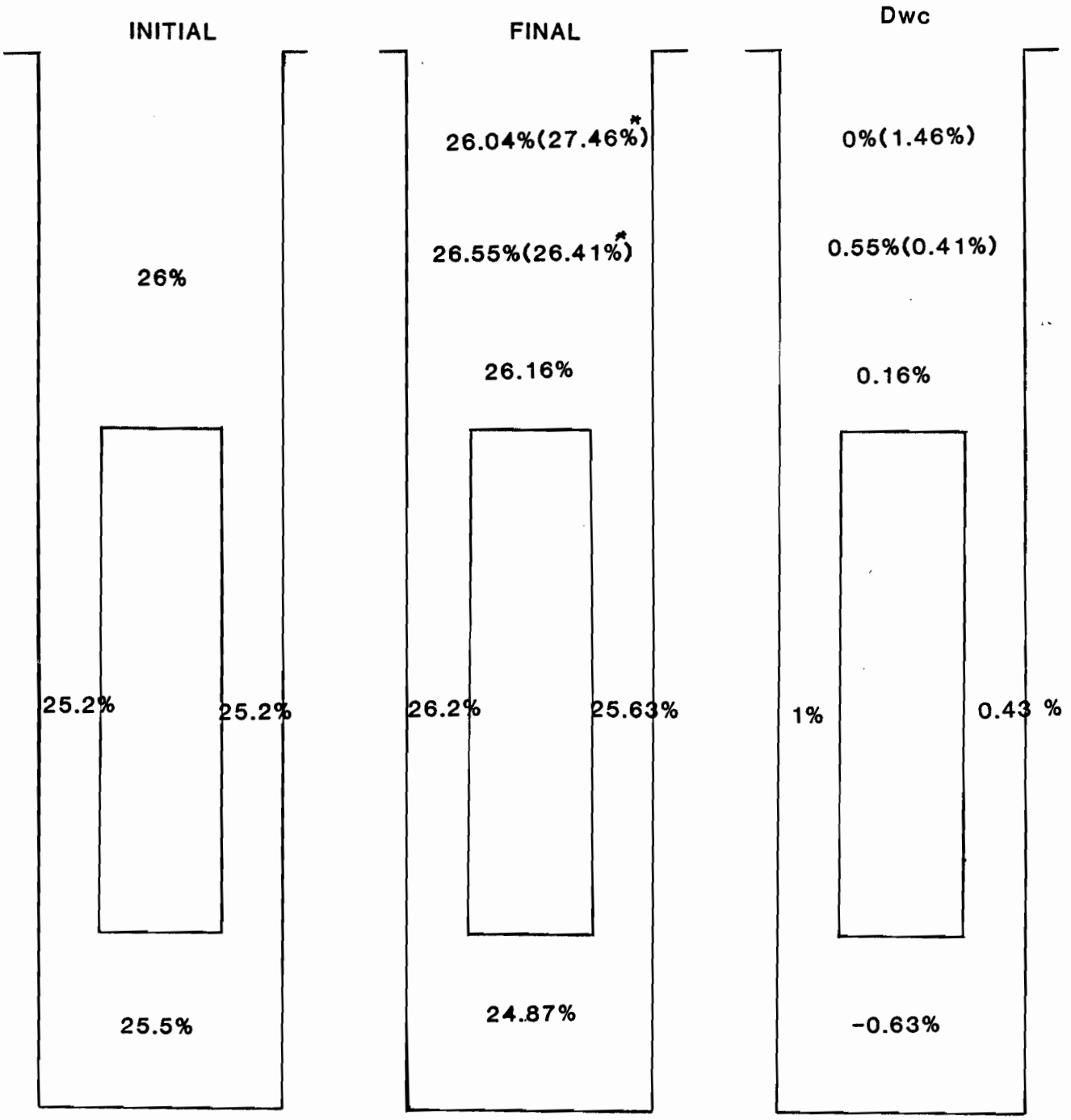

* Sample close to the water intake source

Fig. 4.43

WATER INTAKE FROM BACK

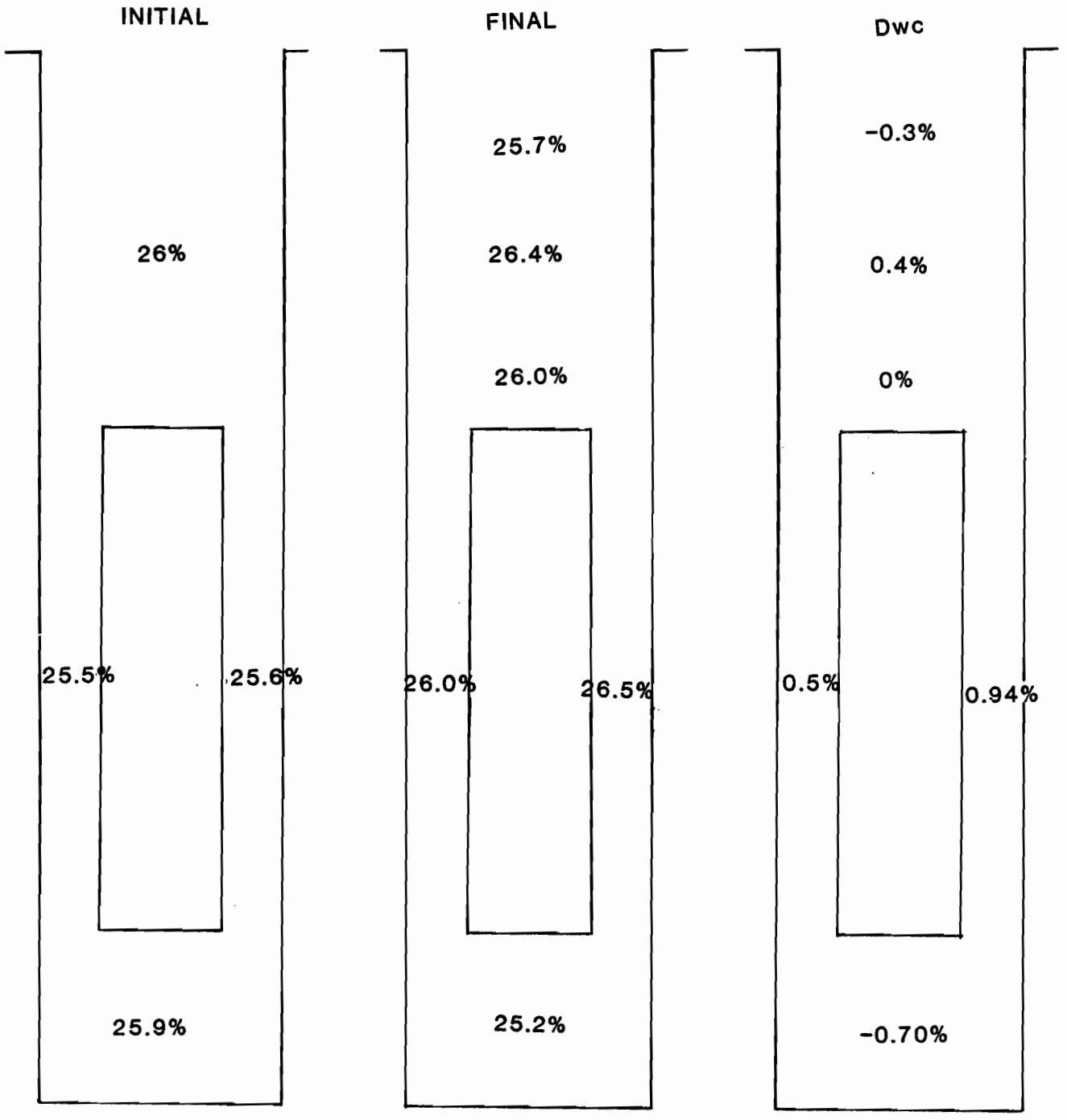

Fig. 4.44

CHAPTER 5

DISCUSSION OF THE ANALYZED AND PREDICTED RESULTS

5.1 Introduction

In this chapter, the applications of the finite element method* are verified by utilizing the proposed model (Chapter 2) to analyze and/or predict the model test results presented in Chapter 4. Comparisons between the finite element results of the proposed model and the experimental results previously reported in Chapter 4 will be made.

The buffer response behaviours which are not feasible to measure directly herein are obtained by data interpretation and analysis and are discussed in terms of velocities, strains, strain rates and stresses.

The finite element technique employed herein adopts the following input characteristics:

5.1.1 Meshes and Boundaries

The model tests described in the previous chapters were modelled by the finite element method for solution by the digital computer. The mesh adopted is shown in Fig. 5.1. In the idealization of the model test, 122 elements and 90 nodal points were used.

Since the sides and the bottom of the disposal hole containing the buffer, and the bottom and top of the waste container were greased it is reasonable to assume that these

---

* Details on the F.E. technique developed are given in Appendix A.

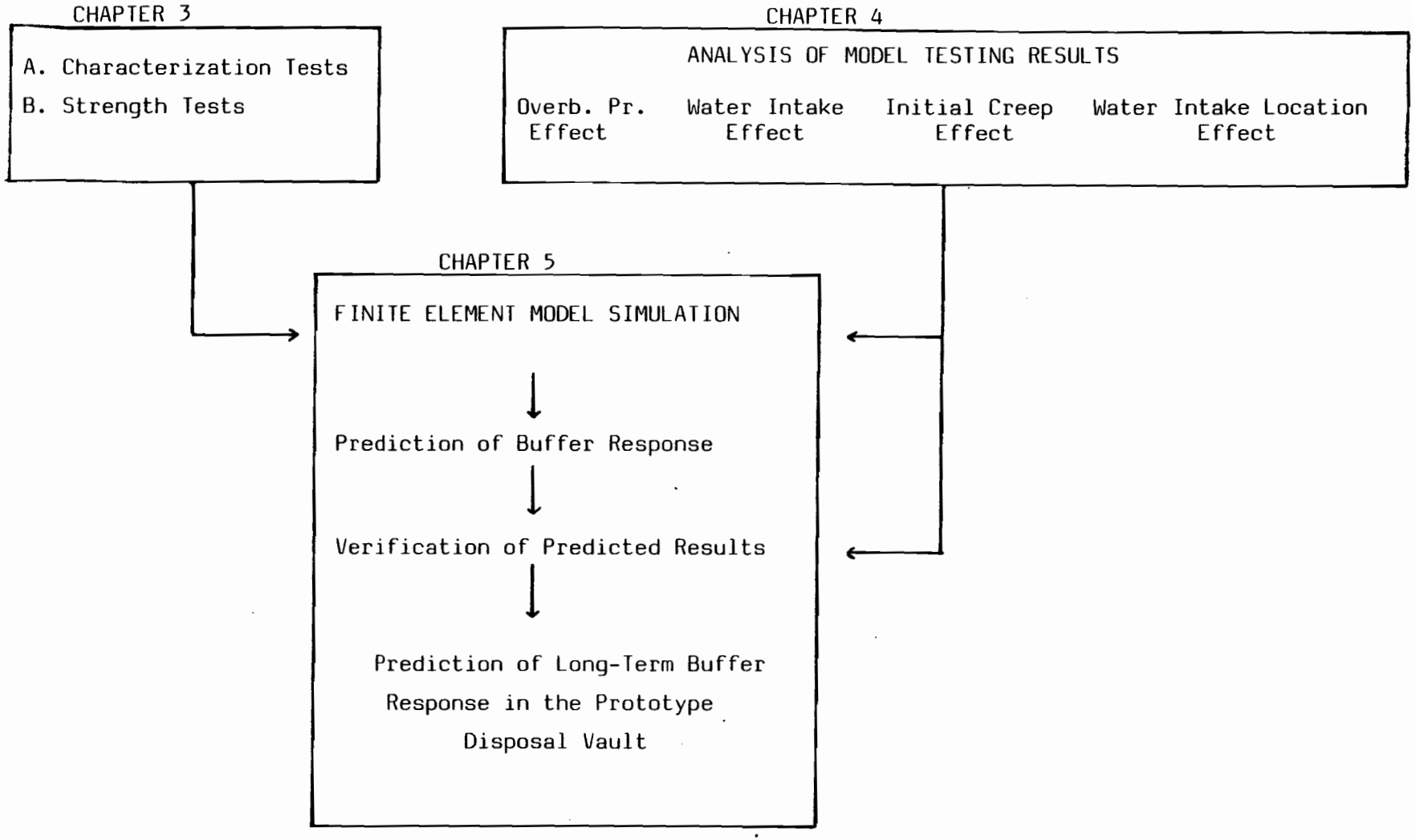

Sequence of Presentation of Test Results, Analyses and Discussions

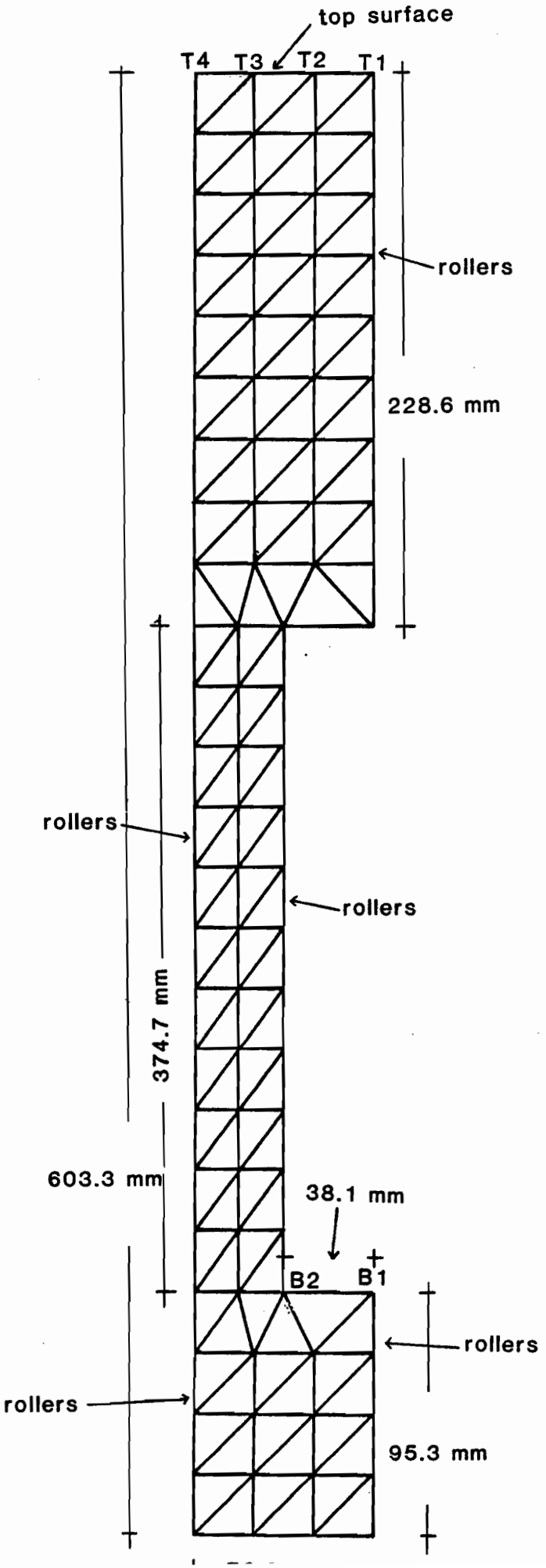

Mesh layout for the model

scale 1:2.54

Fig. 5.1

boundaries are smooth. In the finite element idealization, the boundaries were placed on rollers so that the horizontal movement was restrained on the sides and the vertical movement on the bottom boundary. It is expected that the results from this simplified finite element model would be affected by the boundary conditions imposed.

It has already been found that the friction along the buffer-host rock (concrete) interface was approximately 8 kPa. An attempt to induce the friction existing along the buffer-host rock interface in a form of boundary forces, gave no satisfactory results. For the appropriate simulation of the boundary conditions along the buffer-host rock interfaces, joint (interface) elements must be inserted with constitutive relationships produced from direct shear tests between buffer and rock. Joint (interface) constant strain elements have been used in previous GRC studies on soil cutting and traction problems (Hanna, 1975).

In the finite element analysis, boundary displacements were increased in the appropriate number of increments in order to obtain the final buffer displacement measured in the test, for the boundary nodes in contact with the loading imposed on the buffer as waste container weight and overburden pressure. In Table 5.1 an example is given of the technique, that was used in order to pick the displacement fields corresponding to the measured ones, when the overburden pressure is 36 kPa.

TABLE 5.1 Nodes in Contact with the Waste Container Bottom

Time (days) Under Loading	Measured Boundary Displacement (mm)	Dispacement Obtained from F.E. Analysis (mm)	Increment No.
0	0	0	-
6	.61	.60	5
12	1.12	1.09	9
18	1.32	1.33*	11**

* input boundary final displacement for the Nodes B_1, B_2 (Fig. 5.1)

** input number of increments

Boundary displacements were used as input data instead of boundary stresses in the F.E. model, because through the experimental procedure, displacements were measured at certain time periods.

For each incremental displacement, sufficient iterations for appropriate elastic moduli were provided to ensure convergence and accuracy. The number of iterations depends mainly on the degree of nonlinearity of the stress-strain relationship.

Body forces (buffer self weight) were included in all the analyses made.

5.1.2 Constitutive Relationships

One of the major problems encountered in the simulation of the model test by the finite element technique was the adoption of the most representative constitutive relationships describing the buffer response in the disposal hole. In an initial attempt ,the stress-strain curves obtained from the CU tests for the buffer under axisymmetric conditions already reported in Chapter 3, were used for every element of the finite element model. The resulting stress fields were significantly lower from those expected, mainly for the zone above the waste container up to the top surface of the buffer. Under the actual boundary conditions the buffer material in this area shows low compressibility characteristics, deforms mainly vertically, and the displacements are obtained under considerably higher stresses. The loading patterns in this specific zone resemble those of the one-dimensional consolidation test under no saturation conditions (i.e. compressibility test), where the perfectly confined buffer is compressed vertically. The additional characteristic is the yielding support, i.e. the moving waste container. For the zone above the waste container top the constitutive relationships obtained from the load-deformation test reported in Chapter 3, were used. For the rest of the elements the CU test stress-strain curves were used. These curves represented adequately the buffer response around and below the waste container where the loading conditions theoretically may even produce failure patterns similar to those observed in a foundation problem.

In summary, the main assumptions adopted in the finite element analysis states that because of the different loading conditions, in areas A and B (see Fig. 5.2) of the disposal hole system, the buffer responds in a pattern that is a function of these loading conditions. These buffer response characteri-sitics will be described by two different types of stress-strain curves. This simplifying model neglects any inter-mediate zone necessarily existing between these two areas A and B. This intermediate zone is considered as a part of area A.

In order to demonstrate the effect of the proper modelling of the buffer response through the most representative constitutive relationships, in Figs. 5.2.1 and 5.2.2 the contours of the resulting vertical stress components are plotted when overburden pressure is 120 kPa. Under the label "two types" are the plotted contours where two different sets of constitutive relationships are used. Under the label "one type"the contours of the stresses developed under one set of constitutive relationships - CU stress strain curves - are plotted. From the contours of Fig. 5.2.1 under the label "one type"it is shown that decreased stresses result, which are significantly lower than the induced ones at the bounda ries. On the contrary, the model that uses the assumptions of two different materials, results in a very good agreement with the boundary induced stresses. The increased material stiff-ness is also indicated from Fig. 5.2.2 when the resulting strains are higher, when use of two different sets of constitutive

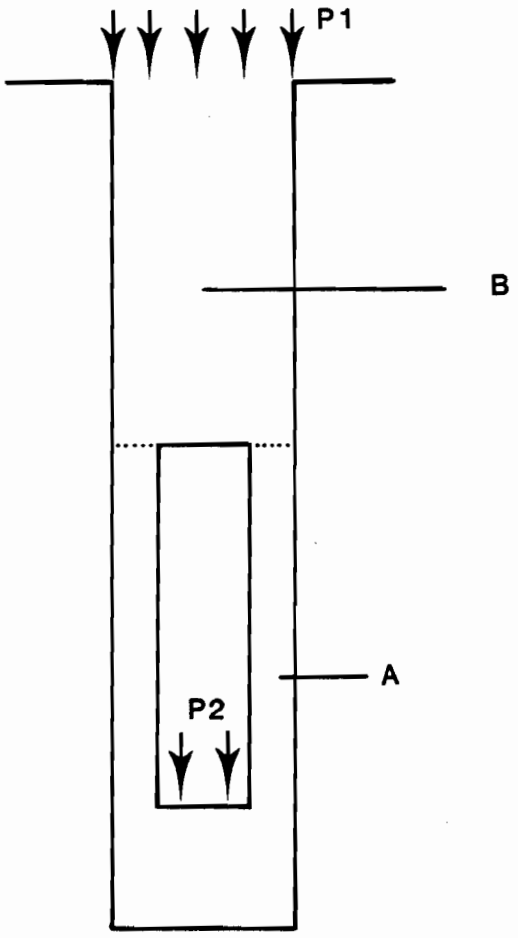

stress–strain curves from

one dimensional compressibility test

stress strain curves

from CU axisymmetrical tests

Fig. 5.2

Final $-\sigma_y-$ contours : Overb.pr. 120 kPa (in kPa)

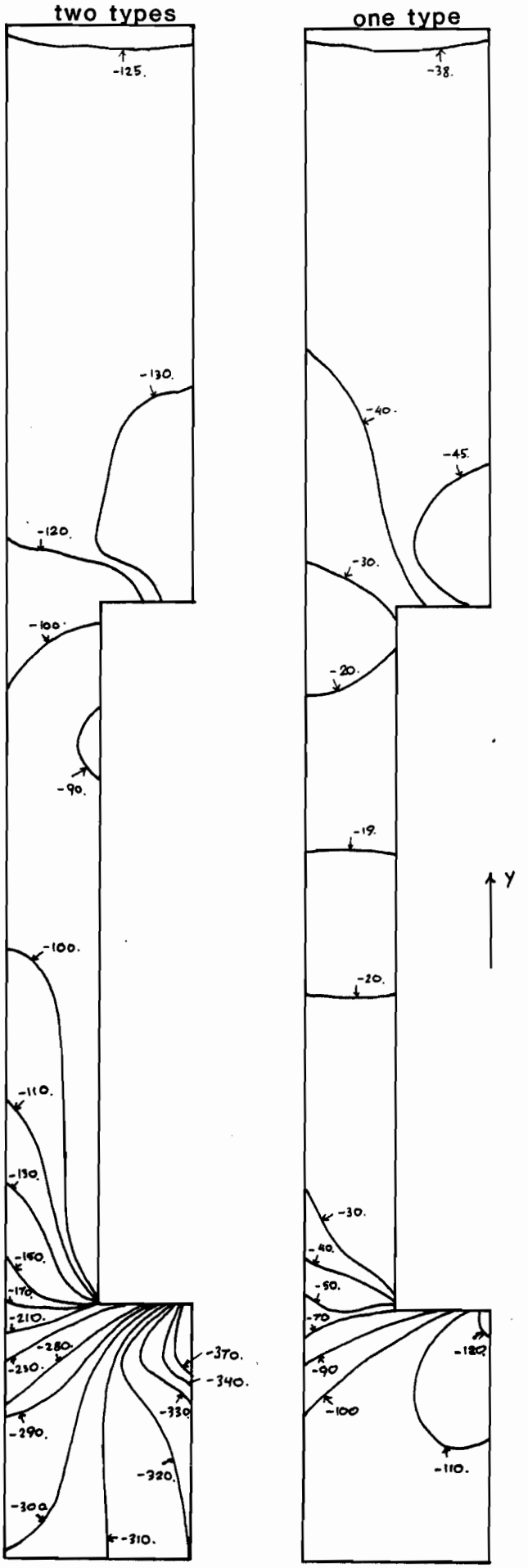

Fig. 5.2.1

Final $-\varepsilon_y-$ contours : Overb.pr. 120 kPa (in %)

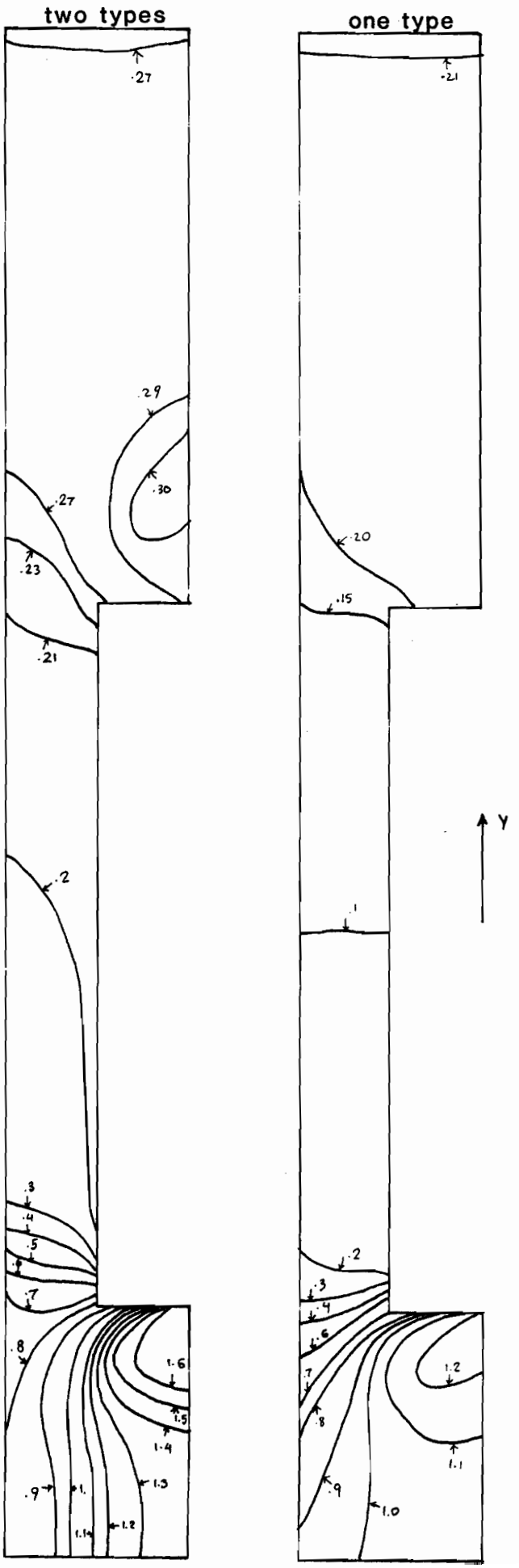

Fig 5.2.2

relationships is made. There is no discontinuity observed from the contours of Fig. 5.2.1, 5.2.2 that should unjustify the use of two different constitutive relationships for the buffer. By using this modelling pattern, the effect of the loading-boundary conditions on the buffer response characteristics is properly taken into account and it results in a better predictive analytical model.

The concept of two differently responding buffers is affected by the relative magnitude of the imposed loads. When the backfill is installed, the overburden pressure increases from 1/10 to 1/3 of the total pressure acting on the buffer underneath the container. Under these conditions an overall one-dimensional compression pattern for the buffer could be adopted. In other words, increasing overburden pressure causes a uniformly distributed one-dimensional compression pattern on the buffer. In Figs. 5.3 and 5.4 the stress-strain curves obtained from CU tests under different confining pressures and from one-dimensional consolidation tests under no saturation conditions, which are adopted for the finite element analysis, are shown.

In general, the nonlinear stress-strain curves expressing the constitutive relationships can be represented directly in digital form or expressed through a mathematical function (Duncan and Change, 1970). In this study, the stress-strain curves obtained from the CU tests and the one-dimensional consolidation tests were described by a number

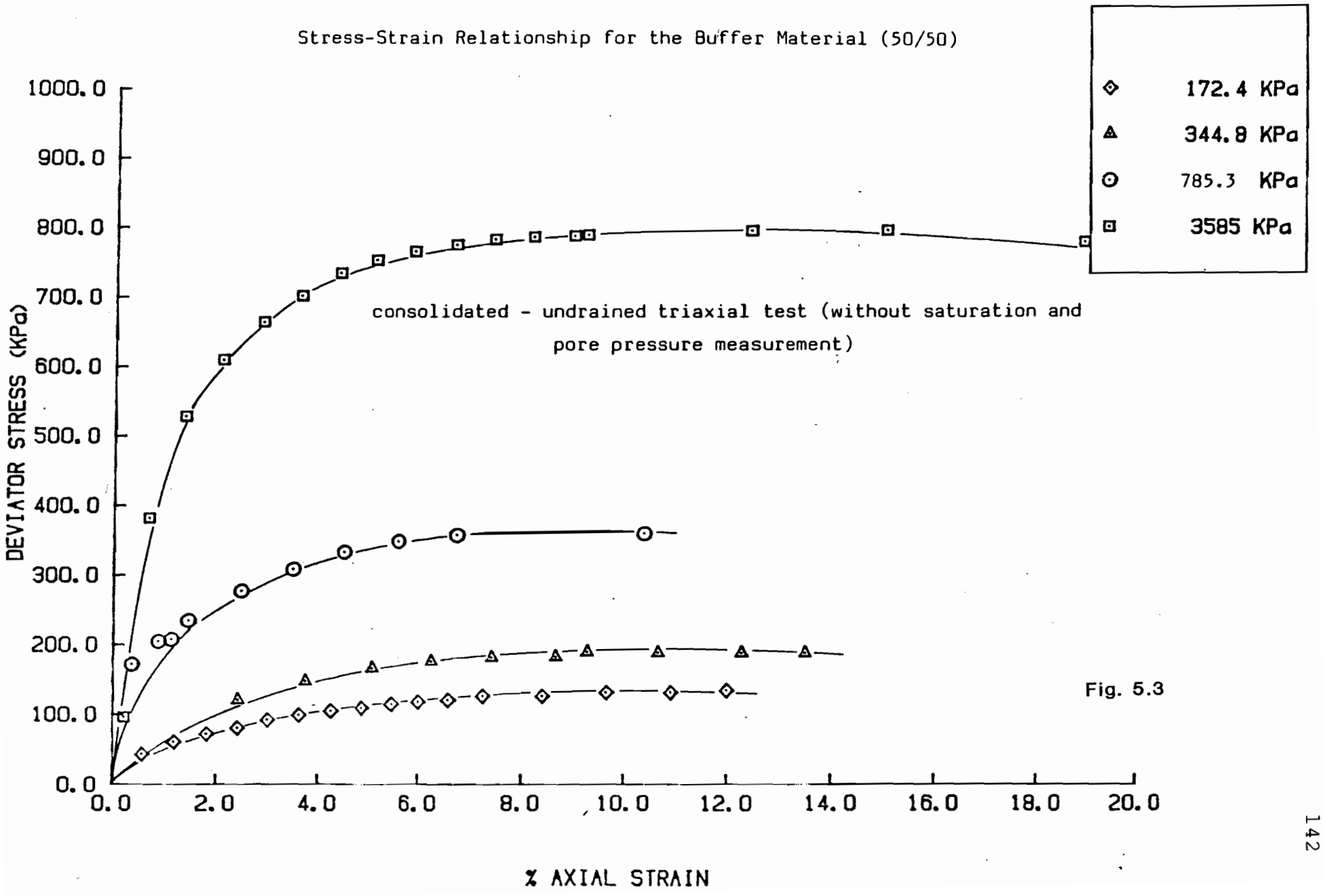
Stress-Strain Relationship for the Buffer Material (50/50)
172.4 KPa
344.8 KPa
785.3 KPa
3585 KPa
consolidated - undrained triaxial test (without saturation and pore pressure measurement)
DEVIATOR STRESS (KPa)
1000.0
900.0
800.0
700.0
600.0
500.0
400.0
300.0
200.0
100.0
0.0
0.0
2.0
4.0
6.0
8.0
10.0
12.0
14.0
16.0
18.0
20.0
% AXIAL STRAIN

Fig. 5.3

Load Deformation Relationship for Buffer Material (50/50)

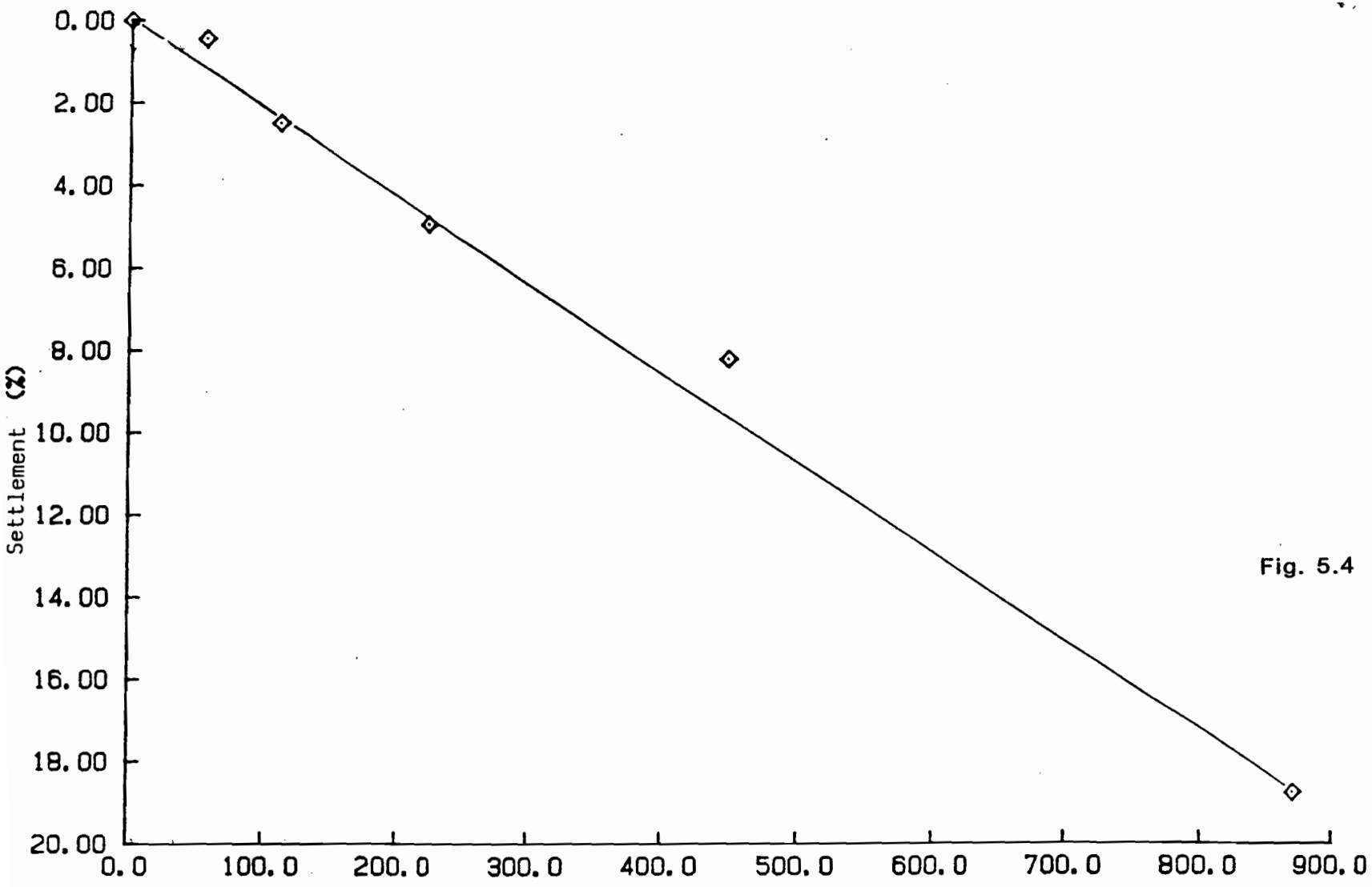

Fig. 5.4

of points, each of which denoted the values of the corresponding stress and strain. The material parameters which are the modulus of elasticity and Poisson's ratio were given initial values and were consequently derived by interpolation. The starting value of the modulus of elasticity was taken as the initial tangent modulus of the stress-strain curve with the lowest confining pressure. The Poisson's ratio for zone A was 0.29 and was obtained as reported in Chapter 3.

For zone B a Poisson's ratio of 0.45 was used.

5.2 Displacements

5.2.1 Vertical Displacements

The vertical displacement contours obtained from the F.E. analysis for the three overburden pressure values are shown in Figs. 5.5, 5.6 and 5.7.

From the vertical displacement contours two different deformation patterns are indicated. The zone above the waste container that is extended up to the top surface is compressed uniformly towards the bottom of the disposal system. This pattern is observed for all three overburden pressure values for all the time periods examined. The most interesting characteristic for this zone is the distribution of the vertical displacement with depth from the top surface as a function of the overburden pressure. When overburden pressure is 120 kPa the vertical displacement at the top of the waste container is 70% of the

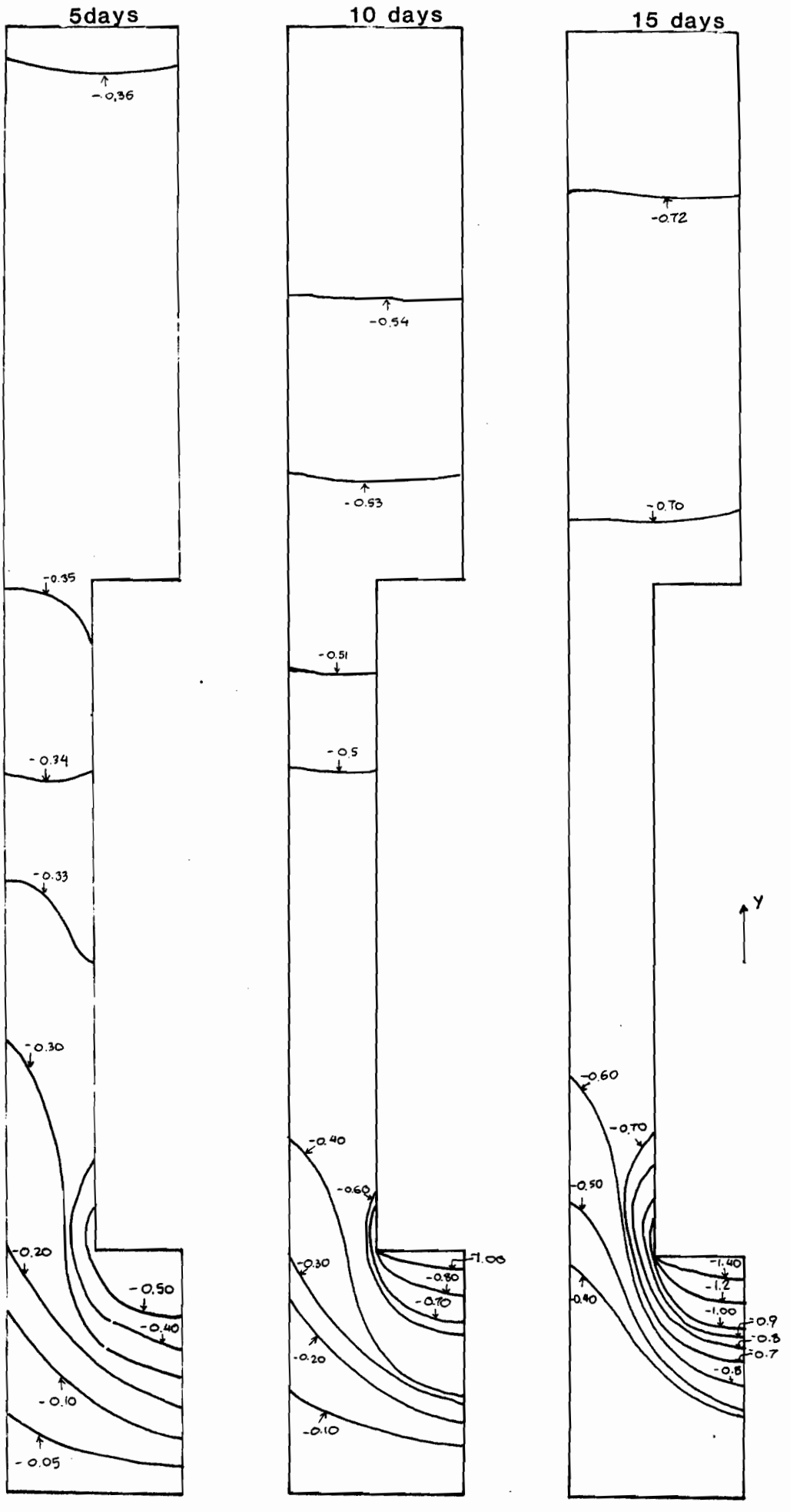
Vertical displacement contours (in mm) .Overb.pr. 0kPa
5days
10 days
15 days
-0.36
-0.35
-0.34
-0.33
-0.30
-0.20
-0.50
-0.40
-0.10
-0.05
-0.54
-0.53
-0.51
-0.5
-0.40
-0.60
-0.30
-1.00
-0.80
-0.70
-0.20
-0.10
-0.72
-0.70
-0.60
-0.70
-0.50
-0.40
-1.40
-1.2
-1.00
-0.9
-0.8
-0.7
-0.6
Y

Fig. 5.5

Vertical displacement contours (in mm) .Overb.pr. 36 kPa

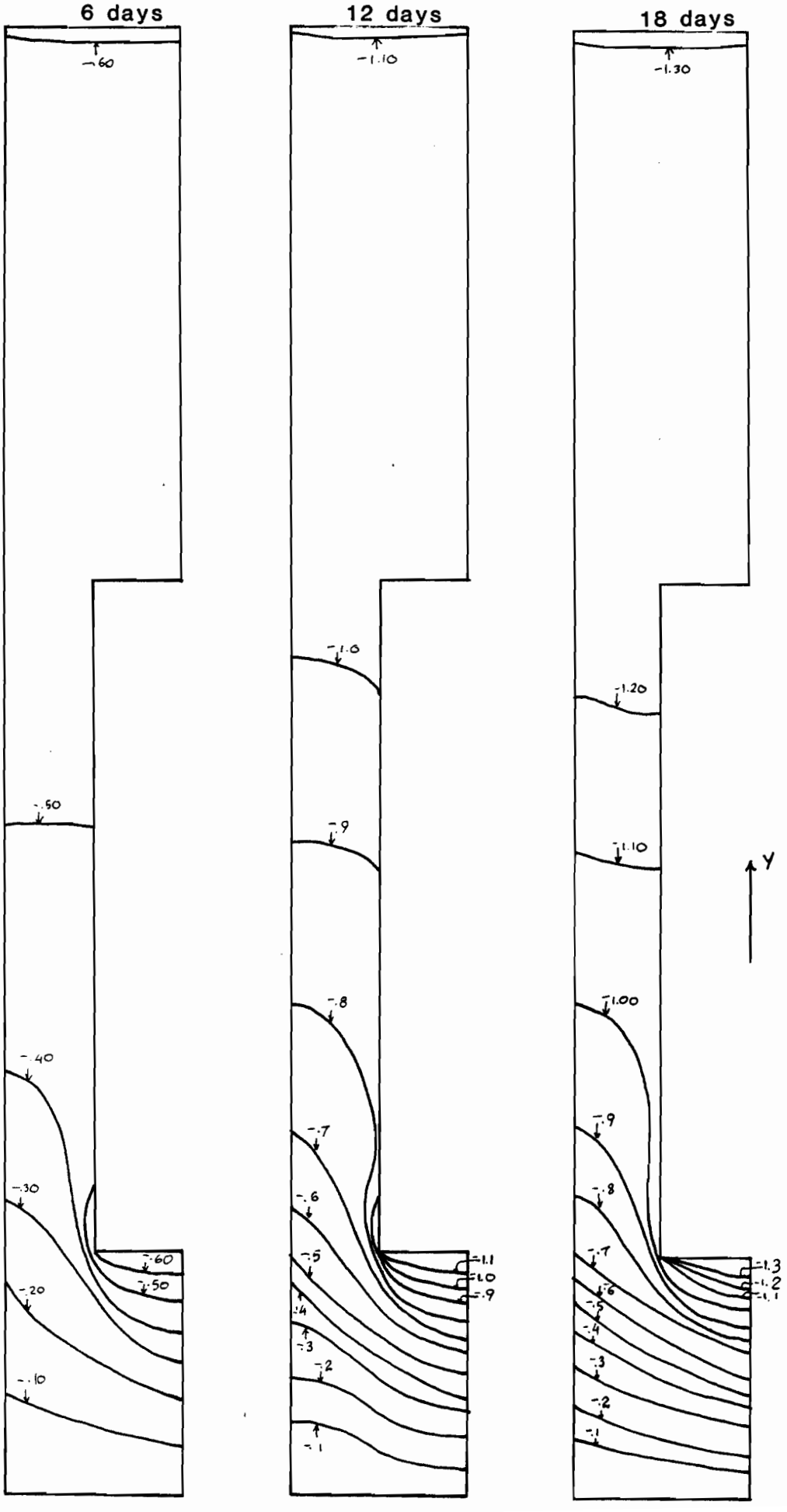

Fig. 5.6

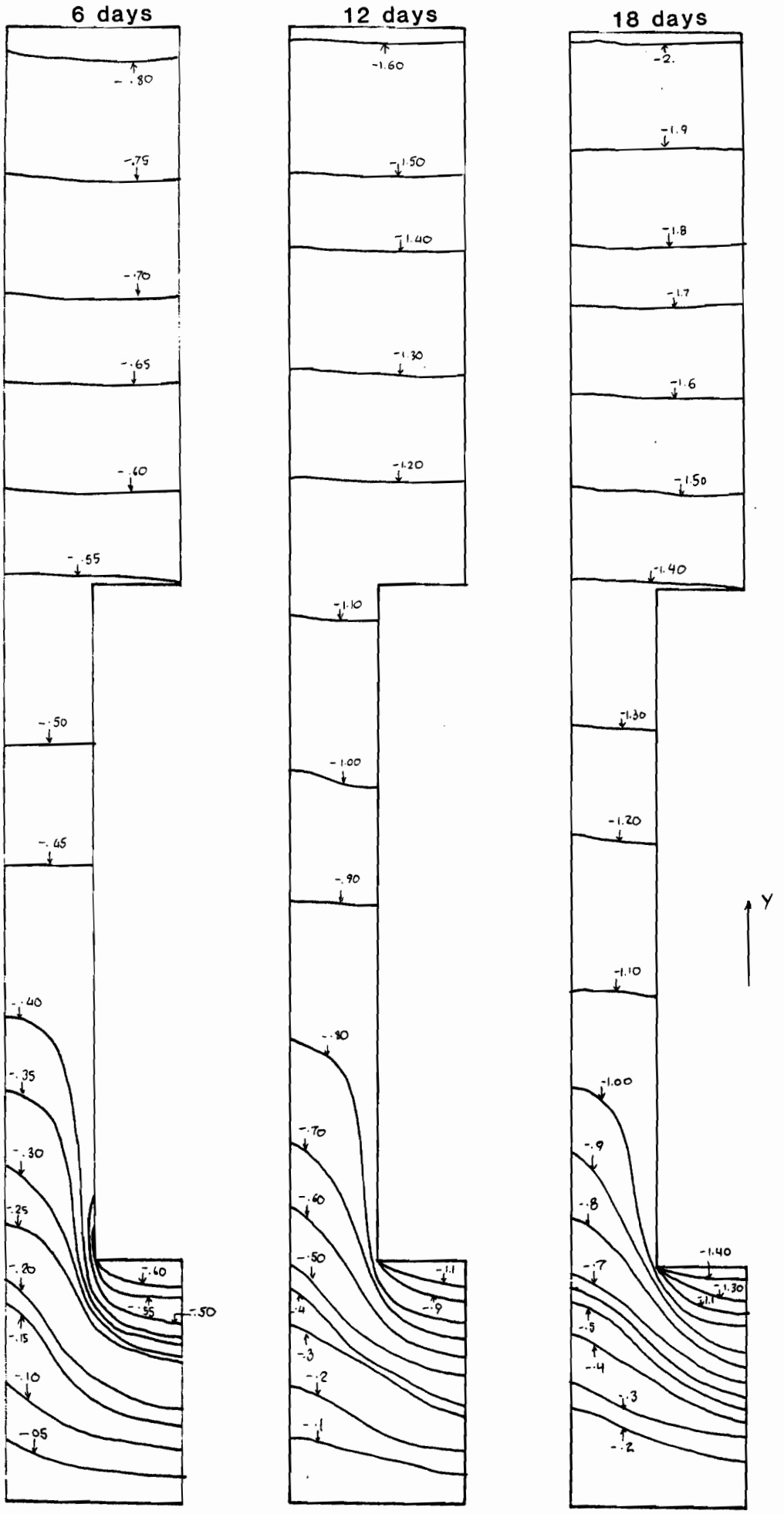
Vertical displacement contours (in mm) .Overb.pr. 120 kPa
6 days
12 days
18 days
-.80
-.75
-.70
-.65
-.60
-.55
-.50
-.45
-.40
-.35
-.30
-.25
-.20
-.15
-.10
-.05
-1.60
-1.50
-1.40
-1.30
-1.20
-1.10
-1.00
-.90
-.80
-.70
-.60
-.50
-.4
-.3
-.2
-.1
-2.
-1.9
-1.8
-1.7
-1.6
-1.50
-1.40
-1.30
-1.20
-1.10
-1.00
-.9
-.8
-.7
-.5
-.4
-.3
-.2
Y

Fig. 5.7

vertical displacement at the surface top while for the other two cases of 0 and 36 kPa the vertical displacements at the top of the waste container are 97 and 91% respectively of that at the top surface for all time periods examined. The separation observed in the experimental results at the zone initially in contact with the top of the waste container is also indicated through the finite element model when comparing the displacements of the nodes located at the top and the bottom of the waste container and when overburden pressure is 0 kPa it comes up to 0.55 mm, when overburden pressure is 36 kPa it is 0.10 mm, and is not observed for the value of 120 kPa overburden pressure.

The pattern of settlement distribution at the zone above the waste container indicates the effect of the separation observed at the top of the waste container on the buffer compressibility characteristics. As already mentioned for the cases of 0 kPa and 36 kPa separation was observed. This separation, that is due to the high cohesive characteristics of the buffer, results in the creation of a "tension" zone above the container top that obviously increases the compressibility characteristics of the buffer that experiences the top load totally unsupported. This zone causes an almost uniform settlement distribution pattern for the zone above the waste container for the cases of 0 and 36 kPa. When overburden pressure increases to 120 kPa this zone is no longer observed and

settlements decrease with depth from the surface top. In Fig. 5.8 the settlements after a 6 day loading period are shown indicating this "tension" zone.

From Fig. 5.8 it can be observedthat for the case of 120 kPa overburden pressure the settlements at the top of the waste container are slightly smaller than those on the same cross-section that are located close to the host-rock-buffer interface. The buffer for the 0 and 36 kPa overburden pressure values looks to be "suspended" for a zone of 50 mm thickness located at the top of the waste container, while it is obviously uniformly compressed when the overburden pressure is 120 kPa. These overburden pressure-dependent patterns at the waste container top affect the settlement distribution by changing the compressibility characteristics of the buffer in that zone.

Another displacement pattern is observed when examining the vertical displacement contours at the zone around and below the waste container. In that zone the container "penetrates" the buffer. The higher settlement values are observed for the nodes in contact with the waste container bottom and are reduced with increasing depth from the container bottomand when approaching the rock-buffer interface. This "penetration" pattern is obvious for all three cases of overburden pressure and is "damped" with depth from the waste container bottom increasing.

After 5 days

Over.pr.: 0 kPa

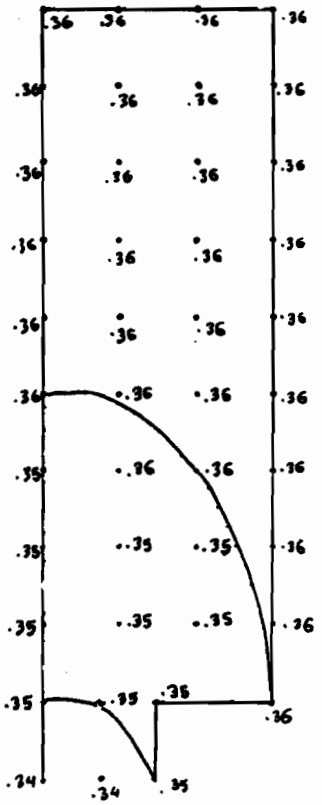

After 6 days

36 kPa

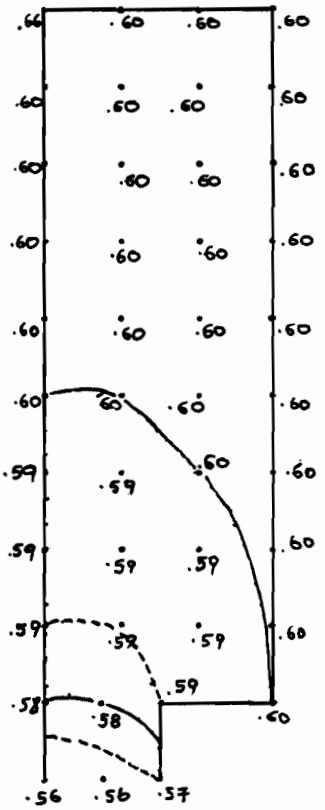

After 6 days

120 kPa

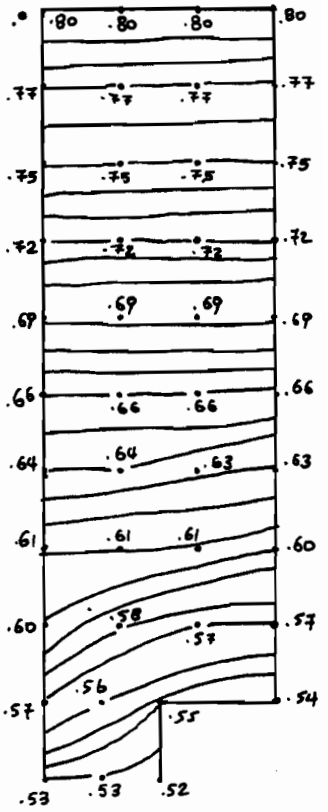

(in mm)

Detailed settlement contours for the zone above the container

Fig. 5.8

5.2.2 Lateral Displacements

The lateral displacement contours are shown in Figs. 5.9, 5.10 and 5.11. The zone where lateral displacements reach measurable values is located close to the bottom corners of the waste container and it extends up to the disposal system bottom. These displacements reach maximum values up to 0.10 mm in nodes close to the bottom corner of the waste container. The general pattern of distribution of the lateral displacements is quite the same for all three cases of overburden pressure and at any time period examined. When the overburden pressure is 120 kPa smalllateral displacements are observed in a zone located close to the top corners of the waste container with maximum values of 0.01 mm.

5.3 Velocities

The instantaneous velocities which were derived from the calculated nodal vertical displacements, show that the zones deformed at a higher rate are located underneath the waste container and at the top surface of the disposal system. Typical velocity contours are shown in Fig. 5.12 for the value of 36 kPa overburden pressure, as experienced by the buffer for 6 days. The velocity contours are obviously similar to the corresponding displacement contours shown previously. The values of the lateral velocities were negligible andmay be ignored.

Lateral displacement contours (in mm) .Overb.pr. 0 kPa

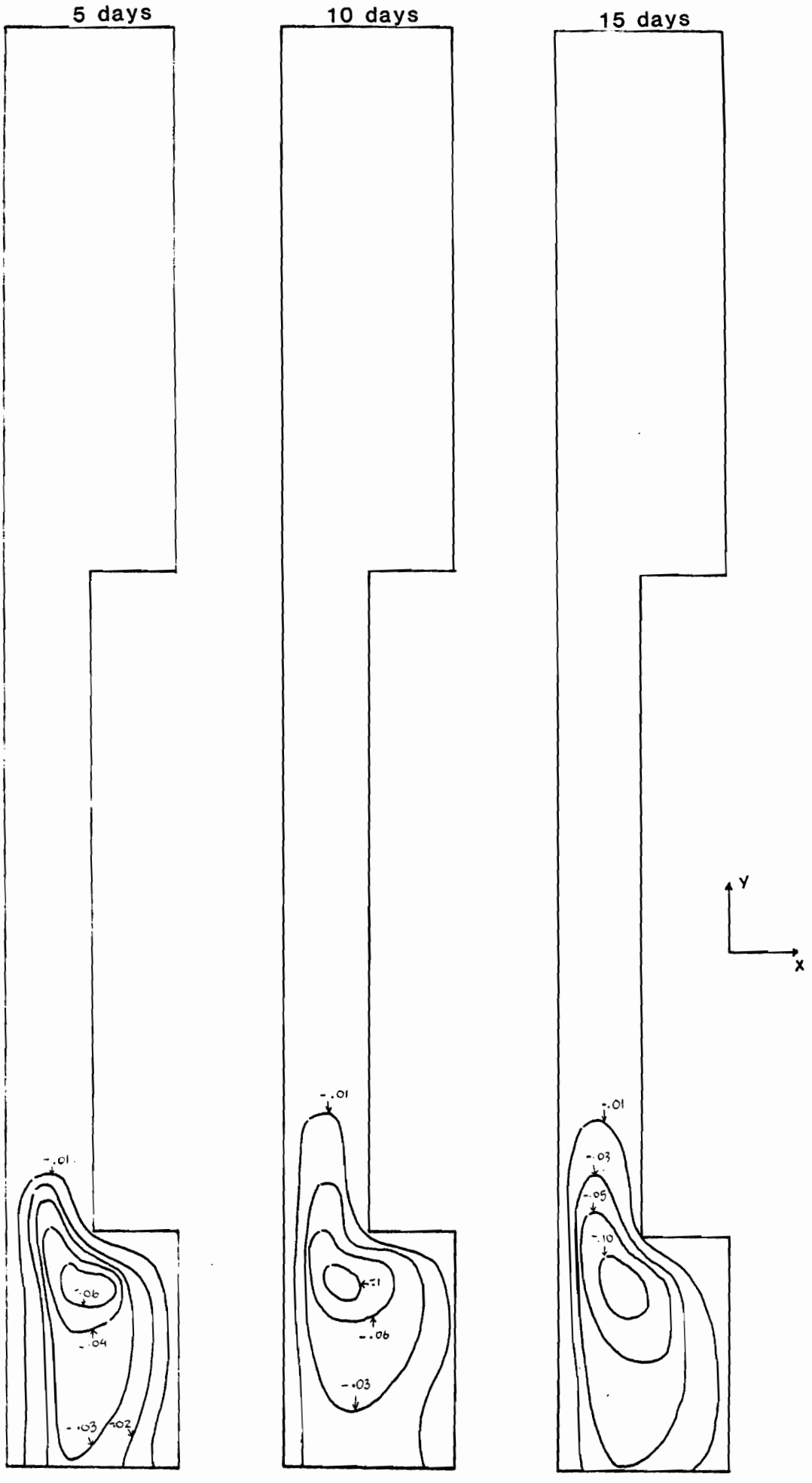

Fig. 5.9

Lateral displacement contours (in mm) .Overb.pr. 36 kPa

Fig. 5.10

Lateral displacement contours (in mm) .Overb.pr. 120 kPa

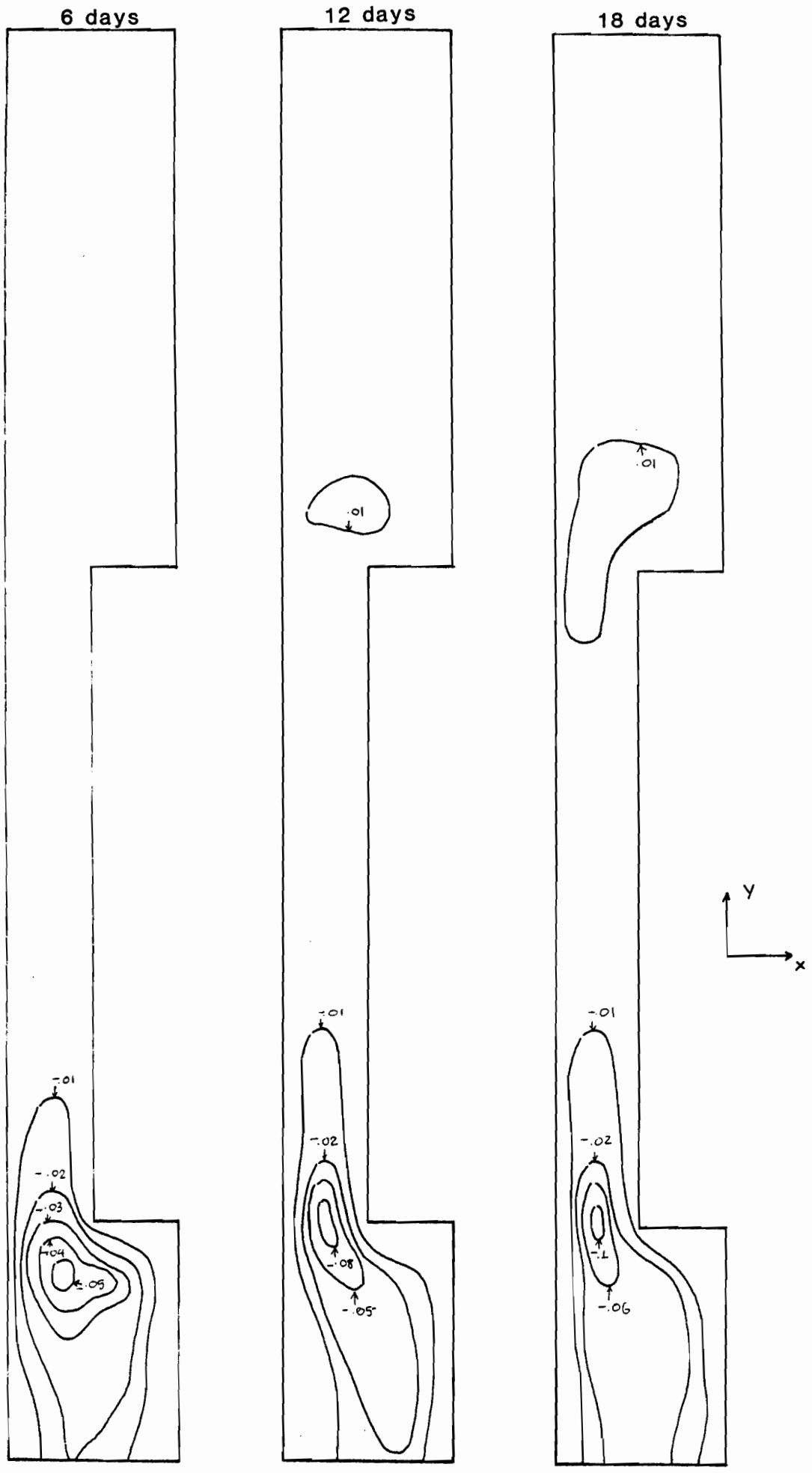

Fig. 5.11

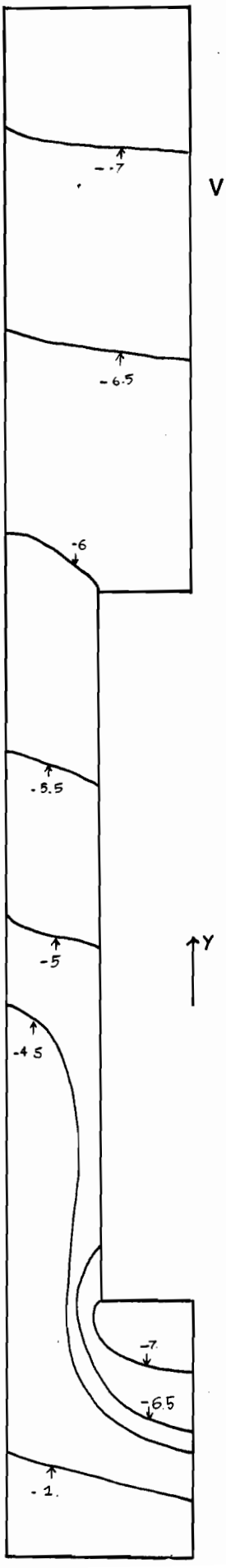

Overb.pr. 36 kPa

Vertical velocity contours after 6 days

(in 10^{-8} m/min)

Fig. 5.12

They also presented a distribution pattern similar to that of the corresponding lateral displacements.

5.4 Strains

5.4.1 Vertical Strains

The straincontours resulting from the calculated strain along the finite element mesh are shown in Figs. 5.13, 5.14 and 5.15. The direction of these strains is the vertical one axis y. In order to obtain a comparison among the three overburden pressure dependent strain fields, in each figure the produced strain fields for the three overburden pressure values are plotted and correspond to the same time period under loading. The general patterns obtained are almost identical and only the strain magnitudes are pressure and time dependent. The strain values obtained at the zone below the waste container are the same for all three cases of overburden pressure, reaching maximum values of 1.6%. It is already indicated that the waste container weight is the main source of buffer strain in that zone and the overburden pressure effect does not cause any significant vertical strain increase. The buffer underneath the waste container deforms vertically in the same pattern while the strain magnitudes attained are essentially overburden pressure independent. For the same zone - beneath the waste container - the vertical strains decrease significantly

Strains $-\varepsilon_y$ - after 6 days (%)

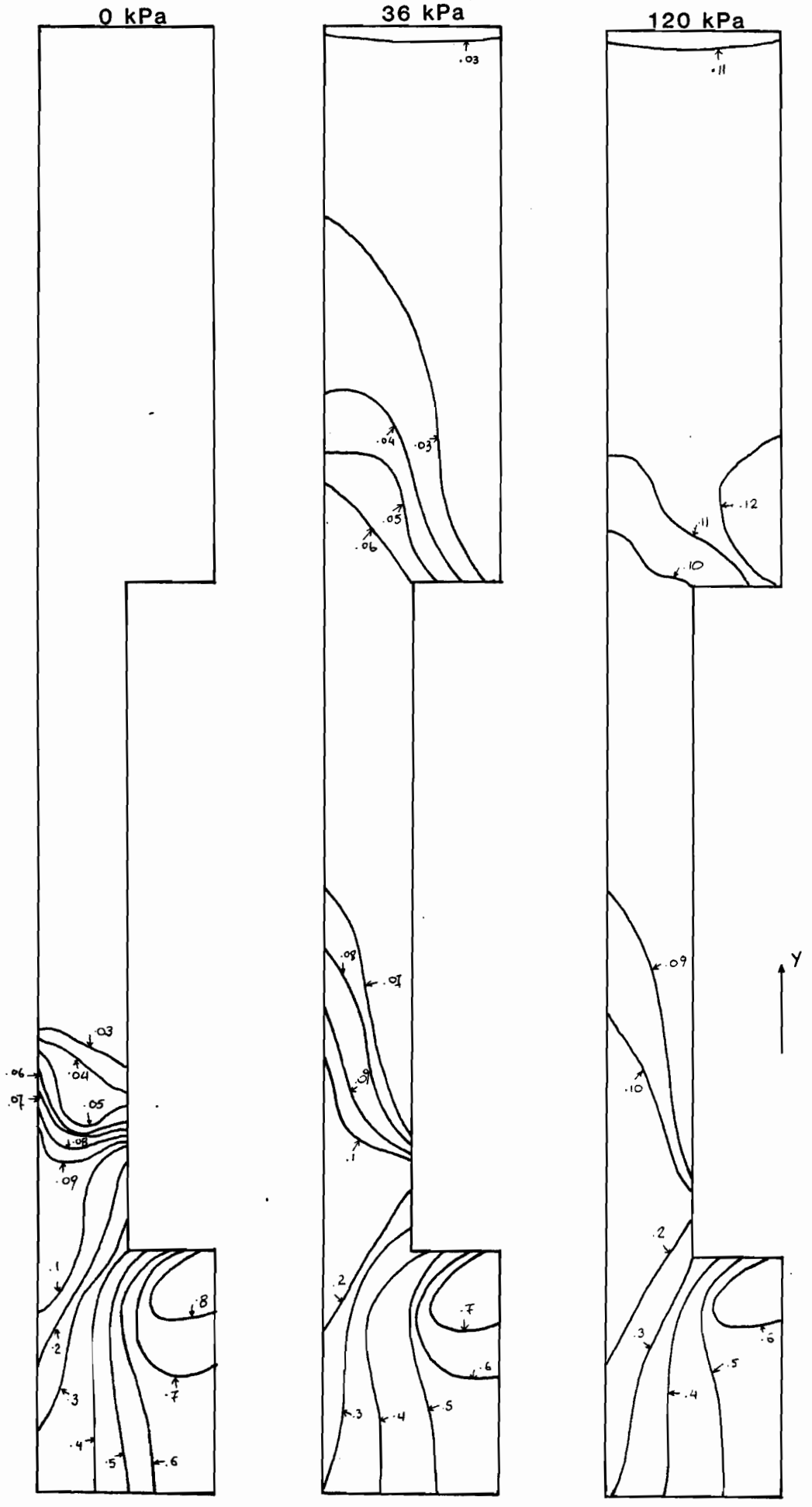

Fig. 5.13

Strains - ε_y - after 12 days (%)

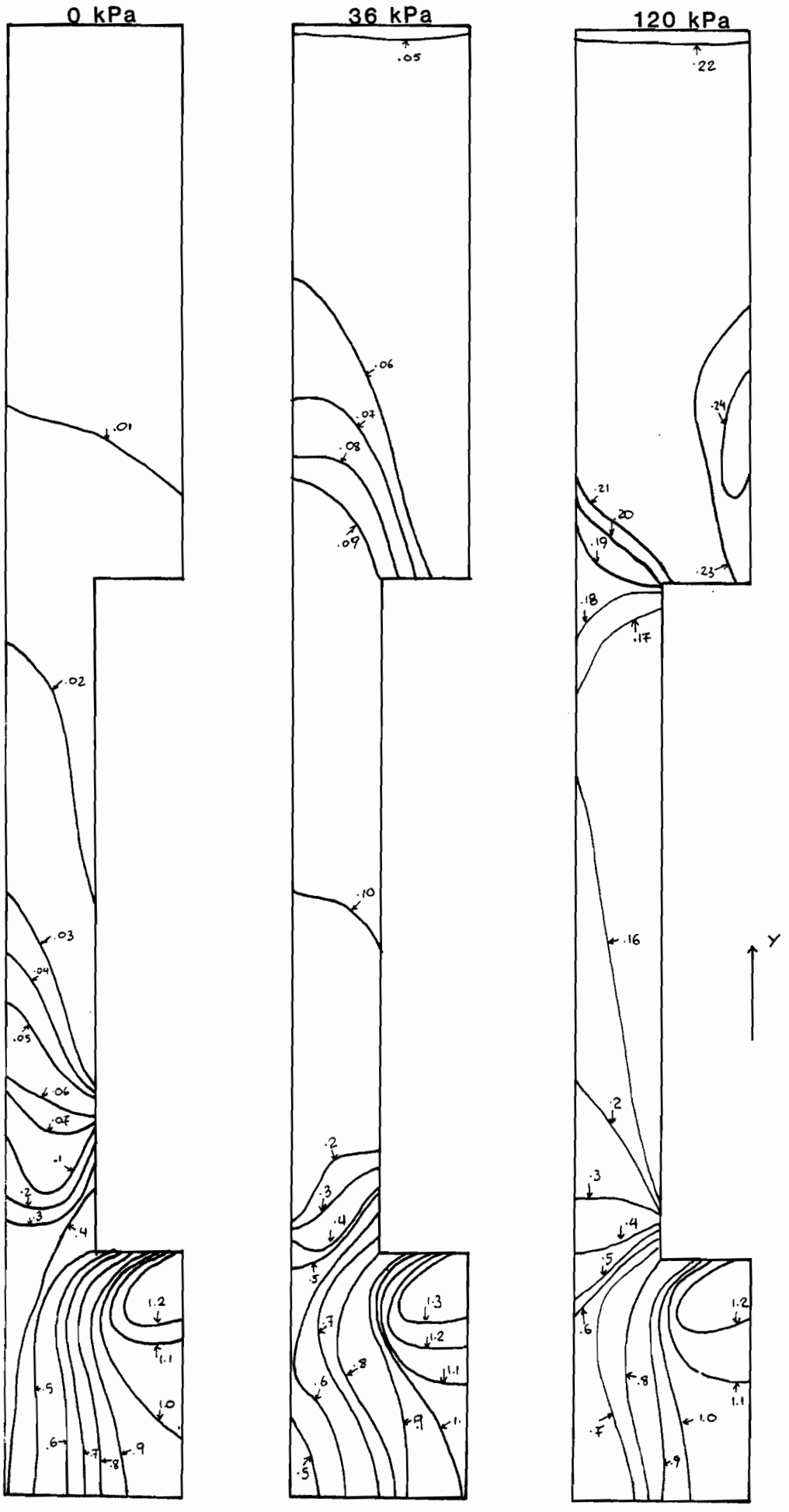

Fig. 5.14

after 10 days

Final strains $-\varepsilon_y-$ (%)

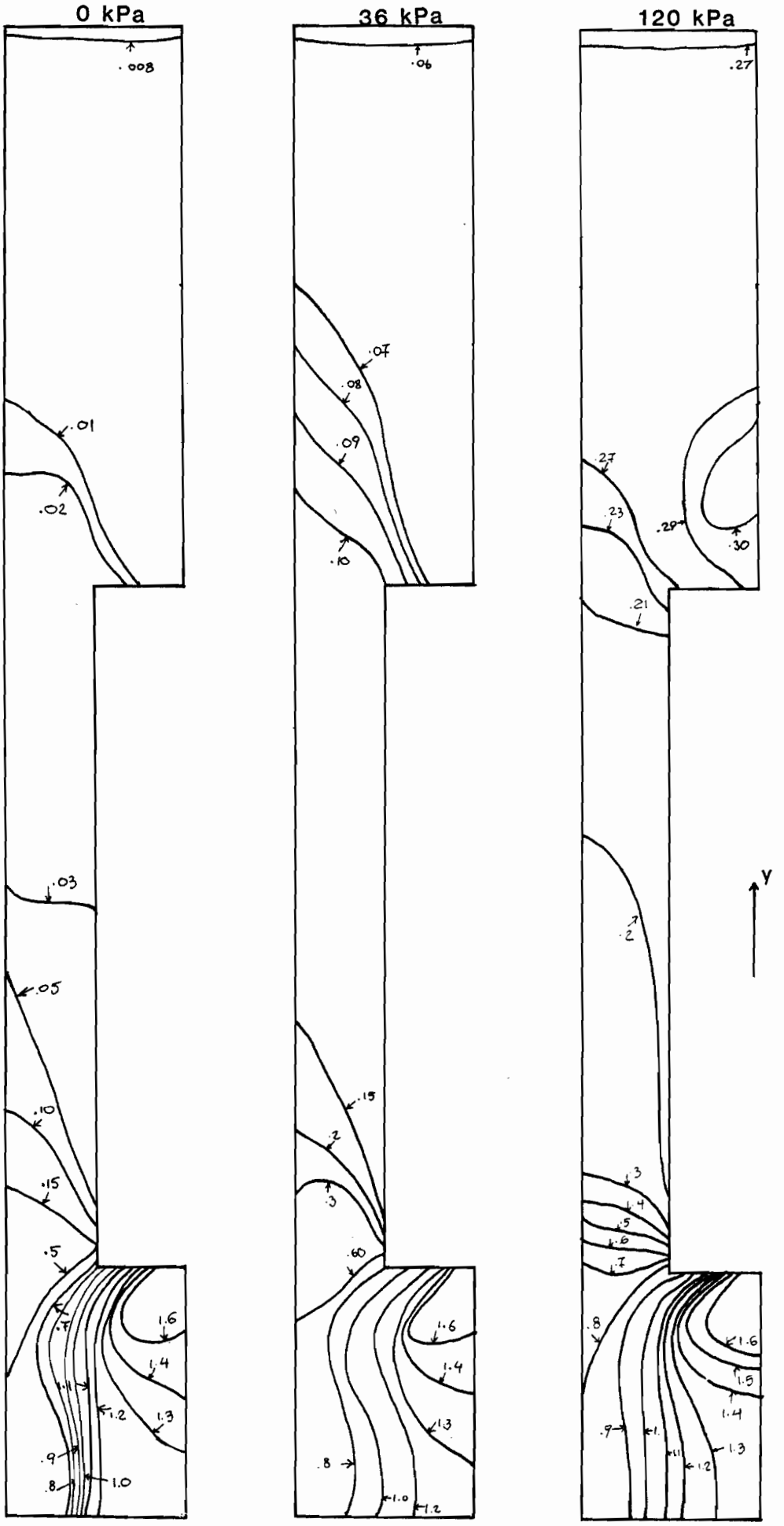

Fig. 5.15

with distance from the central line, vertically or horizontally. The decrease is significant along cross-section nodes located close to the container bottom, where nodes located close to the host rock-buffer interface show strain values half or less of the strain values along the same cross-sections on the central line. For higher depths the strains along the cross-sections are distributed quite uniformly. This pattern, that is almost independent of the overburden pressure values, demonstrates the dominant waste container weight effect on the buffer response in the zone underneath the waste container. The overburden pressure effect is indicated when observing the sizes of the strain bulbs developed in Fig. 5.15, where with the overburden pressure increasing from 0 to 120 kPa the strains show an increase of approximately 7%. This increase is not quite clear in Figs. 5.13 and 5.14, where the obtained bulbs are quite the same in size and shape. The overburden pressure is transferred to the lower buffer zones after longer time periods than the waste container weight because of the buffer compressibility, soil-fluid redistribution and other stress transfer mechanisms. When the overburden pressure is appreciably transferred to the lower buffer zones, the effect in the strain bulb intensity and shape is indicated.

Along the zone around the waste container, the vertical strains increase with overburden pressure increasing quite clearly, at any time period. The maximum values at

this zone are obtained in the area close to the waste container top. Only when the overburden pressure is 120 kPa the strains show a decreasing trend at the area clsoe to the container bottomand then show a constant strain or even a small increase in the zone close to the container top, indicating the overburden pressure effect. The maximum vertical strains for this zone are less than half of the maximum values obtained underneath the waste container. It is expected that the friction generated along the interfaces in that zone would affect the size of strains developed.

When approaching the container top a decrease in strains is observed when pressure is 0 kPa and 36 kPa. The maximum resulting strains are 0.01% and 0.05% respectively. The separation observed at this zone for these pressure values seems to produce a "relief" and a decrease in the vertical compressive strain pattern. The buffer is compressed vertically when pressure is 120 kPa. Maximum strains at .3% are reached in a large part of this zone, indicating uniform vertical compression.

From the finite element model analysis of the vertical strains it can be concluded that vertical strain concentration is expected in the zone underneath the waste container bottom. The increase in overburden pressure will affect the extent of the strain bulb in that zone by increasing it by 7% when pressure increases from 0 to 120 kPa; this effect will be more pronounced at longer

time periods (15 to 18 days). Around the waste container smaller vertical strains are expected indicating that this zone is equally affected by the two loading sources. Above the waste container the buffer shows the lowest vertical strain values, obviously due to the low stresses developed, that are caused by the overburden pressure and by the yielding of the supporting container and the buffer around it.

5.4.2 Shear Strains

The shear strain - ε_{xy} - contours are plotted in Figs. 5.16, 5.17 and 5.18 and appear to provide useful observations and patterns of deformations. While from the vertical strain contours it was shown that the waste container weight clearly is the predominant source of strain, the overburden pressure effect is now equally crucial. Several comments can be made on the maximum values of the shearing strains at certain zones, on the signs of these strains indicating the rotational directions of the nodes, the zones of strain concentration and their dependence on the time and overburden pressure variables.

The zones of higher shearing strain concentration are located close to the bottom corners of the waste container, where the shearing stresses acting on each element prevail against thenormal ones. The maximum values

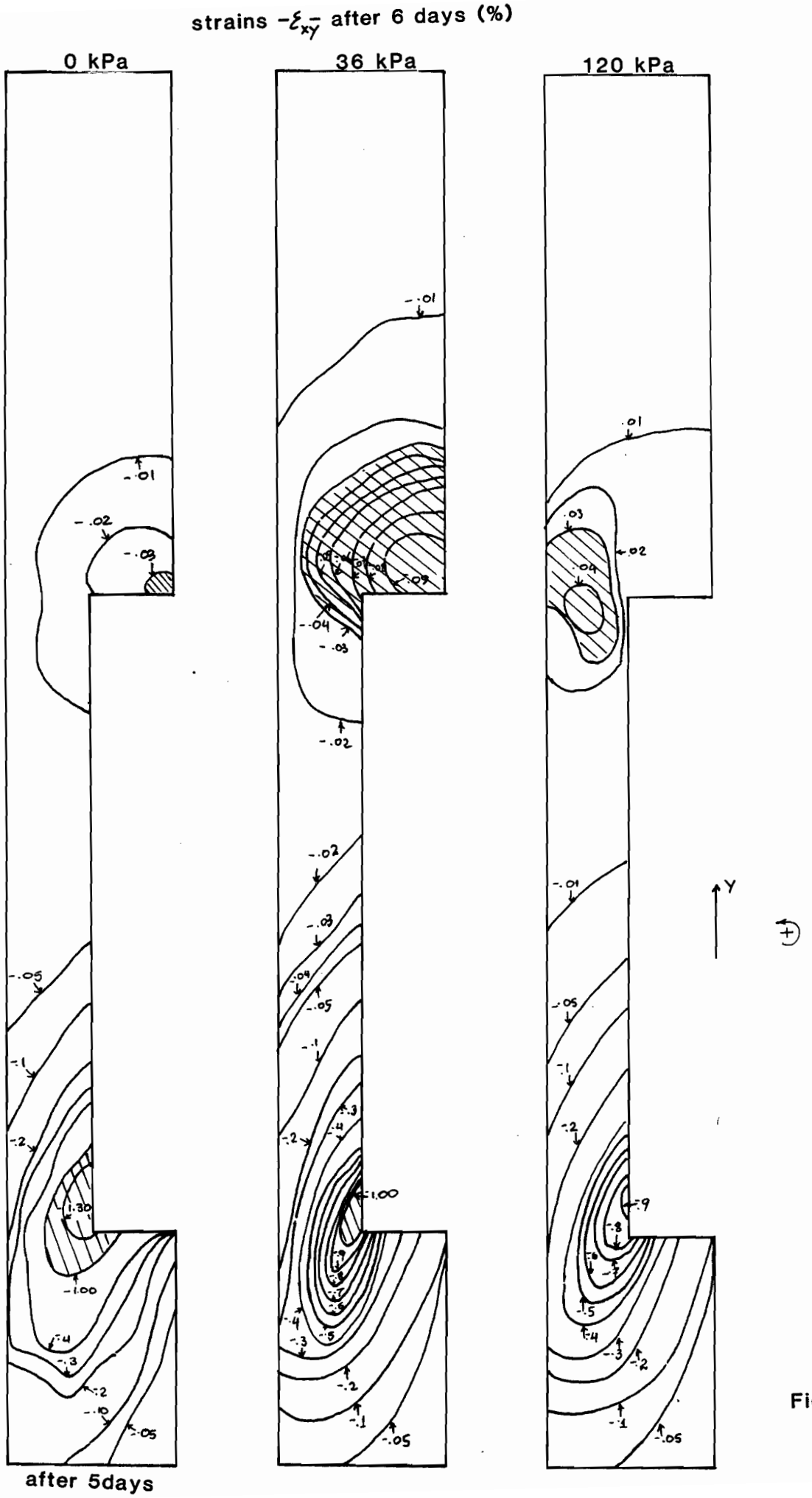
strains $-\varepsilon_{xy}$ after 6 days (%)
0 kPa
36 kPa
120 kPa
Y
+
after 5days

Fig. 5.16

strains $-\varepsilon_{xy}$ 12 days (%)

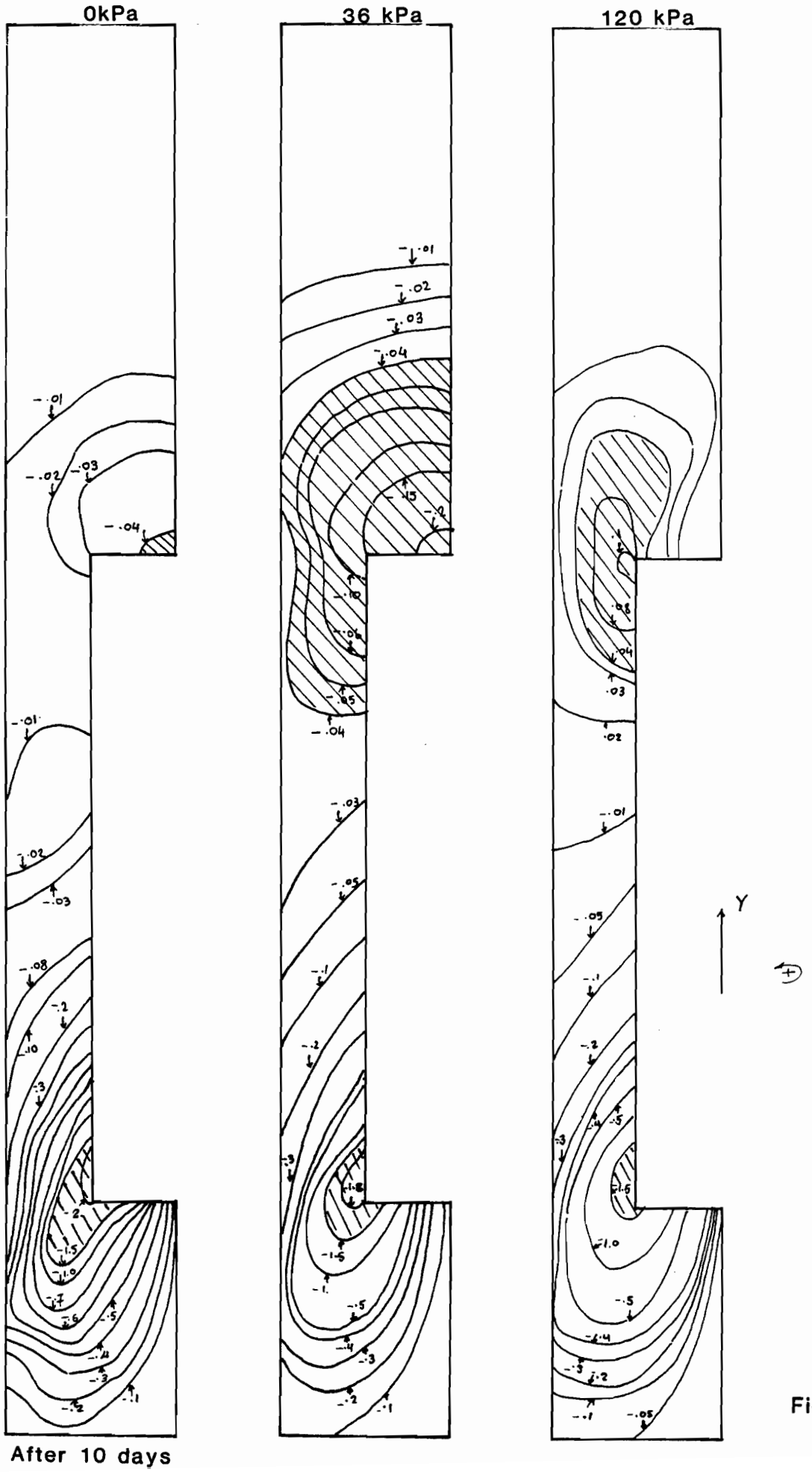

Fig. 5.17

Final strains $-\varepsilon_{xy}$ (%)

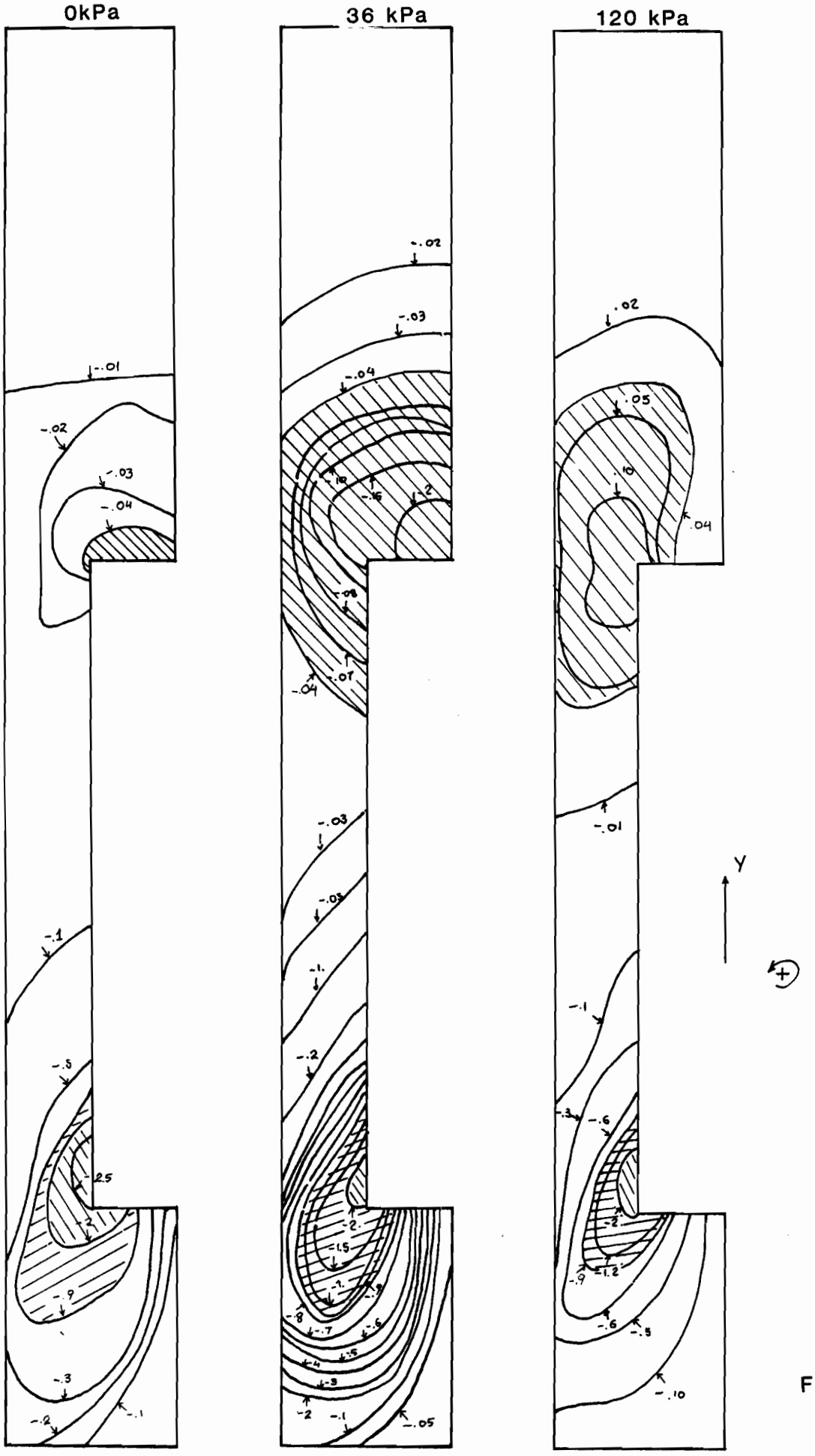

Fig. 5.18

obtained are 2.5% in that zone. In the zone underneath the container and along a significant part of the zone around it the buffer shows a clockwise rotational trend for all three cases of overburden pressure. In the finite element analysis this trend is caused by the interaction between the stresses developed at elements underneath the loading waste container and those located around the waste container that seem to be "pulled down" towards the container bottom.

In the actual condition friction generated along the buffer-waste container interface should increase this rotational pattern of the buffer. The shearing strains are reduced with increasing depth from the waste container bottom and distance from the central line decreasing. The overburden pressure causes significant change in the shearing strain patterns observed. It is clear from Figs. 5.16, 5.17 and 5.18 that when the pressure at the surface top increases from 0 to 120 kPa the shearing strains are decreasing for every time period examined. The shearing strain bulbs are overburden pressure dependent as shown in these figures. The overburdenpressure effect is clear for almost half of the zone underneath the waste container. Close to the disposal hole bottom the strains reach small values and are virtually independent of the overburden pressure effect. The effect of the overburden pressure on the developed shearing strains is inter-related with the increased normal stresses on every element

with pressure increasing compared with the corresponding shearing stresses on the same element. When overburden pressure increases from 0 to 120 kPa the normal stress acting on one element in that area increases from 0 or 1/10 to 1/3 of the shear stress acting on that element. This increase in pressure causes increased vertical strains as it is already shown in 5.4.1 and decreased shearing strains at the same zone. The same pattern of deformation is observed along the zone around the container with shearing strains reaching a maximum value of approximately 1%. The same rotational direction is shown, towards the waste container. The overburden pressure effect is clear once more when approaching the waste container top. Two different shearing patterns are indicated. When over-burden pressure is 0 and 36 kPa due to the yielding support, i.e. the separation at the container top, the buffer shows a trend of moving toward the gap obtained with higher strains close to the central line with clockwise direction. This gap causes increased shear stresses on the elements above the waste container due to lack of support - moved container - which although do not reach any high values, are related to the shear strains, particularly in this zone. The normal stresses acting on every element were transferred not through the support, since there was no contact between buffer and container, but through the shearing resistance at the sides of each element. This stress condition is related to the shearing strain

development in this area.

When overburden pressure is 120 kPa as already mentioned, no gap was observed at the top of the waste container. The pattern of shearing deformation is quite different from that observed for the low pressure values. Higher shear strains are obtained in the zone close to the top corner of the container. The rotational direction is counter-clockwise and indicates the buffer trend of moving towards lower stress levels. The normal stresses acting on the elements at the top of the container are transferred through the support that behaves as a non-yielding one. The shearing is now developed where the yielding support is and this is the buffer around the container. The higher strains are mainly located at the points close to the container buffer interface.

In Fig. 5.19 the structural model of the zone above the container top is illustrated. The zone is considered as a multi-supported beam. In the same figure buffer nodes of deformation are shown.

The shearing strain patterns obtained from the finite element analysis demonstrate the importance of developing high overburden pressure values. Under these values shearing strains are eliminated throughout the buffer, normal strains prevail and result in a uniform compression of the material.

ABOVE THE CONTAINER : SHEAR GENERATION ZONES

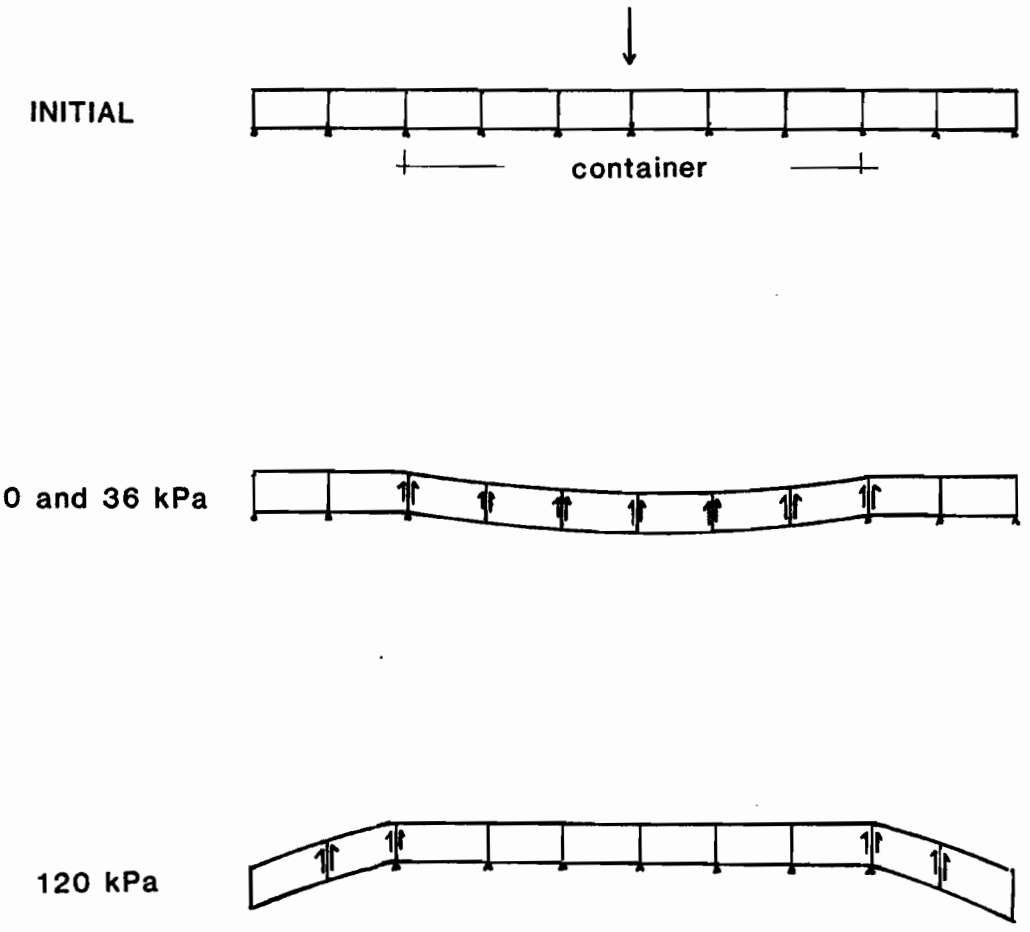

(a)

MODES OF BUFFER DEFORMATION

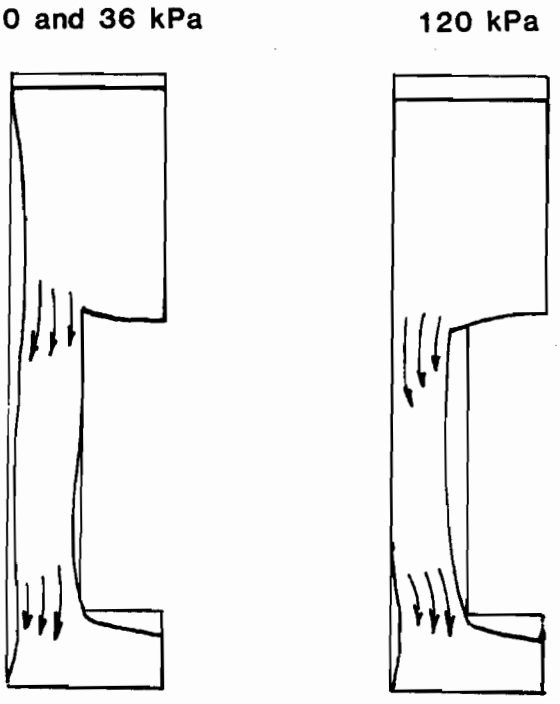

(b)

Fig. 5.19

5.5 Stresses

The final and probably the most important part of the finite element analysis of the disposal system, is the derivation of the stress component distribution patterns along the buffer surface. In Figs. 5.20, 5.21 and 5.22 the final stress component contours are plotted. In order to investigate the overburden pressure effect on the stress pattern development, the stress contours for three different overburden pressure values are plotted in the same figure.

It is clear from Fig. 5.20, where the vertical stress contours are plotted, that the zone of the highest stress concentration is located underneath the waste container. With overburden pressure increasing the vertical stresses increase as well. The stresses on the elements that are in contact with the waste container bottom show a $\pm$ 6-8% deviation from the expected values, i.e. approximately the waste container weight plus the overburden pressure, for these elements.

These vertical stresses decrease with depth from the waste container bottom and when approaching the host rock-buffer interface. For the overburden pressure values of 0 and 36 kPa a significant decrease in the vertical stresses are observed when approaching the container bottom corners, indicating that the waste container weight mainly affects a bulb restricted by the container bottom, the host rock boundaries and two imaginary lines that

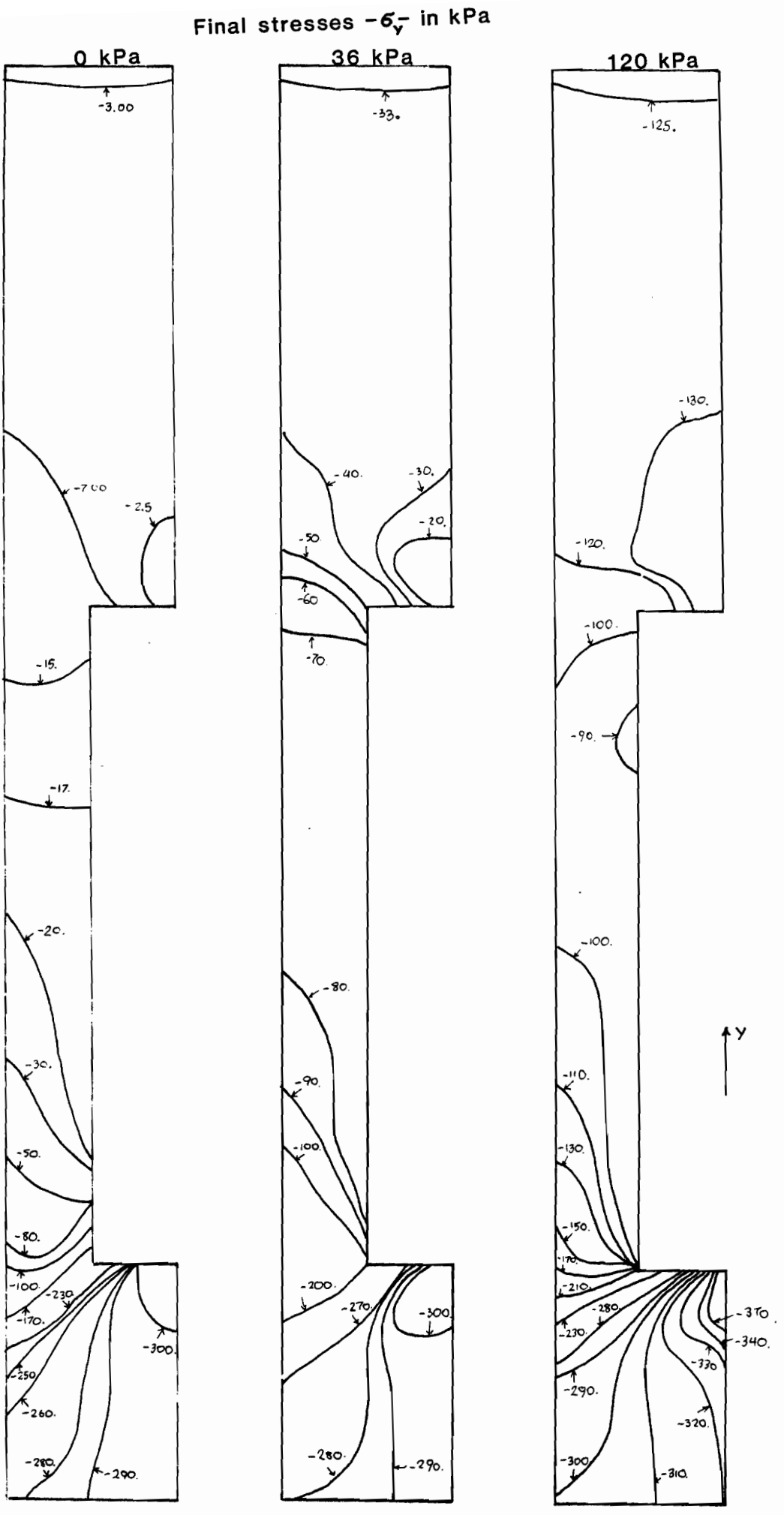
Final stresses $-\sigma_y$ in kPa
0 kPa
36 kPa
120 kPa
-3.00
-7.00
-2.5
-15.
-17.
-20.
-30.
-50.
-80.
-100.
-230.
-170.
-250.
-260.
-280.
-290.
-300.
-33.
-40.
-30.
-20.
-50.
-60
-70.
-80.
-90.
-100.
-200.
-270.
-280.
-290.
-300.
-125.
-130.
-120.
-100.
-90.
-100.
-110.
-130.
-150.
-170.
-210.
-280.
-230.
-290.
-300.
-310.
-320.
-330.
-340.
-370.
y

Fig. 5.20

Final stresses $-\tau_{xy}$ in kPa

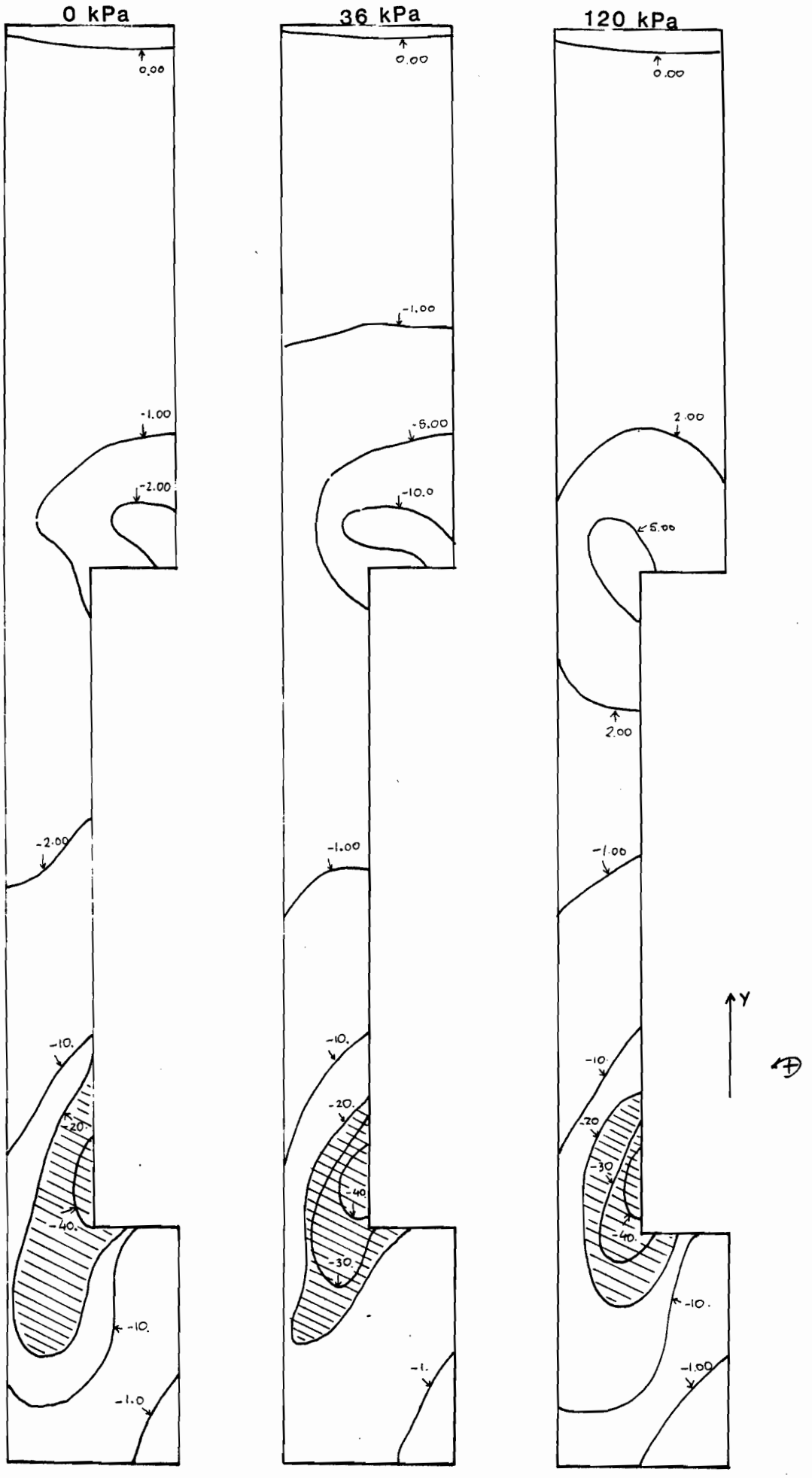

Fig. 5.21

Final stresses $-\sigma_x-$ in kPa

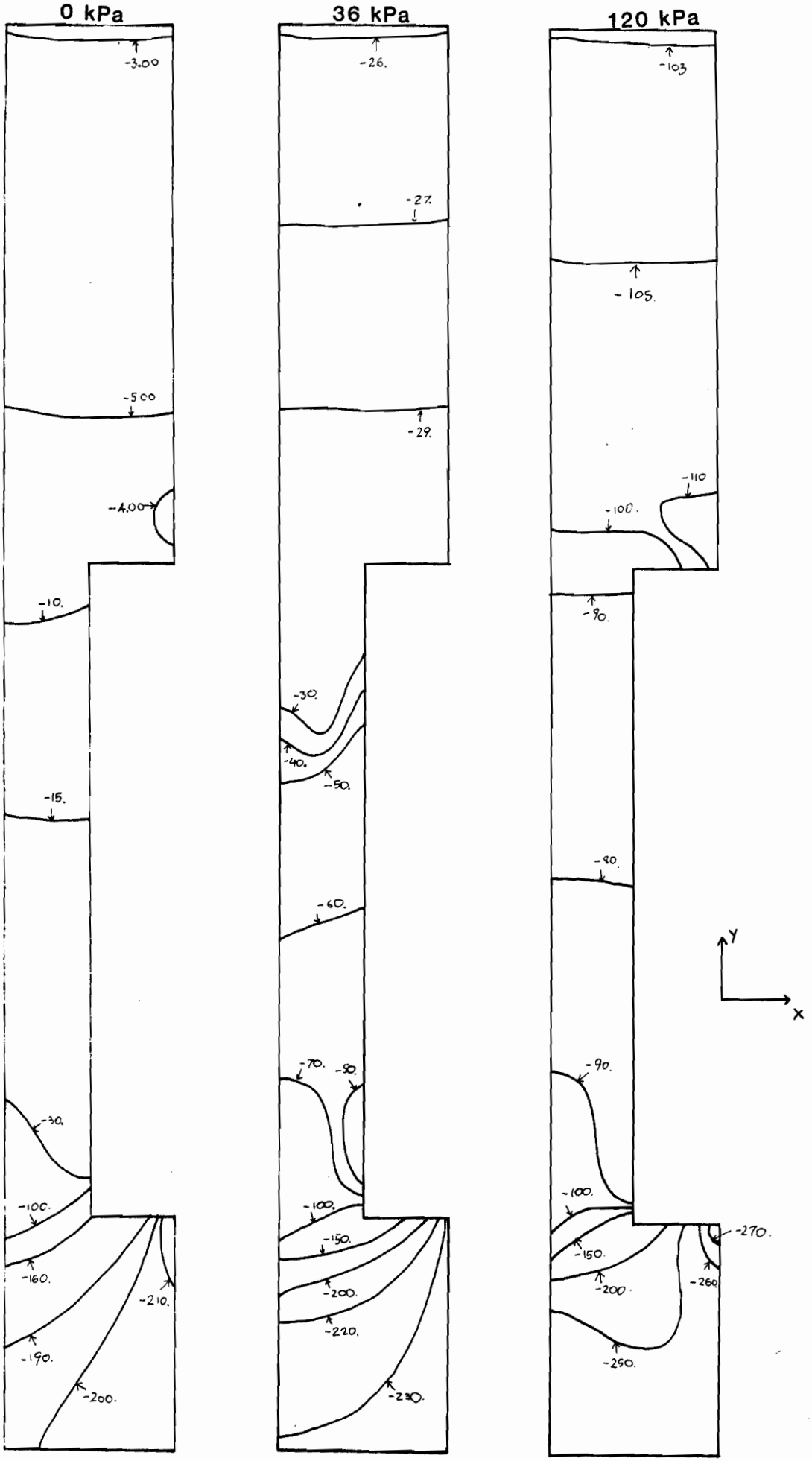

Fig. 5.22

originate from the container bottom corners with a 45° slope fromthe horizontal and terminate atthe host rock boundaries. The same pattern can be expected for the high overburden pressure value of 120 kPa although this bulb is less clear due to the increased overburden pressure effect.

In an attempt to correlate the vertical stress fields obtained for the zone underneath the waste container with vertical stress field obtained using the elasticity theory, the formulae derived by Foster and Alvin (1954) for circular loading on a semi-infinite zone and the solution tabulated by Milovic (1970) that considered circular loading of a finite layer underlain by a rigid base, are used. The results, shown in Fig. 5.23, clearly demonstrate the side boundary effect on the increased buffer rigidity. The effect of confinement on buffer response will be investigated in Section 5.7.

The vertical stresses in the zone around the waste container reach smaller values which decrease with decreasing distance from the container top. When the overburden pressure is 120 kPa stress concentration is observed at the top of the waste container as the buffer is compressed towards the container top.

In Fig. 5.21 the shearing stresses which are developed throughout the buffer are plotted. For the three overburden pressure values the maximum shearing stresses obtained are 40 kPa and are located in the zone around the

VERTICAL STRESSES IN PERCENT OF NORMAL CONTACT PRESSURE AT a-a

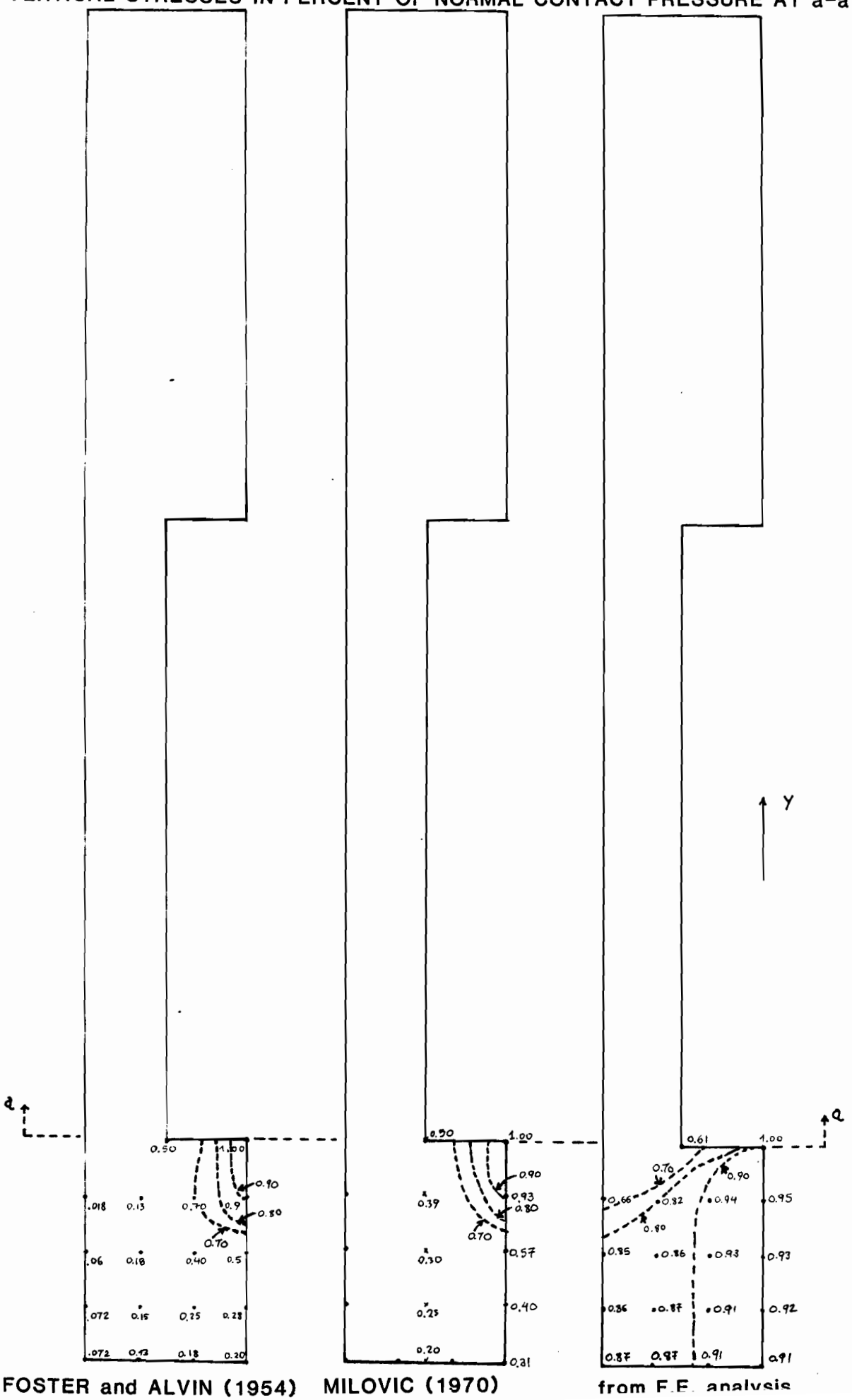

FOSTER and ALVIN (1954) MILOVIC (1970) from F.E. analysis

Fig. 5.23

container bottom corners where shearing patterns of deformation are most significant, as already mentioned in Section 5.4. It is indicated through the shadowed zones that the overburden pressure affects significantly the shearing stress pattern development by decreasing the overall shearing stress components when the pressure increases from 0 to 120 kPa.

In Fig. 5.22 the lateral stress contours are plotted. Higher stress values are once again developed in the zone underneath the waste container (highest lateral stress value of 270 kPa and is obtained when overburden pressure is 120 kPa).

The boundary confinement effect on the buffer response is again indicated as a result of the comparison between elasticity solutions (Milovic, 1970) and the finite element results. The finite element analysis indicates lateral stresses are approximately constant at the zone underneath the container ranging from 0.61 to 0.68 of the contact pressure. On the contrary elasticity solutions give rapid decrease with depth with a maximum stress value of 0.55 and a minimum of 0.05 of the contact pressure. The latter was obtained when approaching the disposal hole bottom.

The examination of Figs. 5.20 through 5.23 leads to the following observations:

1. Stress concentrations at the bottom of the waste container and at the top of it as well, are indicated in all cases. Vertical σ_y, horizontal

σ_x and shearing τ_{xy} stress values are highest in the vicinity of the waste container bottom.

2. The zone transverse to the waste container does not generally experience high stresses.
3. The shearing stresses are significantly affected by the magnitude of the overburden pressure acting at the top surface in a manner indicating that the higher the overburden pressure value the lower the shearing stress development throughout the buffer.
4. The boundary confinement effect on the buffer stiffness is indicated through the finite element developed stress fields as compared to elastic solutions.
5. The observed stress distribution patterns are almost identical for all three overburden pressure values. The only case where the effect of overburden pressure is significant even on the shape of the stress distribution is for the shearing stress pattern developed at the top of the waste container. The zones of high stress concentration are the same for 0 and 36 kPa but differ from the one developed under 120 kPa. The difference is considered as a result of the gap observed at that area (waste container interface) and the stress development and transfer mechanisms which are then produced.

5.6 Effect of Confinement on Buffer Response

It is clearly obvious from both the experimental and analytical model analysis results the importance of the buffer confinement by the surrounding rock. The stress fields obtained from the finite element analysis compared to the simplified analytical solutions gave higher results indicating increased boundary induced material resistance.

In an attempt to obtain a clearer view of the effect of buffer confinement on teh buffer response an "extended" finite element mesh was used with the boundaries located at distances approximately 5B from the waste container where B is the waste container width (Fig. 5.24).

The new mesh consisted of 74 nodes and 106 elements (Fig. 5.25). In the new model the zone above the waste container was ignored for simplification. This resulted in one type of material in the disposal system with constitutive relationships derived from axisymmetrical CU tests. The boundary interfaces were once more considered smooth and the same solution technique as described in Section 5.1 was adopted. In order to obtain stress fields from the model, comparative with those obtained from the actual finite element model, the same boundary displacements were induced at the same boundary cross-sections. The case of overburden pressure equal to 120 kPa is examined in the subsequent figures.

In Figs. 5.26 through 5.28 the final stress component contours necessary to induce the same boundary displacements

Schematic presentation of the "extended" model

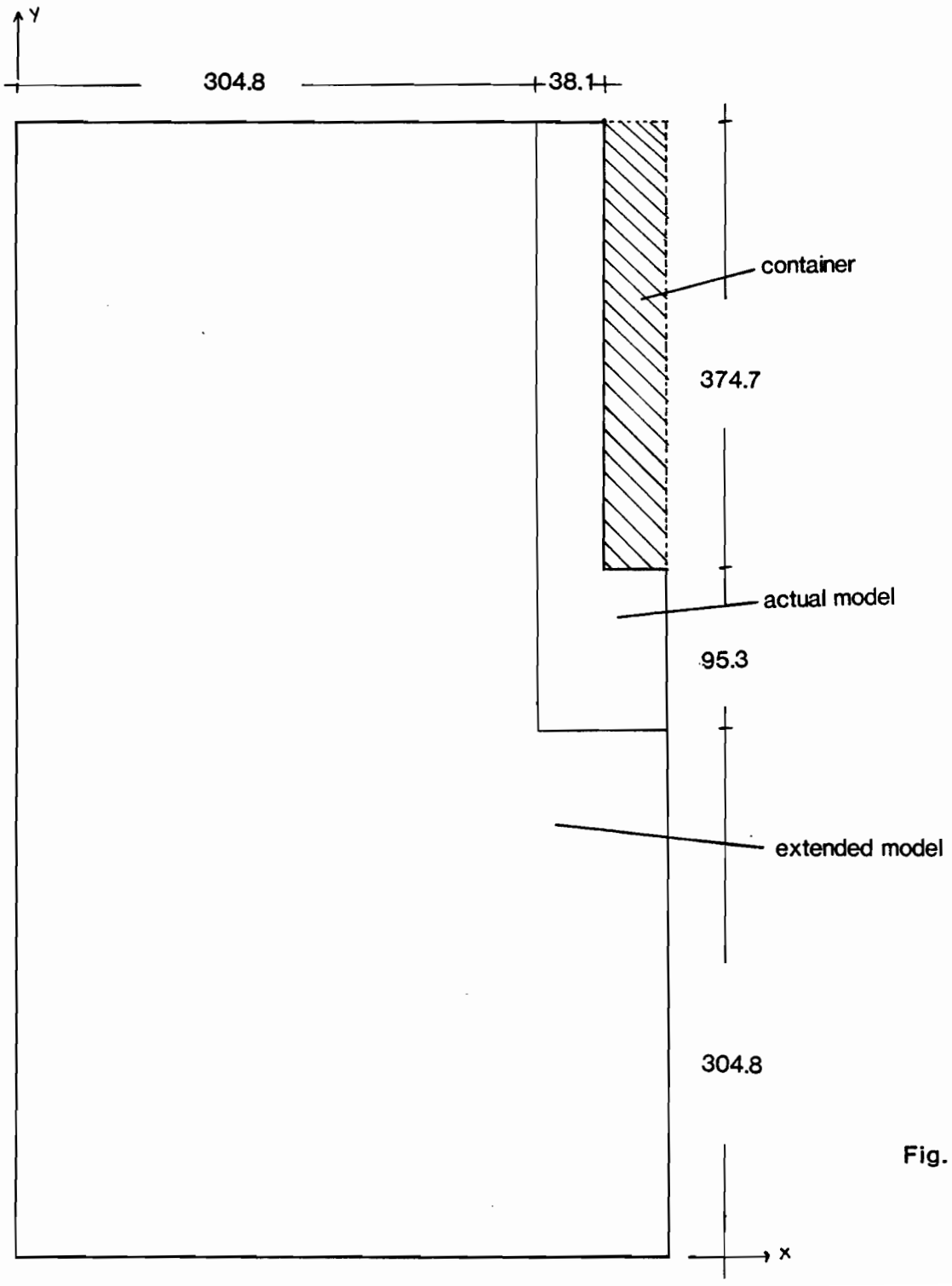

Fig. 5.24

Mesh layout for the "extended" model

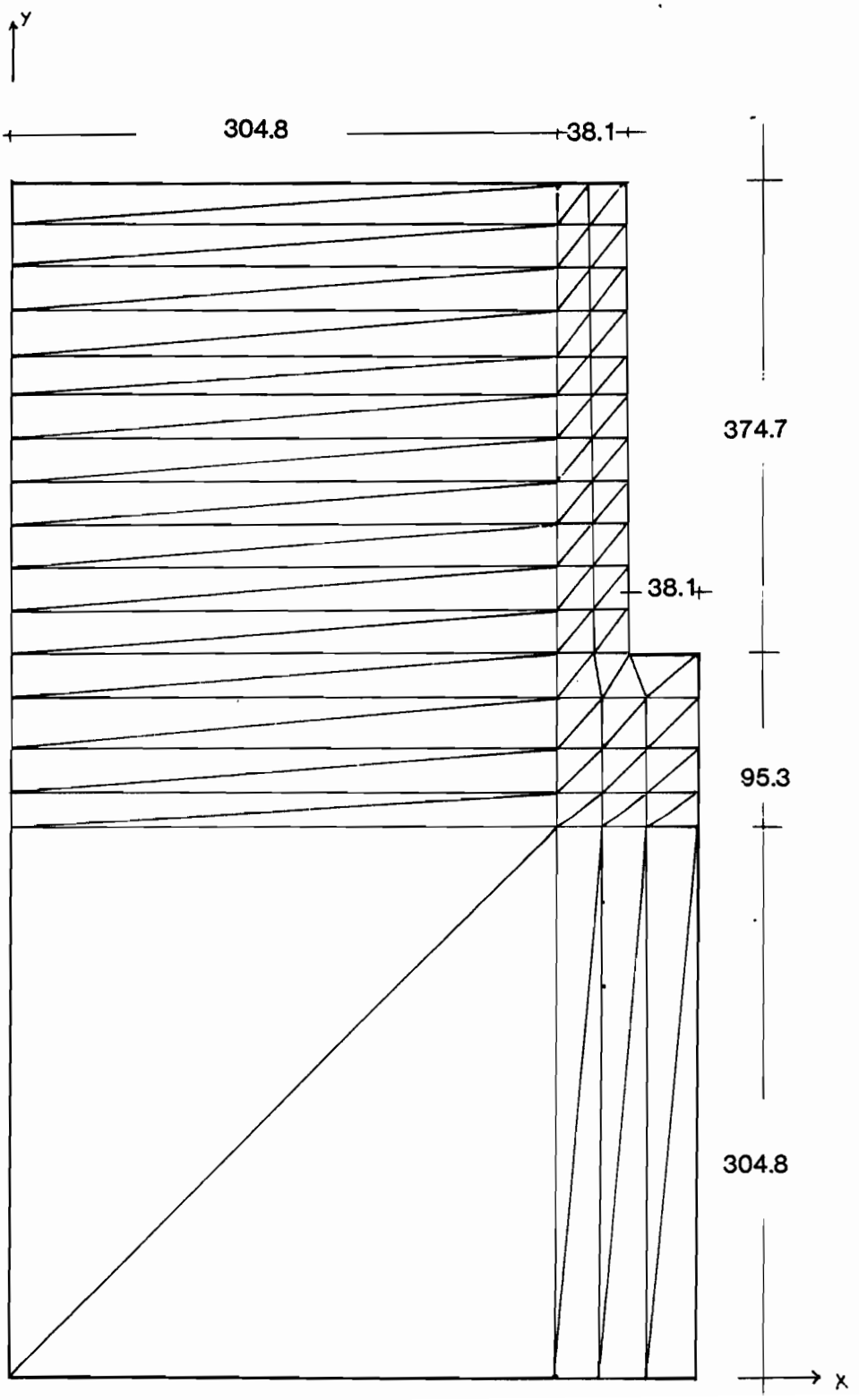

Fig. 5.25

Final stresses $-\sigma_y$ in (kPa

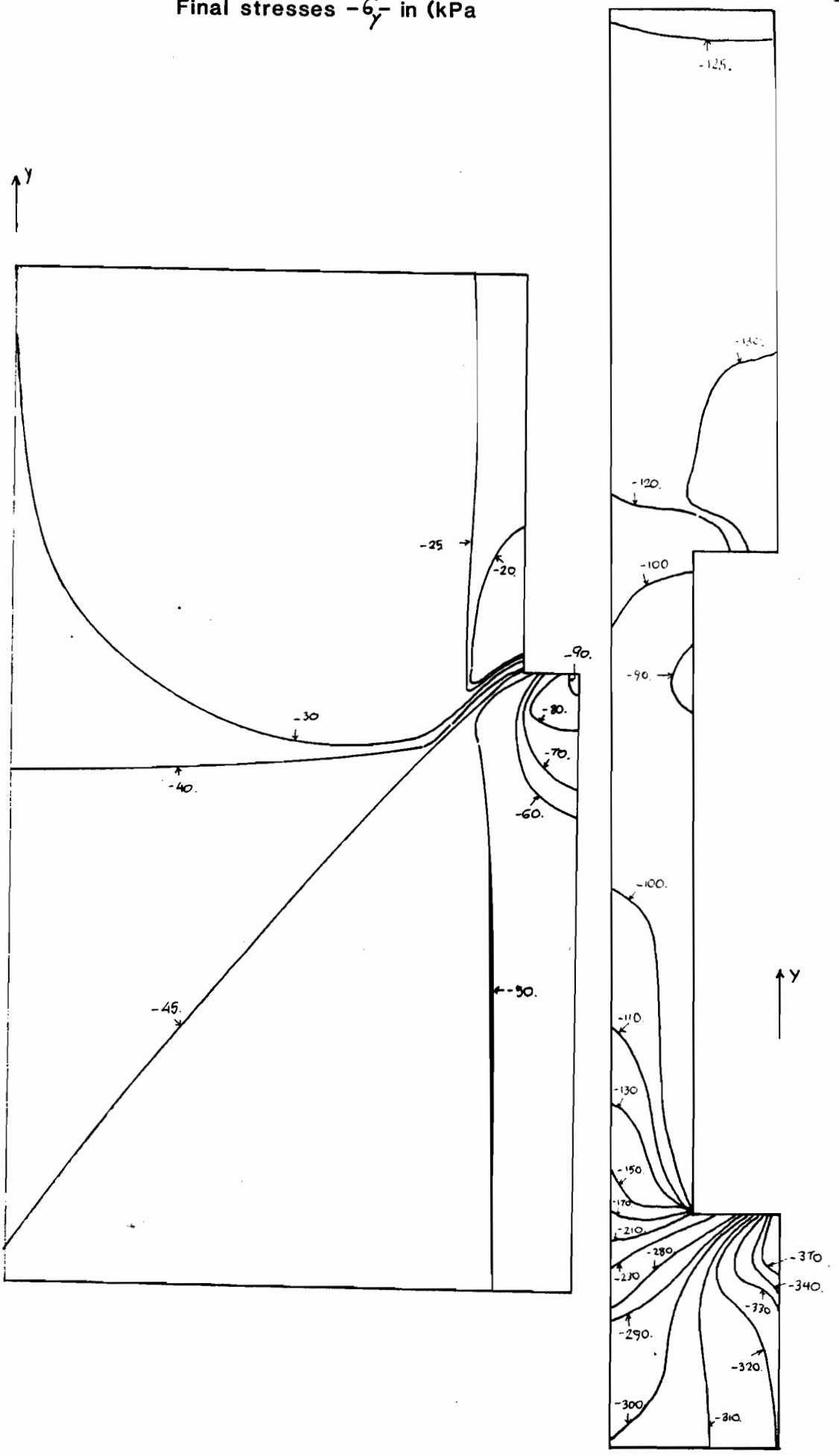

Fig. 5.26

Final stresses $-\bar{\sigma}_{xy}$ in kPa

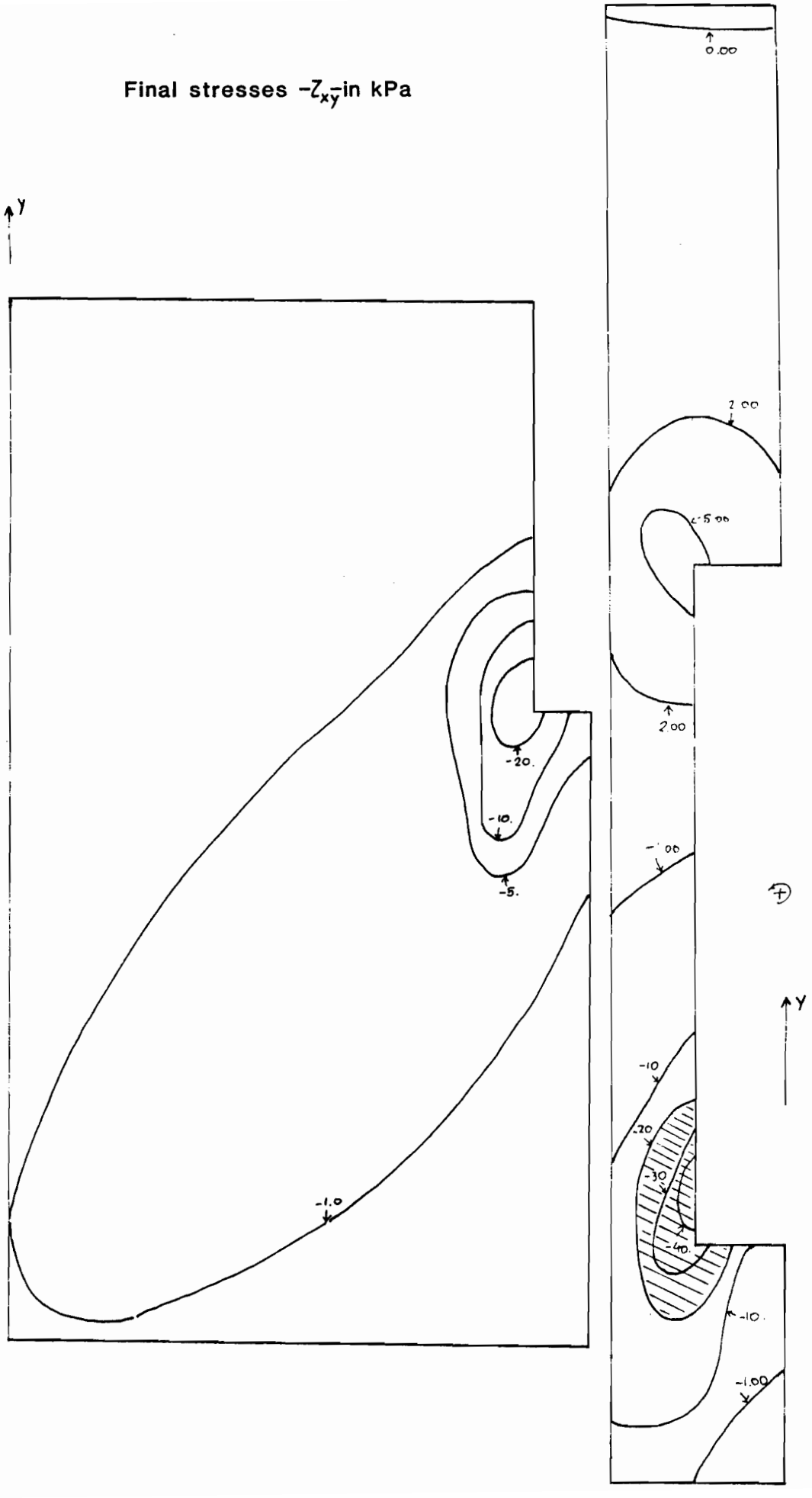

Fig. 5.27

Final stresses $-\sigma_x-$ in kPa

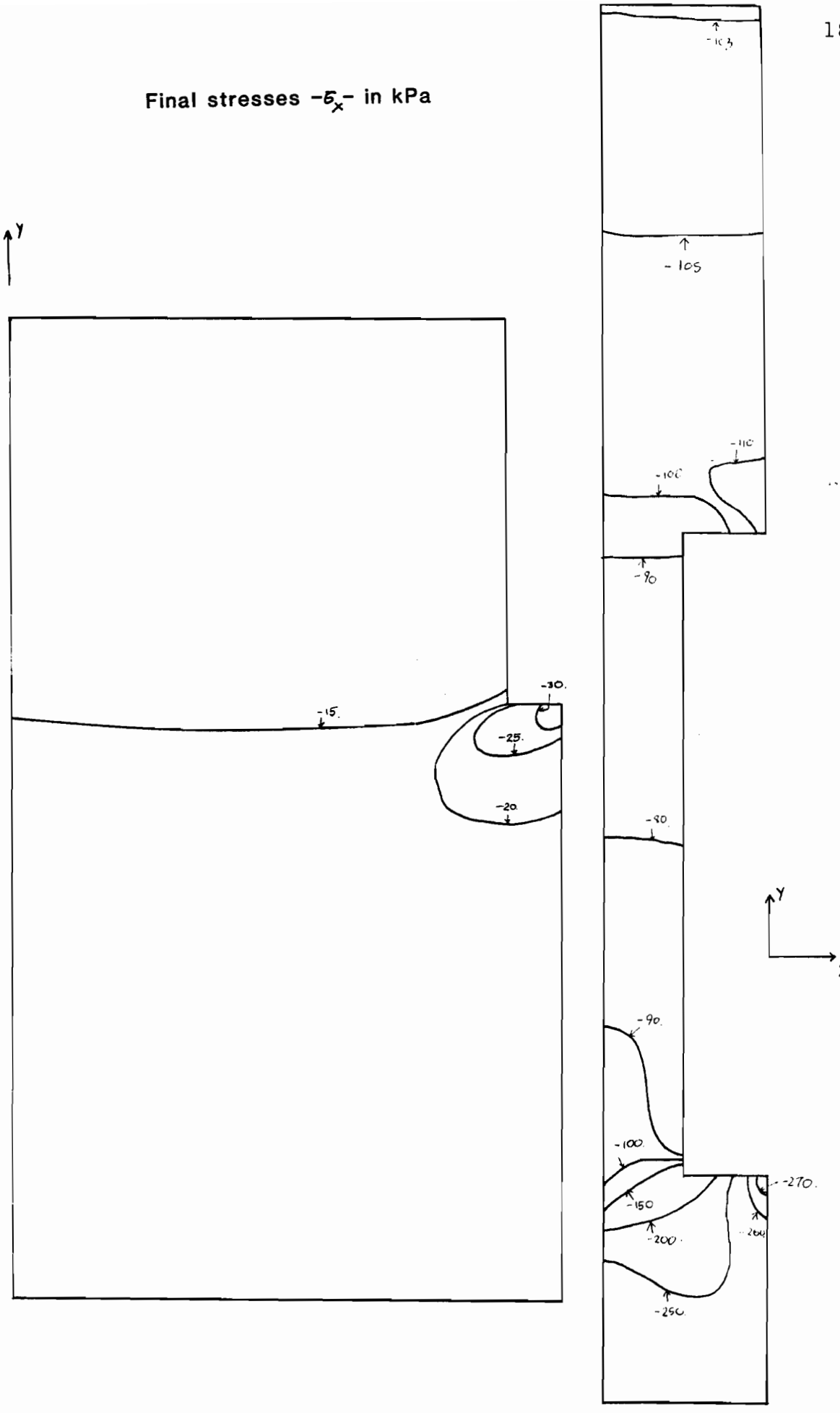

Fig. 5.28

are plotted. In Fig. 5.26 the stress patterns developed are presented. The stress values obtained areconsiderably small and the higher values are approximately 90 kPa or 25% of the corresponding high values obtained in the actual model.

The lateral stress component contours are shown in Fig. 5.28, where the maximum values obtained a small percentage, approximately 10%, of the corresponding values of the actual model.

The shearing stresses which are mainly developed in the vicinity of the waste container bottom corner do not seem to be so significantly affected by the boundary confinement. The effective bulb is approximately identical in area and stress intensity to the corresponding one in the actual finite element model.

The comparison between the stress fields developed in the two finite element models necessary to induce the same boundary displacements leads to the conclusion that the buffer performance is greatly improved due to the confinement by the host rock.

5.7 Comparison Between Measured and Predicted Results

This section presents comparisons between the experimental data reported in Chapter 4, and the finite element analysis presented in the previous sections of this chapter. Such comparisons permit a rational assessment of the admissibility and viability of the finite element method

as a means of predicting the buffer performance in the disposal system. In addition, this section examines the constraints and requirements imposed by the proposed analytical technique.

The discrepancies between the theoretical model and the physical conditions are also evaluated and their significance discussed.

The problem at hand is a mixed boundary value problem with the boundary conditions specified in terms of both displacement and stress. In such problems, the stress and velocity fields must be compatible as there is no apparent independence between the two fields. Therefore, it is essential to establish separate correlations of both the stress distribution and the soil deformation with the physical measurements, before the technique is judged to be satisfactory.

In the present study, the correlation is done in the following fashion:

1. The contours of the nodal displacements obtained from the finite element model proposed are superimposed on the contours obtained from the recorded grid deformation to demonstrate the similarities and discrepancies in the deformation patterns.
2. The boundary values of the calculated stress fields obtained from the finite element solution are compared with the boundary stresses which are imposed on the buffer.

5.7.1 Comparison Between Measured and Calculated Displacement Fields

In Figs. 5.29 through 5.37 the calculated displacement contours are superimposed on the corresponding measured ones.

It must be recalled that the host rock-buffer interfaces and the waste container-buffer interfaces are smooth and no friction is generated along these interfaces. It must also be recalled that in the finite element analysis provided, the boundary conditions were all described by means of boundary displacements that were the actual final measured boundary displacements at the cross-sections where loading was applied. At these boundary nodes as input displacement values, the average measured values along the boundary cross-sections were given (i.e. at the surface top and underneath the waste container).

The results presented in Figs. 5.29 through 5.37 offer a satisfactory predictive picture of the buffer deformation time history. At the same time they strongly demonstrate the importance of the assumptions adopted regarding the boundary conditions in this specific problem and indicate further improvement of these assumptions.

The finite element solution generally results in higher displacement values throughout the buffer. This is more clear along the zones around the waste container and must be attributed to the adopted boundary conditions, i.e. no friction along the interfaces.

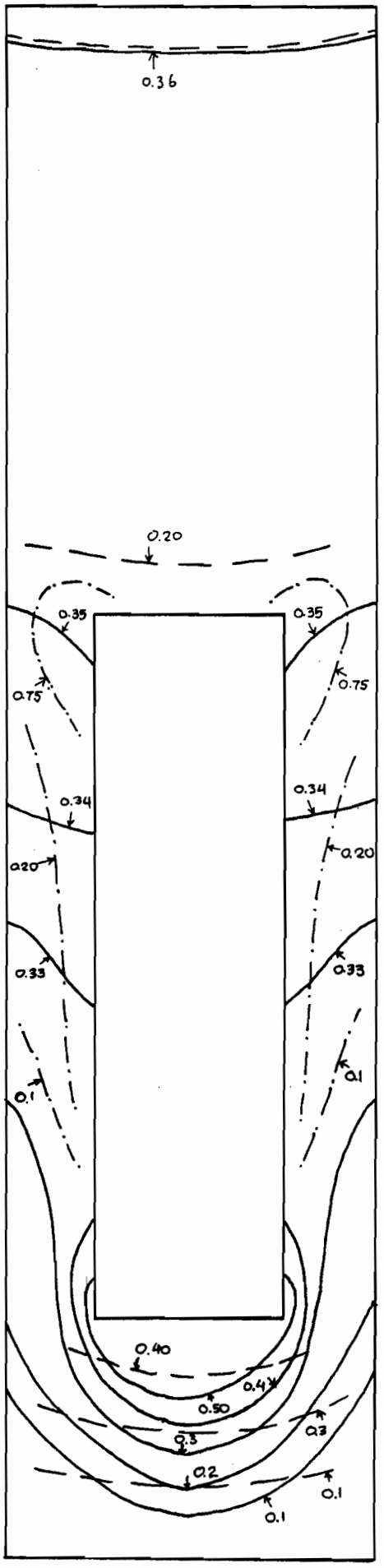

Vertical displacement contours

Overb. pr. : 0 kPa

after 5 days

——— : from F.E.

– – – – : measured

—·—·— measured upwar

(in mm)

Fig. 5.29

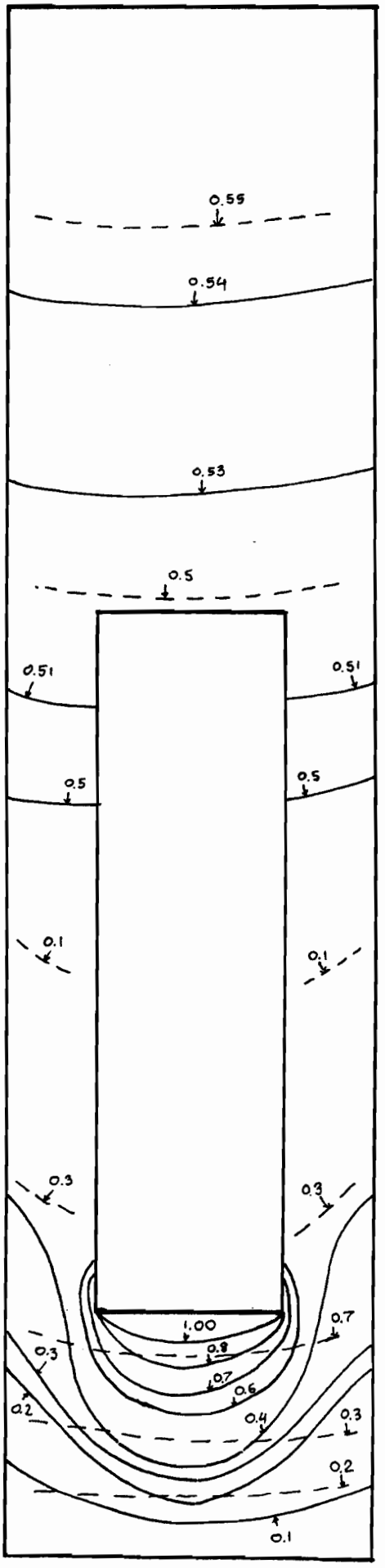

Vertical displacement contours

Overb. pr. : 0 kPa

after 10 days

——— : from F.E.

– – – – – – :measured

(in mm)

Fig. 5.30

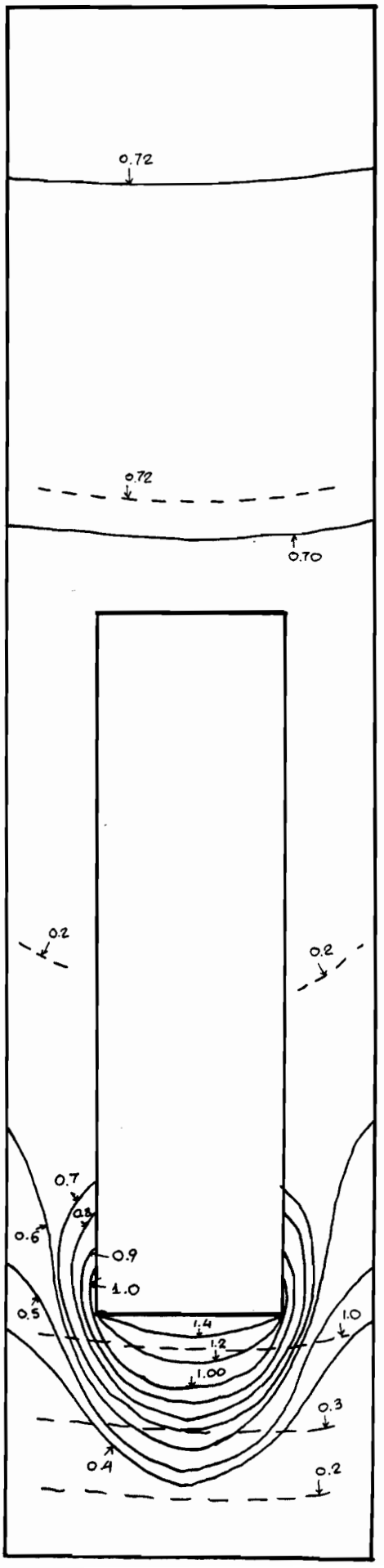

Vertical displacement contours

Overb. pr. : 0 kPa

after 15 days

———: from F.E.

– – – – :measured

(in mm)

Fig. 5.31

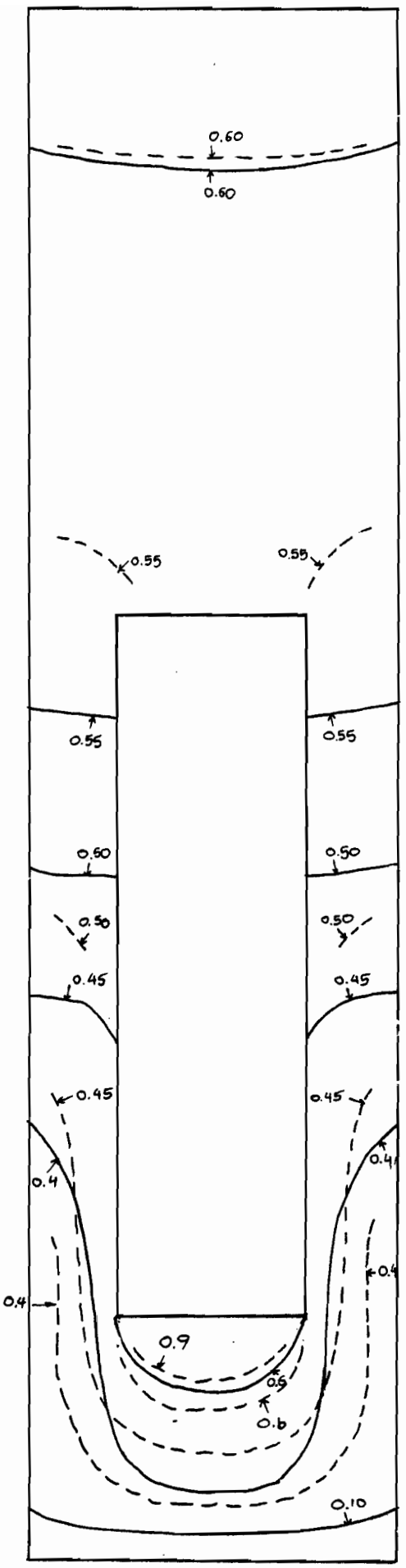

Vertical displacement contours

Overb. pr. : 36 kPa

after 6 days

———— : from F.E.

– – – – – : measured

(in mm)

Fig. 5.32

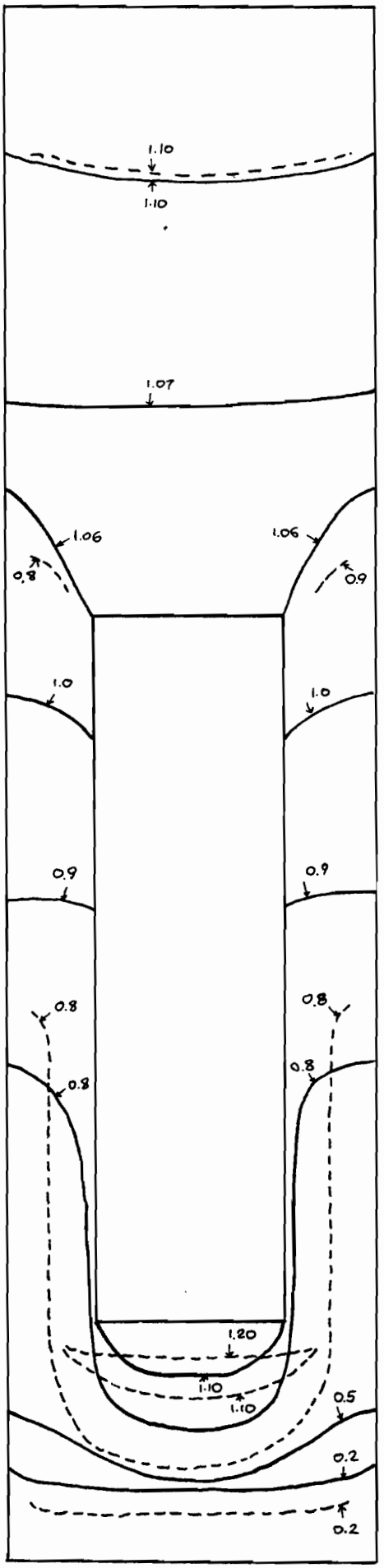

Vertical displacement contours

Overb. pr. : 36 kPa

after 12 days

——— : from F.E.

– – – – : measured

(in mm)

Fig. 5.33

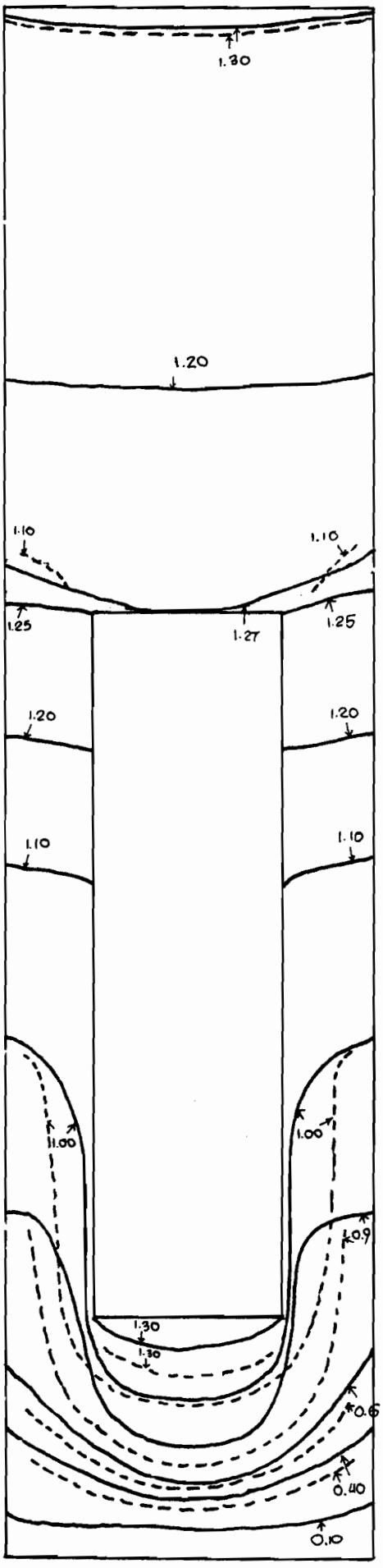

Vertical displacement contours

Overb. pr. : 36 kPa

after 18 days

——— : from F.E.

------: measured

(in mm)

Fig. 5.34

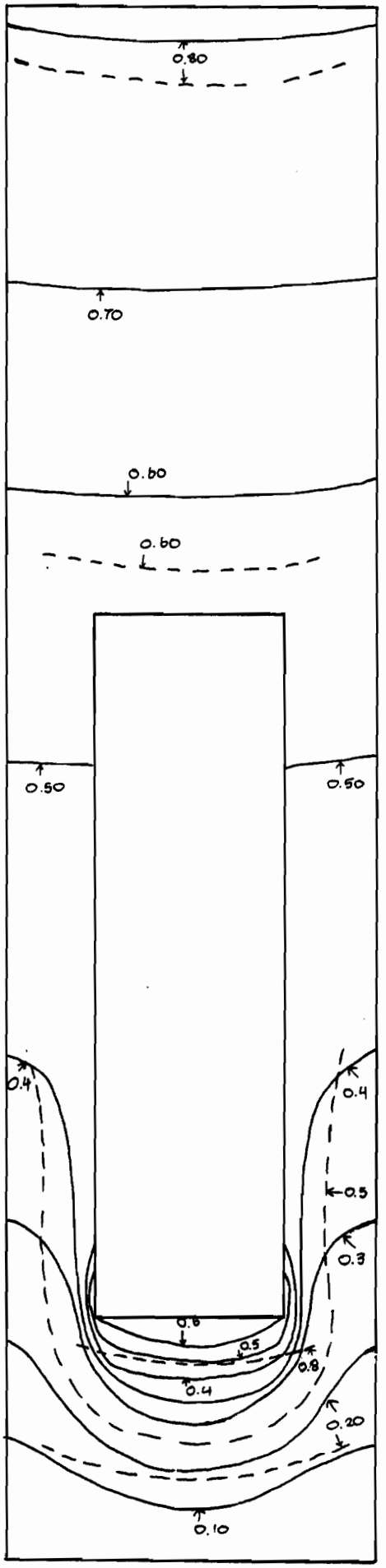

Vertical displacement contours

Overb. pr. : 120 kPa

after 6 days

———: from F.E.

– – – –: measured

(in mm)

Fig. 5.35

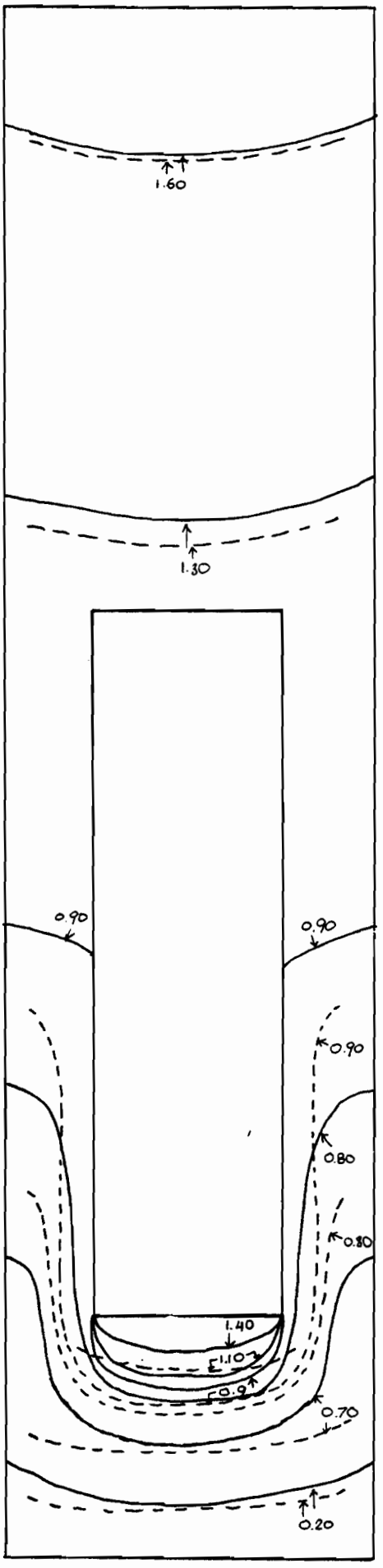

Vertical displacement contours

Overb. pr. : 120 kPa

after 12 days

——— : from F.E.

– – – — : measured

(in mm)

Fig. 5.36

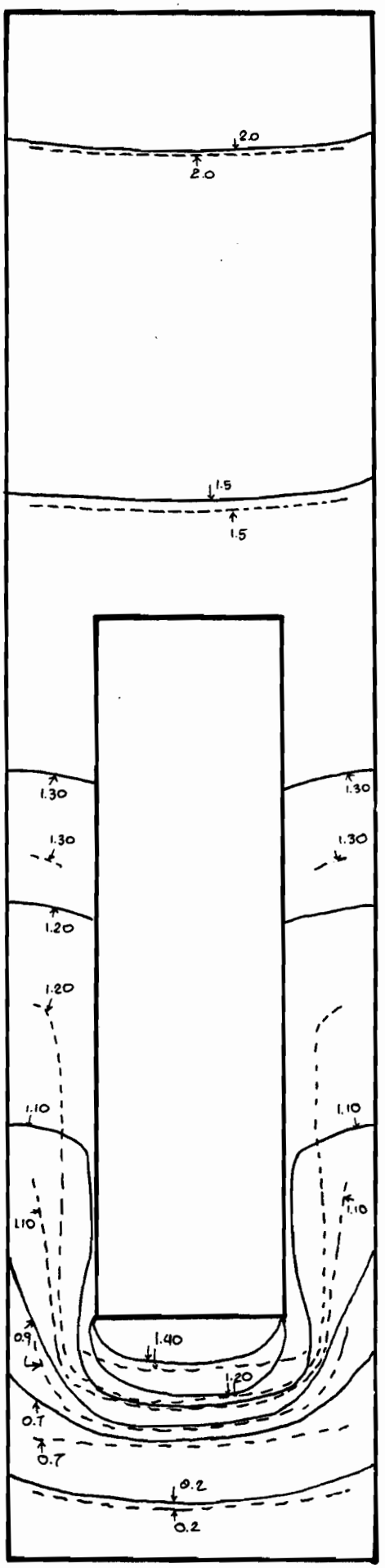

Vertical displacement contours

Overb. pr. : 120 kPa

after 18 days

——— : from F.E.

– – – – : measured

(in mm)

Fig. 5.37

Above the waste container as well as underneath it there is good agreement between the measured and calculated results. This agreement is improved with time and increasing overburden pressure. The agreement between the measured and predicted vlaues at the zone underneath the waste container is considered as very good for the final displacement contours, Figs. 5.34 and 5.37. Where disagreement is rather obvious is along the zone around the waste container and when overburden pressure is 0 kPa, where the measured values indicate an initial upward movement of the buffer.

As already mentioned, the superimposed results demonstrate the necessity of further improved boundary condition models in an attempt to predict the actual buffer behaviour quite accurately. What can be adopted in an improved finite element model is the use of the joint elements along the interfaces. These joint elements will represent the interface characteristics along the buffer-host rock and buffer-container discontinuities. The literature on the development and use of joint elements in structural engineering, rock mechanics and soil mechanics is quite extensive and several joint element models have been investigated in an attempt for a fully representative modelling of the discontinuities in concrete-steel interfaces, rock cracks and soil-machine interaction problems. Previous GRC studies have adopted thejoint element modelling when dealing with soil-cutting problems (Hanna, 1975).

5.7.2 Comparison Between Measured and Calculated Boundary Stresses

The boundary stresses calculated from the finite elements model solution are compared to the actual ones at the same boundary cross-sections. The stress values obtained from the finite element analysis at the top surface are in exceptional agreement with the actual ones at these boundary nodes. Both values, i.e. actual and predicted, are found to be quite close, only 4 to 8% apart.

This discrepancy can be attributed to factors such as the assumptions regarding the boundary conditions, i.e. smooth interfaces, and the constitutive realtionships used. The stress-strain curves used were CU axisymmetric test results and it is already proved (Campanella, Vaid, 1974) that when adopted for plane strain creep problems they yield lower stress values. Plane strain triaxial tests would provide more representative stress-strain curves for the particular disposal system model.

5.8 Water Intake Condition Finite Element Simulation

Simulation of the disposal system under water intake conditions has to deal with numerous problems which result from the buffer-absorbed water interaction characteristics.

New constitutive relationships under higher degrees of saturation must be used for certain zones of saturation

which vary with time due to the continuing water absorption process. Fluid flow through unsaturated swelling soil and its effects on the buffer engineering characteristics is the new condition. An acceptable procedure to simulate the disposal system under water intake conditions should consist of the general following steps:

1. Determination of the moisture profile at any time period, using the method described by Yong and Wong (1973)
2. Creation of saturation zones and adoption of appropriate constitutive relationships for every zone. Reference for this procedure is a previous GRC study reported by Yong, Sciadas and Siu (1982)
3. Solution for every time period of the F.E. model after the zones are defined and described by the appropriate constitutive relationships and the buffer swelling characteristics.
4. Steps No. 2 and 3 are repeated with new saturation zones as the water front advances.

The procedure previously described deals with the continuously varying buffer response due to the water absorption by using different types of engineering materials, i.e. described by different constitutive relationships.

The most difficult part of this procedure is the appropriate modelling of the swelling potential of the buffer in a constitutive relationship pattern that would be also a function of the degree of saturation.

5.8.1 Long-Term Buffer Response Investigation Under Water Intake Conditions

In order to investigate the long-term buffer response under water intake conditions, a simplified finite element simulation was adopted. The strength of the buffer in the zones around and underneath the waste container was considered as decreased by 50% of the strength under the lower confining pressure of the CU tests (i.e. 172.4 kPa). In other words, for the zone around and underneath the waste container the stress-strain curve used, produced 50% lower stresses. The simplifying assumption mentioned above, concerning strength changes with saturation level in the simple model cannot be easily defended. The rationale for the model lies in the observation that strength does indeed decrease as saturation increases, and vice versa. This technique was used by Yong, Sciadas and Siu (1982) when dealing with the stability of unsaturated slopes with changing degrees of saturation. The results from this model were compared with the corresponding F.E. model results under no water intake conditions. It must be noted that in both F.E. models the input boundary pressure values simulated the backfilled tunnel conditions. Comparison showed that when, due to water intake the buffer strength becomes 50% lower, the settlements increase at the zone underneath the waste container by a ratio of 3 over the corresponding settlements under no water intake conditions. Maximum displacements in that zone reach the value of 7.44 mm (2.29 mm under no

water intake). An increase in settlements with an average ratio of 2.53 is also observed in the zone located above the waste container as a result of the increased buffer compressibility around and underneath the waste container.

In addition to the increased settlements, the lateral displacements are increased by a ratio ranging from 1.14 to 3.21. The developed strains also demonstrated the increased buffer compressibility due to the water intake. Increased vertical strains by a ratio of 3 over the corresponding ones under no water intake conditions were developed throughout the buffer area. The strain rates were higher under no water intake conditions and when correlated with the strains, it was shown that the time period necessary to reach the final strains was shorter under water intake conditions by 22% of the time period needed under no water intake conditions. The effect of the increased buffer compressibility on the time period necessary to reach the final strain values was also demonstrated through the experimental results and presented in Chapter 4.

From the comparison between the simplified water intake F.E. model and themodel under no water intake conditions, it can be concluded that even under these extreme conditions - strength of buffer decreased by 50% of the lower one under no water intake - the system stability is ensured, with maximum strain values reaching 7%, and higher displacements at 7 mm.

The buffer response under water intake conditions was furthermore investigated. The buffer strength at this time was considered as decreased by 84%. This percentage was selected after comparing the CBR test results - Table 5.2 - under soaked and non-soaked conditions. Under soaked conditions, the stresses necessary to produce the same penetration as under non-soaked conditions, were lower by an average value of 84% when compared to the corresponding stresses under non-soaked conditions. The F.E. analysis under these constitutive relationships, resulted in very

TABLE 5.2

Test Condition	Swell (%)	Penetration (mm)	Stress (kPa)
no soaking		2.5	675
		5.0	1175
		7.5	1583
		10.0	1767
		12.7	1933
soaked	2.6	2.5	117
		5.0	158
		7.5	208
		10.0	275
		12.7	383

high settlement values at the zone located underneath the waste container with a maximum value of 38.56 mm. Vertical strains at the same zone reached values averaging 36% under the same stresses which under no water intake conditions produced only 2% vertical strains. The results from this analysis where the buffer responds with a strength decreased by 84% indirectly demonstrate the

disposal system stability. It was shown that in order to obtain high strain values and unstable conditions, the buffer strength needs to become a small fraction, i.e. 14% approximately, of the corresponding buffer strength under no water intake conditions.

5.9 High Overburden Pressure Conditions Simulation

It has already been mentioned that the theme of this investigation concentrates on the long-term creep characteristics of the buffer material under both operating and extreme loading conditions that should be caused by certain unaccountables.

The buffer response was investigated under simulated high overburden pressure conditions through the F.E. technique. The results obtained are summarized in Figs. 5.38, 5.39 and 5.40 and demonstrate the effect of the overburden pressure on the waste container developed settlements, on the final vertical strains which are developed along the zone underneath the waste container and on the time required for the final strains to be achieved, or else for the system stabilization to be obtained. In this simulation it is assumed that the total amount of the overburden pressure imposed on the buffer top surface is transferred to the bottom of the waste container, hence to the buffer material underneath it. The buffer response was investigated up to 960 kPa of overburden pressure, or 8 times

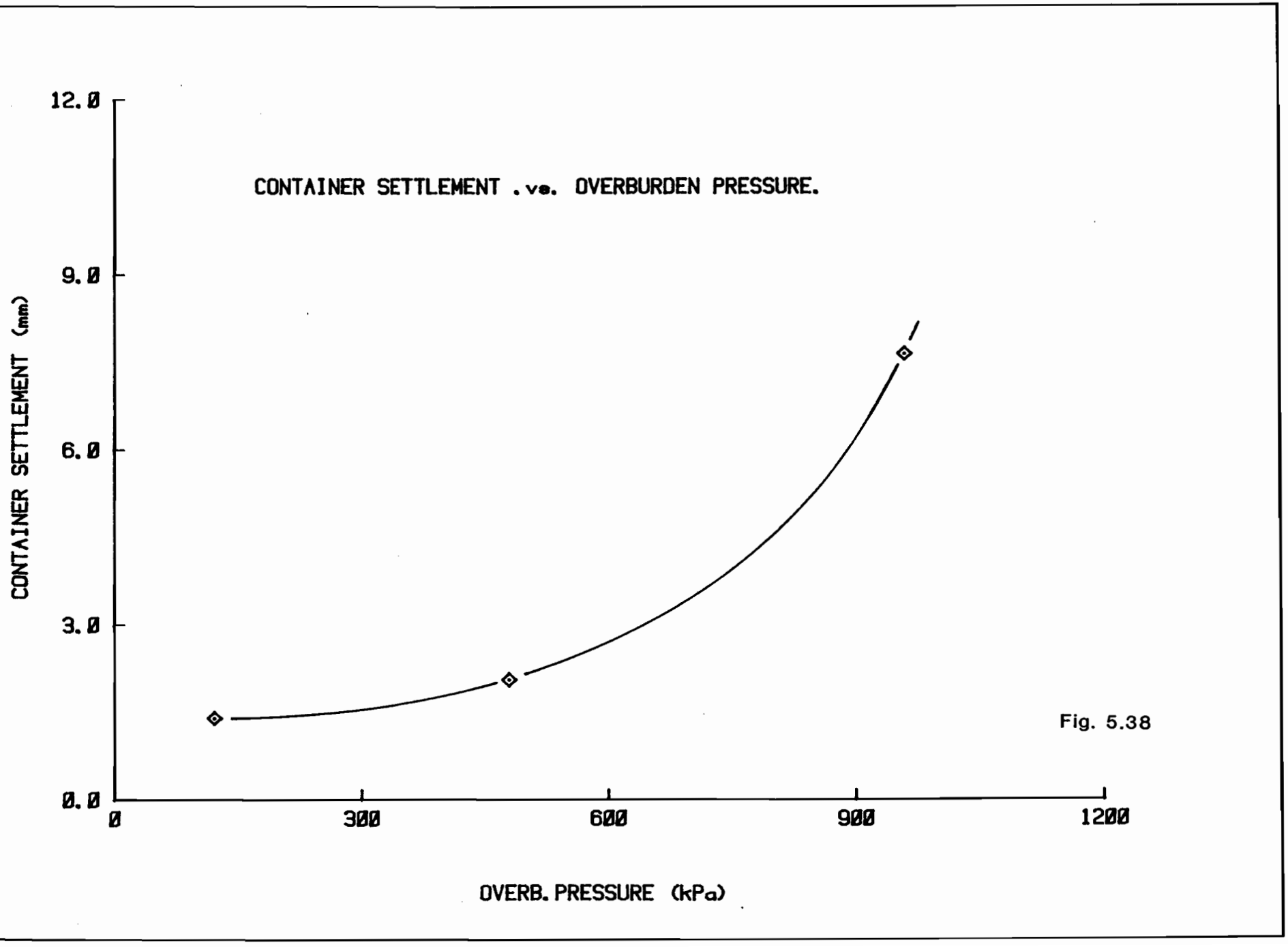
CONTAINER SETTLEMENT .ve. OVERBURDEN PRESSURE.
CONTAINER SETTLEMENT (mm)
12.0
9.0
6.0
3.0
0.0
0
300
600
900
1200
OVERB. PRESSURE (kPa)

Fig. 5.38

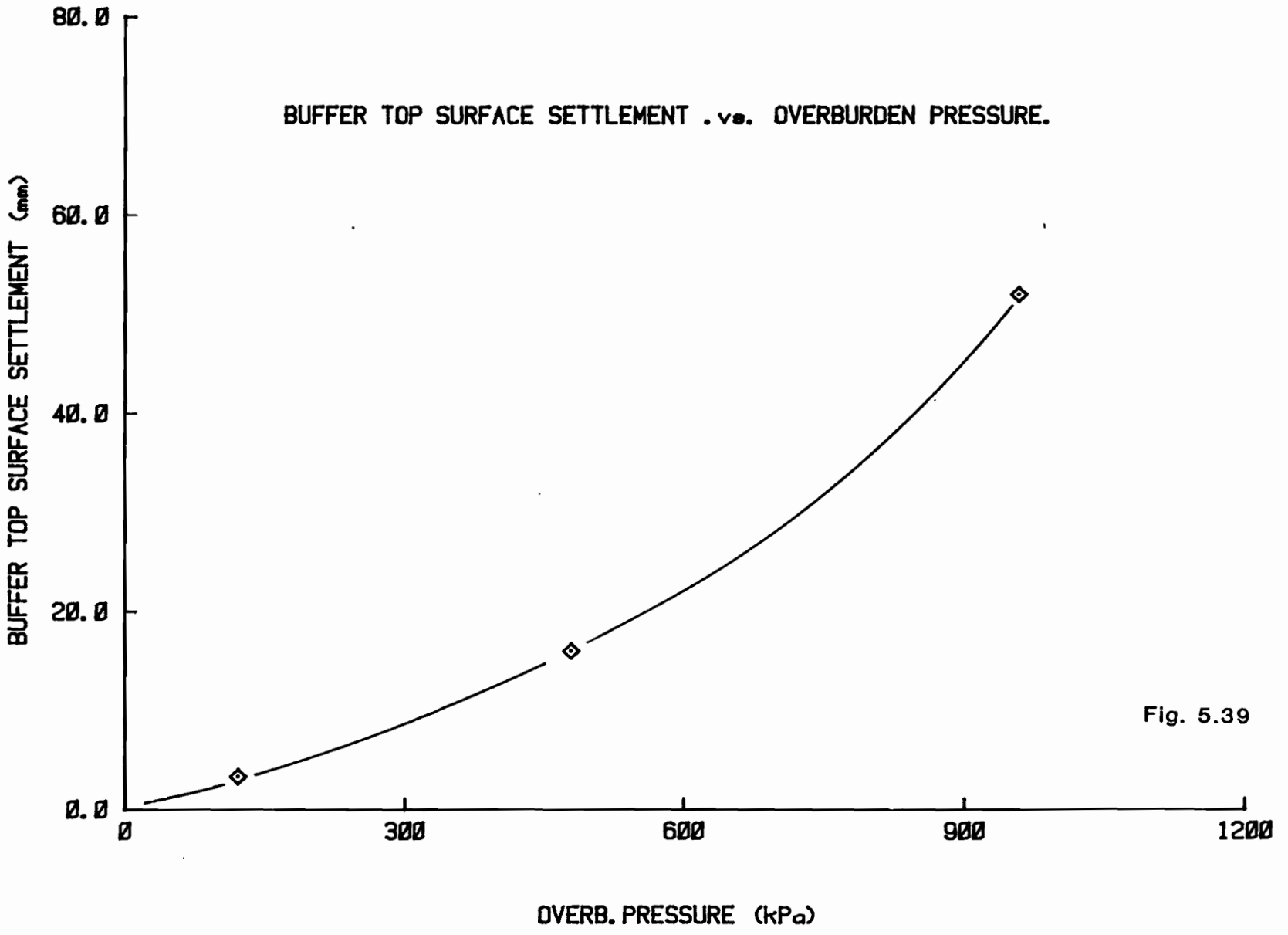
BUFFER TOP SURFACE SETTLEMENT .vs. OVERBURDEN PRESSURE.
BUFFER TOP SURFACE SETTLEMENT (mm)
80.0
60.0
40.0
20.0
0.0
0
300
600
900
1200
OVERB. PRESSURE (kPa)

Fig. 5.39

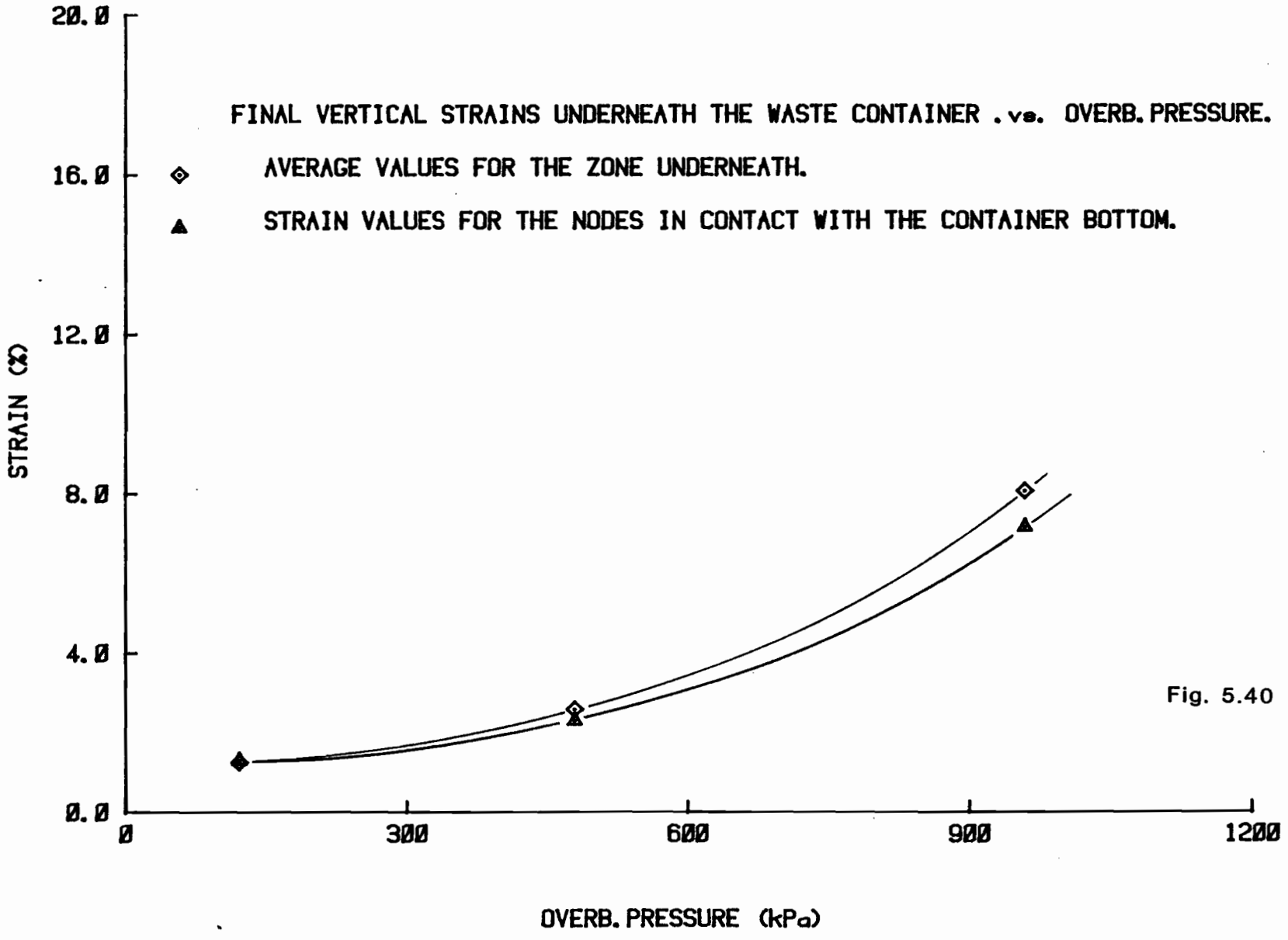
FINAL VERTICAL STRAINS UNDERNEATH THE WASTE CONTAINER .vs. OVERB. PRESSURE.
AVERAGE VALUES FOR THE ZONE UNDERNEATH.
STRAIN VALUES FOR THE NODES IN CONTACT WITH THE CONTAINER BOTTOM.
STRAIN (%)
20.0
16.0
12.0
8.0
4.0
0.0
0
300
600
900
1200
OVERB. PRESSURE (kPa)

Fig. 5.40

the expected operating overburden pressure value that is experienced by the buffer due to the backfill weight. Vertical strains developed underneath the waste container increase from 1.25% to 8% (average values) with pressure increasing, at the same time settlements increase from 1.4 mm to 7.64 mm.

Figures 5.38 through 5.40 present the results of the simulation analysis quite clearly and can be used in any case of prediction of buffer response under different overburden pressure values.

5.10 Long-Term Buffer Response Prediction in the Prototype Disposal System

There were two main objectives of the modelling technique adopted for the investigation of the buffer response in the disposal system. The first objective was to obtain on a non-quantitative basis, useful observations of the buffer response, i.e. general patterns of the soil particle movement under different boundary conditions and the second one was to predict by means of the experimentally measured results the buffer response in the actual disposal vault. In order to achieve the second objective certain principles of similitude had to be satisfied. According to Roscoe (1968) the investigator must asses not only all the physical quantities that are relevant to the problem but also to use judgement to reduce them to a working minimum by selecting the most significant parameters.

The similitude principles as stated by Rocha (1953, 1957) and analyzed by Roscoe (1968) were satisfied by using in the model disposal system the buffer material in the same initial condition as in the actual disposal system and by inducing the same stresses on the model as on the prototype, thereby ensuring the identity of stress-strain curves in model and prototype. This procedure was suggested by Roscoe (1968) when the self-weight effect is not significant. In our case self-weight produced an increase in stresses of approximately 5%. It was also stated by Roscoe (1968) that when these similitude principles are fulfilled the time effects will be proportional to h^2 where h is the linear scale ratio. In other words, what would be obtained after a time period t in the model, should be obtained after a time period $t*h^2$ in the prototype.

In order to offer a predictive model of the buffer response in the prototype and at the same time to avoid any deficiencies of the similitude theory when interpreting the model test results to prototype results, two F.E. models were used.

The first model had the dimensions of the model disposal system and the second one had the dimensions of the prototype one. The same boundary conditions were imposed in both models - frictionless interfaces, two dimensional analysis - and also the same boundary pressures were given as input data simulating the backfilled tunnel

conditions. The results obtained from the F.E. analysis demonstrated the "scaling effect" on the buffer response and provided scale factors in order to predict the buffer response in the prototype.

Comparison between the results obtained from the F.E. analysis generated the following observations:

1. The nodal settlements in the zone underneath the waste container in the prototype were higher than the nodal settlements in the same zone in the model. The ratio between the settlements ranged from 8.32 to 14.89 with an average value of 12.80. The settlements resulted in both prototype and model for the zone underneath the waste container are shown in Table 5.3. In the same zone the lateral displacements in the prototype were 5.06 to 15.00 times the lateral displacements in the model with an average value of 9.98. The increase in both vertical and lateral displacements is a result of the increased geometry of the prototype disposal vault. The rigid boundaries are not close to the waste container because both the diameter of the disposal vault and the distance from the disposal system bottom are increased and the overall buffer compressibility is higher, due to the lower degree of confinement produced by the rigid boundaries.

The increase in both settlements and lateral displacements is again significant in the zone above the waste container where settlements are 15.54 to 20 times higher with an average value of 16. Lateral displacements are

TABLE 5.3

Node	Prototype Settlement (mm)	Model Settlement (mm)
1	0.0	0.0
2	0.0	0.0
3	0.0	0.0
4	0.0	0.0
5	3.07	.30
6	3.33	.24
7	2.68	.18
8	2.49	.17
9	7.17	.73
10	7.79	.59
11	6.37	.44
12	5.21	.36
13	11.01	1.20
14	13.09	.99
15	9.07	.66
16	7.60	.56
17	14.90	1.79
18	13.32	1.00

also increased in a range of 3 to 11.43 with an average of 7.00. The resulting higher nodal displacements along zone once more demonstrate the dimensional effect on the buffer response. The same increase is also observed along the zone around the waste container. The average values of the ratios abovementioned can be used as scale factors in order to interpret the displacements found from the model tests to the displacements expected in the prototype disposal system.

2. The vertical strains in the zone underneath the waste container in the prototype, are found to be higher than the corresponding ones in the model with ratios ranging from 1.2 to 1.79 with an average of 1.57. This increase in strains indicates mainly the change in the compressibility characteristics of the buffer due to the increased geometry of the disposal system. Increase in vertical strains is also found in the zone above the waste container with an average ratio of 1.13 (ratios ranging from 1.04 to 1.33). The overall average values of the ratio of increase in vertical strains along the buffer surface should be 1.41. This increase in strains indicates that the compressibility characteristics of the buffer if modelled by means of a suitable parameter should show a non-linear upward increasing trend with geometrical size of the disposal system increasing. The same conclusion can also be derived if the average value of the vertical

displacement increase - 14.4 - is compared to linear scale ratio - 8 - herein called "minimum expected displacement increase". The percentage of "non-expected" displacement increase is (14.4-8)/14.4 = 0.44 approximately equal to 0.41.

3. The vertical strain rates developed in the prototype are approximately equal with the corresponding ones in the model with an average ratio value of 0.97. Combining the strain rate values with the strains, the time necessary to obtain these values is 1.14 to 1.29 times higher in the prototype. This time scale factor of 1.20 can be used when the correlation between the time effects in prototype and model is sought. In other words, when maximum displacements in the model are obtained in 15 days, in the prototype it would be expected to be obtained in 15 * 1.2 = 18 days. The similitude theory should give 15 * 8^2 = 960 days.

4. The stresses obtained in the prototype are found to be higher by an average ratio of 1.10 (range 1.02 - 1.19) for the vertical stresses, an average ratio of 1.10 (range 1.02 - 1.23) for the lateral stresses and an average ratio of 0.5 (0.1 - 1.00) for the shear stresses.

From the comparison presented, the following scale factors are derived and will be used in order to project the model test results to predicted buffer response characteristics in the prototype disposal system.

Vertical displacement:	14.40
Lateral displacement:	8.50
Vertical strain:	1.41
Lateral strain:	3.00
Shear strain:	1.70
Vertical strain rate:	0.97
Vertical stress	1.10
Lateral stress	1.10
Shear stress	0.50
Time factor:	1.20 (similitude theory = 64)

It is assumed that the above scale factors are constant at any time period and are independent of overburden pressure and location on the buffer surface.

As a result the following conclusions can be derived for the buffer response in the prototype disposal system, projected through both the experimental and theoretical time scale factors:

For the zone underneath the waste container:

1. Under minimum overburden pressure values or else where the tunnel is not backfilled, higher settlement values will be obtained after 22 days (theory: 38 months) under the loading conditions experienced due to the waste container weight. Until that time the buffer will deform mainly vertically while, the corresponding vertical instantaneous strain rates will decrease to the value of 5.5×10^{-5} %/min and the vertical strains will reach their peak

value of approximately 2.24% after 23 days (40 months).

2. When the tunnel is backfilled immediately after the waste container installation, the generated high overburden pressure value of 120 kPa will cause a maximum displacement of approximately 23.8 mm after 23 days (theory: 40 months) while the vertical instantaneous strain rates will decrease to the value of 5.5×10^{-5}%/min
3. Under water intake conditions from a point located at the bottom of the disposal vault, when the tunnel is not backfilled and when creep due to waste container weight is finished (i.e. after 26 days (theory: 44 months) approximately , additional settlements must be expected due to the increased buffer compressibility characteristics. This additional creep will continue for approximately 19 days (theory: 33 months) and will cause additional settlements of 17.38 mm. Under backfilled tunnel conditions the additional creep will continue for approximately the same time period and additional settlement values equal to 17.28 mm will be reached.
4. When water intake is allowed from points located around or above the waste container due to possible unfavourable local rock cracks, additional creep is expected with resulting settlement increases of only 15% to 18%.

5. The effect of water intake during the 47 month creep period under no water intake conditions, was also examined. Under these conditions it must be expected that the higher additional settlement values will be reached at shorter time periods, i.e. 16 days (theory: 28 months) after water intake is allowed.

As already mentioned the results obtained from both the experimental and analytical study of the buffer response characteristics in the model offer a 60 day period (theory: 4 to 5 year time period) observation of the buffer response in the prototype disposal vault. During this period the buffer will creep under the operating loading conditions and reach its higher displacement and strain values. Water intake will produce additional creep in the buffer with higher additional settlement values obtained in a 19 day (theory: 33 months) period under after water intake is allowed.

Under no waterintake conditions, for longer than a 34 day (theory: 5 year) period the buffer will deform with an instantaneous creep rate decreasing as shown in Fig. 5.41 where the relationship with time is plotted for the maximum vertical instantaneous strain rates at the zone underneath the waste container, for the three overburden pressure values. From Fig. 5.41 a linear relationship between the ln $\dot{\varepsilon}$ and ln t can be derived.

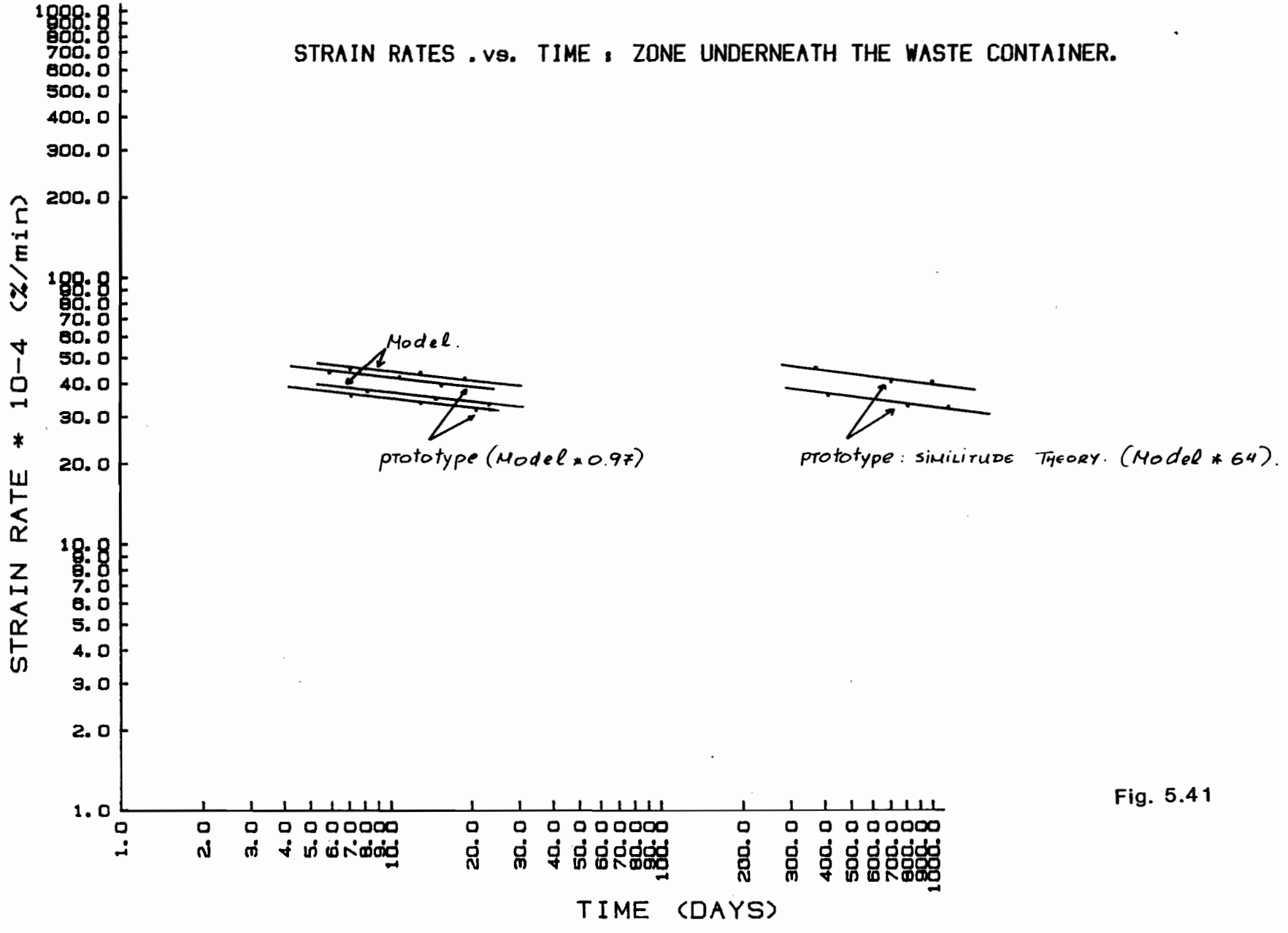
STRAIN RATES . vs. TIME : ZONE UNDERNEATH THE WASTE CONTAINER.
STRAIN RATE * 10-4 (%/min)
TIME (DAYS)
Model.
prototype (Model * 0.97)
prototype : similitude Theory. (Model * 64).

Fig. 5.41

$$\dot{\varepsilon}(t) = A \cdot t^{-m} \qquad (5.1)$$

where A is a function of the overburden pressure value and takes values between 4.5×10^{-3} and 5.4×10^{-3} (%/min)

t is time in days

m is the slope of the relationship with value 0.110.

The simple relationship derived, is similar to that obtained by Mitchell (1976) that predicts the strain rate at any time as a function of the deviator stress level and a reference strain rate value.

By means of eq. (5.1), it is possible to predict the strain rate at which the buffer will deform, as a function of the overburden pressure variable at any time at the zone underneath the waste container where the higher strain rate values are obtained.

5.10.1 Relationships Between Strain Rate and Deviator Stress

In Fig. 5.42 the relationships between the measured maximum strain rate values and the corresponding deviator stresses are illustrated, at different time intervals (t = 6, 12 and 18 days), under the three overburden pressure values applied (i.e. 0, 36 and 120 kPa).

Deviator stress is defined herein as the difference $\sigma_1 - \sigma_3$, where σ_1 is the maximum stress (almost invariably

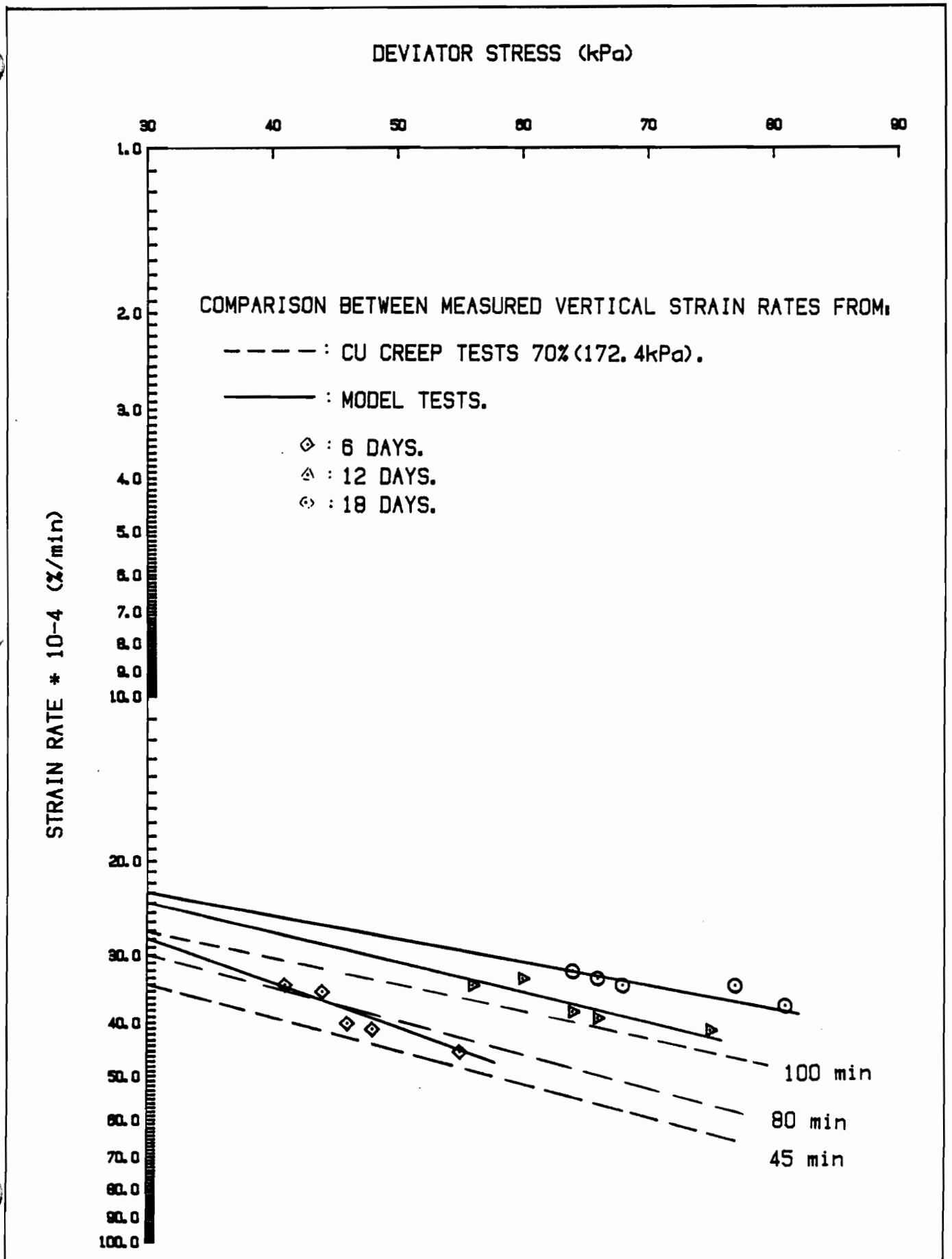
DEVIATOR STRESS (kPa)
30
40
50
60
70
80
90
STRAIN RATE * 10-4 (%/min)
1.0
2.0
3.0
4.0
5.0
6.0
7.0
8.0
9.0
10.0
20.0
30.0
40.0
50.0
60.0
70.0
80.0
90.0
100.0
COMPARISON BETWEEN MEASURED VERTICAL STRAIN RATES FROM:
: CU CREEP TESTS 70% (172.4kPa).
: MODEL TESTS.
: 6 DAYS.
: 12 DAYS.
: 18 DAYS.
100 min
80 min
45 min

Fig. 5.42

equal to the vertical stress) and σ_3 is the minimum stress. For the derivation of the deviator stress-strain rate relationship, data from the zone underneath the waste container were used, where the higher values of either the deviator stresses or the strain rates were developed.

The pattern of relationship observed between strain rate and deviator stress, illustrated in Fig. 5.42 was also observed for other zones of the buffer surface with lower developed strain rate and deviator stress values.

As anticipated, the strain rate increases with deviator stress. A linear relationship between log strain rate values and deviator stresses is imposed. This pattern of behaviour was also observed by Mitchell, Campanella and Singh (1968) for undisturbed San Francisco mud, and later by Kavazanjan and Mitchell (1980) for the undrained creep of remoulded San Francisco bay mud (soft clay). Investigations on the silicate-grouted sand as reported by Koenzen (1977) show evidence of linearity for the relationship between strain rate and stress.

The linear realtionships between the strain rate and deviator stress illustrated in Fig. 5.42 lead to an average value of slope $a = 0.0044 \frac{\%/min}{kPa}$.

In order to correlate the results obtained from the model tests to those obtained from the CU creep tests, in Fig. 5.42 the relationships between the CU creep test strain rates and the deviator stresses are plotted for several time periods and initial loading levels and for

confining stresses equal to 172.4 kPa.

The relationships resulting when confining stress is 172.4 kPa and initial loading level 70% follow the same pattern as those obtained from the model tests. The slopes from these CU creep test relationships vary from 1.6×10^{-3} to .009 $\frac{\%/min}{kPa}$ with an average value at .0056 $\frac{\%/min}{kPa}$. From Fig. 5.42 it is indicated that the CU creep test under confining stress equal to 172.4 kPa and initial loading level 70% can successfully duplicate the relationship resulting from the model testing.

From both Figs. 5.41 and 5.42 a long-term prediction of the buffer response can be achieved at any time period or for any known deviator stress value. For instance, at a time t, the strain rate value from Fig. 5.41 can be obtained and with this strain rate value and the time t, the corresponding deviator stress from Fig. 5.42 can be obtained. When a deviator stress value is known the resulting strain rate value at any time can also be obtained.

The values derived from both these figures are expected to be higher than the ones observed along the zones around and above the container but will be in better agreement with those observed in the zone underneath the waste container. In any case, these figures could be used as a simple model in order to obtain a prediction for the long-term buffer response.

The CU creep test results can also be used in order to obtain a long-term prediction for the buffer response

because as shown in Fig. 5.42, the rheological patterns indicated from the model tests are quite close to those from the CU creep tests.

CHAPTER 6

SUMMARY AND CONCLUSIONS

6.1 Summary

The primary goal of this study was to investigate the buffer response characteristics in the in-hole disposal system under different loading and water intake conditions. In addition, the derivation of an analytical model was attempted in order to provide a rational means for predicting the buffer performance.

The buffer performance was predicted through application of the finite element method; the predicted performance was compared to the experimental surficial measurements obtained through use of the "glass box" photographic technique and application of the visioplasticity approach.

The finite element method provides a convenient framework for field or laboratory investigations of complex boundary value problems, thus providing a means of properly incorporating the buffer properties and boundary conditions into a rational overall theory. The solution by the finite element method provides knowledge of detailed stress and deformation fields within the loaded soil, and contact stresses at the soil-container and soil-boundary interfaces at various time periods. Consequently, a relatively complete description of the load-deformation behaviour of the buffer material was obtained.

The main features of the finite element model adopted in this study can be summarized as follows:

a) Idealization

1. Two different patterns of buffer response are described by the constitutive relationships adopted. In the zone above the waste container the buffer behaviour is described by means of a stress-strain curve obtained from one-dimensional compressibility test. Around and underneath the waste container CU tests resulted in stress-strain curves, describing the buffer response.

2. The buffer mass is modelled by plane-strain continuum elements representing a region in which plastic deformations take place.

b) Boundary Conditions

The boundary conditions for the analytical model can be either specified pressure, specified displacement or both.

c) Nonlinear Analysis

In the model developed, the stress-strain relations obtained from laboratory tests are used in the analysis to predict the load-deformation behaviour of the soil. The direct digital form is used to incorporate the constitutive laws into the finite element model. The solution is obtained by the incremental method of analysis improved by iterating a few times in each increment of loading.

6.2 Conclusions

The present study addressed the problem of examining the buffer response characteristics under actual boundary conditions in order to develop a better knowledge of the long-term buffer performance. It must be looked upon as one more step in the direction of using model testing in soil mechanics in order to obtain correct predictions of the prototype performance through observations of the model.

In its immediate application, the proposed analysis provides a complete description of the buffer long-term performance in the in-hole disposal system.

The following is a short summary of the specific conclusions arrived at in this study:

(1) Under normal operating conditions - i.e. empty or backfilled tunnel, no water intake - the buffer material suffers mainly vertical deformation with maximum vertical strain values up to 1.6%. Maximum settlements are observed mainly underneath the waste container, evidently due to the highest vertical pressure experienced. The nodal displacement depends mainly on its location relative to the container and the disposal vault boundary. Separation between the buffer material and the waste container at the top of the container resulted, due to the high cohesive characteristics of the soil and the boundary effects of the system, was observed as well.

(2) The analysis of the experimental results demonstrated the overburden pressure effect on the buffer response characteristics. Increased overburden pressure produced higher settlements throughout the buffer surface. Furthermore, higher final strain rates are developed in the buffer with high overburden pressure values, and the time period for the creep to end is increased with overburden pressure, indicating the stress level effect on the creep of the buffer. Finite element simulation of high overburden pressure conditions demonstrated the buffer high resistance characteristics even for overburden pressure values 8 times higher than the maximum operating values.

(3) Water intake conditions demonstrated the high swelling potential of the buffer and the overall change in the compressibility characteristics. Additional settlements were observed after water intake was allowed, especially for low overburden pressure values. After several water entry positions were examined, the potentially most crucial one for the system stability was located at the bottom of the disposal vault. The initial creep - no water intake - effect on the buffer response under subsequent water intake conditions was demonstrated through the lower amount of absorbed water and smaller additional settlements produced.

(4) Finite element simulation of both the model and prototype system resulted in the derivation of the scale factors that were necessary to project the results

obtained to buffer predictive behaviour in the prototype disposal system.

(5) The rheological patterns of buffer behaviour that resulted from the scale model tests were correlated with the rheological patterns resulting from the axi-symmetrical tests. An additional simple model was provided from data acquisition regarding the buffer long-term response characteristics.

CHAPTER 7

RECOMMENDATIONS FOR FURTHER STUDY

Future studies should be focused on the further reduction of the number of simplifying assumptions which were currently adopted in the development of the analytical model. They should also improve the experimental procedure with resulting higher accuracy.

Specifying the recommended points of further investigation it should be stated:

1. The importance of prediction through the finite element technique of the buffer response in the in-hole disposal system under water intake conditions. The problems to be solved are linked with the modelling of the swelling properties of the buffer, and the adoption of the appropriate constitutive relationships to take into account the continuous decrease in strength with water front advancing through the buffer.
2. The necessity of using joint (interface) elements with accompanying proper constitutive relationships in order to obtain representative descriptions of the boundary conditions in the in-hole disposal system. In addition, it should be investigated the effect of using the stress-strain results

from axisymmetric tests in a problem considered as a two-dimensional one.

3. The possibility of modelling the buffer response under the constant loading conditions, by means of one rheological model that should take into account the time effect on the buffer response characteristics in the specific geometry of the in-hole disposal system.
4. The accuracy of the cornerstone of the experimental procedure, i.e. the reduction of the unknown variables of the problem that were reflected in the laboratory through the adopted "glass box" technique, should be investigated by modelling the in-hole disposal system and using X-ray radiographic techniques in order to monitor any soil particle movement in a three dimensional space.

These recommended points of further study should improve the finite element model predictions of the buffer material under more complicated boundary conditions and would justify the "glass box" technique use for a highly complicated boundary value problem.

BIBLIOGRAPHY

1. Abdel-Hady and Herrin (1966) "Characteristics of soil asphalt as a rate process", Journal of the Highway Division, ASCE, Vol. 92, No. HW1, Proc. Paper 4719, pp. 49-69

2. Alfrey, T. (1948)"Mechanical Behaviour of High Polymers" International Publishers, New York

3. Anderson H.W. and Dodd J.S. (1966) "Finite element method applied to rock mechanics",Proc. 1st Congress, Int. Soc. for Rock Mechanics, Lisbon

4. Bishop A.W. (1966) "The strength of soils as engineering materials", Geotechnique, Vol. 16, pp. 89-130

5. Campanella R.G. and Vaid Y.P. (1977) "Time-dependent behaviour of undisturbed clay", Journal of the Geotech. Eng. Div., ASCE, Vol. 103, No. GT7, Proc. Paper 13065 pp. 693-709

6. Chen (1972) "Wedge and cone indentation of soils", Ph.D. Thesis, McGill University

7. Chen D.S. (1975) "A probabilistic representation for drained creep in clays", Ph.D. Thesis, McGill University

8. Christensen R.W. and Wu T.H. (1964) "Analysis of clay deformation as a rate process", Journal of the Soil Mechanics and Foundations Division, ASCE, Vol. 90, No. SM6, pp. 125-159

9. Clough R.W. and Pirtz D (1958) "Earthquake resistance of rock-fill dams", Trans. Am. Soc. Civ. Engrs., 123, 792

10. Desai C.S. (1972) "Overview, trends and projections theory and application of the finite element method in Geotechnical engineering, state-of-the-art", Proc. of the Symposium on the Application of the Finite Element Method in Geotechnical Engineering, Vicksburg, Miss.

11. Desai C.S. and Abel J.F. (1978) "Introduction to the Finite Element Method", Van Nostrand Reinhold Co., New York

12. Duncan J.M. and Chang C.Y. (1970) "Nonlinear analysis of stress and strain in soils", Journal of the Soil Mechananics and Foundations Division, ASCE, Vol. 96, No. 5, pp. 1629

13. El Mamlouk (1980) "Energy analysis and prediction of track-soil interaction", Ph.D. Thesis, McGill University

14. Eyring H., Glasstone S. and Laidler K.J. (1941) "The theory of rate processes", McGraw Hill Co., New York

15. Foster, C.R. and Ahlvin R.G. (1954) "Stresses and deflections induced by a uniform circular load", Proc. High. Res. Board, Vol. 33, pp. 467-470

16. Freitag D.R., Schafer R.L., and Wismer R.D. (1970) "Similitude studies of soil-machine systems", Journal of Terramechanics, Vol. 7, No. 2, pp. 25 to 59

17. Fung Y.C. (1965) "Foundations of solid mechanics", Prentice Hall Inc., Englewood Cliffs, New Jersey

18. Geuze E.G.W.A. (1964) "Rheological and mechanical models of saturated clay particle systems", Proc. IUTAM, Grenoble, France, pp. 90-99

19. Goldstein, , Misumsky and Lapidys (1961) "The theory of probability and statistics in relation to the rheology of soils", Proc. 5th ICOSMFE, Vol. 1, pp. 123-126

20. Goodman R.E., Taylor R.L. and Brekke T.L. (1968) "A model for the mechanics of jointed rock", Journal of Soil Mechanics and Foundation Division, ASCE, Vol. 94, No. SM3

21. Gross B. (1953) "Structure of the theory of linear viscoelasticity", Proc. 2nd Int. Cong. on Rheology, Oxford, pp. 220-227

22. Haefeli R. (1953) "Creep problems in soil, snow and ice", Proc. 3rd ICSMFE, Vol. 3, pp. 238-251

23. Hanna A.W. (1975) "Finite element analysis of soil cutting and traction", Ph.D. Thesis, McGill University

24. Herrin M., and Jones G. (1963) "Behaviour of bituminous material from the viewpoint of the absolute rate theory", Proc. Assn. of Asphalt Paving Technologists, Ann Arbor, Mich., Vol. 32

25. Hildebrand R.B. (1956) "Introduction to numerical analysis", McGraw-Hill Book Co., Inc., New York

26. Hogan M. (1953) "The engineering application of the absolute rate theory to plastics", Bulletin, Univ. of Utah, Salt Lake City, Utah, No. 62

27. Komamura F., Huang R.J. (1974) "New rheological model for soil behaviour", Journal of the Geotechnical Eng. Div., ASCE, Vol. 100, No. GT7, pp. 10675

28. Kondner R.L. and Green G.E. (1962) "Lateral stability or rigid poles subjected to a ground-line thrust", Highway Res. Bd. Bull., 342, pp. 124

29. Ladanyi B. (1972) "An engineering theory of creep of frozen soils", Canadian Geotechnical Journal, 9, 63

30. McKyes E.S. (1969) "Yielding of a remoulded clay under complex stress states", Ph.D. Thesis, McGill University

31. Milovic D.M. (1970) "Contraintes et deplacements dans une couche elastique d'epaisseuz limitee, produits par une fondation circulaire", Le Genie Civil, T.147, No. 5, pp. 281-285

32. Mitchell J.K. and Singh A. (1968) "General stress-strain-time function for soils", Journal of the Soil Mechanics and Foundations Div., ASCE, Vol. 94, No. SM4, pp. 5728

33. Myrayama S. and Shibata T. (1958) "On the rheological characters of clay", Part 1. Disaster Prevention Research Inst., Kyoto Univ., Bulletin No. 26

34. Myrayama S. and Shibata T. (1961) "Rheological properties of clays", Proc. 5th ICSMFE, Vol. 1, pp. 269-273

35. Myrayama S. and Shibata T. (1964) "Flow and stress relaxation of clays", Proc. IUTAM, Grenoble, France, pp. 99-130

36. Ngo D. and Scordelis A.C. (1967) "Finite element analysis of reinforced concrete beams", Journal of the American Concrete Institute, Vol. 69

37. Prevost J.H. (1976) "Undrained stress-strain-time behaviour of clays", Journal of the Geotechnical Engineering Div., ASCE, Vol. 102, No. FT12, pp. 12644

38. Rocha M. (1953) "Similarity conditions in model studies of soil mechanics problems", Laboratoria Nacional de Engenharia Civil, Lisbon, Publ. No. 35, 1953

39. Rocha M. (1957) "The possibility of solving soil mechanics problems by the use of models", Proc. 4th Int. Conf. Soil Mech., London 1957, 1, 183

40. Roscoe K.H. (1968) "Soils and model tests", Journal of Strain Analaysis, Vol. 3, No. 1, pp. 57-64

41. Roscoe K.H. and Poorooshasb H.B. (1963) "A fundamental principle of similarity in model tests for earth pressure problems", Proc. 2nd Asian Conf. Soil Mech., Tokyo, 1, 174

42. Schuring D.J. and Emori R.I. (1964) "Soil deforming processes and dimensional analysis", Society of Automotive Engineers, Milwaukee

43. Scott R.F. (1969) "The freezing process and mechanics of frozen ground", U.S. Army, Hanover, N.H.

44. Sylvestre-Williams R. (1973) "Indendation and traffica-bility studies on clay", Ph.D. Thesis, McGill University

45. Vyalov S.S. and Skibisky A.M. (1957) "Rheological processes in frozen soils and dense clays", Proc. 4th ICOSMFE, Vol. 1, pp. 120-124

46. Vyalov S.S. and Skibisky A.M. (1961) "Problems of the rheology of soils", Proc. 5th ICOSMFE, Vol. 1, pp. 387-391

47. V yalov S.S. (1965) "Plasticity and creep of a cohesive medium", Proc. 6th ICOSMFE, Vol. 1, pp. 402-406

48. Vyalov S.S. and Meschyan S.R. (1969) "Creep and long-term strength of soils subjected to variable load", Proc. 7th ICOSMFE, Vol. 1, pp. 423-431

49. Yang C.T. and Thompsen E.G. (1951) "Plastic flow in a lead extrusion", ASME, paper No. 52- F-18

50. Yong R.N. (1973) "On the physics of unsaturated flow in expansive soils", Proc. 3rd Int. Conf. on Expansive Soils, Haifa, Israel, Vol. 2.

51. Yong R.N. and Chen D.S. (1969) "Analysis of creep of clays using retardation time distribution", Proc. 5th Int. Congr. Rheology, Kyoto, University Park Press, Vol. 2, pp. 309-314

52. Yong R.N. and Webb (1969) "Energy dissipation and draw-bar pull prediction in soil-wheel interaction", 3rd Int. Conf., I.S.T.V.S., Essen, West Germany

53. Yong R.N. and Windisch E.J. (1970) "Determination of wheel contact stresses from measured instantaneous soil deformations", Journal of Terramechanics, Vol. 7, No. 3 and 4, pp. 57-67

54. Yong R.N. and Wong H.Y. (1973) "Engineering problems in unsaturated soils", Civil Engineering and Public Works Review.

55. Yong R.N., Sciadas N., Siu S. (1982) "Stability analysis of unsaturated slopes", Proceedings of the conference on engineering and construction in tropical and residual soils, ASCE, Honolulu Hawaii

56. Yong, R.N., Fattah, E.A., Sciadas, N. (1984) "Vehicle Traction Mechanics", Elsevier Science Publishers, The Netherlands.

57. Zienkiewicz D.C., Vailliappan S., and King I.P. (1970), Elasto plastic solutions of engineering problems initial stress, finite element approach", ISNME, Vol. 1, p. 75

58. Zienkiewicz O.D. (1971) "The finite element method in engineering science", 2nd Edition, McGraw-Hill Co. New York.

APPENDIX A

FINITE ELEMENT TECHNIQUE AS APPLIED TO THE PRESENT PROBLEM

A1 Introduction

For a given problem, development of a reliable numerical technique involves various steps as depicted in Fig. A.1. These steps essentially represent a trial and error procedure which requires the examination of factors such as idealization of the problem as a discretized body, numerical characteristics and constitutive laws. In the figure, the first two factors are indicated by dashed lines, whereas the trial and error procedure for constitutive laws is shown by solid lines (Desai, 1972).

A numerical technique for solving soil-structure interaction problems can be developed in progressive stages. In the initial recognition phase, the action is observed and noted to be repetitive. The recognition phase is gradually supplanted by an "equivalent" model. For complicated problems, the idealization stage can be difficult and would require a number of trials before a model for acceptable accuracy can be evolved. The final model may be arrived at after a number of trials.

The second step of developing a solution technique is arriving at a representative constitutive law. A constitutive law for soil is usually dependent on a number of factors such as density, stress history, water content, and

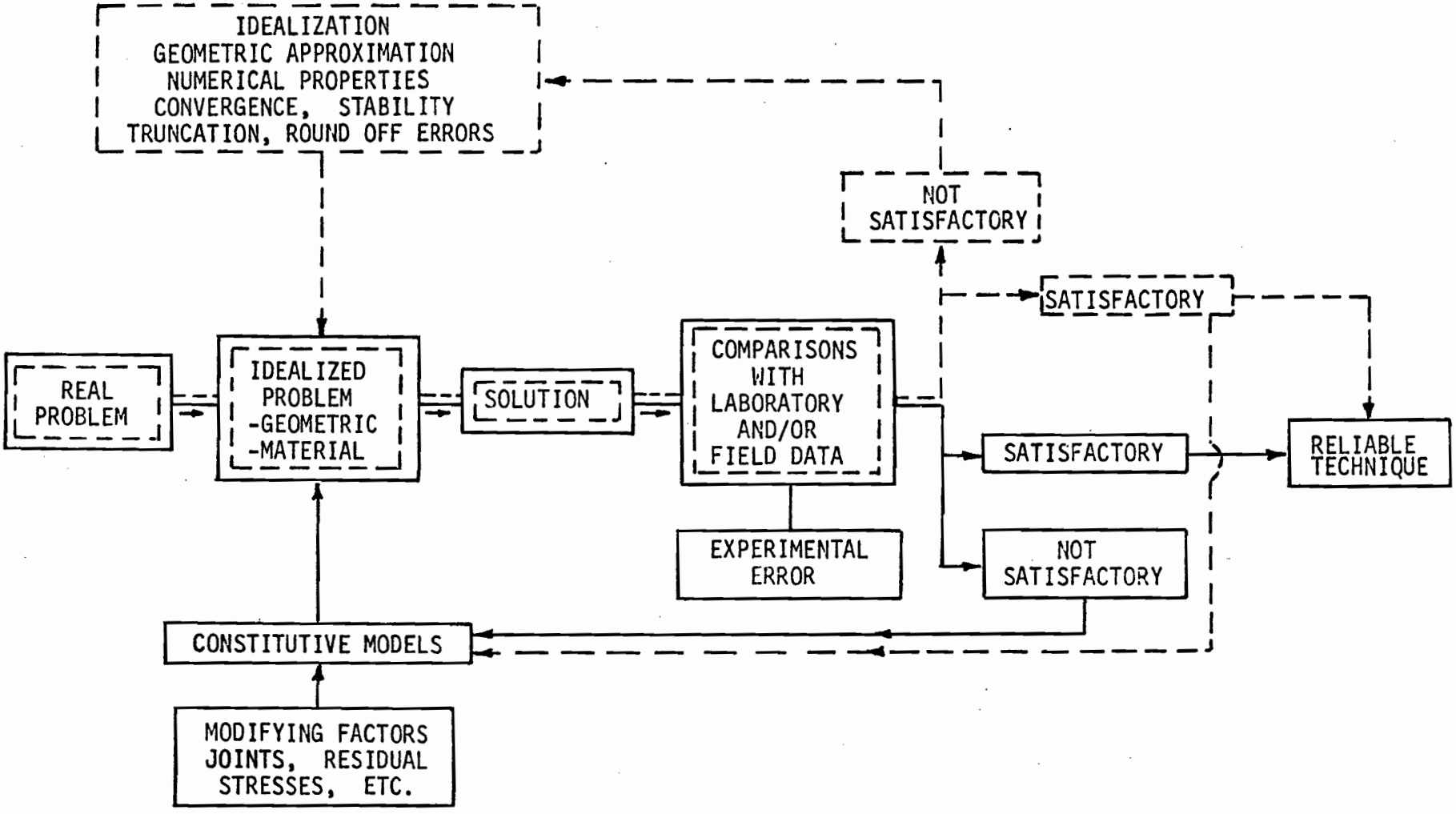

Fig. A.1 - DEVELOPMENT OF A RELIABLE NUMERICAL TECHNIQUE AFTER DESAI (1972)

the existence of discontinuities. The constitutive relation can be established through the application of several distinct phases of study. First, some specific behaviour is observed and studied. Second, having noted the behaviour, factors involved in the behaviour are identified and their relation ascertained in a cause-and-effect manner. Mathematical equations are required to quantitatively describe the cause-and-effect relation, and hence, the behaviour. Resorting to mathematical equations is possible only when both input and output quantities can be expressed in some form of numerical description.

Many numerical techniques can be attempted in developing a solution for a particular problem; among them the limit equilibrium, the finite difference, and the finite element method. The main advantage of the finite element method lies in its capacity of handling relatively complex problems. This was the main reason that the method was chosen in this study to investigate the long-term creep response characteristics of the buffer in the in-hole disposal system.

A2 Idealization

In developing an analytical model for problems dealing with the soil as an engineering material, it is essential that proper appreciation be given to the material performance and boundary conditions. The appropriate framework defined by using realistic similarities between physical and

mathematical boundary conditions will ensure a higher order of predictability with the developed analytical model. The observation of soil deformation and failure patterns during a loading process often provides the basis for the development of valid models leading to solutions of forces and stress fields.

The initial step in developing an analytical model using the finite element approach consists of idealization of the problem by drawing a finite element mesh which simulates the presence of the soil mass. The construction of the finite element mesh requires that the type and number of elements included should be adequate to attain the correct flexibility of the continuum.

For the proper idealization of the problem by a finite element model, certain characteristics must be incorporated in such a model so that it can represent the various elements. One of these characteristics is the displacement patterns that are observed along the buffer-container and buffer-host rock interfaces. The nature of the interface behaviour depends upon the roughness of the boundaries and the friction and adhesion of the soil. Most finite element analyses have been performed using one of the two following limiting assumptions concerning the characteristics of a soil-rigid interface interaction (Hanna, 1975):

1. that the interface is perfectly rough, with no possibility of slip between the rigid interface

and the soil, or

2. that the interface is perfectly smooth, with no possibility for shear stresses which would retard relative movements between the rigid interface and the soil.

Experimental and actual field evidence, show that these assumptions generally are not realistic. For a realistic analysis of the problem, it is essential that any relative displacement or discontinuity in the deformation field should be taken into consideration. According to Hanna (1975) the plane strain continuum elements used in the finite element analysis (constant strain triangular element, for example) cannot satisfactorily model the soil deformation behaviour in a case where discontinuities may develop. In order to include behaviour features as development of discontinuities, idealized discrete elements representative of those features must be incorporated in the overall model. Attempts to develop such elements were made by Goodman (1968), ZienKiewicz et al. (1970), in reinforced concrete by Ngo and Scordelis (1967), in soil-structure interaction problems by Clough and Duncan (1971) and Hanna (1975).

A3 Formulation of the Problem

The analysis of plane strain problems by the finite element method has been fully described in many publications (Zienkiewicz, 1971). The derivations will not be presented here, only the general formulation and the

essential features of the procedure required for the analysis of the present problem will be discussed.

From basic energy principles, for a body to be in equilibrium, its potential energy expressed as a functional π should assume a stationary value in a class of admissable variations (δu_i) of the displacements U_i of the equilibrium state. The functional π is given by:

$$\pi(U_i) = y - w$$

where y = strain energy, and

w = work done

In a detailed form the above equation can be written as:

$$\pi(U_i) = \int_V \frac{1}{2} \tau_i \varepsilon_i \, dV - \int_V F_i U_i \, dV - \int_B T_i U_i \, dB \quad (A.1)$$

where τ_i = stress tensor

ε_i = strain tensor

F_i = body force field

T_i = surface force field, and

B,V represents the body boundary and volume, respectively.

In a matrix notation eqn. (A.1) becomes:

$$\pi(U_i) = \int_V \frac{1}{2} \tau^T \varepsilon \, dV - \int_V U^T F \, dV - \int_B U^T T \, dB \quad (A.2)$$

Using a stress-strain relationship of the form:

$$\tau = C^i \varepsilon$$

where C^i is a stress-strain matrix at stress level i, eq. (A.) can now be written as:

$$\pi(U_i) = \int_V \frac{1}{2} \varepsilon^T C^i \varepsilon \, dV - \int_V U^T F \, dV - \int_B U^T T \, dB \quad (A.3)$$

Assuming a displacement field given by:

$$U = \phi \, a \quad (A.4)$$

where ϕ is the coordinate matrix of the nodal points, and a are generalized coordinates.

It is possible to represent a in terms of ϕ and U by premultiplying both sides of eq. (A.4) by ϕ^{-1}, giving:

$$a = h \, U$$

where $h = \phi^{-1}$

The strain vector can now be obtained by differentiating the displacement vector U with respect to ϕ and can be expressed as:

$$\varepsilon = \phi' \, h \, U \quad (A.5)$$

where ϕ' is the ϕ matrix after the necessary differentiation. Substituting eq. (A.5) into eq. (A.3) yields:

$$\pi(U_i) = \frac{1}{2} \int_V U^T h^T \phi'^T C^i \phi' \, h \, U \, dV - \int_V U^T F \, dV - \int_B U^T T \, dB \quad (A.6)$$

After proper integration and conversion of the body forces F and surface tractions T to nodal forces, eq. (A.8) can be written as:

$$\pi(U_i) = \frac{1}{2} U^T K U - U^T f \quad (A.7)$$

where f are the lumped nodal point forces.

From the theorem of minimum potential energy, in an equilibrium state the variation of the functional vanishes, i.e.:

$$\delta\pi(U_i) = \frac{\pi(U_i)}{U_i} = 0 \qquad \text{(A.8)}$$

Applying the condition set by eq. (A.8) to eq. (A.7), yields

$$\delta\pi(U_i) = K\,U - f = 0$$

or

$$K\,U = f \qquad \text{(A.9)}$$

where K is the element stiffness matrix.

Solving eq. (A.), subject to the boudnary conditions, provides both the stress and deformation fields.

A4 Boundary Conditions

In the two-dimensional problem considered in this study, the boundary conditions can be either specified forces, specified displacements or both. If the boundary condition is that of an applied load, the value of the load is simply added to the appropriate components of the vector f in eq. (A.9). Equivalent nodal point forces due to body forces and surface tractions are calculated and assembled concurrently with the element stiffnesses. The body forces in a triangular element due to gravity are lumped as one-third values at each nodal point comprising the triangle.

In case displacement or kinematic boundary conditions are specified, as in the present study, the stiffness matrix

K has to be suitably altered to account for the specified displacements (see Fig. A.1.1 and A.1.2).

If the i^{th} element of the deflection vector U is specified to be Δ, the corresponding row of the stiffness matrix is made zero and the diagonal term is made unity, i.e.,

$$K_{ii} = 1$$
$$K_{ij} = 0 \text{ for } i \neq j,\ j = 1,\ldots n \qquad \text{(A.10)}$$

The corresponding force element, f_i, is then set equal to the prescribed displacement value Δ. One major disadvantage of this procedure is that the altered stiffness matrix, K is no longer symmetrical leading to added storage requirements while solving for the unknown displacements. An additional modification, however, will restore the symmetry of the K matrix as outlined below.

In addition to satisfying eq. (A.10), all elements in the i^{th} column, except the diagonal element K_{ii}, are set equal to zero as in eq. (A.11) the symmetrical nature of K matrix is retrieved.

$$K_{ii} = 1$$
$$K_{ji} = 0 \text{ for } i \neq j,\ j = 1,\ldots n \qquad \text{(A.11)}$$

The force vector f on the right-hand side of eq. (A.9) now has to be altered as:

$$f_i = \Delta$$
$$f_j = f_i - K_{ji}\ \Delta, \text{ for } i \neq j,\ j=1,..n \qquad \text{(A.12)}$$

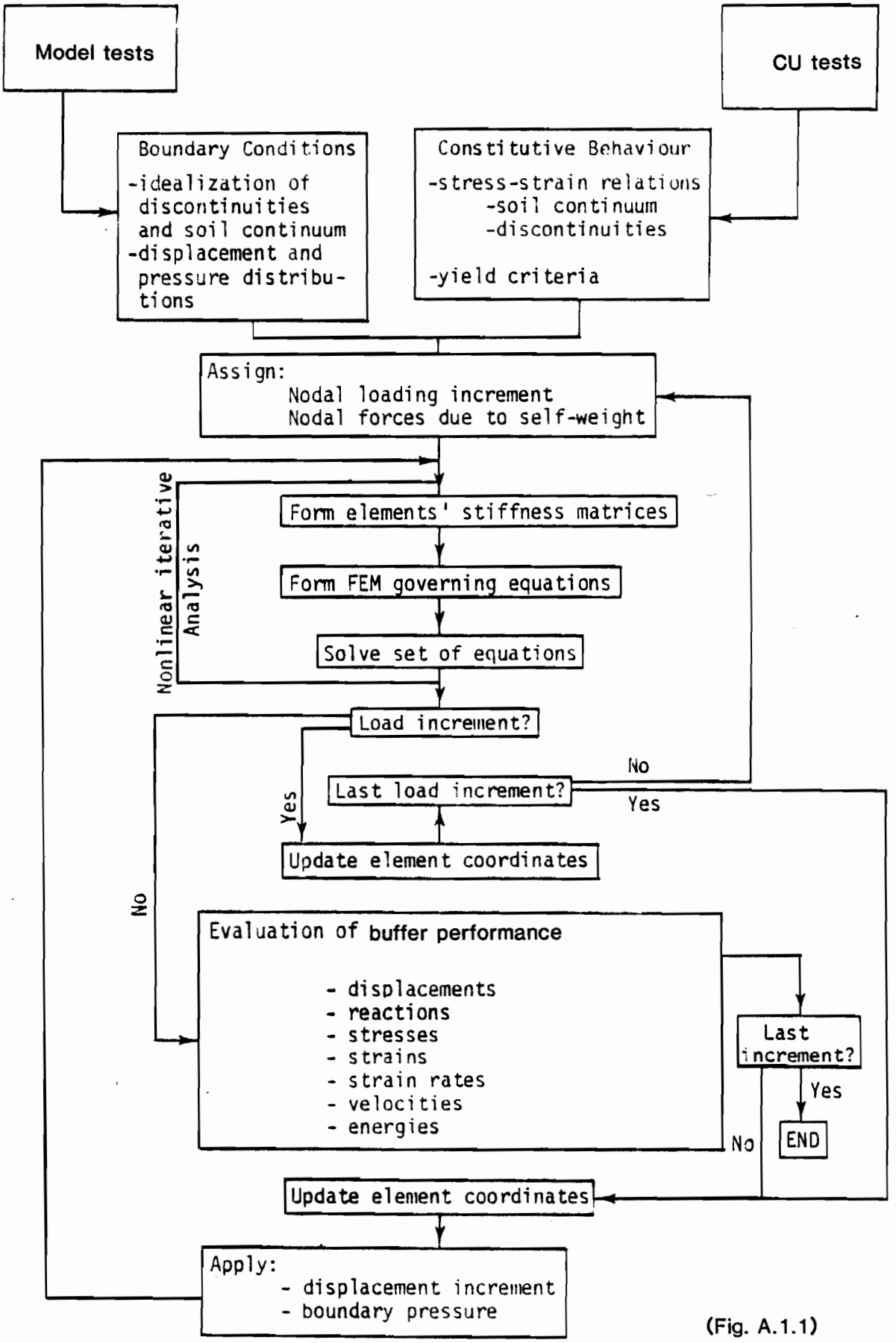

(Fig. A.1.1)

Finite element implementation where the boundary condition of uniform vertical pressure prevails.

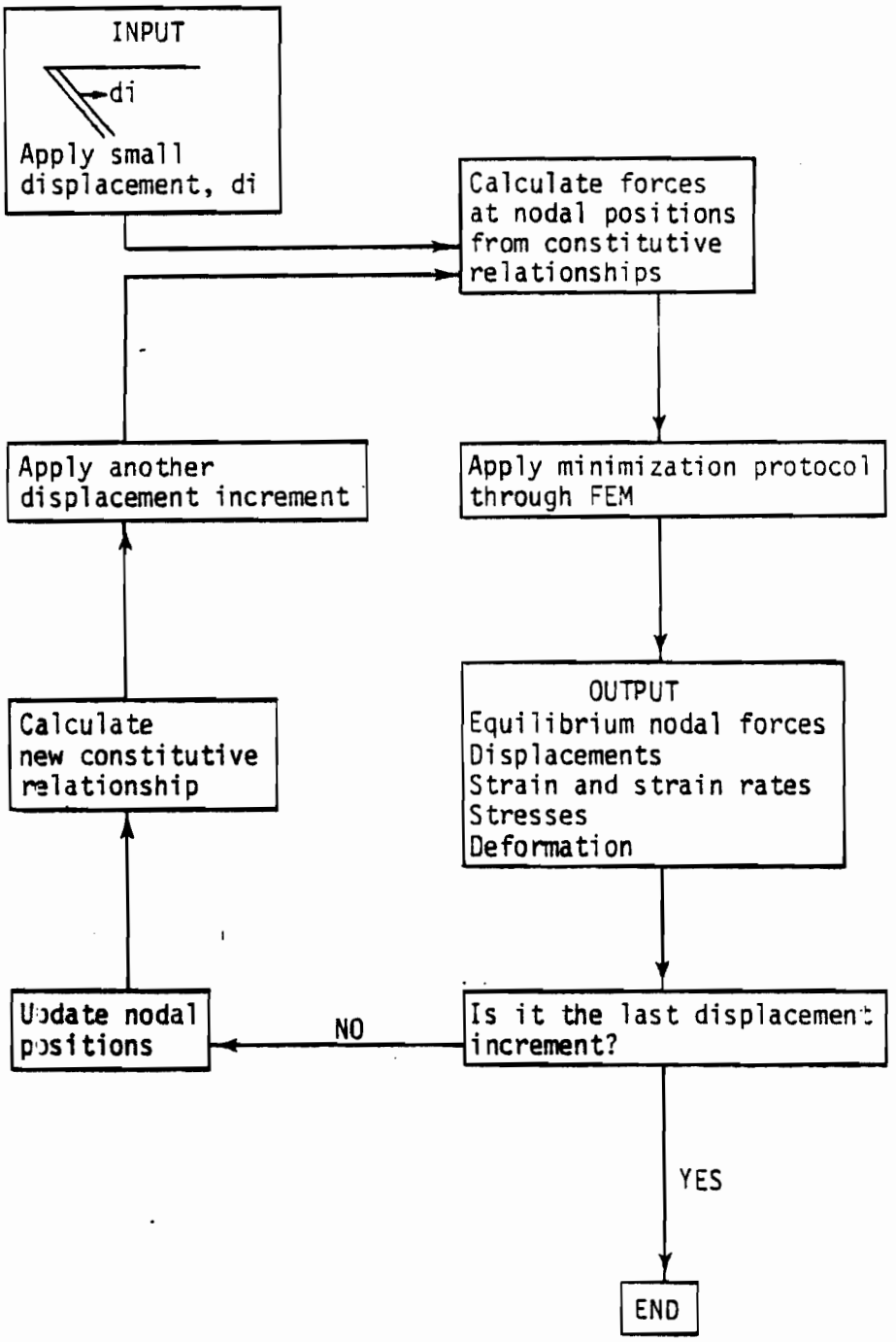

Simplified flow scheme for computation using the FEM of analysis

Fig. A.1.2 After Yong,Fattah and Sciadas,1984

Thus, eqs. (A.10), (A.11) and (A.12) can be used together to achieve the desired purpose. The method is discussed in more detail in Zienkiewicz' book (1971); it is very easy to program and is adopted in the computer program used in this work.

A5 Constitutive Relationships for Soils and Finite Element Nonlinear Analysis

A set of equations that defines the stress-strain behaviour of a material represents the constitutive law for the material. Constitutive relations for soils are derived, based on some simplified assumptions for the behaviour of the material. The number of variables occurring in the law would depend upon the complexity of the model chosen to simulate soil behaviour. Nonlinear analysis by the finite element method or other numerical techniques will be influenced by the nature of the model chosen. In general, the more complex the model, the more the number of variables to be taken into account and the more involved the nonlinear analysis. Moreover, for a realistic analysis, it must be possible to obtain values for the constants involved in the constitutive law from laboratory experiments.

The simplest constitutive law will be the one that assumes that soil behaviour can be represented by a linear, elastic material. This linear, elastic model has been used by many research workers in their investigations.

Other workers have considered soil to be elasto-plastic or nonlinearly elastic.

The elasto-plastic approach idealizes the stress-strain curve for the soil, and uses the equations of elasticity in the elastic range and the equations of plasticity in the plastic range. The nonlinear elastic approach, on the other hand, does not idealize the stress-strain curve, but uses the equations of elasticity to solve for the stress state even after yielding has occurred in the soil. Any degree of nonlinearity can be accounted for in this approach. The elasto-plastic approach appears sound from a theoretical standpoint, but the practical problems involved in defining a yield limit and a flow law are quite a handicap. In as much as the nonlinear elastic analysis represents the actual stress-strain relation obtained from tests, it seems reasonable to expect fairly good results from this type of analysis.

It is to be recognized that anisotropy in materials can be of two types. Material anisotropy represents different elastic properties in different directions. In nonlinear materials, stress-induced anisotropy always exists and this may be coupled with material anisotropy. The principal stresses under a loaded condition will seldom be the same, and this will result in different elastic values in different directions depending on the stress level. This causes stress-induced anisotropy. It is generally difficult to take this anisotropy into account

without elaborate testing or simplifying assumptions.

A6 Method of Analysis

In this particular study, nonlinearities occur in two different forms. The first is material or physical nonlinearity, which results from nonlinear constitutive laws. The second is geometric nonlinearity, which derives from finite changes in the geometry of the deforming body (Desai and Abel, 1972).

Material nonlinearity alone encompasses problems in which the stresses are not linearly proportional to the strains, but in which small displacements and small strains are considered. Displacements refer to the changes in the overall geometry of the soil body, whereas strains are related to internal deformations. Because of the small displacements encountered in some cases, local distortions of an element can be ignored and the areas of the original undeformed element can be ignored in computing stresses. In this case the linear strain-displacement equations written for plane strain problems as:

$$\varepsilon_x = \frac{u}{x} \qquad \varepsilon_y = \frac{v}{y}$$

$$\gamma_{xy} = \frac{v}{x} + \frac{u}{y}$$

are used.

The most general category of nonlinear problems is the combination of the material and geometric nonlinearities.

It involves nonlienar constitutive behaviour as well as large strain and finite displacements.

Nonlinear stress-strain behaviour may be approximated in finite element analyses by assigning different modulus values to each of the elements into which the soil is subdivided for purposes of analysis. The modulus value assigned to each element is selected on the basis of the stress or strain in each element. Because the modulus values depend on the stresses, and the stresses in turn depend on the modulus values, it is necessary to make repeated analyses to ensure that the modulus values correspond to the stress conditions for each element in the system.

Two techniques for approximate nonlinear analyses by the finite element method have been tried (Desai and Abel, 1972). These are:

1. Direct iteration method, shown in Fig. A.2. By this method, the same change in soil external loading is analysed repeatedly. After each analysis, the values of stress and strain within each element are examined to determine if they satisfy the appropriate nonlinear stress-strain relationship. If the values of stress and strain do not correspond, a new value of modulus is selected for that element for the next analysis. The main advantage of this technique is the capability of the procedure to represent stress-

strain relationships in which the stress decreases with increasing strain after reaching a peak value. The shortcoming of the iterative procedure is that it can only give the solution for the final level of applied load, and cannot consider the load and deformation history of the soil.

2. Incremental method, shown in Fig. A.3. In this procedure, the soil loading is considered to be applied in small increments. If the state of stress and strain at the start of an increment is known in each element, the state at the end of the increment can be found by an addition of incremental changes. The constitutive relationship to be used for each element may be determined at the beginning of each interval. Thus, the nonlinear stress-strain relationship is approximated by a series of straight lines. The principal advantage of this procedure is that it provides a relatively complete description of the load-deformation behaviour, as results are obtained for each of the intermediate states corresponding to an increment of loading.

In the present study, it is essential that the buffer deformation and stress fields are obtained and examined as time-dependent variables. For this purpose the incremental procedure was employed. The technique adopted makes use

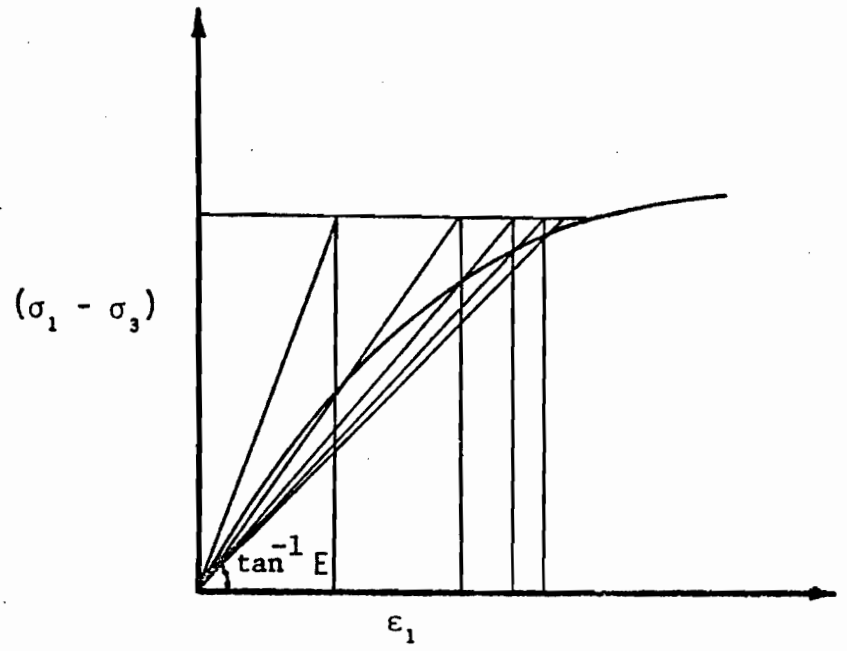

Fig. A.2 DIRECT ITERATION PROCEDURE

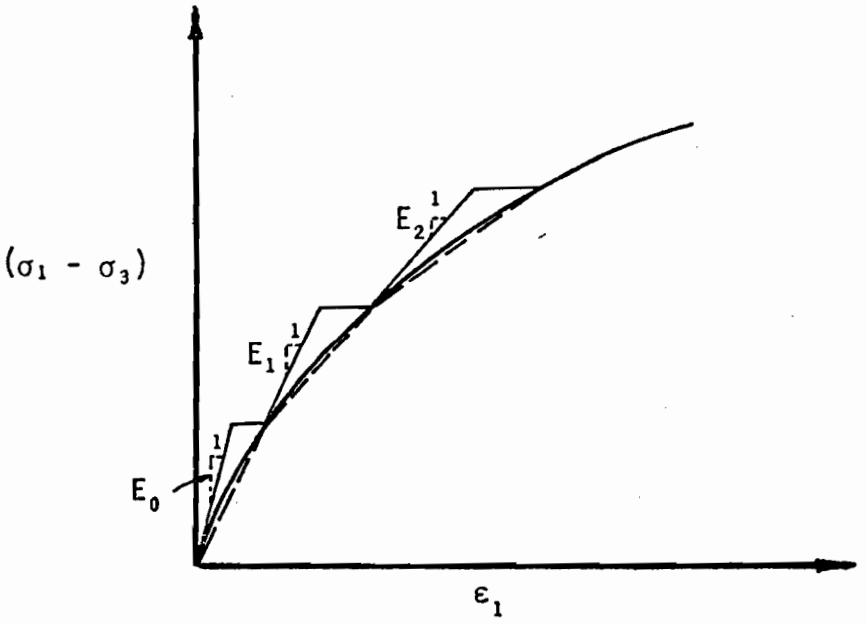

Fig. A.3 INCREMENTAL PROCEDURE

of the CU triaxial stress-strain curves to compute the value of the elastic modulus, E, during each increment. The value of Poisson's ratio V is kept constant in the analysis.

APPENDIX B

B1: Characterization and Index Properties of Avonlea Clay

B2: Swell Test Set-Up and Sample Preparation

B3: Triaxial Test Sample Preparation

Fig. B.1 X-Ray Diffractograms of AECL Avonlea Clay

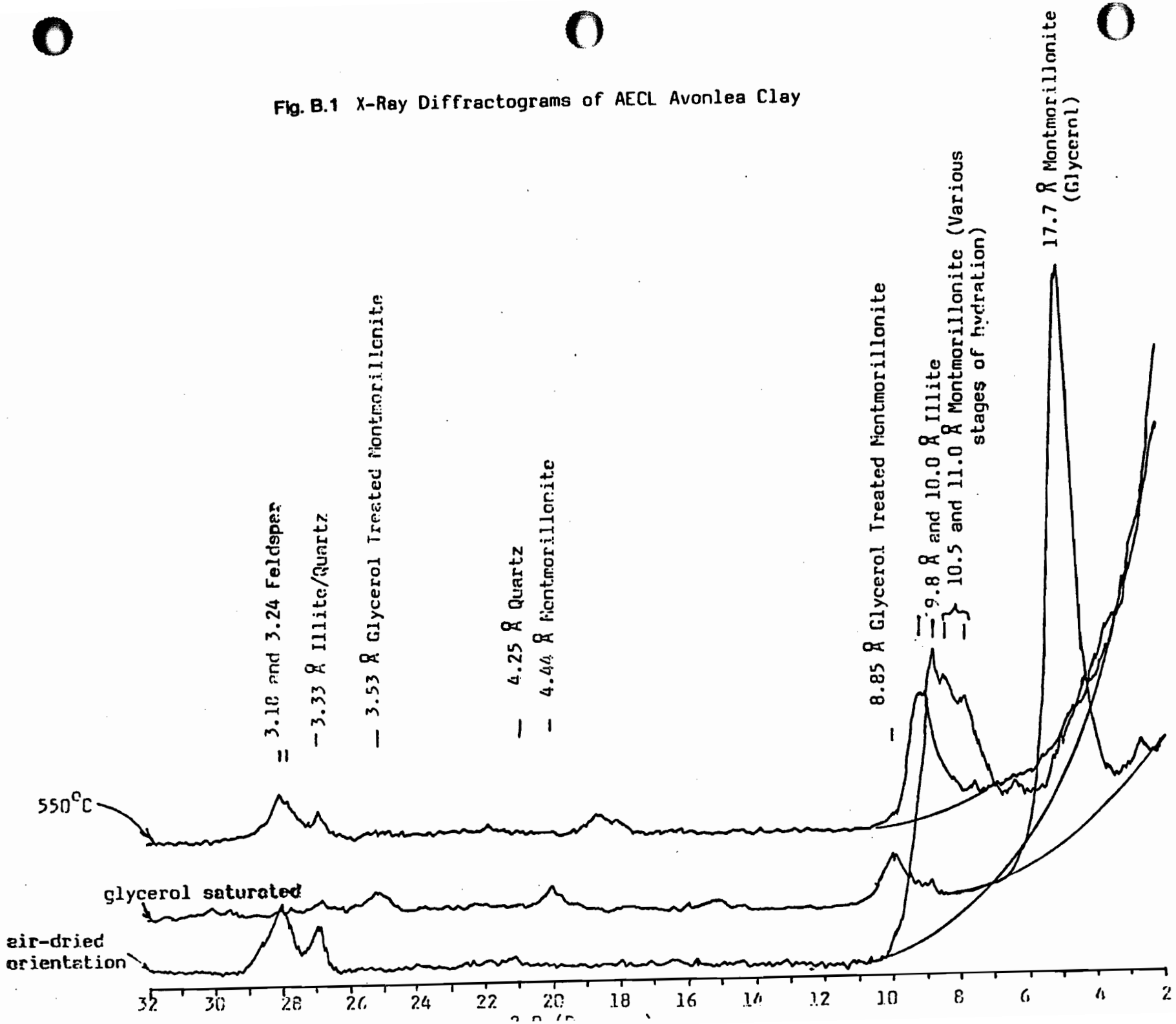

hydraulic head (10 cm granitic groundwater) was used in the test. Continuous readings were taken using the data acquisition system until relatively stable values were reached. A schematic diagram of the swelling pressure apparatus is shown in Fig. B.2. The measurement device is a cylindrical load cell, rated at 4.45 kN. The load cell top cap assembly is kept in contact with the sample by means of a steel holding rod firmly anchored to a rigid frame. Granitic groundwater is connected to the bottom of the sample from a constant hydraulic head reservoir. The resultant swelling pressure induced across the sample is electronically displayed and recorded on the data acquisition system.

The equipment used for the free swell measurement is shown in Fig. B.3. Instead of a load cell, a displacement transducer with a $\pm$ 25.4 mm travel is used to determine the change in specimen height as indicated by the relative movement of the lightweight top cap. The on-going output is also displayed electronically and recorded on the data acquisition system. The effect of side friction during sample and/or cap movement is minimized by using an interior lining of teflon material in teh consolidation cell.

B3 Triaxial Test Sample Preparation

A specimen 76 mm in height by 38 mm in diameter, was trimmed from a buffer sample compacted at the optimum

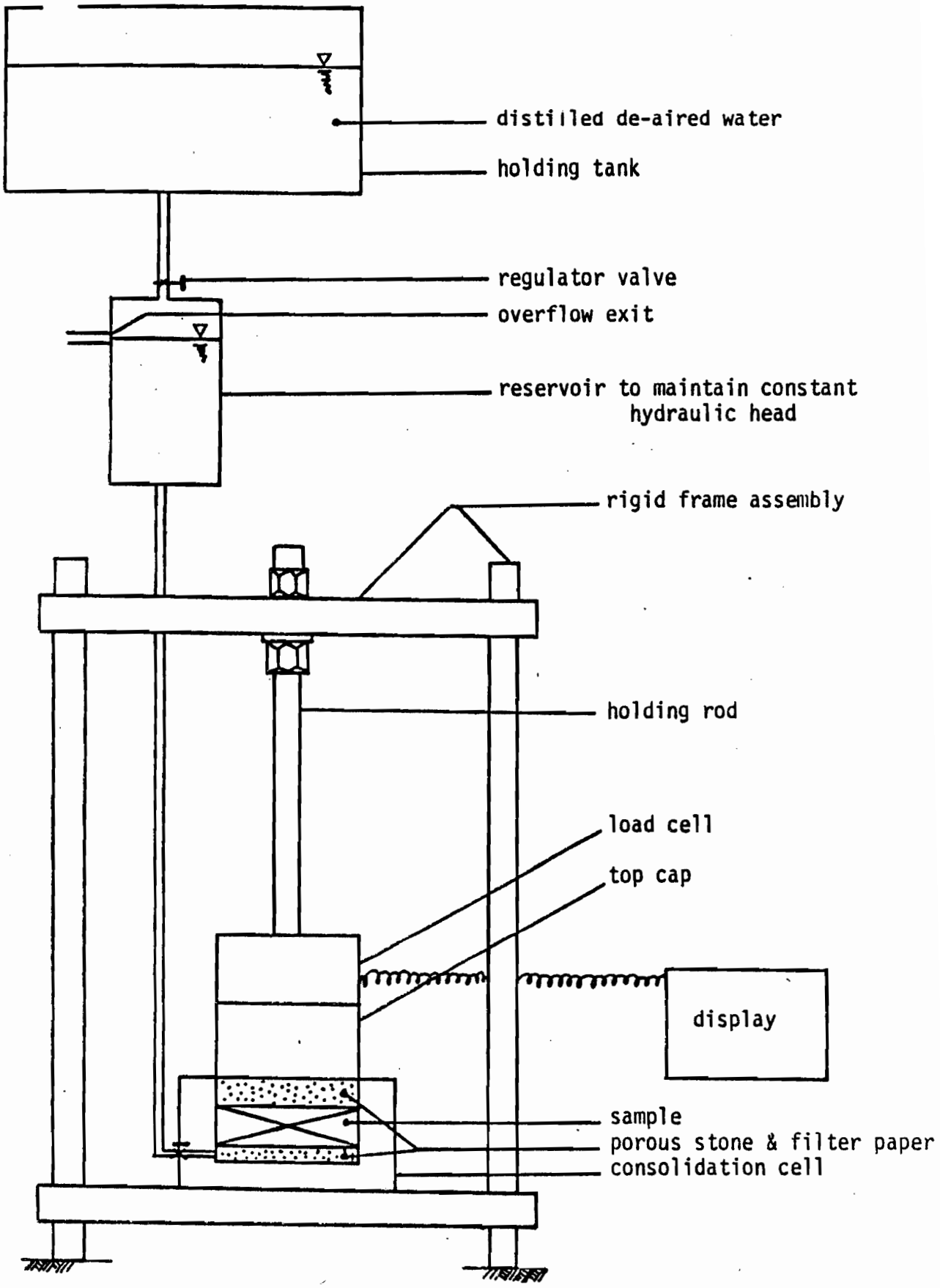

Fig. B.2 Apparatus for Swelling Pressure Determination

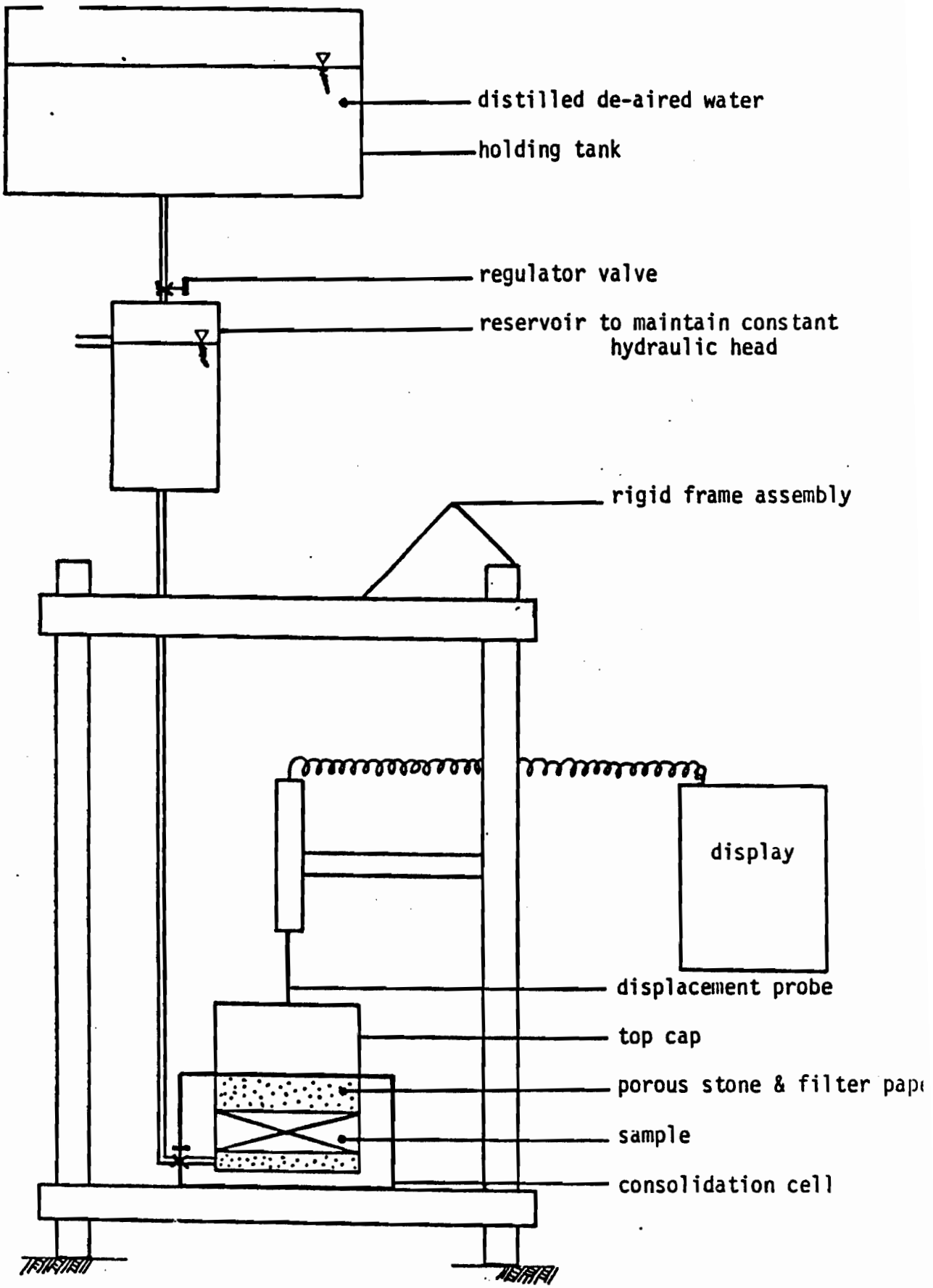

Fig. B.3 Apparatus for Free Swell Determination

moisture content. Some trimmings were used to determine the initial water content of the sample. The dimensions of the specimen were then carefully measured using a Vernier and weighed. After fitting the sample with side filter drains, enclosing it in two latex membranes and connecting to top drainage, it was set-up in a triaxial cell. The sample was then consolidated incrementally to the desired pressure (without back pressure for saturation). At each consolidation pressure, the sample was allowed to consolidate beyond the t_{100} value.

Upon completion of the consolidation stage the sample was loaded axially with a constant strain machine to failure. The rate of deformation was selected with regard to the t_{100} value during consolidation to allow full equilibration of pore pressure during loading. Load and deformation were measured by a Gould(Statham) load cell and a Hewlett Packard DCDT, respectively. Both of which were connected to the data acquisition system. After failure the sample was measured, weighed and the final water content was determined.

APPENDIX C

C1: Computer Program for F.E. Analysis

C2: Computer Program for Data Manipulation

C1 Computer Program for F.E. Analysis

The programs used in the present study were grouped under a series named "MAIN" and were based on Zienkiewicz's program (1971). These programs were developed by Hanna (1975) at the Geotechnical Research Centre and can handle non-linear material properties, and the different methods used to perform the non-linear analysis and idealize the continuum usually classified the type of the program.

"MAIN 1" and "MAIN 2" (Figs. C.1-C.2) use an incremental-iterative method without predictions to solve non-linear problems. "MAIN 1" is a general routine developed to handle problems with no discontinuities in the deformation field, the joint analysis was incorporated in "MAIN 2" to handle such problems.

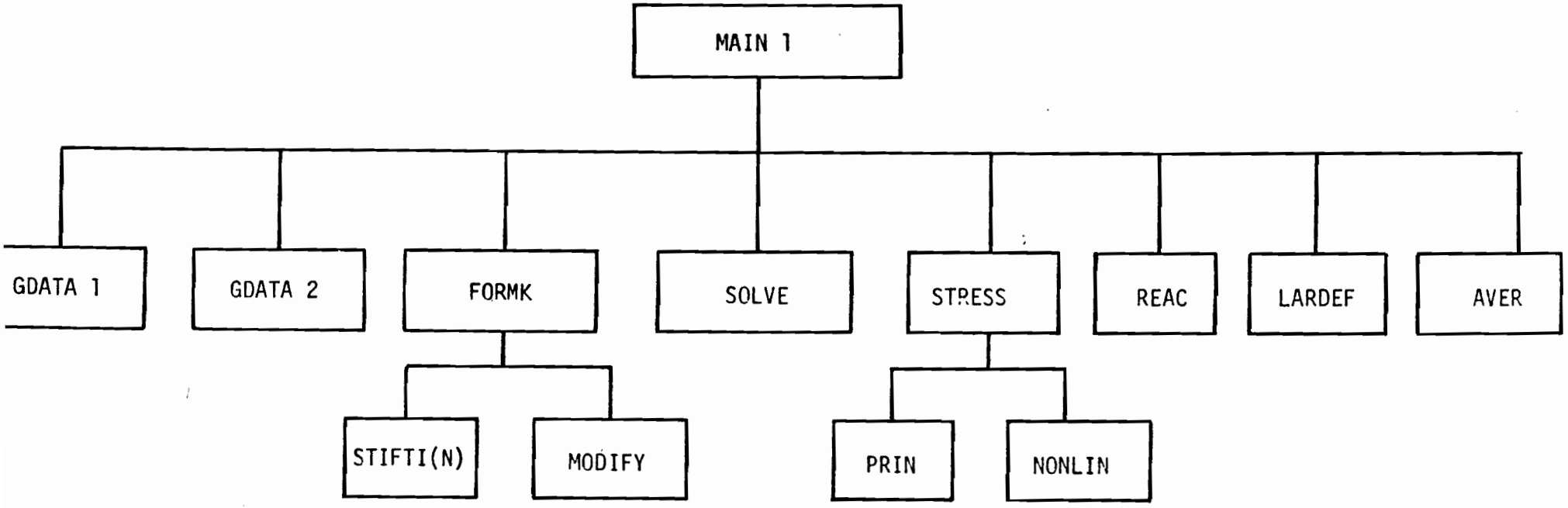

Fig. C1 - MAIN 1 SUBPROGRAM LINKAGE

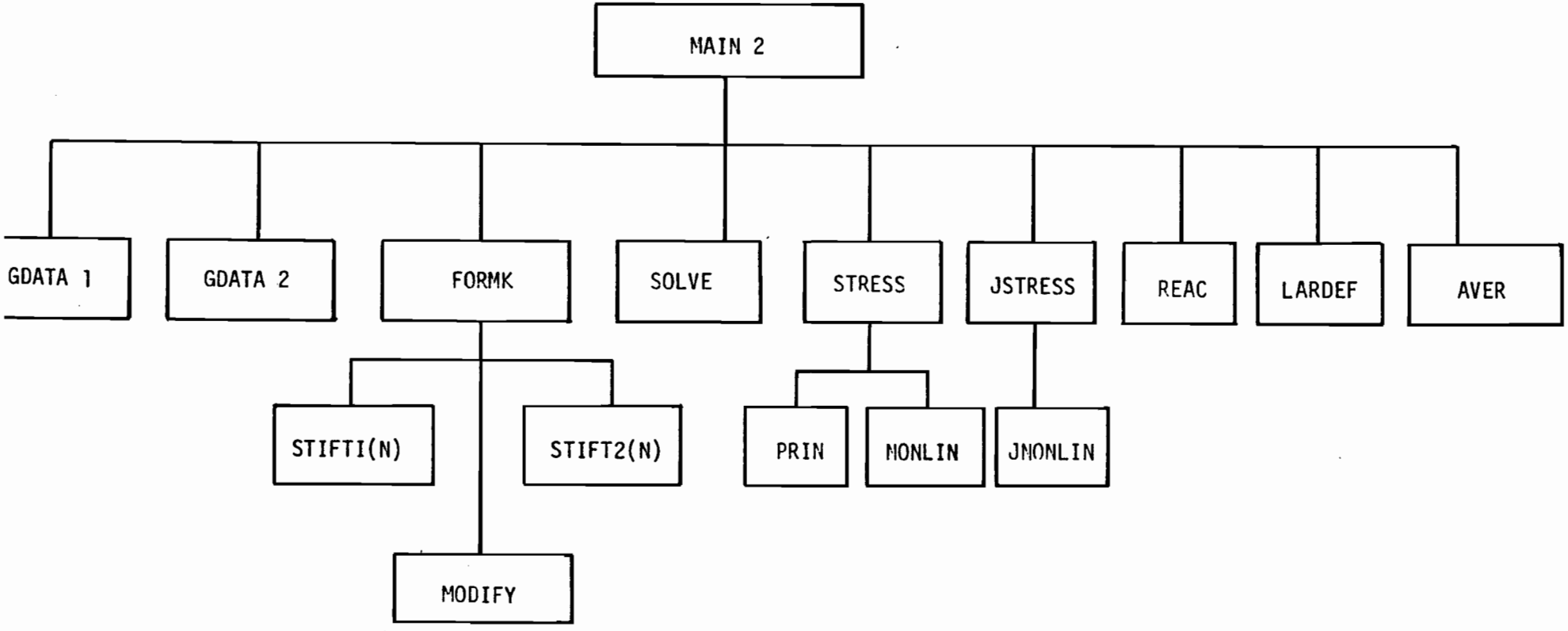

Fig. C2 - MAIN 2 SUBPROGRAM LINKAGE

FLOW CHARTS

PROGRAM MAIN 2

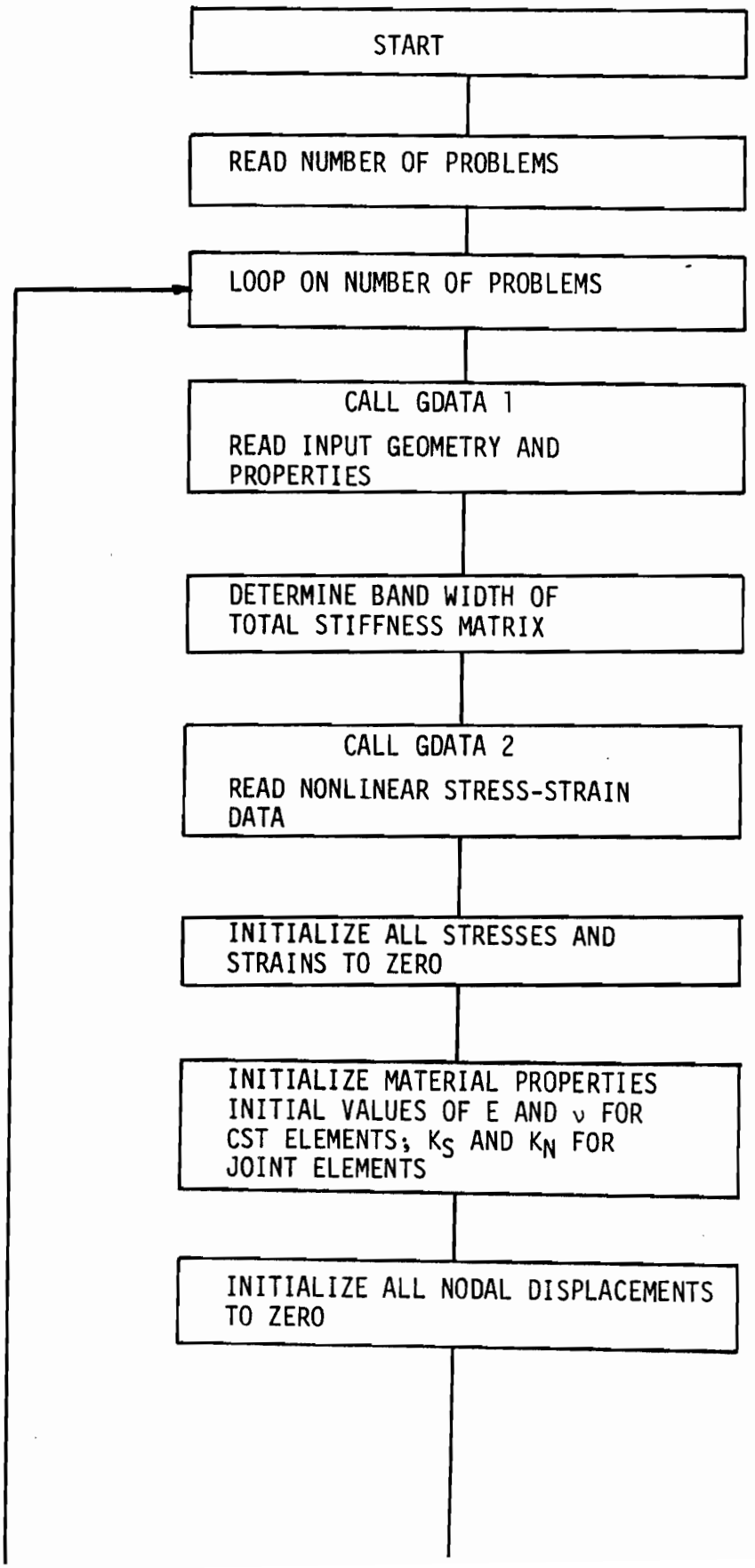

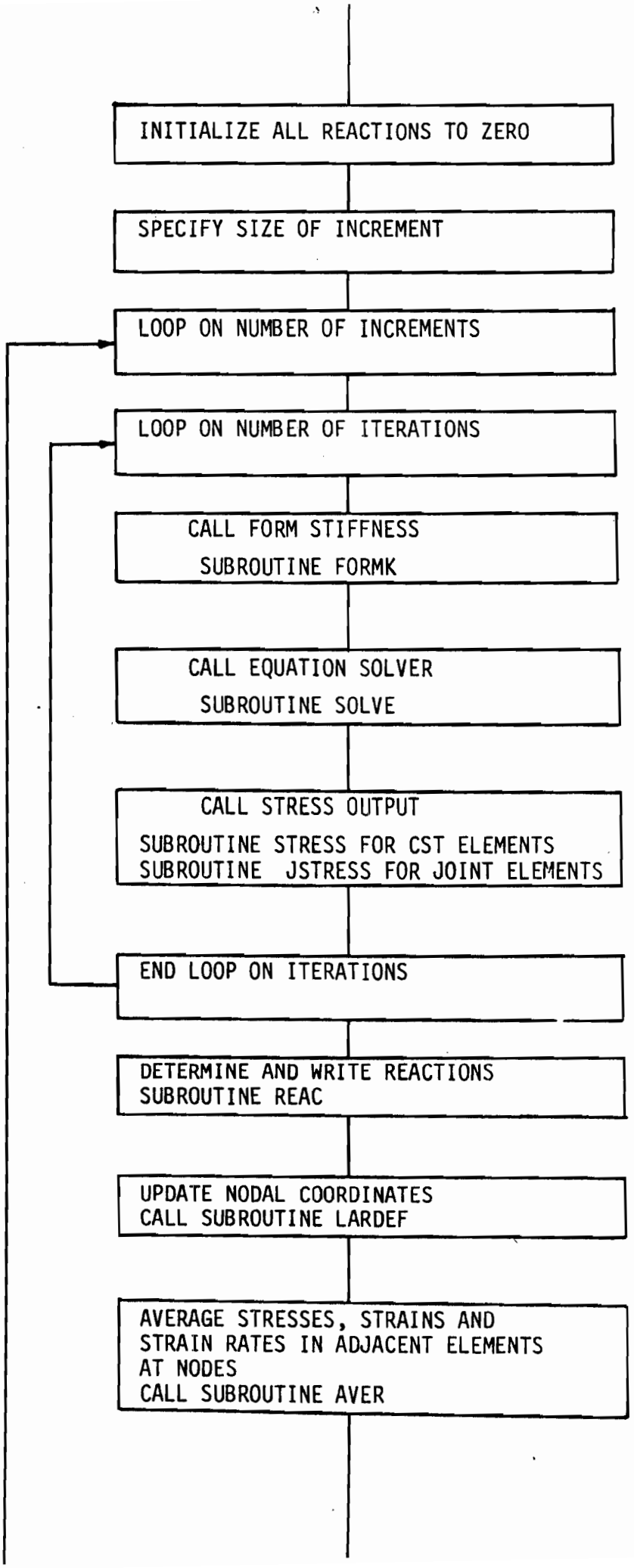
INITIALIZE ALL REACTIONS TO ZERO
SPECIFY SIZE OF INCREMENT
LOOP ON NUMBER OF INCREMENTS
LOOP ON NUMBER OF ITERATIONS
CALL FORM STIFFNESS
SUBROUTINE FORMK
CALL EQUATION SOLVER
SUBROUTINE SOLVE
CALL STRESS OUTPUT
SUBROUTINE STRESS FOR CST ELEMENTS
SUBROUTINE JSTRESS FOR JOINT ELEMENTS
END LOOP ON ITERATIONS
DETERMINE AND WRITE REACTIONS
SUBROUTINE REAC
UPDATE NODAL COORDINATES
CALL SUBROUTINE LARDEF
AVERAGE STRESSES, STRAINS AND
STRAIN RATES IN ADJACENT ELEMENTS
AT NODES
CALL SUBROUTINE AVER

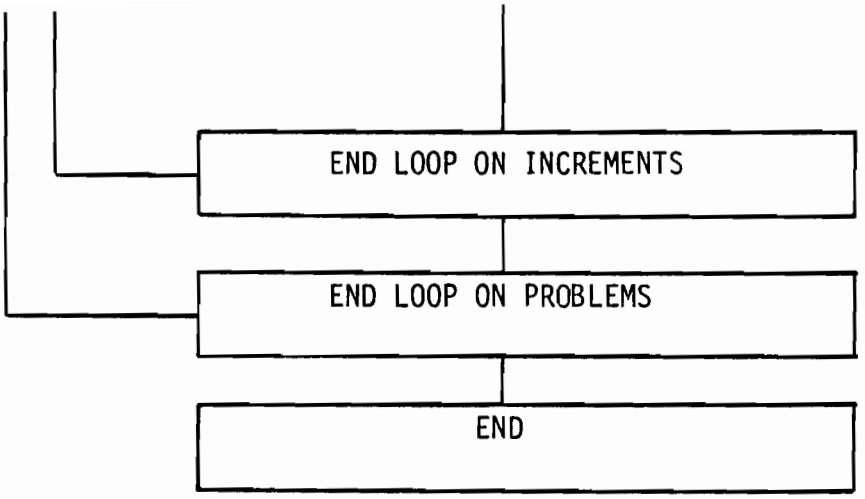
END LOOP ON INCREMENTS
END LOOP ON PROBLEMS
END

SUBROUTINE GDATA 1

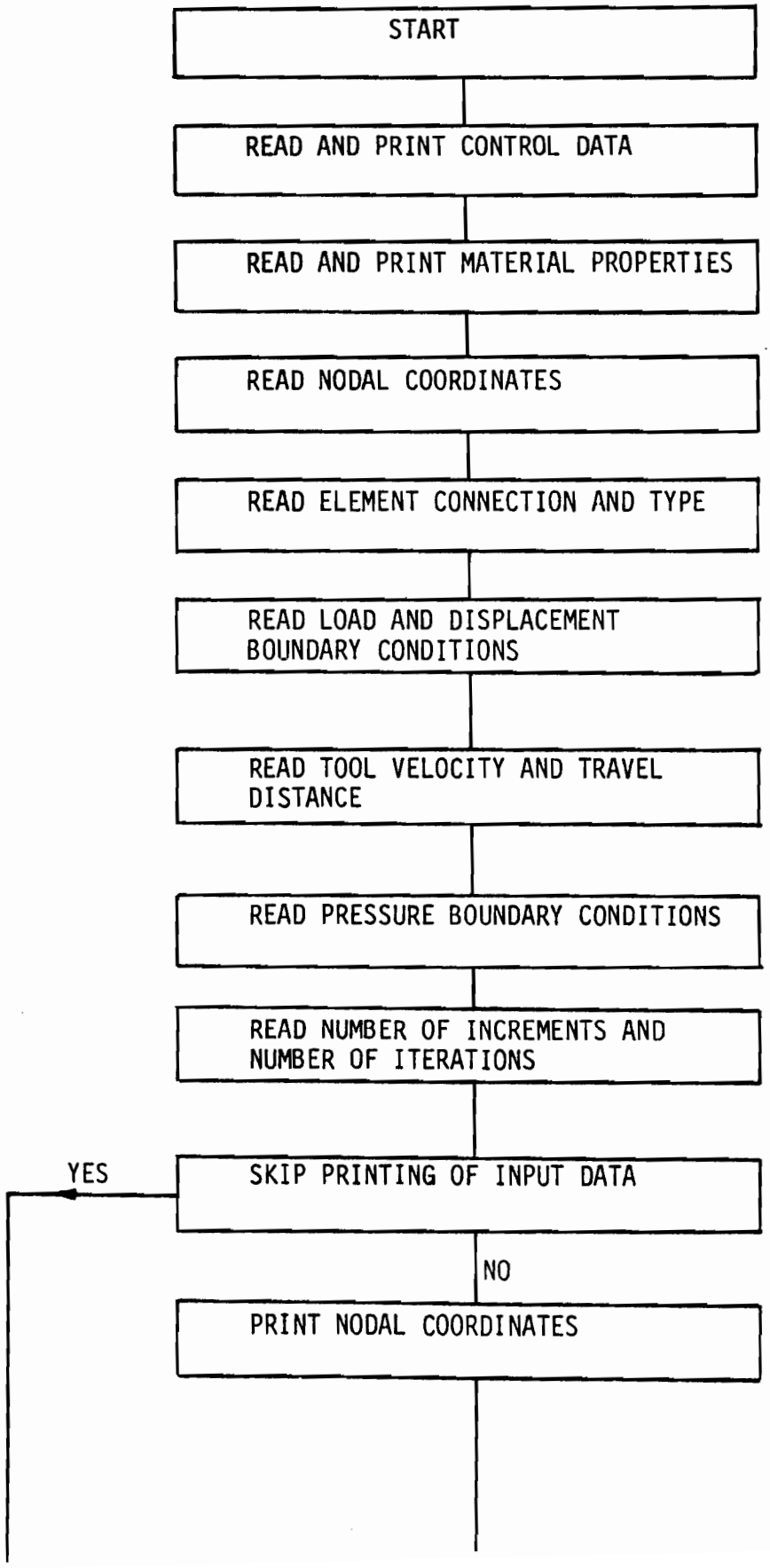

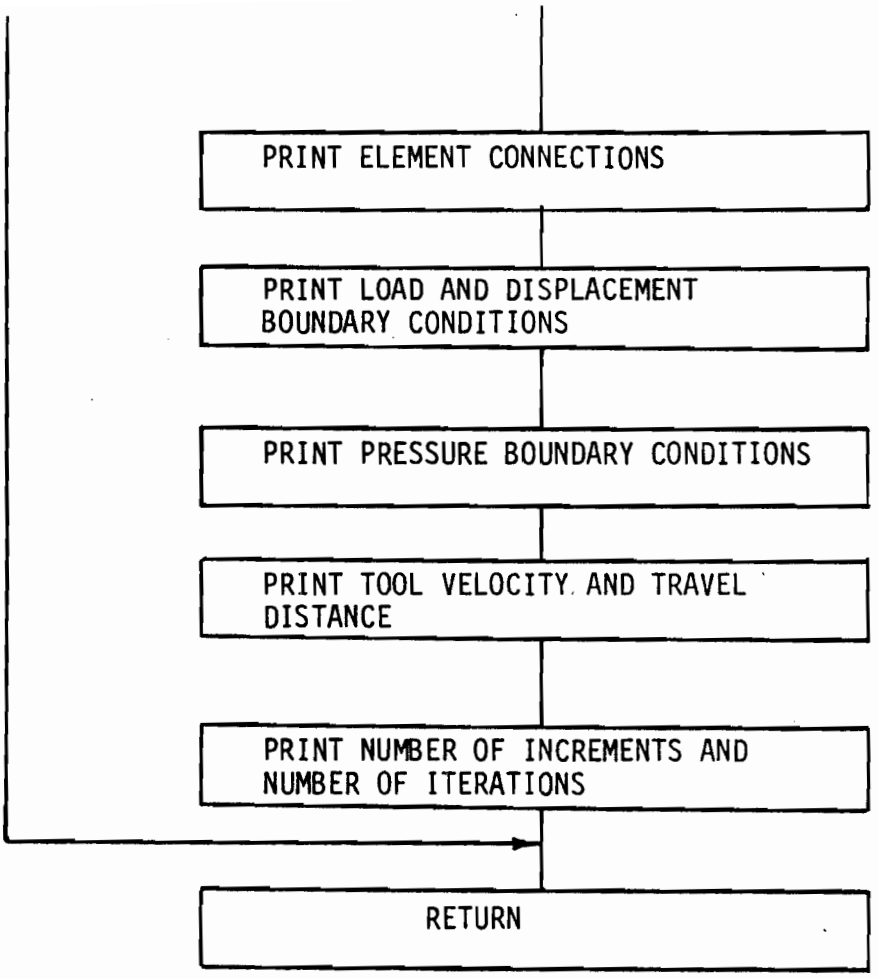
PRINT ELEMENT CONNECTIONS
PRINT LOAD AND DISPLACEMENT BOUNDARY CONDITIONS
PRINT PRESSURE BOUNDARY CONDITIONS
PRINT TOOL VELOCITY AND TRAVEL DISTANCE
PRINT NUMBER OF INCREMENTS AND NUMBER OF ITERATIONS
RETURN

SUBROUTINE GDATA 2

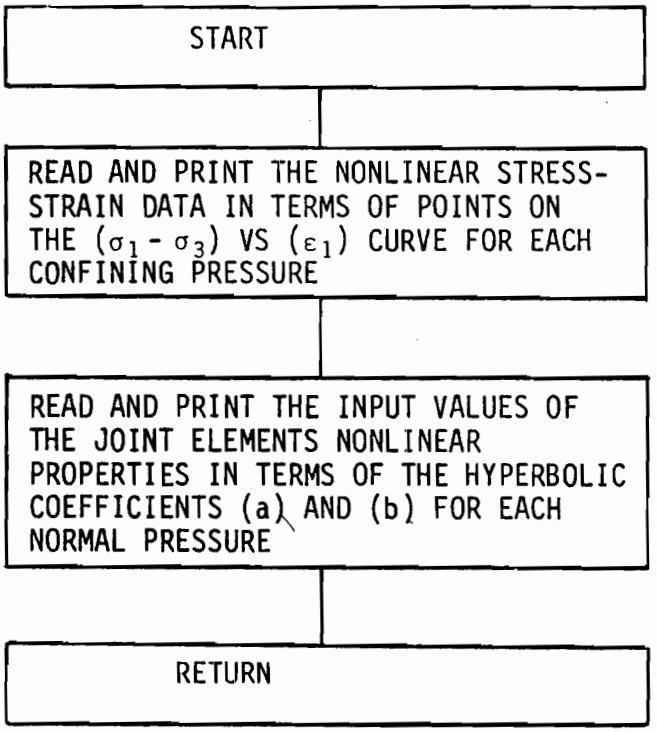

SUBROUTINE FORMK

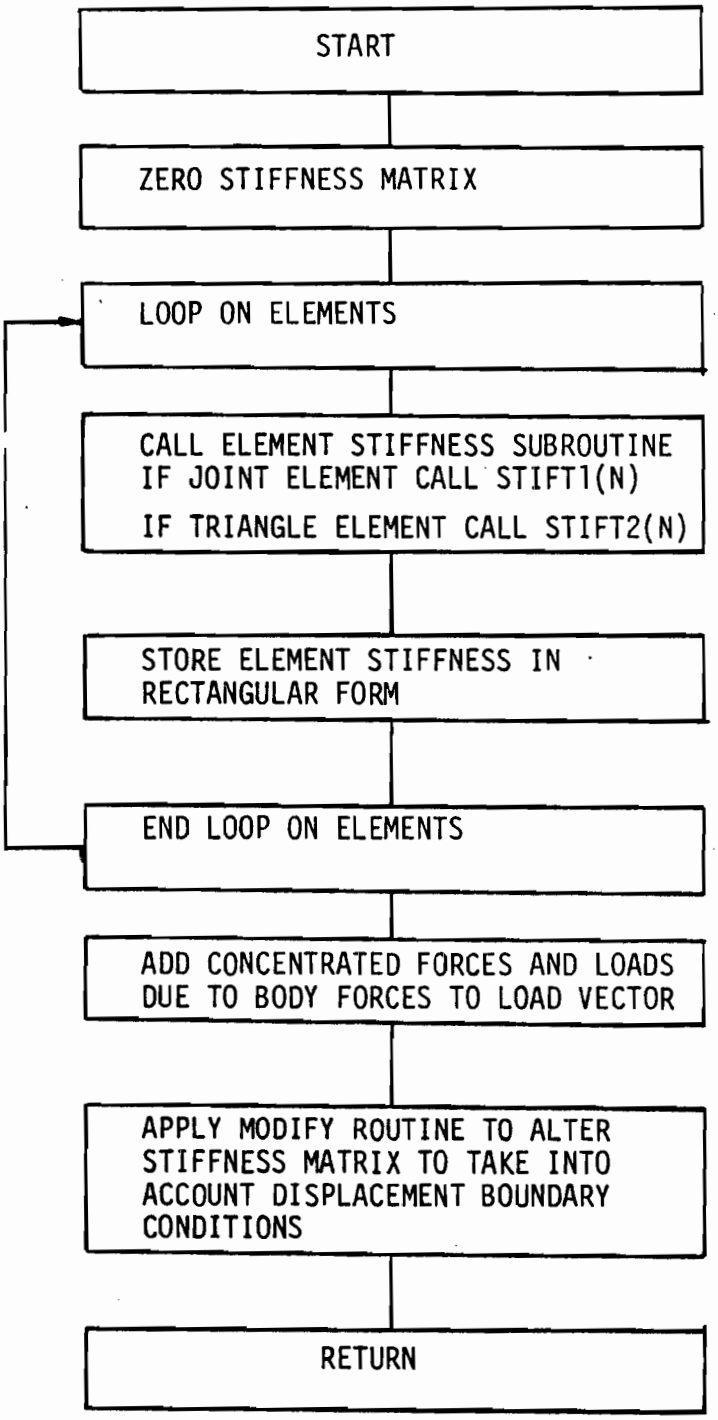

SUBROUTINE STIFT1(N)

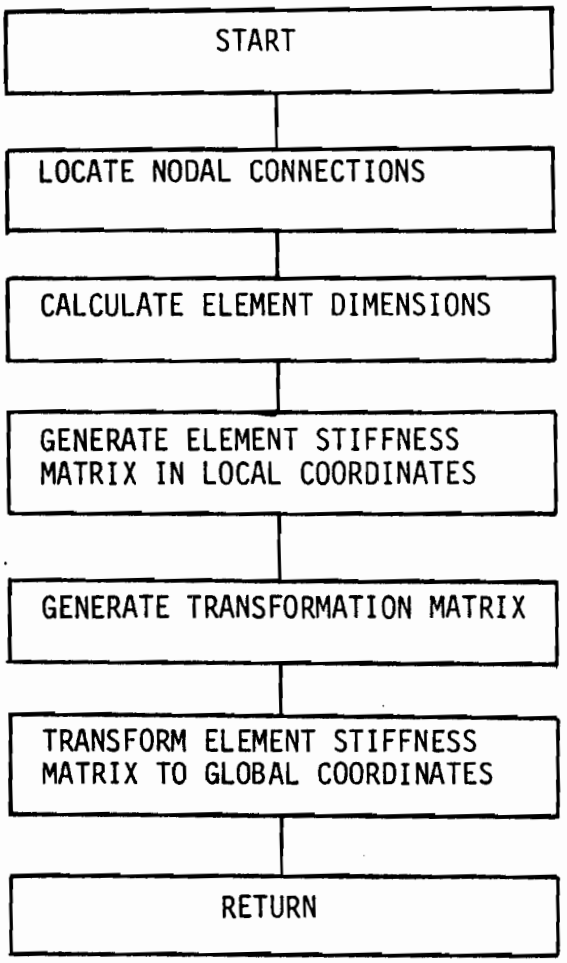

SUBROUTINE STIFT2(N)

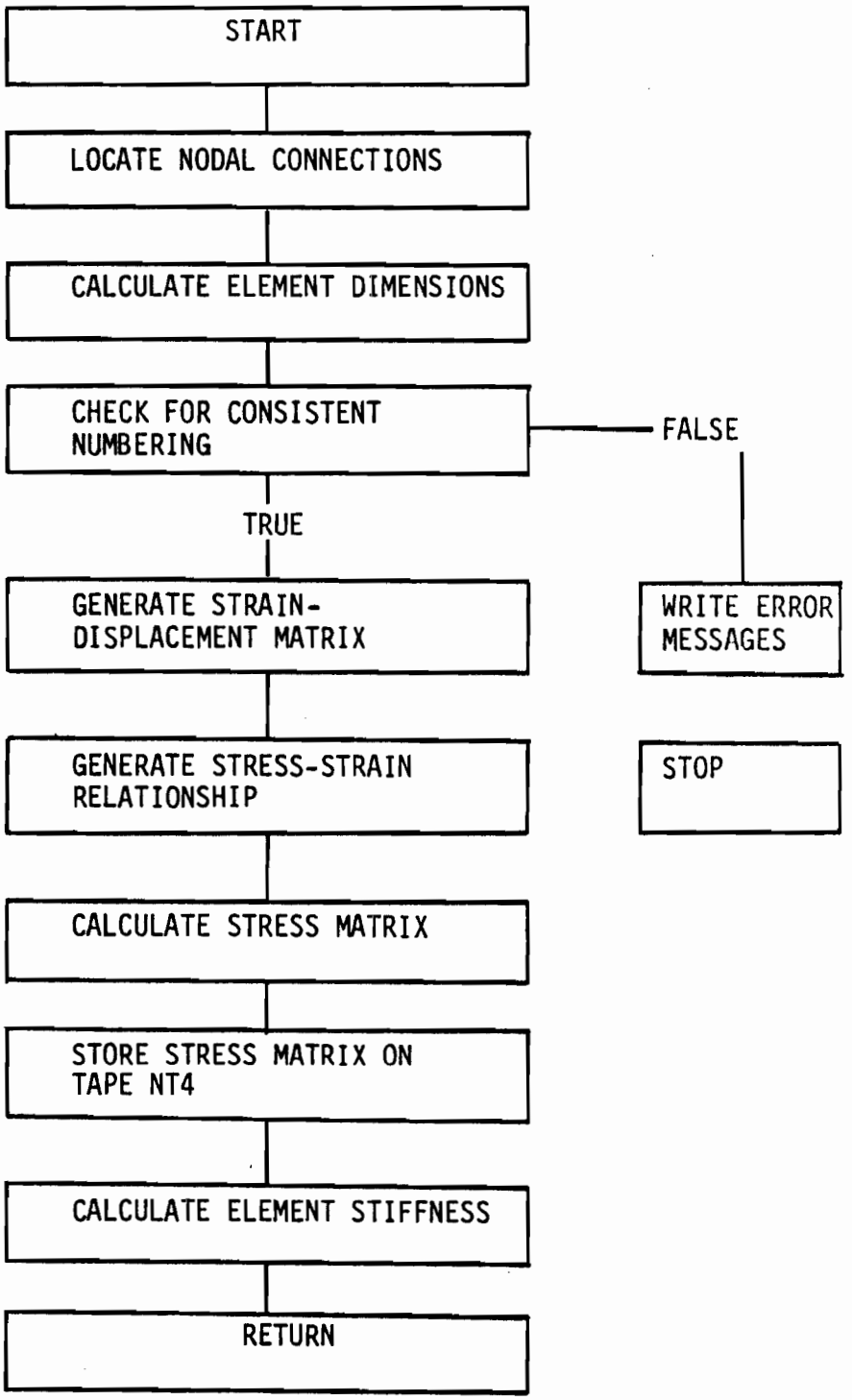

SUBROUTINE MODIFY

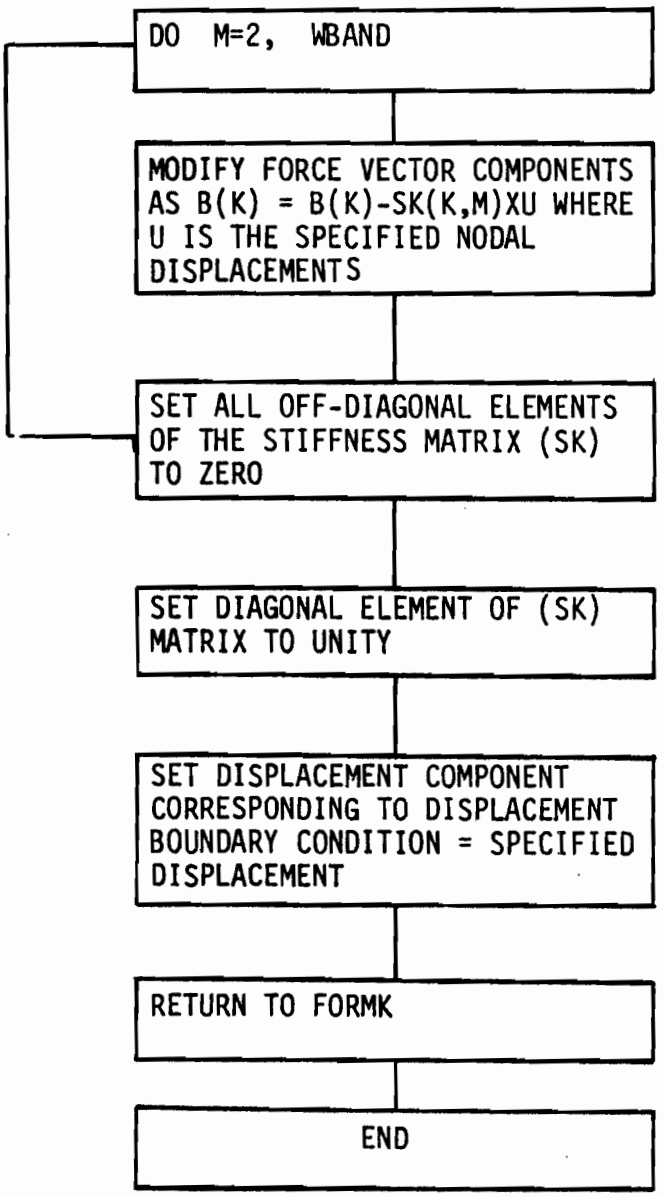

SUBROUTINE SOLVE

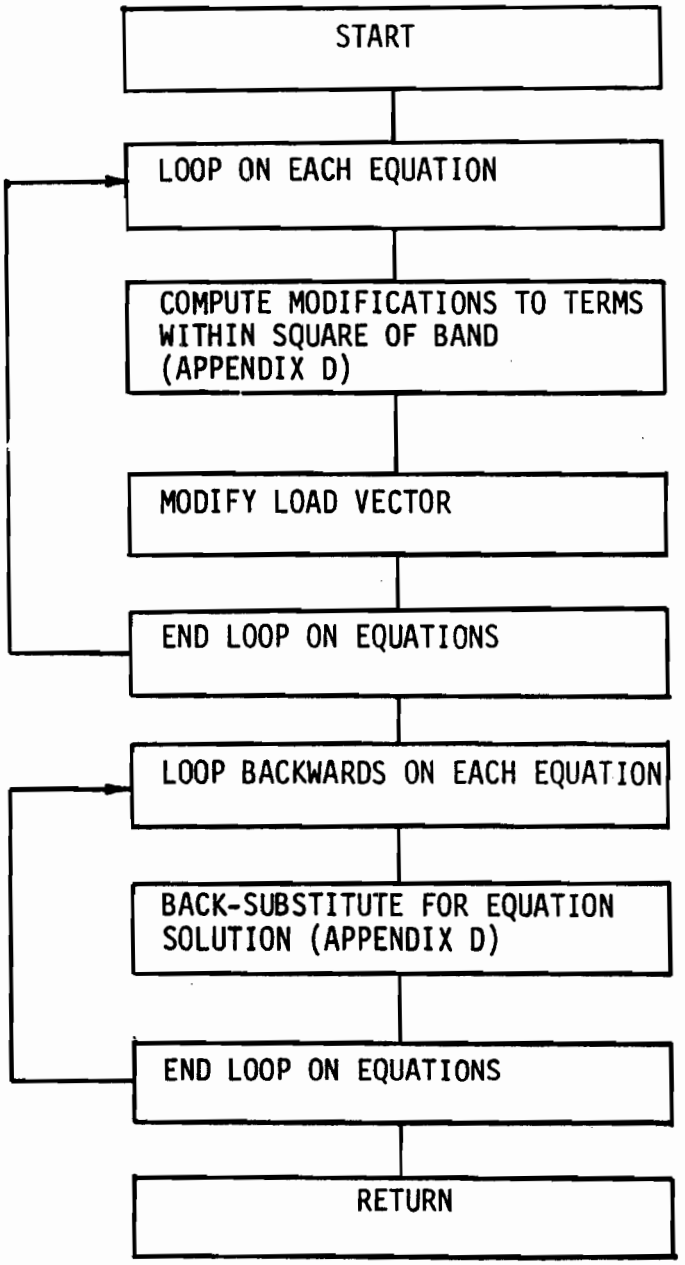

SUBROUTINE STRESS

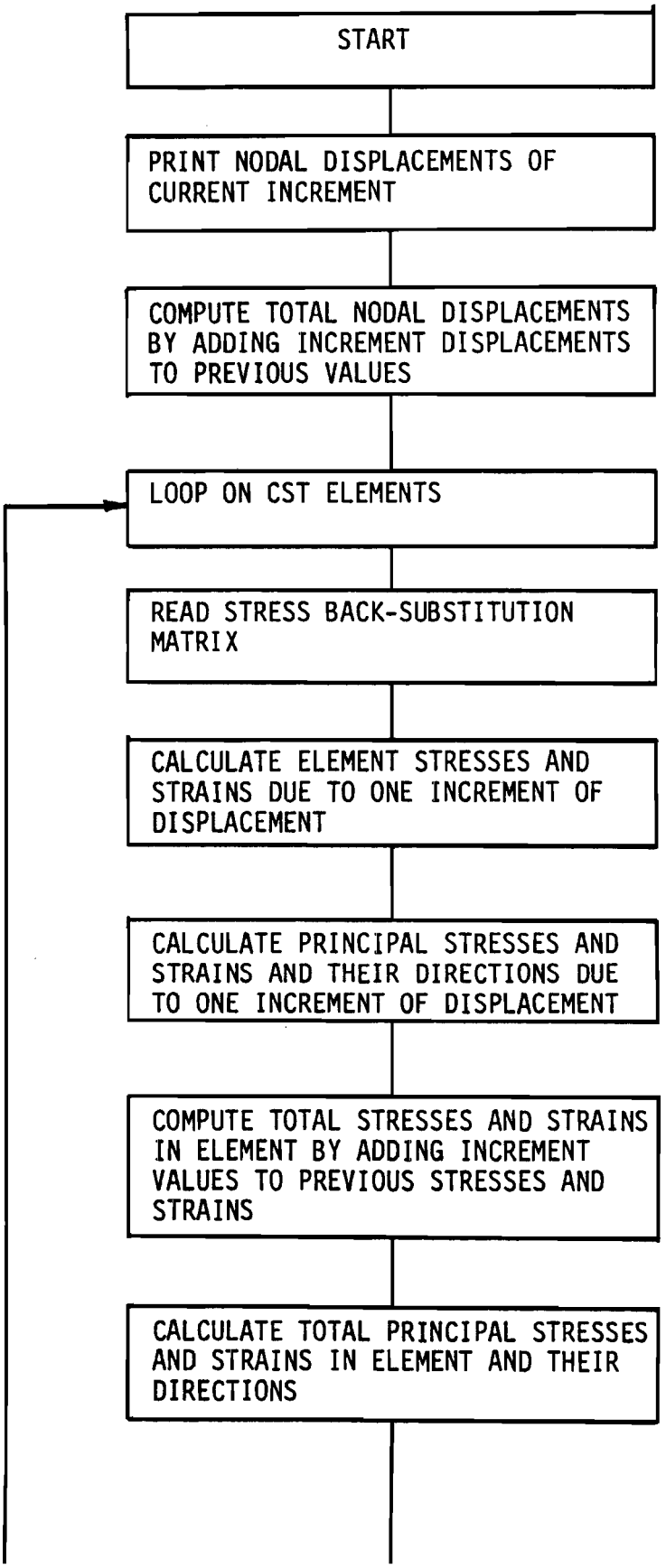

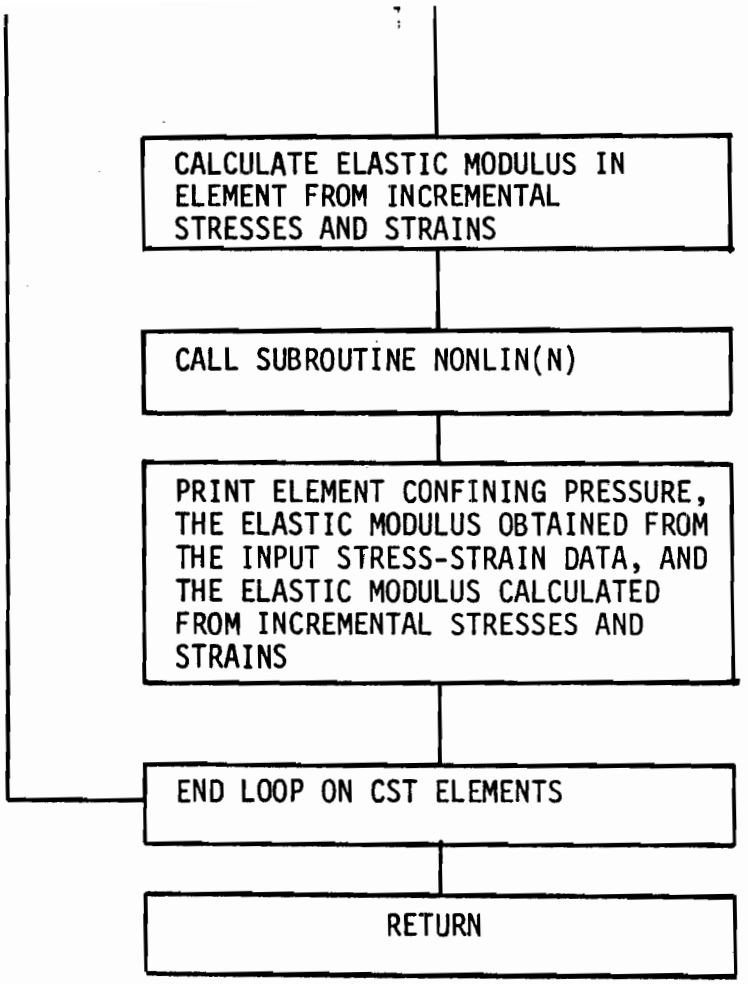
CALCULATE ELASTIC MODULUS IN ELEMENT FROM INCREMENTAL STRESSES AND STRAINS
CALL SUBROUTINE NONLIN(N)
PRINT ELEMENT CONFINING PRESSURE, THE ELASTIC MODULUS OBTAINED FROM THE INPUT STRESS-STRAIN DATA, AND THE ELASTIC MODULUS CALCULATED FROM INCREMENTAL STRESSES AND STRAINS
END LOOP ON CST ELEMENTS
RETURN

SUBROUTINE JSTRES

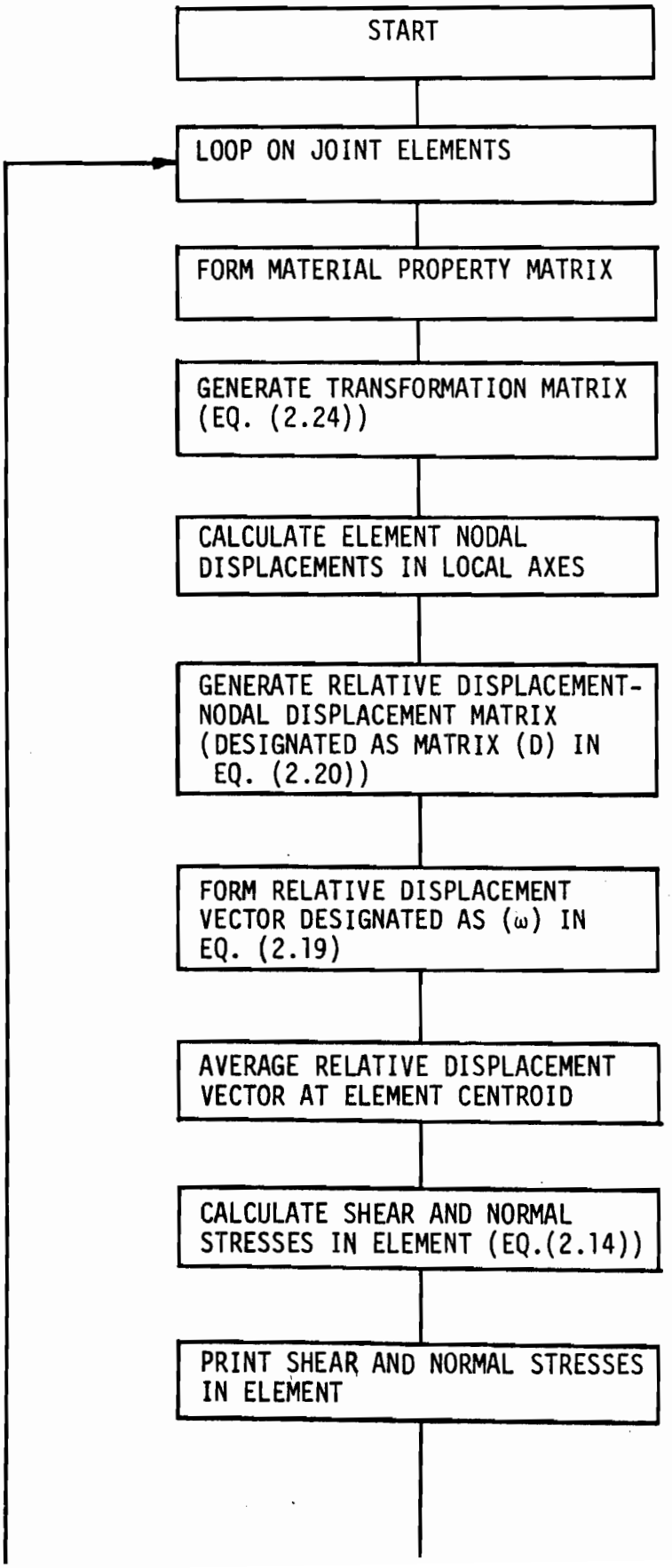

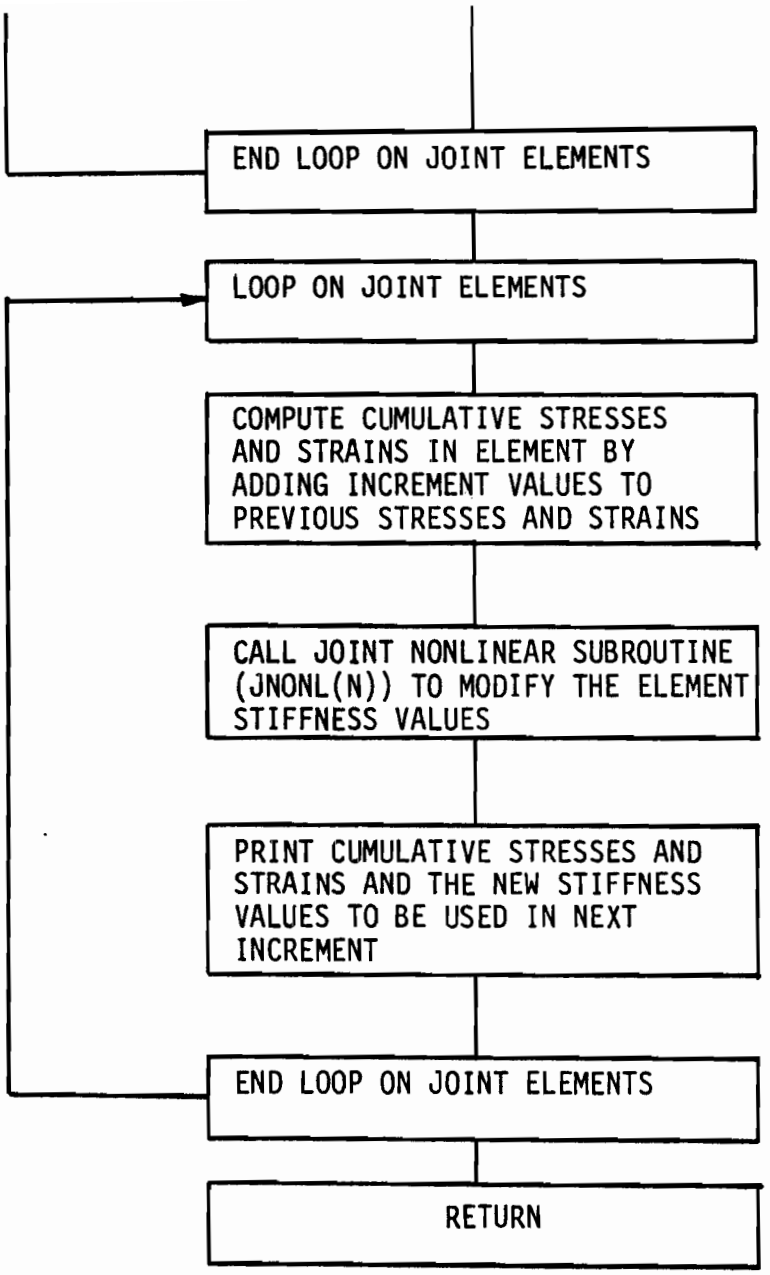
END LOOP ON JOINT ELEMENTS
LOOP ON JOINT ELEMENTS
COMPUTE CUMULATIVE STRESSES AND STRAINS IN ELEMENT BY ADDING INCREMENT VALUES TO PREVIOUS STRESSES AND STRAINS
CALL JOINT NONLINEAR SUBROUTINE (JNONL(N)) TO MODIFY THE ELEMENT STIFFNESS VALUES
PRINT CUMULATIVE STRESSES AND STRAINS AND THE NEW STIFFNESS VALUES TO BE USED IN NEXT INCREMENT
END LOOP ON JOINT ELEMENTS
RETURN

SUBROUTINE REAC

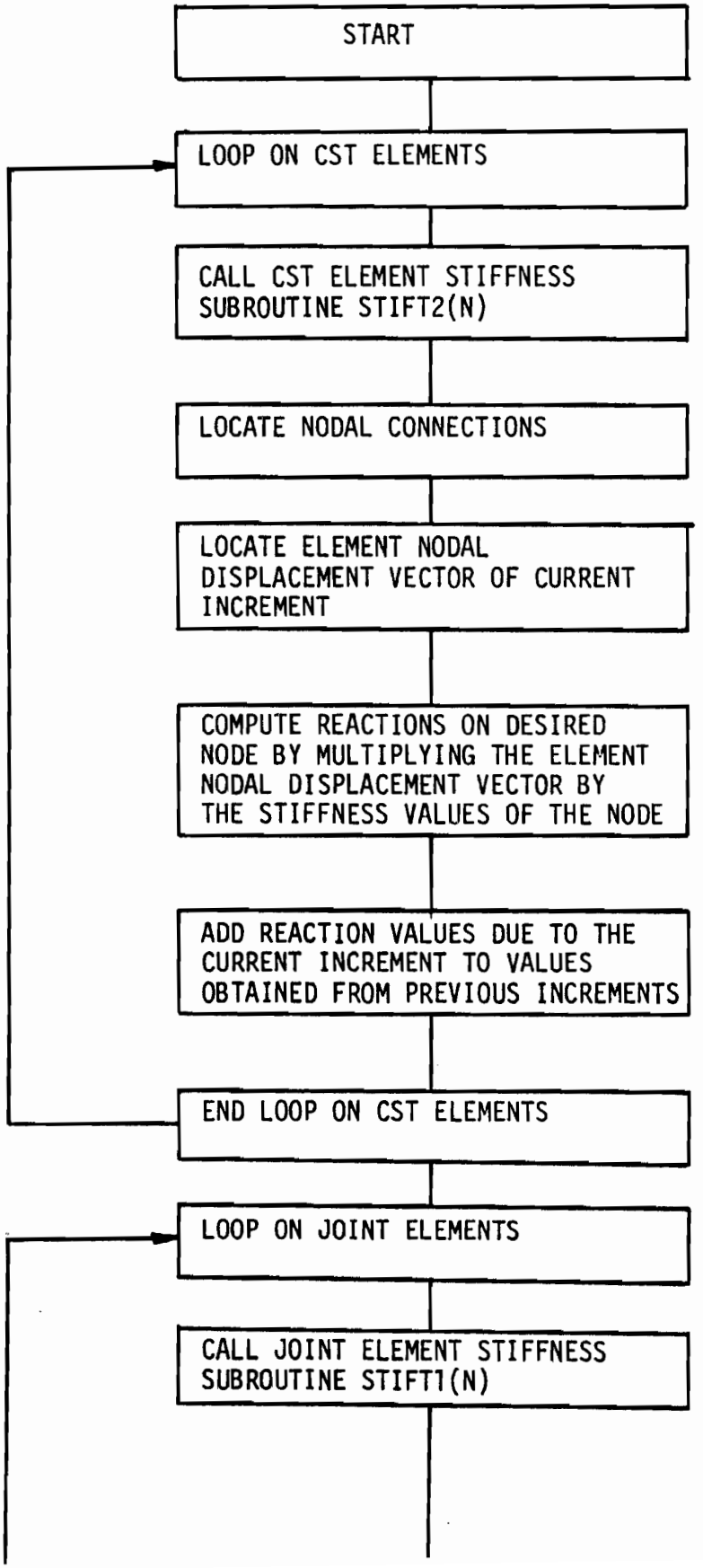

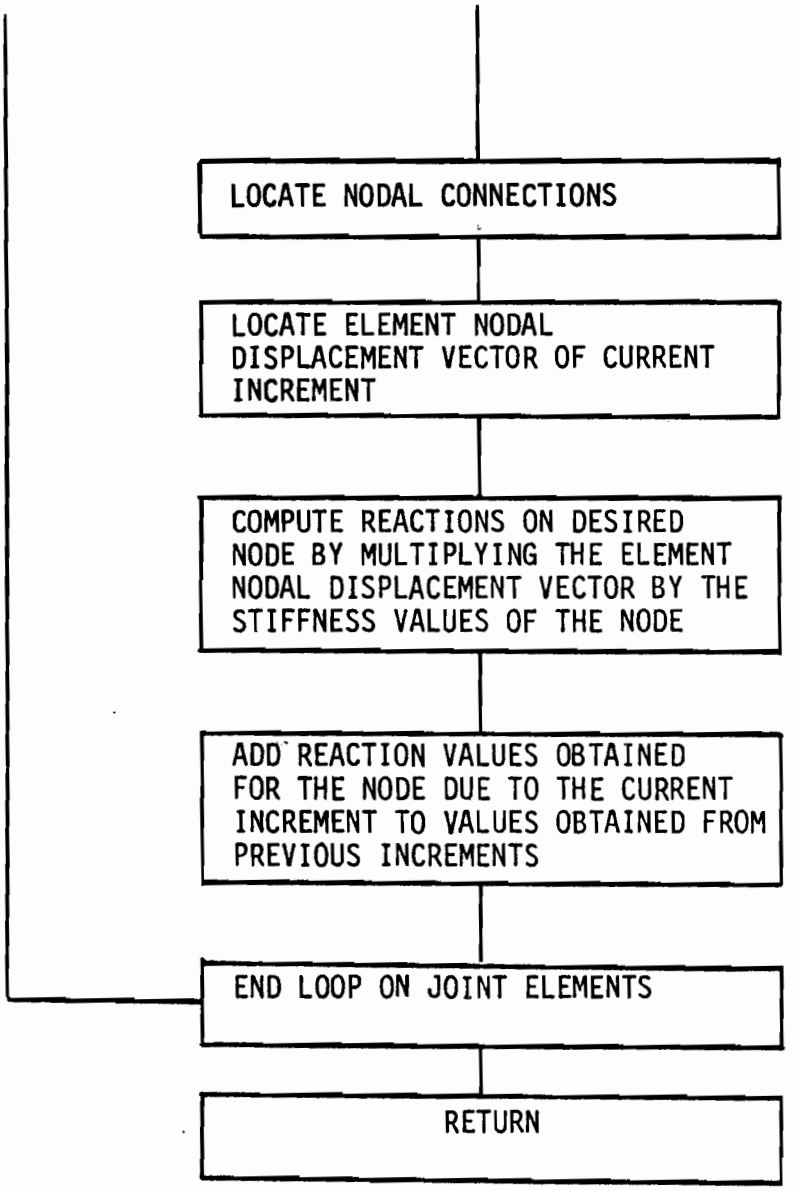
LOCATE NODAL CONNECTIONS
LOCATE ELEMENT NODAL DISPLACEMENT VECTOR OF CURRENT INCREMENT
COMPUTE REACTIONS ON DESIRED NODE BY MULTIPLYING THE ELEMENT NODAL DISPLACEMENT VECTOR BY THE STIFFNESS VALUES OF THE NODE
ADD REACTION VALUES OBTAINED FOR THE NODE DUE TO THE CURRENT INCREMENT TO VALUES OBTAINED FROM PREVIOUS INCREMENTS
END LOOP ON JOINT ELEMENTS
RETURN

SUBROUTINE LARDEF

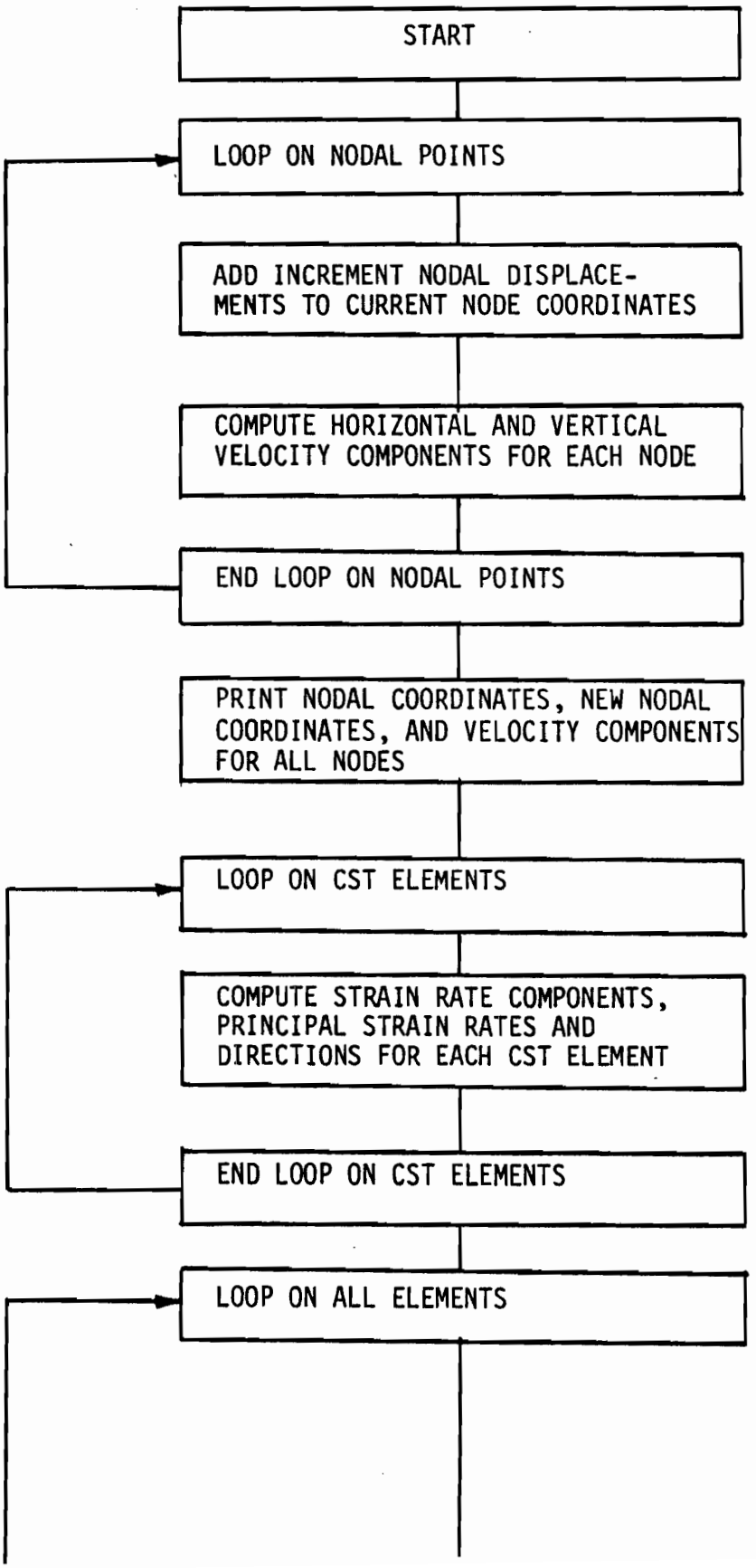

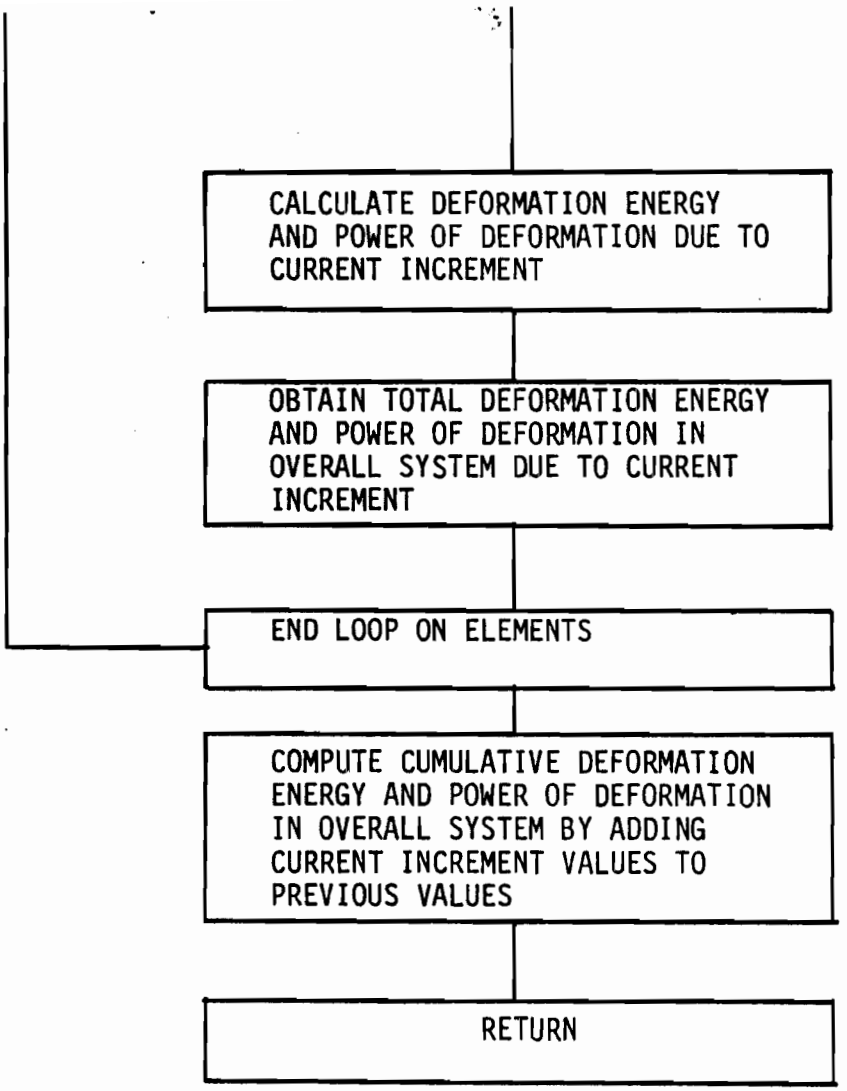
CALCULATE DEFORMATION ENERGY AND POWER OF DEFORMATION DUE TO CURRENT INCREMENT
OBTAIN TOTAL DEFORMATION ENERGY AND POWER OF DEFORMATION IN OVERALL SYSTEM DUE TO CURRENT INCREMENT
END LOOP ON ELEMENTS
COMPUTE CUMULATIVE DEFORMATION ENERGY AND POWER OF DEFORMATION IN OVERALL SYSTEM BY ADDING CURRENT INCREMENT VALUES TO PREVIOUS VALUES
RETURN

SUBROUTINE NONLIN(N)

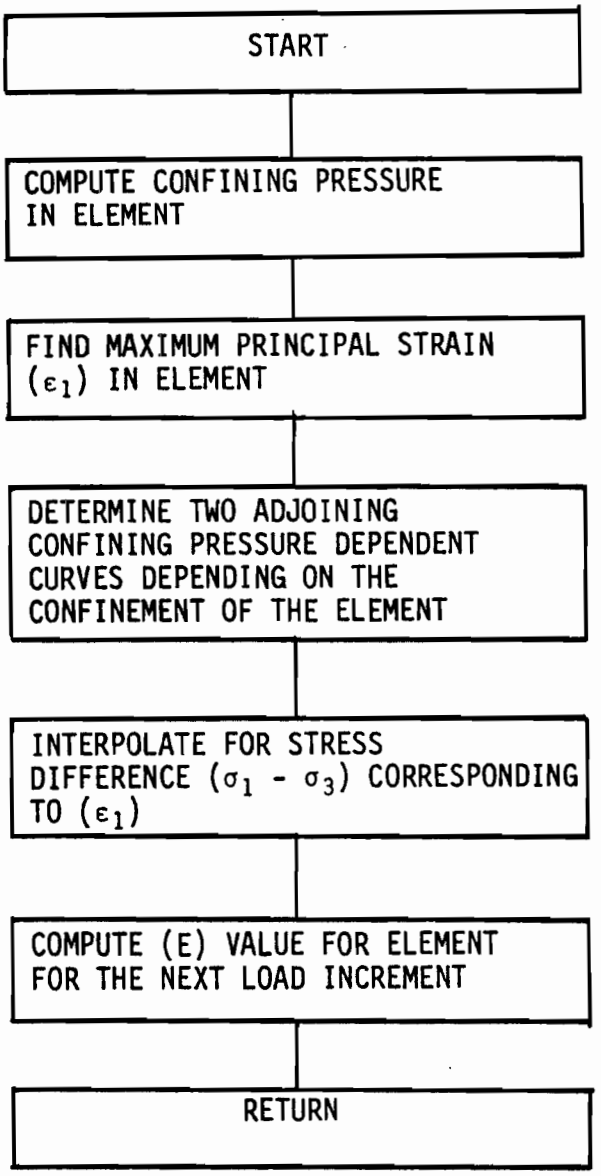

SUBROUTINE JNONL(N)

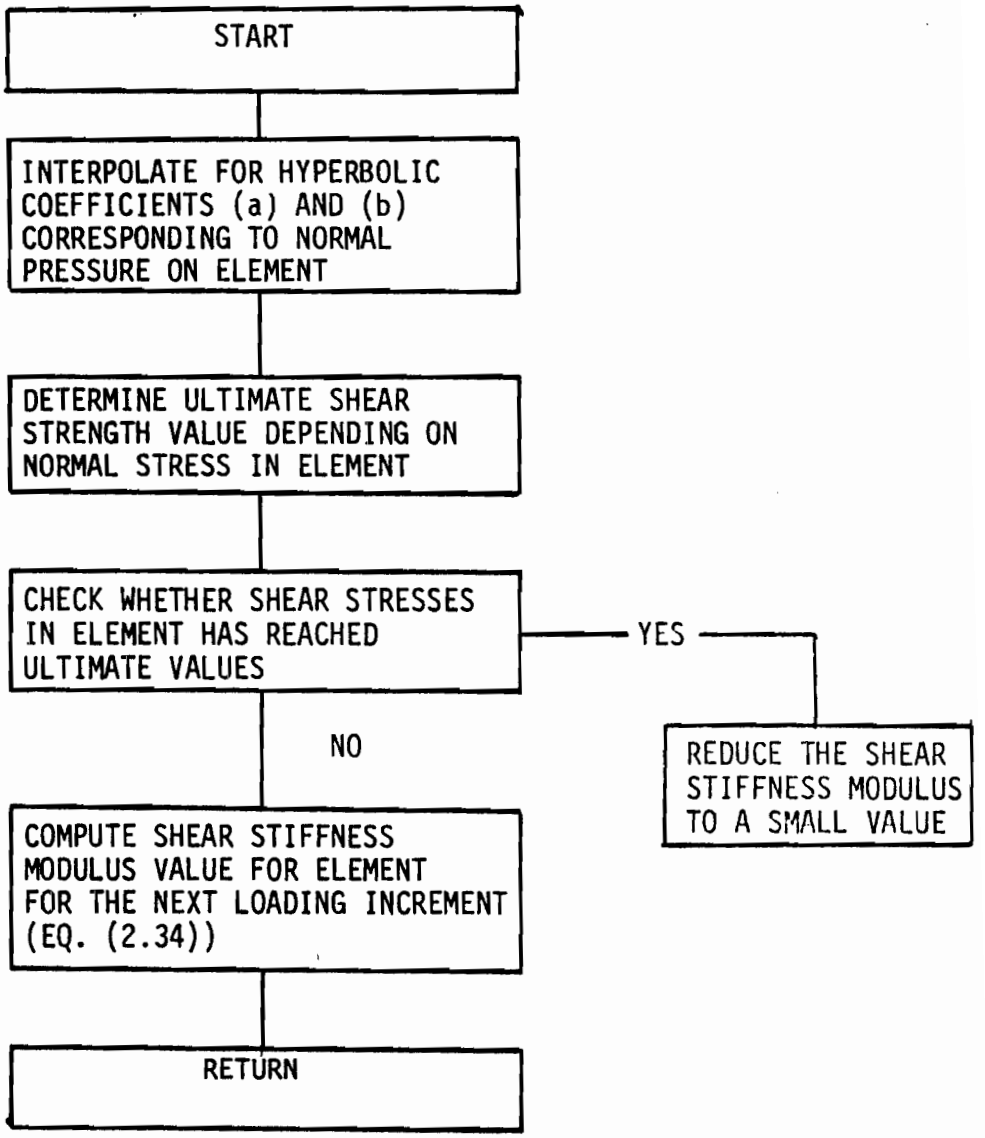

SUBROUTINE AVER

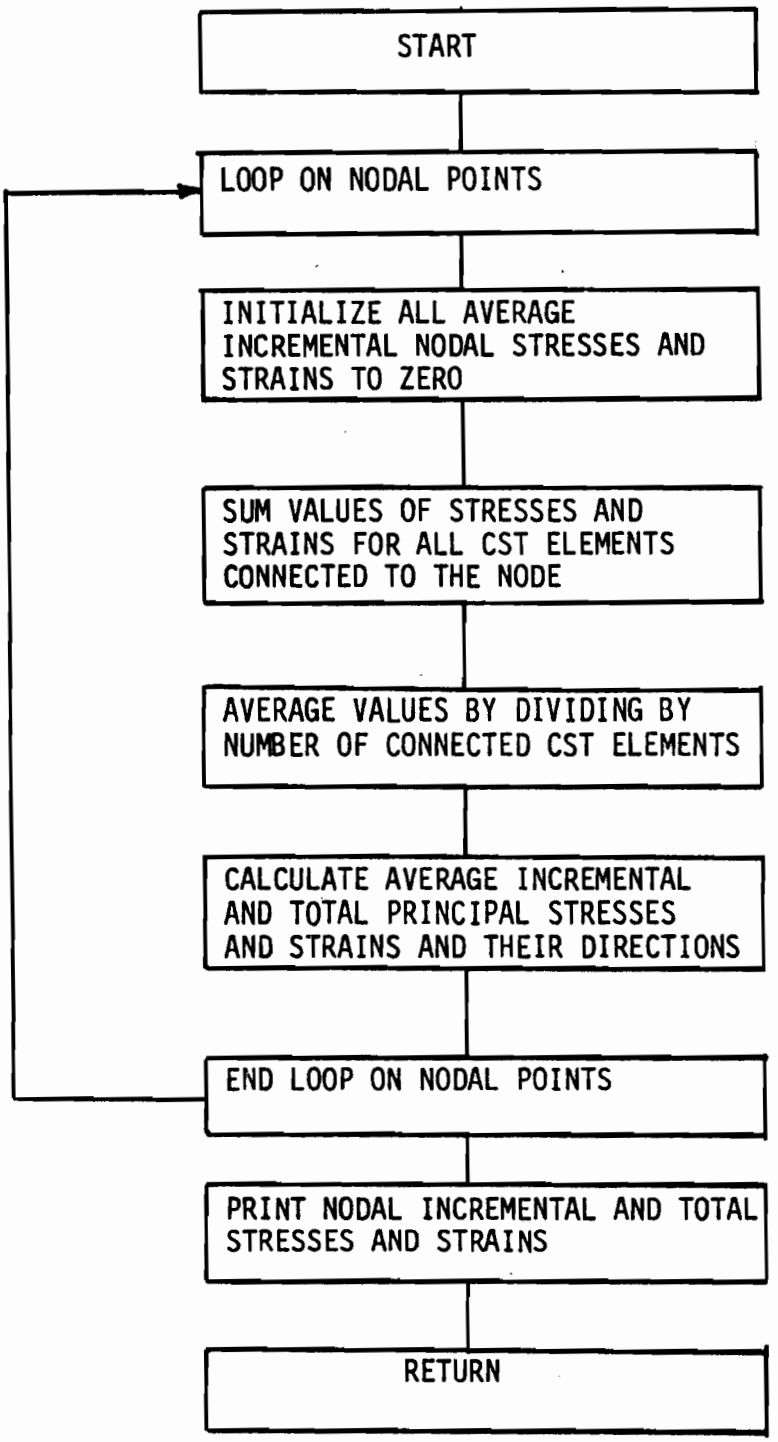

```
C       ALL RESULTS ARE PER UNIT WIDTH
C       CONTROL MAIN PROGRAM
      COMMON/CONTR/TITLE(12),NP,NE,NB,NDF,NCN,NLD,NMAT,NSZE,LL,NT4,
     1,NOPC,NCMAT,INDEX,IOUT,INCOUT(20)
      COMMON/DATA/CORD(200,2),NOP(200,4),IMAT(200),NBC(60),JX(200),
     1UY(200),IBC(10),JBC(10),PRE(10),T(200),XDEN,YDEN,ORX(200),ORY
     2,PRCORD(200,2),CODE(200)
      COMMON/ANAL/NOINC,KOUNT,NTEST,LTEST,NITER,NCITER,VEL,IND,GRTP
     1SPC
      COMMON/STIFF/ESTIFM(12,12),A(200,3,6),B(200,3,6),SA(510,75),
     1AREA(200),C(510),K(8),N(8),MBAND,D(510),AR(510)
      COMMON/STRES/DISTO(2,200),SIGTO(200,4),SIPTO(200,3),SMAXTO(20
     1SMINTO(200),ANGTO(200),EANGTO(200),EMAXTO(200),EALMTO(200),
     2FORCE(200,4),STR(200,3),PSIGTO(200,4),PSTRTO(200,3),PDISTO(2,
      COMMON/NONL/NCUR(3),CRA(3,10),NPTS(3,10),MG(30),GAM(30),
     1EY(3,10,30),GAMOC(3,10,30),PRESTR(200),PREDEV(200),CONPRE(200
      COMMON/DEF/DX(200),DY(200),VX(200),VY(200),EPSX(200),EPSY(200
     1GAMXY(200),EPSI1(200),EPSI2(200),PSI(200),CSUMD,CSUMPR
      COMMON/ELAS/E,ENFO,ENU,EF(200),EC(200),DKSIJ,DKNIJ,DASII,DKNI
     1EA(10)
      COMMON/JOINT/T1(8,8),BL(8,8),AL(200),ANG(200),DKS(200),DKN(20
     1SD(2,2),W(200,2),P(200,2),V(200,2),AVP(200,2),CV(200,2),
     2CAVP(200,2),ECV(200,2),PCAVP(200,2),B1(8,8)
      COMMON/JNONL/NVAI(2),CNP(2,10),AH(2,10),BH(2,10)
      COMMON/AVRG/AVSMAX(200),AVSMIN(200),AVANG(200),AVTMX(200),
     1AVTAN(200),AVTANG(200),AVSMX(200),AVSMN(200),AVSANG(200),
     2AVSTMX(200),AVSTMN(200),AVSTAN(200),AVPSI1(200),AVPSI2(200),
     3AVPSI(200)
      INTEGER MBAND
C
C                 INITIALIZE TAPE NO.
C                 AND NUMBER OF CORNER NODE MAX.
C
      NPROB=1
C
C                 LOOP ON NO. OF PROBLEMS
C
      DO 400 NPE=1,NPROB
C
C                 READ INPUT GEOMETRY AND PROP.
C
      NTEST=0
      LTEST=1
      CALL GDATA1
      NSTF=N2*NDF
C
C                 DETERMINATION OF BAND WIDTH
C                 FIND LARGEST DIFFERENCE IN NODAL NUMBERS
C                 IN ANY ELEMENT
      JJ=0
      DO 350 N=1,NE
      DO 350 I = 1,4
      DO 360 L = I ,4
      KK=IABS(NOP(N,I)-NOP(N,L))
      IF(KK-JJ) 360,360,365
```

```
  365 JJ=KK
  360 CONTINUE
  350 CONTINUE
C                     COMPUTE BAND WIDTH AS 2*JJ+NO. OF DEGREES
C                     OF FREEDOM
      NBAND=2*JJ+2
      WRITE(6,12)  NBAND
C
C                     READ NONLINEAR STRESS-STRAIN VALUES
C
      IF(NTEST.EQ.ITEST) GO TO 300
      CALL GDATA2
C
C                     INITIALIZE ALL STRESSES AND STRAINS
C
  300 DO 200 N=1,NE
      IF(IMAT(N).EQ.3) GO TO 104
      IF(NOP(N,3).NE.NOP(N,4)) GO TO 101
      DO 500 I=1,4
  500 SIGTO(N,I)    = 0.
      DO 301 I=1,3
  301 STRTO(N,I)    = 0.
      SMAXTO(N)    =0.
      SMINTO(N)    = 0.
      EMAXTO(N)    = 0.
      EMINTO(N)    = 0.
      PRESTR(N)=0.0
      PREDEV(N)=0.0
      COMPRE(N)=0.
      IF(IMAT(N).EQ.1)  EF(N)=F
      IF(IMAT(N).EQ.2)  EZ(N)=EZERO
C
C                           INITIALIZE JOINT STRESS-STRAIN PROPERTIES
      GO TO 200
  101 DKN(N)=DKNIJ
      DKS(N)=DKSIJ
      GO TO 105
  104 DKN(N)=DKNII
      DKS(N)=DKSII
  105 DO 102 I=1,2
      CV(N,I)=0.0
  102 CAVP(N,I)=0.0
  200 CONTINUE
      CSUMPD=0.0
      CSUMPW=0.0
C
C                     INITIALIZE ALL NODAL DISPLACEMENTS TO ZERO
C
      DO 600 N=1,NP
      DO 600 J=1,2
  600 DISTO(J,N)=0.0
C
C                     INITIALIZE ALL REACTIONS TO ZERO
C
```

```
      DO 437 J=1,NE
      M=NBC(J)
      N=2*M-1
      L=2*M
      AP(N)=0.0
      AR(L)=0.0
  437 CONTINUE
C                     INCREMENTAL LOADS AND DISPLACEMENTS
      DO 800 K=1,NE
      NN=NBC(K)
      UX(NN)=UX(NN)/NOINC
      UY(NN)=UY(NN)/NOINC
  800 CONTINUE
      IF (NOPC.EQ.0) GO TO 711
      DO 710 LI=1,NOPC
  710 PRE(LI)=PRE(LI)/NOINC
  711 CONTINUE
C                     LOOP ON NO. OF INCREMENTS
C
      KOUNT=1
      DO 700 IK=1,NOINC
      DO 980 I12=1,IOUT
      IF(IK.EQ.INCOUT(I12)) GO TO 981
  980 CONTINUE
      INDEX=0
      GO TO 982
  981 INDEX=1
  982 DO 714 L=1,NOITER
      NITER=L
C     REWIND NT4
C     REWIND NT5
C
C
C                     FORM STIFFNESS MATRIX THEN SOLVE
C                     SIMULTANEOUS EQUATIONS
      CALL FORMK
      CALL SOLVE
C
C                     CALCULATE STRESSES
C
      CALL STRESS
      CALL JSTRES
C
C                     ITERATE ON ELASTIC MODULUS
C
      IF(NTEST.EQ.ITEST) GO TO 713
  714 CONTINUE
C                           DETERMINATION OF REACTIONS
      IF(NITER.NE.NOITER)GO TO 440
      DO 438 L=1,NE
      M=NBC(L)
      DO 901 N1=1,NE
      IF(NOP(N1,3).NE.NOP(N1,4))GO TO 706
      NCN=3
      GO TO 707
```

```
706     NCN=4
707     DO 901 I=1,NCN
        IF(NOP(N1,I)-M)  901,705,901
705     N=N1
        J=I
        IF(CODE(M))  438,438,422
422     CALL REAC(J,P,M)
901     CONTINUE
438     CONTINUE
440     CONTINUE
C                                   WRITE REACTIONS
        IF(NITER.NE.NCITER)GO TO 441
        IF(INDEX.EQ.0) GO TO 983
        WRITE(6,203)
  983   DO 439 K=1,ND
        M=NBC(K)
        N=2*M-1
        L=2*M
C                       ADD BODY FORCES TO FIRST INCREMENT
        IF(CODE(4).NE.1.)GO TO 501
        AR(N)=AR(N)-D(N)
        GO TO 503
501     IF(CODE(4).EQ.2.)GO TO 502
        AR(N)=AR(N)-D(N)
502     AR(L)=AR(L)-D(L)
503     CONTINUE
        IF(INDEX.EQ.0) GO TO 439
        WRITE(6,201)  M,AR(N),AR(L)
439     CONTINUE
441     CONTINUE
C
C                       CHANGE ELEMENT COORDINATES
C
  713   IF(NOINC.EQ.1) GO TO 712
        CALL LANDEF
C                       AVERAGE STRESSES, STRAINS AND STRAIN RATES
C                       IN ADJOCENT ELEMENTS
        CALL AVER
        KOUNT=KOUNT+1
  700   CONTINUE
  712   CONTINUE
  400   CONTINUE
   12   FORMAT('0',5X,'BAND WIDTH=',I5)
201     FORMAT(I5,2F15.6)
  203   FORMAT('1',5X,'TABLE 11 - REACTIONS'//10X,'X-REACTIONS',4X,
       1'Y-REACTIONS')
        STOP
        END
C-----------------------------------------------------------------
        SUBROUTINE GDATA1
        COMMON/CONTRL/TITLE(12),NP,NE,NB,NOP,NCN,NLD,NMAT,NSOP,LI,NT4
       1,NOPC,NCMAT,INDEX,IOUT,INCOUT(20)
        COMMON/DATA/COORD(200,2),NOP(200,4),IMAT(200),NBC(60),UX(200)
       1UY(200),IBC(10),JBC(10),PRE(10),T(200),XDEN,YDEN,CRX(200),CR
```

```
     2,PRCORD(200,2),CODE(200)
      COMMON/ANAL/NOINC,KOUNT,NTEST,LTEST,NITER,NOITER,VEL,END,GRTE
     1SPC
      COMMON/STIFF/ESTIFM(12,12),A(200,3,6),B(200,3,6),SK(510,75),
     1AREA(200),C(510),R(8),H(8),NBAND,D(510),AR(510)
      COMMON/ELAS/E,ENEO,ENU,EE(200),EC(200),DKSIJ,DKNIJ,DKSII,DKNI
     1EA(10)
      INTEGER NBAND
C
C                    READ AND PRINT TITLE AND CONTROL
      READ(5,7) TITLE
      WRITE(6,100) TITLE
      READ(5,1) NP,NE,NB,NDF,NMAT,NCMAT,NOPC,XDEN,YDEN,I1
      WRITE(6,9)
      WRITE(6,10) NP,NE,NB,NDF,NMAT,NCMAT,NOPC,XDEN,YDEN,I1
C                    READ AND PRINT MATERIAL DATA
      READ(5,*) E,ENEO,ENU,DKSIJ,DKNIJ,DKSII,DKNII
      WRITE(6,108)
      WRITE(6,18) E,ENEO,ENU,DKSIJ,DKNIJ,DKSII,DKNII
C                    READ NODAL POINT DATA
      WRITE(6,102)
      DO 900 N=1,NP
      READ(5,*) I,(COORD(N,M),M=1,2)
      WRITE(6,2)  I,(COORD(N,M),M=1,2)
  900 CONTINUE
C                    READ ELEMENT DATA
      WRITE(6,103)
      DO 901 N=1,NE
       READ(5,3)  I,(NOP(N,M),M=1,4),IMAT(N),T(N)
      WRITE(6,3)  I,(NOP(N,M),M=1,4),IMAT(N),T(N)
  901 CONTINUE
C                    READ BOUNDARY DATA
C     CODE=0.0,SPECIFIED LOAD IN X AND Y DIRECTIONS
C     CODE=1.0,SPECIFIED DISPLACEMENT IN X DIRECTION-LOAD IN Y DIR
C     CODE=2.0,SPECIFIED LOAD IN X DIRECTION-DISPLACEMENT IN Y DIR
C     CODE=3.0,SPECIFIED DISPLACEMENT IN X AND Y DIRECTIONS
      READ(5,*) (NBC(I),I=1,NB)
      DO 822 K=1,NB
      NN=NBC(K)
      READ(5,*) CODE(NN),UX(NN),UY(NN)
  822 CONTINUE
C        READ MULTIPLE GROUSER ELEMENT VELOCITY AND
C         HORIZONTAL TRAVEL DISTANCE
      READ(5,*) THD,VEL
C                    READ BOUNDARY PRESSURE CONDITIONS
      IF(NOPC.EQ.0.) GO TO 110
      DO 490 L=1,NOPC
      READ(5,*)  IBC(L),JBC(L),PRE(L)
  490 CONTINUE
C                    READ NO. OF INCREMENTS
  110 READ(5,*) NOINC,NOITER
      READ(5,*) IOUT
      READ(5,*) (IACOUT(I),I=1,IOUT)
  480 IF(I1.NE.0) GO TO 500
```

```
C                    PRINT INPUT DATA
      WRITE(6,106)
      DO 19 N=1,NB
      NN=NBC(N)
   19 WRITE(6,11) NN,CODE(NN),UX(NN),UY(NN)
      IF(NOPC.EQ.0) GO TO 113
      WRITE(6,475)
      WRITE(6,510) (IBC(L),JBC(L),PRE(L),L=1,NOPC)
  113 CONTINUE
      IF(NTEST.EQ.ITEST) GO TO 300
      WRITE(6,301)
      GO TO 112
  300 WRITE(6,303)
  301 FORMAT(//,1X,'NONLINEAR ANALYSIS'//)
  303 FORMAT(//,1X,'LINEAR ANALYSIS'//)
  112 WRITE(6,105) NOINC,NOITER
  500 CONTINUE
    1 FORMAT(7I5,2F10.3,I5)
    2 FORMAT(I10,2F10.5)
    3 FORMAT(5I5,F10.3)
    4 FORMAT(2I5)
    7 FORMAT(12A4)
    8 FORMAT(2F10.2,3A4,F4.1)
    9 FORMAT(6X,'NP',6X,'NE',6X,'NB',6X,'NDF',6X,'NMAT',4X,'NCMAT'
     14X,'NOPC',7X,'DENSITY'/62X,'X',11X,'Y')
   10 FORMAT(7I8,2F10.3,I5)
  100 FORMAT('1',5X,12A4//5X,'TABLE 1 - INPUT GEOMETRY AND PROPERT
     1)
  102 FORMAT(///1X,'NODAL POINTS')
  103 FORMAT(///1X,'ELEMENTS')
  106 FORMAT(///1X,'BOUNDARY CONDITIONS')
  105 FORMAT(1X,'NO. OF INCREMENTS=',I5/1X,'NO. OF ITERATIONS=',I5
  108 FORMAT(1H0,'MATERIAL PROPERTIES')
  115 FORMAT(2I5,E10.3)
  475 FORMAT('0',2X,'PRESSURE BOUNDARY CONDITIONS',//,16X,'I',3X,'
     12X,'PRESSURE')
   11 FORMAT(I5,F10.3,2E15.7)
  510 FORMAT(5X,2I5,E10.3)
   12 FORMAT(24I3)
   13 FORMAT(F10.3,2E15.7)
   14 FORMAT(2F10.2,F10.3,4E10.5)
      RETURN
      END
         SUBROUTINE GDATA2
      COMMON/CONTR/TITLE(12),NP,NE,NB,NDF,NCN,NLD,NMAT,MSLV,LI,NI4
     1,NOPC,NCMAT,INDEX,IOUT,INCOUT(20)
      COMMON/NONL/NCUR(3),CPR(3,10),NPTS(3,10),EG(30),SAN(30),
     1PY(3,10,30),GAMOC(3,10,30),PRESTP(200),PREDEV(200),CONPRE(20
      COMMON/JNONL/NVAI(2),CNP(2,10),AN(2,10),BN(2,10)
C
C                    DATA FOR NONLINEAR MATERIAL PROPERTIES
C                    THE INPUT CURVE FOR EACH CONFINING PRESSURE IS
C                    (SIGMA1-SIGMA3) VS EPSILON1
C
```

```
C                    START READING NON-LINEAR INPUT DATA
C
      READ(5,95) TMAT
      WRITE(6,1000) TMAT
 1000 FORMAT(//,5X,'TYPE OF MATERIAL=',1X,A4)
      WRITE(6,66)
C
C                 NCURV IS THE NUMBER OF NONLINEAR CURVES INPUT
C
      READ(5,*) (NCUR(I),I=1,NCMAT)
      DO 3000 I=1,NCMAT
      NCURV=NCUR(I)
      IF (NCURV) 304,304,310
  304 WRITE(6,452)
      STOP
  310 DO 330 NC=1,NCURV
      READ(5,*) CPR(I,NC),NPTS(I,NC)
      WRITE (6,459) NC,CPR(I,NC),NPTS(I,NC)
      NPT=NPTS(I,NC)
      READ(5,*) (EG(LP),LP=1,NPT)
      READ(5,*) (GAM(LP),LP=1,NPT)
      WRITE(6,465)
      DO 330 LP=1,NPT
      EY(I,NC,LP)=EG(LP)
      GAMOC(I,NC,LP)=GAM(LP)
      WRITE(6,472) EY(I,NC,LP),GAMOC(I,NC,LP)
  330 CONTINUE
 3000 CONTINUE
C                          DATA FOR JOINT NONLINEAR PROPERTIES
C                          THE INPUT VALUES FOR EACH NORMAL PRESSURE
C                          ARE HYPERBOLIC COEFFICIENTS A AND B
      IF(NMAT.EQ.NCMAT)GO TO 601
      NL=NCMAT+1
      READ(5,100)  (NVAL(I),I=NL,NMAT)
      WRITE(6,67)
      DO 600 I=NL,NMAT
      NVALUE=NVAL(I)
      IF(NVALUE)603,603,604
603   WRITE(6,609)
      STOP
604   WRITE(6,607)
      DO 605 NV=1,NVALUE
      READ(5,606)  CNP(I,NV),AH(I,NV),BH(I,NV)
      WRITE(6,608)  NV,CNP(I,NV),AH(I,NV),BH(I,NV)
605   CONTINUE
600   CONTINUE
601   CONTINUE
609   FORMAT(5X,'ERROR IN NVALUE CARD')
606   FORMAT(3F10.3)
607   FORMAT(2X,'NUM.     NORMAL PRESS.    A-VALUE     B-VALUE')
608   FORMAT(2X,I5,3(F10.3,5X))
100   FORMAT(6I5)
67    FORMAT(//,5X,'TABLE 3 - JOINT NONLINEAR CURVES'///)
   95 FORMAT(A4)
```

```
  452 FORMAT(5X,'ERROR IN NCURVE CARD')
  110 FORMAT(E10.3,I5)
  459 FORMAT(10X,' NUM.      CONF. PRESS.        NUM. OF POINTS',/
     19X,I5,10X,E10.3,8X,I5)
  465 FORMAT(4X,' DEV. STRESS',3X,'AXIAL STRAIN')
  472 FORMAT(5X,E10.3,5X,E10.3)
   66 FORMAT('1',5X,'TABLE 2 - NONLINEAR CURVES',//)
  120 FORMAT(7F10.4)
      RETURN
      END
      SUBROUTINE STIFT1(N)
C                          JOINT ELEMENT
      COMMON/CONTR/TITLE(12),NP,NE,NB,NDF,NCN,NLD,MNAT,MSZE,LI,NI4,
     1,NOPC,NCMAT,INDEX,IOUT,INCOUT(20)
      COMMON/DATA/CORD(200,2),NOP(200,4),IMAT(200),NBC(60),JX(200),
     1HY(200),IBC(10),JBC(10),PRS(10),T(200),XDEN,YDEN,ORX(200),ORY
     2,ZBCORD(200,2),CODE(200)
      COMMON/STIFF/ESTIFM(12,12),A(200,3,6),B(200,3,6),SK(510,75),
     1AREA(200),C(510),R(8),H(8),WBAND,D(510),AR(510)
      COMMON/JOINT/T1(8,8),BI(8,8),AL(200),ANG(200),DKS(200),DKN(20
     1SD(2,2),W(200,2),P(200,2),V(200,2),AVP(200,2),CV(200,2),
     2CAVP(200,2),PCV(200,2),PCAVP(200,2),B1(8,8)
      I=NOP(N,1)
      J=NOP(N,2)
      K=NOP(N,3)
      L=NOP(N,4)
      IF(CORD(I,1).EQ.CORD(J,1)) GO TO 11
      ANG(N)=ATAN((CORD(J,2)-CORD(I,2))/(CORD(J,1)-CORD(I,1)))
      GO TO 12
11    ANG(N)=90.0/57.29578
12    CONTINUE
      AL(N)=SQRT((CORD(J,2)-CORD(I,2))**2+(CORD(J,1)-CORD(I,1))**2)
      ORX(N)=(CORD(I,1)+CORD(J,1)+CORD(K,1)+CORD(L,1))/4.
      ORY(N)=(CORD(I,2)+CORD(J,2)+CORD(K,2)+CORD(L,2))/4.
C                    J O I N T  E L E M E N T
C                          SUBROUTINE STIFF JOINT
C                          STIFM IS STIFFNESS MATRIX
      DO 3 I=1,8
      DO 3 J=1,8
3     ESTIFM(I,J)=0.0
      ESTIFM(1,1)=DKS(N)*AL(N)/3.0
      ESTIFM(1,3)=ESTIFM(1,1)/2.0
      ESTIFM(1,5)=-ESTIFM(1,3)
      ESTIFM(1,7)=-ESTIFM(1,1)
      ESTIFM(2,2)=DKN(N)*AL(N)/3.0
      ESTIFM(2,4)=ESTIFM(2,2)/2.0
      ESTIFM(2,6)=-ESTIFM(2,4)
      ESTIFM(2,8)=-ESTIFM(2,2)
      ESTIFM(3,3)=ESTIFM(1,1)
      ESTIFM(3,5)=-ESTIFM(1,1)
      ESTIFM(3,7)=-ESTIFM(1,1)/2.0
      ESTIFM(4,4)=ESTIFM(2,2)
      ESTIFM(4,6)=-ESTIFM(2,2)
      ESTIFM(4,8)=-ESTIFM(2,2)/2.0
```

```
      ESTIFM(5,5)=ESTIFM(1,1)
      ESTIFM(5,7)=ESTIFM(1,1)/2.0
      ESTIFM(6,6)=ESTIFM(2,2)
      ESTIFM(6,8)=ESTIFM(2,2)/2.0
      ESTIFM(7,7)=ESTIFM(1,1)
      ESTIFM(8,8)=ESTIFM(2,2)
      DO 4 K=1,7
      K1=K+1
      DO 4 J=K1,8
4     ESTIFM(J,K)=ESTIFM(K,J)
C                              DETERMINE TRANSFORMATION MATRIX
      R=COS(ANG(N))
      S=SIN(ANG(N))
      DO 5 I=1,8
      DO 5 J=1,8
5     T1(I,J)=0.0
      DO 6 I=1,8
      J=I
6     T1(I,J)=R
      DO 7 I=1,7,2
      J=I+1
7     T1(I,J)=S
      DO 8 I=2,8,2
      J=I-1
8     T1(I,J)=-S
C                              TRANSFORM STIFFNESS MATRIX TO GLOBAL AXES
      DO 9 I=1,8
      DO 9 J=1,8
      BL(I,J)=0.0
      DO 9 L=1,8
9     BL(I,J)=BL(I,J)+ESTIFM(I,L)*T1(L,J)
      DO 10 I=1,8
      DO 10 J=1,8
      ESTIFM(I,J)=0.0
      DO 10 L=1,8
10    ESTIFM(I,J)=ESTIFM(I,J)+BL(L,I)*T1(L,J)
      RETURN
      END
      SUBROUTINE STIFF2(N)
      COMMON/CONTR/TITLE(12),NP,NE,NB,NDF,NCN,NLD,NMAT,NBAND,LI,MI4
     1,NOPC,NCMAT,INDEX,IOUT,INCOUT(20)
      COMMON/DATA/COORD(200,2),NOP(200,4),EMAT(200),NBC(60),JA(200)
     1UY(200),IBC(10),JBC(10),PRE(10),T(200),XDEL,YDEL,DRA(200),DR
     2,PPCORD(200,2),CCDE(200)
      COMMON/STIFF/ESTIFM(12,12),A(200,3,6),B(200,3,6),SK(510,75),
     1AREA(200),C(510),R(8),H(8),WBAND,D(510),AM(510)
      COMMON/ELAS/E,ENPO,ENU,RE(200),EC(200),DKSIJ,DKNIJ,DKSII,DKN
     1EA(10)
      INTEGER WBAND
C
C                         DETERMINE ELEMENT CONSTANTS
C
      I=NOP(N,1)
      J=NOP(N,2)
```

```
      K=NOP(N,3)
      ORX(N)=(CORD(I,1)+CORD(J,1)+CORD(K,1))*0.333333
      ORY(N)=(CORD(I,2)+CORD(J,2)+CORD(K,2))*0.333333
C
C                  SET UP LOCAL COORDINATE SYSTEM
C
      AJ=CORD(J,1)-CORD(I,1)
      AK=CORD(K,1)-CORD(I,1)
      BJ=CORD(J,2)-CORD(I,2)
      BK=CORD(K,2)-CORD(I,2)
      AREA(N)=(AJ*BK-AK*BJ)/2.
      IF(AREA(N).LE.0.) GO TO 220
C
C                  FORM STRAIN DISP. MATRIX
C                  AND SAVE ON TAPE
C
      A(N,1,1)=BJ-BK
      A(N,1,2)=0.
      A(N,1,3)=BK
      A(N,1,4)=0.
      A(N,1,5)=-BJ
      A(N,1,6)=0.
      A(N,2,1)=0.
      A(N,2,2)=AK-AJ
      A(N,2,3)=0.
      A(N,2,4)=-AK
      A(N,2,5)=0.
      A(N,2,6)=AJ
      A(N,3,1)=AK-AJ
      A(N,3,2)=BJ-BK
      A(N,3,3)=-AK
      A(N,3,4)=BK
      A(N,3,5)=AJ
      A(N,3,6)=-BJ
C     WRITE(NT5) N,((A(I,J),J=1,6),I=1,3)
C
C                  FORM STRESS STRAIN MATRIX
C
      COMM=EE(N)/((1.+ENU)*(1.-ENU*2.)*AREA(N))
      ESTIFM(1,1)=COMM*(1.-ENU)
      ESTIFM(1,2)=COMM*ENU
      ESTIFM(1,3)=0.
      ESTIFM(2,1)=ESTIFM(1,2)
      ESTIFM(2,2)=ESTIFM(1,1)
      ESTIFM(2,3)=0.
      ESTIFM(3,1)=0.
      ESTIFM(3,2)=0.
      ESTIFM(3,3)=EE(N)/(2.*(1.+ENU)*AREA(N))
C
C                  B IS THE STRESS BACKSUBSTITUTION
C                  MATRIX AND IS SAVED ON TAPE
      DO 205 I=1,3
      DO 205 J=1,6
      B(N,I,J)=0.
```

```
      DO 205 K=1,3
  205 B(N,I,J)=B(N,I,J)+ESTIFM(I,K)/2.*A(N,K,J)
C     WRITE(NT4)  N,((B(I,J),J=1,6),I=1,3)
C
C                     ESTIFM IS STIFFNESS MATRIX
      DO 210 I=1,6
      DO 210 J=1,6
      ESTIFM(I,J)=0.
      DO 210 K=1,3
210   ESTIFM(I,J)=ESTIFM(I,J)+B(N,K,I)/2.*A(N,K,J)
      RETURN
C                           ERROR EXIT FOR BAD CONNECTIONS
220   WRITE(6,100) N
100   FORMAT('ZERO OR NEGATIVE AREA ELEMENT NO',I4/'EXECUTION TERMI
     1N')
      STOP
      END
C -----------------------------------------------------------------
      SUBROUTINE FORMK
C
C                     FORMS STIFFNESS MATRIX
      COMMON/CONTR/TITLE(12),NP,NE,NB,NDF,NCY,MID,NMAT,NSZF,LI,NT4
     1,NOPC,NCMAT,INDEX,ICUT,INCOUT(20)
      COMMON/DATA/CORD(200,2),NOP(200,4),IMAT(200),NBC(60),NX(200)
     1NY(200),IBC(10),JBC(10),PBC(10),T(200),XDEN,YDEN,GAX(200),GAY
     2,PRCORD(200,2),CODE(200)
      COMMON/ANAL/NOINC,KOUNT,MTEST,LTEST,NITER,NOITER,VEL,IND,GRT,
     1SPC
      COMMON/STIFF/ESTIFM(12,12),A(200,3,6),B(200,3,6),SK(510,75),
     1AREA(200),C(510),L(8),J(8),NBAND,D(510),AR(510)
      DIMENSION XE(3,2)
      INTEGER NBAND
C
C                     ZERO STIFFNESS MATRIX
C
      DO 300 N=1,NSZF
      C(N)=0.0
      D(N)=0.0
      DO 300 M=1,NBAND
300   SK(N,M)=0.
C                     SCAN ELEMENTS
C
      DO 400 N=1,NE
      IF(IMAT(N).EQ.2)  ENU=.45
      IF(NOP(N,3).EQ.NOP(N,4)) GO TO 100
      CALL STIFT1(N)
      GO TO 101
100   CALL STIFT2(N)
101   CONTINUE
C
C                     RETURNS ESTIFM AS STIFFNESS MATRIX
C
C                     STORE ESTIFM IN SK
C                     FIRST ROWS
```

```
C
      IF(NOP(N,3).EQ.NOP(N,4)) GO TO 307
      NCN=4
      GO TO 308
  307 NCN=3
  308 DO 360 JJ=1,NCN
      NROWB=(NOP(N,JJ)-1)*NDF
      IF(NROWB)360,305,305
  305 DO 350 J=1,NDF
      NROWB=NROWB+1
      I=(JJ-1)*NDF+J
C
C                     THEN COLUMNS
C
      DO 330 KK=1,NCN
      NCOLB=(NOP(N,KK)-1)*NDF
      DO 320 K=1,NDF
      L = (KK-1)*NDF + K
      NCOL = NCOLB + K + 1 -NROWB
C                 SKIP STORING IF BELOW BAND
C
      IF(NCOL)320,320,310
  310 SK(NROWB,NCOL)=SK(NROWB,NCOL)+ESTIFM(I,L)
  320 CONTINUE
  330 CONTINUE
  350 CONTINUE
  360 CONTINUE
  400 CONTINUE
C
C                     ADDITION OF CONCENTRED FORCES
C
      DO 297 I=1,NF
      N=NBC(I)
      K=2*N
      IF(CODE(N)-1.) 295,295,296
  296 IF(CODE(N).EQ.2.) GO TO 301
  298 IF(CODE(N)-3.) 425,297,425
  295 C(K)=C(K)+UY(N)
      IF(CODE(N).NE.0.0) GO TO 297
  301 C(K-1)=C(K-1)+UX(N)
      GO TO 297
  425 WRITE(6,426) N
      STOP
  297 CONTINUE
  426 FORMAT(5X,'ERROR IN CODE NUMBER-NODE-EXECUTION TERMINATED',I
C
C                     NORMAL PRESSURE BOUNDARY CONDITION
C
      IF(NOPC) 306,306,250
  250 DO 302 L=1,NOPC
      I=IBC(L)
      J=JBC(L)
      PP=PPE(L)/2.0
      DX=(COORD(I,2)-COORD(J,2))*PP
```

```
      DY=(COORD(J,1)-COORD(I,1))*PP
      II=2*I
      SINA=0.0
      COSA=1.0
      C(II-1)=C(II-1)+(COSA*DX+SINA*DY)
      C(II)=C(II)-(SINA*DX-COSA*DY)
      JJ=2*J
      C(JJ-1)=C(JJ-1)+(COSA*DX+SINA*DY)
      C(JJ)=C(JJ)-(SINA*DX-COSA*DY)
      IF(J.EQ.87)  C(JJ)=C(JJ)-(SINA*DX-COSA*DY)
  302 CONTINUE
  306 CONTINUE
C
C                    CALCULATION OF LOADS DUE TO BODY FORCES
C
      IF(KOUNT.GT.1) GO TO 30
      IF(XDEN)  880,882,880
  882 IF(YDEN) 880,30,880
  880 DO 20 II=1,NE
      IF(NOP(II,3).NE.NOP(II,4))  GO TO 20
      DO 85 I=1,3
      JJ=NOP(II,I)
      XE(I,1)=COORD(JJ,1)
   85 XE(I,2)=COORD(JJ,2)
      VOL=0.166667*(XE(2,1)*(XE(3,2)-XE(1,2))+XE(1,1)*(XE(2,2)-
     1XE(3,2))+XE(3,1)*(XE(1,2)-XE(2,2)))
      UT=VOL*XDEN
      VT=VOL*YDEN
      DO 86 I = 1,3
      JJ=NOP(II,I)
      C(2*JJ-1)=C(2*JJ-1)+UT
   86 C(2*JJ)=C(2*JJ)+VT
   20 CONTINUE
   30 CONTINUE
C
C
C                    TRANSFER LOAD VECTOR TO D
      DO 601 I=1,NSZF
      D(I)=C(I)
  601 CONTINUE
C                    DISPLACEMENT BOUNDARY CONDITIONS
C
C
      DO 401 J=1,NF
      M=NBC(J)
      U=UX(M)
      N=2*M-1
      IF(CODE(M))  401,401,311
  311 IF(CODE(M)-1.0)  401,325,331
  331 IF(CODE(M).EQ.2.) GO TO 335
      IF(CODE(M)-3.)  401,340,401
  325 CALL MODIFY(SK,C,NSZF,MBAND,N,U)
      GO TO 401
  340 CALL MODIFY(SK,C,NSZF,MBAND,N,U)
```

```
  335 U=UY(M)
      N=N+1
      CALL MODIFY(SK,C,NSZF,WBAND,N,U)
  401 CONTINUE
      RETURN
      END
C -----------------------------------------------------------------
      SUBROUTINE MODIFY(SK,B,NUEQ,WBAND,N,U)
      DIMENSION SK(510,75),B(510)
      INTEGER WBAND
C                  SUBROUTINE MODIFY MODIFIES THE STIFFNESS MATRIX
C                  SO AS TO ACCOUNT FOR THE SPECIFIED DISPLACEMENTS
      DO 240 M=2,WBAND
      K=N-M+1
      IF(K) 210,210,220
  220 B(K)=B(K)-SK(K,M)*U
      SK(K,M)=0.0
  210 K=N+M-1
      IF(NUEQ-K) 240,230,230
  230 B(K)=B(K)-SK(N,M)*U
      SK(N,M)=0.0
  240 CONTINUE
      SK(N,1)=1.0
      B(N)=U
      RETURN
      END
C -----------------------------------------------------------------
      SUBROUTINE SOLVE
C
C     SPECIFICATION STATEMENTS
C
      COMMON/CONTRL/TITLE(12),NP,NE,NM,NDF,NCN,NLD,NMAT,NSZF,LI,NI4
     1,NOPG,NCMAT,INDEX,IOUT,INCOUT(20)
      COMMON/STIFF/ESTIFM(12,12),A(200,3,6),B(200,3,6),SK(510,75),
     1AREA(200),C(510),P(8),H(8),WBAND,D(510),AL(510)
      INTEGER WBAND
C
C                          REDUCE MATRIX
C
      DO 300 N = 1,NSZF
      I = N
      DO 290 L=2,WBAND
      I = I + 1
      IF(SK(N,L)) 240,290,240
  240 G =SK(N,L)/SK(N,1)
      J = 0
      DO 270 K=L,WBAND
      J = J + 1
      IF(SK(N,K)) 260,270,260
  260 SK(I,J)=SK(I,J) - G*SK(N,K)
  270 CONTINUE
      SK(N,L)=G
C
C                     ADD LOAD VECTOR
```

```
C                    FOR EACH EQUATION
C
      C(I)=C(I)-G*C(N)
  290 CONTINUE
  300 C(N)=C(N)/SK(J,1)
C
C                    BACK-SUBSTITUTION
C
      N=NSZP
  350 N = N - 1
      IF(N)500,500,360
  360 L = N
      DO 400 K=2,MBAND
      L = L + 1
      IF(SK(N,K))370,400,370
  370 C(N)=C(N)-SK(N,K)*C(L)
  400 CONTINUE
      GO TO 350
C
  500 CONTINUE
      RETURN
      END
C -----------------------------------------------------------------
      SUBROUTINE STRESS
      COMMON/CONTR/TITLE(12),NP,NE,NB,NDF,NCN,NLD,NMAT,NSZP,LI,NT4
     1,NOPC,NCMAT,INDEX,IOUT,TNCOUT(20)
      COMMON/DATA/CORD(200,2),NOP(200,4),IMAT(200),NBC(60),UX(200)
     1UY(200),IBC(10),JBC(10),PRE(10),T(200),XDEN,YDEN,ORX(200),OR
     2,PRCORD(200,2),CODE(200)
      COMMON/ANAL/NOINC,KOUNT,MTEST,LTEST,NITER,NOITER,VEL,THD,GRT
     1SPC
      COMMON/STIFF/FSTIFM(12,12),A(200,3,6),B(200,3,6),SK(510,75),
     1AREA(200),C(510),P(8),E(8),MBAND,D(510),AR(510)
      COMMON/STRES/DISTO(2,260),SIGTO(200,4),STRTO(200,3),SMAXTO(2
     1SMINTO(200),ANGTO(200),EANGTO(200),EMAXTO(200),EMINTO(200),
     2FORCE(200,4),STR(200,3),PSIGTO(200,4),PSTRTO(200,3),PDISTO(2
      COMMON/NONL/NCUR(3),CBR(3,10),NPTS(3,10),EG(30),GAM(30),
     1EY(3,10,30),GAMOC(3,10,30),PRESIN(200),PREDEV(200),CONPRE(20
      COMMON/ELAS/I,ENTO,ENU,EE(200),EC(200),DKSIJ,DKNIJ,DKSII,DKN
     1EA(10)
      DIMENSION DIS(2,260)
      EQUIVALENCE(DIS,C)
      INTEGER MBAND
C     REWIND NT4
C     REWIND NT5
C
C
C                    PRINT DISPLACEMENTS
      IF(NITER.NE.NOITER) GO TO 902
      IF(INDEX.EQ.0) GO TO 902
      WRITE(6,100) KOUNT
      WRITE(6,117) (N,(DIS(J,N),J=1,NDF),N=1,NP)
  902 CONTINUE
C
```

```
C                    NODAL DISPLACEMENTS DUE TO EACH INCREMENT ARE
C                    CUMULATIVELY ADDED TO THOSE EXISTING BEFORE
C
      IF(NITER.NE.1) GO TO 601
      DO 230 M=1,NP
      DO 230 J=1,2
      PDISTO(J,M)=DISTO(J,M)
  230 DISTO(J,M)=DISTO(J,M)+DIS(J,M)
  601 DO 602 M=1,NP
      DO 602 J=1,2
  602 DISTO(J,M)=PDISTO(J,M)+DIS(J,M)
      IF(NITER.NE.NCITER) GO TO 903
      IF(INDEX.EQ.0) GO TO 903
      WRITE(6,112)
      WRITE(6,117)  (M,(DISTO(J,M),J=1,2),M=1,NP)
  903 CONTINUE
C
C                    CALCULATE ELEMENT FORCES
C                    CALCULATE ELEMENT STRAINS
C
      DO 200 NC=1,NE
      IF(IMAT(N).EQ.2)  ENU=.45
      N=NC
      IF(NOP(NC,3).NE.NOP(NC,4)) GO TO 200
C     READ(NT4)  N,((B(I,J),J=1,6),I=1,3)
C     READ(NT5)  N,((A(I,J),J=1,6),I=1,3)
      DO 260 I =1,3
      M=NOP(N,I)
      IF(M.EQ.0)GO TO 260
      K = (I - 1)*NDF
      DO 240 J =1,NDF
      IJ = J + K
  240 R(IJ) = DIS(J,M)
  260 CONTINUE
      IA = K + NDF
      DO 500 I=1,4
  500 FORCE(N,I)=0.
      DO 300 I = 1,3
      STR(N,I)=0.
      DO 300 J = 1,IA
      STR(N,I)=STR(N,I)+(A(N,I,J)*R(J))/(2.*AREA(N))
  300 FORCE(N,I)=FORCE(N,I)+B(N,I,J)*R(J)
      FORCE(N,4)=FORCE(N,4)+ENU*(FORCE(N,1)+FORCE(N,2))
  200 CONTINUE
C                    CALCULATE PRINCIPAL STRESSES
C                    AND DIRECTIONS
C
C
      DO 600 N = 1,NE
      IF(NOP(N,3).NE.NOP(N,4)) GO TO 600
  250 G = (FORCE(N,1)+ FORCE(N,2))/2.
      Q=SQRT(((FORCE(N,2)-FORCE(N,1))/2.)**2+ FORCE(N,3)**2)
      SMAX=G+Q
      SMIN=G-Q
```

```
      IF(FORCE(N,2).EQ.SMIN)GO TO 700
      ANG=57.29578*ATAN(FORCE(N,3)/(FORCE(N,2)-SMIN))
      GO TO 210
  700 ANG = 90.
  210 CONTINUE
  600 CONTINUE
C                    CALCULATE PRINCIPAL STRAINS AND
C                                 DIRECTIONS
      DO 800 N=1,NE
      IF(NOP(N,3).NE.NOP(N,4)) GO TO 800
      E=(STR(N,1)+STR(N,2))/2.
      F=SQRT(((STR(N,2)-STR(N,1))/2.)**2+(STR(N,3)/2.)**2)
      EMAX=E+F
      EMIN=E-F
      IF(STR(N,2).EQ.EMIN) GO TO 900
      EANG=57.29578*ATAN((STR(N,3)/2.)/(STR(N,2)-EMIN))
      GO TO 220
  900 EANG=90.
  220 CONTINUE
  800 CONTINUE
C
C                    CUMULATIVE STRESSES AND STRAINS
C
      IF(NITER.NE.1) GO TO 802
      DO 801 N=1,NE
      IF(NOP(N,3).NE.NOP(N,4)) GO TO 801
      DO 290 I=1,3
      PSTRTO(N,I)=STRTO(N,I)
  290 STRTO(N,I)=STRTO(N,I)+STR(N,I)
      DO 304 I=1,4
      PSIGTO(N,I)=SIGTO(N,I)
  304 SIGTO(N,I)=SIGTO(N,I)+FORCE(N,I)
  801 CONTINUE
      GO TO 806
  802 DO 807 N=1,NE
      IF(NOP(N,3).NE.NOP(N,4)) GO TO 807
      DO 803 I=1,3
  803 STRTO(N,I)=PSTRTO(N,I)+STR(N,I)
      DO 805 I=1,4
  805 SIGTO(N,I)=PSIGTO(N,I)+FORCE(N,I)
  807 CONTINUE
  806 CONTINUE
C
C                    TOTAL PRINCIPAL STRESSES AND STRAINS AND DIRECT
C
      DO 301 N=1,NE
      IF(NOP(N,3).NE.NOP(N,4)) GO TO 301
      C1=(SIGTO(N,1)+SIGTO(N,2))/2.
      D1=SQRT(((SIGTO(N,2)-SIGTO(N,1))/2.)**2+SIGTO(N,3)**2)
      SMAXTO(N)=C1+D1
      SMINTO(N)=C1-D1
      IF(SIGTO(N,2).EQ.SMINTO(N)) GO TO 701
      ANGTO(N)=57.29578*ATAN(SIGTO(N,3)/(SIGTO(N,2)-SMINTO(N)))
      GO TO 702
```

```
  701 ANGTC(N)=90.0
  702 CONTINUE
      E1=(STRTC(N,1)+STRTO(N,2))/2.
      F1=SQRT(((STRTO(N,2)-STRTO(N,1))/2.)**2+(STRTO(N,3)/2.)**2)
      EMAXTC(N)=E1+F1
      EMINTO(N)=E1-F1
      IF(STRTO(N,2).EQ.EMINTC(N)) GO TO 703
      EANGTC(N)=57.29578*ATAN((STRTO(N,3)/2.)/(STRTO(N,2)-EMINTO(N)
      GO TO 704
  703 EANGTC(N)=90.0
  704 CONTINUE
  301 CONTINUE
C
C                    CALL SUBROUTINE NONLIN
C
      IF(NTEST.EQ.LTEST) GO TO 307
      DO 305 N=1,NF
      IF(IMAT(N).EQ.2) ENU=.45
      IF(NOP(N,3).NE.NOP(N,4)) GO TO 305
      IF(STR(N,1).EQ.0.) GO TO 937
      EC(N)=(FORCE(N,1)-ENU*(FORCE(N,2)+FORCE(N,4)))/STR(N,1)
      GO TO 938
937   IF(STR(N,2).EQ.0.) GO TO 940
      EC(N)=(FORCE(N,2)-ENU*(FORCE(N,1)+FORCE(N,4)))/STR(N,2)
      GO TO 938
940   EC(N)=RE(N)
  938 CONTINUE
      CALL NONLIN(N)
  305 CONTINUE
  307 CONTINUE
C
C                    WRITE INTERPOLATED STRESS DIFFERENCE VALUES
C                    CORRESPONDING TO EPSILON1
C
      IF(NTEST.EQ. LTEST) GO TO 1003
      IF(NITER.NE.NCYTER) GO TO 1003
      IF(INDEX.EQ.0) GO TO 1003
      WRITE(6,1000)
      DO 1003 N=1,NF
      IF(NOP(N,3).NE.NOP(N,4)) GO TO 1003
      WRITE(6,1002) N,CONPRM(N),EE(N),PRESTR(N),PERDEV(N),EC(N)
 1003 CONTINUE
C
C                    FORMATS
C
100   FORMAT('1',10X,'INCREMENT NO.',I5//
     15X,'TABLE 4 - DISPLACEMENT INCREMENT'/
     27X,'NODE',6X,'X-DISPLACEMENT',3X,'Y-DISPLACEMENT')
  117 FORMAT(I10,2F16.5)
  112 FORMAT(///,5X,'TABLE 5 - TOTAL DISPLACEMENT'/
     1                                        7X,'NODE',6X,'X-DISPLACE
     23X,'Y-DISPLACEMENT')
 1000 FORMAT('0',5X,'TABLE 8 - INTERPOLATED VALUES'//
     1'      ELEMENT    CONF. PRESS.          MODULUS        PRIN. STR.
```

```
     2 DEV. STRESS        MODULUS'/
     3'                                  TANGENT
     4                    CHECK')
 1002 FORMAT     (5X,I4,8X,F10.5,5X,F10.3,6X,F10.6,6X,F10.4,6X,F10.3
      RETURN
      END
      SUBROUTINE JSTRES
C                    J O I N T  E L E M E N T
C     SUBROUTINE JOINT STRESS
      COMMON/CONTR/TITLE(12),NP,JF,NB,NDF,NCN,NLD,NMAT,NSZF,LI,NI4,
     1,NOPC,NCMAT,INDEX,IOUT,INCOUT(20)
      COMMON/DATA/COORD(200,2),NOP(200,4),IMAT(200),NBC(60),UX(200),
     1UY(200),IBC(10),JBC(10),PRE(10),T(200),XDEN,YDEN,URX(200),URY
     2,PLCORD(200,2),CODE(200)
      COMMON/ANAL/NOINC,KOUNT,NTEST,LTEST,NITER,NCITER,VEL,TRD,GRTI
     1SPC
      COMMON/STIFF/ESTIFM(12,12),A(200,3,6),B(200,3,6),SK(510,75),
     1AREA(200),C(510),E(8),H(8),MBAND,D(510),AE(510)
      COMMON/JOINT/T1(8,8),BL(8,8),AI(200),ANG(200),DKS(200),DKN(20
     1SD(2,2),W(200,2),Z(200,2),V(200,2),AVP(200,2),CV(200,2),
     2CAVP(200,2),ECV(200,2),PCAVP(200,2),B1(8,8)
      DIMENSION DIS(2,260)
      EQUIVALENCE (DIS,C)
      IF(NITER.NE.NOITER) GO TO 901
      WRITE(6,6000)
      WRITE(6,604)
901   CONTINUE
      DO 301 N=1,NE
C                    FORM STRESS-STRAIN MATRIX
      IF(NOP(N,3).EQ.NOP(N,4)) GO TO 301
      DO 1 I=1,2
      DO 1 J=1,2
    1 SD(I,J)=0.0
      SD(1,1)=DKS(N)
      SD(2,2)=DKN(N)
      DO 7 I=1,2
    7 V(N,I)=0.0
C                    DETERMINE TRANSFORMATION MATRIX
      E=COS(ANG(N))
      S=SIN(ANG(N))
      DO 13 I=1,8
      DO 13 J=1,8
   13 T1(I,J)=0.0
      DO 14 I=1,8
      J=I
   14 T1(I,J)=E
      DO 15 I=1,7,2
      J=I+1
   15 T1(I,J)=S
      DO 16 I=2,8,2
      J=I-1
   16 T1(I,J)=-S
C                    ELEMENT NODAL DISPLACEMENTS
      DO 260 I=1,4
```

```
      M=NOD(N,I)
      IF(M.EQ.0) GO TO 260
      K=(I-1)*NDF
      DO 240 J=1,NDF
      IJ=J+K
  240 R(IJ)=DIS(J,M)
  260 CONTINUE
C                     DISPLACEMENTS WITH RESPECT TO ELEMENT LOCAL AXES
      DO 12 I=1,8
      H(I)=0.0
      DO 12 IJ=1,8
   12 H(I)=H(I)+T1(I,IJ)*R(IJ)
      X=-AL(N)/2.
      DO 1000 II=1,2
C                     FORM STRAIN-DISPLACEMENT MATRIX
      F=1.-2.*X/AL(N)
      G=1.+2.*X/AL(N)
      DO 2 I=1,2
      DO 2 J=1,8
    2 B1(I,J)=0.0
      B1(1,1)=-F/2.
      B1(1,3)=-G/2.
      B1(1,5)=G/2.
      B1(1,7)=F/2.
      B1(2,2)=-F/2.
      B1(2,4)=-G/2.
      B1(2,6)=G/2.
      B1(2,8)=F/2.
C                     FORM RELATIVE  DISPLACEMENT VECTOR
      DO 3 I=1,2
      W(N,I)=0.0
      DO 3 J=1,8
    3 W(N,I)=W(N,I)+B1(I,J)*H(J)
C                     AVERAGE RELATIVE DISPLACEMENT
      DO 11 I=1,2
   11 V(N,I)=V(N,I)+W(N,I)
C                     FIND SHEAR AND NORMAL STRESSES
      DO 4 I=1,2
      P(N,I)=0.0
      DO 4 J=1,2
    4 P(N,I)=P(N,I)+SD(I,J)*W(N,J)
      IF(NITER.NE.NOITER) GO TO 1000
 1000 X=X+AL(N)
C                     FIND AVERAGE SHEAR AND NORMAL STRESSES ACROSS
C                     THE ELEMENT
      DO 10 I=1,2
   10 V(N,I)=V(N,I)/2.
      DO 6 I=1,2
      AVP(N,I)=0.0
      DO 6 J=1,2
    6 AVP(N,I)=AVP(N,I)+SD(I,J)*V(N,J)
      ANG(N)=ANG(N)*(360./(2.0*3.141593))
      IF(NITER.NE.NOITER) GO TO 301
      WRITE(6,4000) N,ANG(N),AL(N),ORX(N),ORY(N),V(N,1),V(N,2),AVP(
```

```
     1AVP(N,2)
  301 CONTINUE
C                       CUMMULATIVE AVERAGE STRESSES AND DISPLACEMENTS
      IF(NITER.NE.NCITER) GO TO 902
      WRITE(6,5000)
      WRITE(6,605)
902   CONTINUE
      DO 2000 N=1,NE
      IF(NOP(N,3).EQ.NOP(N,4)) GO TO 2000
      IF(NITER.NE.1) GO TO 601
      DO 9 I=1,2
      PCV(N,I)=CV(N,I)
      PCAVP(N,I)=CAVP(N,I)
      CV(N,I)=CV(N,I)+V(N,I)
    9 CAVP(N,I)=CAVP(N,I)+AVP(N,I)
  601 DO 17 I=1,2
      CV(N,I)=PCV(N,I)+V(N,I)
   17 CAVP(N,I)=PCAVP(N,I)+AVP(N,I)
C                       CALL JOINT NONLINEAR SUBROUTINE
      IF(NTEST.EQ.ITEST) GO TO 2000
      CALL JNONLN(N)
      IF(NITER.NE.NCITER) GO TO 2000
      WRITE(6,300) N,CV(N,1),CV(N,2),CAVP(N,1),CAVP(N,2),DKS(N),DK
 4000 FORMAT('0',I5,4(F10.3),2F10.7,2F10.6)
  300 FORMAT('0',I5,4F10.7,F15.7,F15.5)
 2000 CONTINUE
 6000 FORMAT(//,5X,'TABLE 9 - STRESSES AND DISPLACEMENTS IN JOINT
     1ING')
 5000 FORMAT(//,5X,'TABLE 10 - CUMMULATIVE STRESSES AND DISPLACEME
     1 JOINT ELEMENTS')
  604 FORMAT('0',5X,'N',4X,'ANGLE',4X,'LENGTH',6X,'CENTROID',12X,'
     1E DISPLACEMENT',13X,'AVERAGE STRESS'/32X,'X',9X,'Y',9X,'SHEA
     2'NORMAL',10X,'SHEAR',9X,'NORMAL')
  605 FORMAT('0',4X,'N',5X,'CUMMULATIVE DISPLACEMENTS',4X,'CUMMULA'
     1TRESSES',10X,'STIFFNESS VALUES'/12X,'SHEAR',10X,'NORMAL',9X,
     2',10X,'NORMAL',8X,'SHEAR',11X,'NORMAL')
      RETURN
      END
      SUBROUTINE KFAC(J,A,N)
      COMMON/CONTR/TITLE(12),NP,NE,NB,NDF,NCN,NLD,NMAT,NSEP,LI,NT4
     1,NOPC,NCMAT,INDEX,IOUT,INCOUT(20)
      COMMON/DATA/CORD(200,2),NOP(200,4),IMAT(200),NBC(60),UX(200)
     1UY(200),IBC(10),JBC(10),PRE(10),T(200),XDEN,YDEN,OSX(200),OR
     2,PSCORD(200,2),CODE(200)
      COMMON/STIFF/ESTIFN(12,12),A(200,3,6),B(200,3,6),SK(510,75),
     1AREA(200),C(510),R(8),H(8),WBAND,D(510),AR(510)
      DIMENSION U(8)
      INTEGER WBAND
C
C                       RECALCULATE STIFFNESS MATRIX FOR ELEMENT N
C
      IF(NOP(N,3).NE.NOP(N,4)) GO TO 504
      CALL STIFT2(N)
      J1=2*NOP(N,1)-1
```

```
      J2=2*NOP(N,1)
      K1=2*NOP(N,2)-1
      K2=2*NOP(N,2)
      L1=2*NOP(N,3)-1
      L2=2*NOP(N,3)
      U(1)=C(J1)
      U(2)=C(J2)
      U(3)=C(K1)
      U(4)=C(K2)
      U(5)=C(L1)
      U(6)=C(L2)
      IF(CODE(N).NE.1.) GO TO 501
      I=2*J-1
      K=2*NOP(N,J)-1
      SUM=0.0
      DO 425 L=1,6
  425 SUM=SUM+ESTIFM(I,L)*U(L)
      AR(K)=AR(K)+SUM
      GO TO 503
  501 IF(CODE(N).EQ.2.) GO TO 502
      I=2*J-1
      K=2*NOP(N,J)-1
      SUM=0.0
      DO 426 L=1,6
  426 SUM=SUM+ESTIFM(I,L)*U(L)
      AR(K)=AR(K)+SUM
  502 I=2*J
      K=2*NOP(N,J)
      SUM=0.0
      DO 427 L=1,6
  427 SUM=SUM+ESTIFM(I,L)*U(L)
      AR(K)=AR(K)+SUM
  503 CONTINUE
      GO TO 3
  504 CALL STIFT1(N)
      I1=2*NOP(N,1)-1
      I2=2*NOP(N,1)
      J1=2*NOP(N,2)-1
      J2=2*NOP(N,2)
      K1=2*NOP(N,3)-1
      K2=2*NOP(N,3)
      L1=2*NOP(N,4)-1
      L2=2*NOP(N,4)
      U(1)=C(I1)
      U(2)=C(I2)
      U(3)=C(J1)
      U(4)=C(J2)
      U(5)=C(K1)
      U(6)=C(K2)
      U(7)=C(L1)
      U(8)=C(L2)
      IF(CODE(N).NE.1.) GO TO 1
      I=2*J-1
      K=2*NOP(N,J)-1
```

```
      SUM=0.0
      DO 2 L=1,8
    2 SUM=SUM+ESTIFM(I,L)*U(L)
      AR(K)=AR(K)+SUM
      GO TO 3
    1 IF(CODE(M).EQ.2.) GO TO 4
      I=2*J-1
      K=2*NOP(N,J)-1
      SUM=0.0
      DO 5 L=1,8
    5 SUM=SUM+ESTIFM(I,L)*U(L)
      AR(K)=AR(K)+SUM
    4 I=2*J
      K=2*NOP(N,J)
      SUM=0.0
      DO 6 L=1,8
    6 SUM=SUM+ESTIFM(I,L)*U(L)
      AR(K)=AR(K)+SUM
    3 CONTINUE
      RETURN
      END
      SUBROUTINE LABOTH
      COMMON/CONTR/TITLE(12),NJ,NE,NB,NDF,NCN,NLD,NMAT,NSZF,L1,NF4,
     1,NOPC,NCMAT,INDEX,IOUT,INCOUT(20)
      COMMON/DATA/CORD(200,2),NOP(200,4),IMAT(200),MBC(60),DX(200),
     1UY(200),IBC(10),JBC(10),PRS(10),T(200),XDEN,YDEN,ORX(200),OR
     2,PRCORD(200,2),CODE(200)
      COMMON/ANAL/NOINC,KOUNT,NTEST,LTEST,NITER,NCITER,VEL,THD,GRT
     1SPC
      COMMON/STIFF/ESTIFM(12,12),A(200,3,6),B(200,3,6),SA(510,75),
     1AREA(200),C(510),R(8),E(8),NBAND,D(510),AR(510)
      COMMON/STRES/DISTO(2,260),SIGTO(200,4),STRTO(200,3),SMAXTO(2
     1SMINTO(200),ANGTO(200),EANGTO(200),EMAXTO(200),EMINTO(200),
     2FORCE(200,4),STR(200,3),PSIGTO(200,4),PSTRTO(200,3),PDISTO(2
      COMMON/DEF/DX(200),DY(200),VX(200),VY(200),EPSX(200),EPSY(20
     1GAMXY(200),EPSI1(200),EPSI2(200),PSI(200),CSUMPD,CSUM2D
      COMMON/JOINT/T1(8,8),EL(8,8),AL(200),AMS(200),DRS(200),DRN(2
     1SD(2,2),W(200,2),P(200,2),V(200,2),AVP(200,2),CV(200,2),
     2CAVP(200,2),PCV(200,2),PCAVP(200,2),B1(8,8)
      DIMENSION DIS(2,260)
      EQUIVALENCE (DIS,C)
C
C                    REPLACE ELEMENT COORDINATES WITH NEW COORDINATE
C
      DO 100 N=1,NE
      PRCORD(N,1)=CORD(N,1)
      PRCORD(N,2)=CORD(N,2)
      CORD(N,1)=CORD(N,1)+DIS(1,N)
      CORD(N,2)=CORD(N,2)+DIS(2,N)
  100 CONTINUE
C
C                    COMPUTATION OF VELOCITY COMPONENTS
C
      TT=(THD/NOINC)/VEL
```

```
      J=KOUNT
      DO 200 N=1,NE
      DX(N)=DIS(1,N)
      DY(N)=DIS(2,N)
      VX(N)=DX(N)/TT
      VY(N)=DY(N)/TT
  200 CONTINUE
      IF(INDEX.EQ.0) GO TO 984
      WRITE(6,1)
      WRITE(6,2)  (N,PRCORD(N,1),PRCORD(N,2),CORD(N,1),CORD(N,2),VX
     1VY(N),N=1,NP)
C
C                     CALCULATION OF STRAIN RATES AND DIRECTION OF PR
C                     STRAIN RATE
C
  984 DO 300 N=1,NE
      IF(NOP(N,3).NE.NOP(N,4)) GO TO 300
      EPSX(N)=STR(N,1)/TT
      EPSY(N)=STR(N,2)/TT
      GAMXY(N)=STR(N,3)/TT
      E=(EPSX(N)+EPSY(N))/2.
      F=SQRT(((EPSY(N)-EPSX(N))/2.)**2+(GAMXY(N)/2.)**2)
      EPSI1(N)=E+F
      EPSI2(N)=E-F
      IF(EPSY(N).EQ.EPSI2(N)) GO TO 301
      PSI(N)=57.29578*ATAN((GAMXY(N)/2.)/(EPSY(N)-EPSI2(N)))
  301 PSI(N)=90.0
      GO TO 300
  300 CONTINUE
C                     PLASTIC WORK OF DEFORMATION AND POWER OF DEFORM
      SUMPW=0.0
      SUMPD=0.0
      DO 121 IK=1,NE
      IF(NOP(IK,3).NE.NOP(IK,4)) GO TO 123
      IF(KOUNT.EQ.1) GO TO 101
      DUP=0.5*(SIGTO(IK,1)+PSIGTO(IK,1))*STR(IK,1)+0.5*(SIGTO(IK,2
     1TO(IK,2))*STR(IK,2)+0.5*(SIGTO(IK,3)+PSIGTO(IK,3))*STR(IK,3)
      GO TO 102
  101 DUP=0.5*(SIGTO(IK,1)*STR(IK,1)+SIGTO(IK,2)*STR(IK,2)+SIGTO(I
     1STR(IK,3))
  102 CONTINUE
      DUPV=DUP*AREA(IK)
      PDOF=DUPV/TT
      GO TO 124
  123 DUP=CAVP(IK,1)*V(IK,1)+CAVP(IK,2)*V(IK,2)
      DUPV=DUP*AL(IK)
      PDOF=DUPV/TT
C                     TOTAL INCREMENTAL PLASTIC WORK AND POWER OF DEF
C
  124 SUMPW=SUMPW+DUPV
      SUMPD=SUMPD+PDOF
  121 CONTINUE
C                     CUMULATIVE PLASTIC WORK AND POWER OF DEFORMATIO
C
```

```
      CSUMPW=CSUMPW+SUMPW
      CSUMPD=CSUMPD+SUMPD
      IF(INDEX.EQ.0) GO TO 985
      WRITE(6,122) KOUNT,SUMPW,SUMPD,CSUMPW,CSUMPD
    1 FORMAT('1',5X,'TABLE 12- VELOCITY AND NEW CO-ORDINATES'//
     1           8X,'NODE',3X,'X-COORD',9X,'Y-COORD',3X,'N-X-COORD',5X
     2'N-Y-COORD',5X,'X-VELOCITY',5X,'Y-VELOCITY')
    2 FORMAT('0',7X,I3,5X,F10.7,3X,F10.7,3X,F10.7,3X,F10.7,3X,E12.5
     1E12.5)
  122 FORMAT('1',5X,'TABLE 14 - PLASTIC WORK AND POWER OF DEFORMATI
     1           15X,'INCREMENT NO.',I5//15X,'TOTAL INCREMENTAL PLA
     1WORK=',F20.9/15X,'TOTAL INCREMENTAL POWER OF DEFORMATION=',F2
     115X,'CUMULATIVE PLASTIC WORK=',F20.9/15X,'CUMULATIVE POWER OF
     2FORMATION=',F20.9)
  985 RETURN
      END
      SUBROUTINE AVER
C             THIS SUBROUTINE AVERAGE STRESSES,STRAINS AND STRAINRA
C             AT NODAL POINTS AND THEN PROCEEDS TO CALCULATE PRINCI
C             VALUES AND DIRECTIONS
      COMMON/CONTR/TITLE(12),NP,NE,NB,NDF,NCN,NLD,NMAT,NSOF,LI,NT4,
     1,NOPC,NCMAT,INDEX,IOUT,INCOUT(20)
      COMMON/DATA/CORD(200,2),NOP(200,4),IMAT(200),NBC(60),UA(200),
     1UY(200),IBC(10),JBC(10),PBR(10),T(200),XDEN,YDEN,ORX(200),ORY
     2,PRCORD(200,2),CODE(200)
      COMMON/STRES/DISTO(2,200),SIGTO(200,4),STRTO(200,3),SMAXTO(20
     1SMINTO(200),ANGTO(200),RANGTO(200),EMAXTO(200),EMINTO(200),
     2FORCE(200,4),SCR(200,3),PSIG2O(200,4),PSTRTO(200,3),PDISTO(2
      COMMON/DEF/DX(200),DY(200),VX(200),VY(200),EPSX(200),EPSY(200
     1GAMXY(200),EPSI1(200),EPSI2(200),PSI(200),CSUM2D,CSUM2W
      COMMON/AVRG/AVSMAX(200),AVSMIN(200),AVANG(200),AVTMX(200),
     1AVTMN(200),AVTANG(200),AVSMX(200),AVSMN(200),AVSANG(200),
     2AVSTMX(200),AVSTMN(200),AVSTAN(200),AVPSI1(200),AVPSI2(200),
     3AVPSI(200)
      DIMENSION SFORCE(200,4),SSIGTO(200,4),SSTRTO(200,3),SSTR(200
     1SEPSX(200),SEPSY(200),SGAMXY(200)
      DO 100 L=1,NP
C             INITIALIZATION
      DO 800 I=1,4
      SFORCE(L,I)=0.0
  800 SSIGTO(L,I)=0.0
      DO 900 I=1,3
      SSTR(L,I)=0.0
  900 SSTRTO(L,I)=0.0
      SEPSY(L)=0.0
      SEPSY(L)=0.0
      SGAMXY(L)=0.0
C             VALUES FOR ADJACENT  ELEMENTS
      NOEL=0
      DO 400 N1=1,NE
      DO 400 I=1,3
      IF(NOP(N1,3).NE.NOP(N1,4)) GO TO 401
      IF(NOP(N1,I)-L) 400,300,400
  300 N=N1
```

```
      NOEL=NOEL+1
      DO 500 J=1,4
      SFORCE(L,J)=SFORCE(L,J)+FORCE(N,J)
500   SSIGTO(L,J)=SSIGTO(L,J)+SIGTO(N,J)
      DO 501 J=1,3
      SSTR(L,J)=SSTR(L,J)+STR(N,J)
501   SSTRTO(L,J)=SSTRTO(L,J)+STRTO(N,J)
      SEPSX(L)=SEPSX(L)+EPSX(N)
      SEPSY(L)=SEPSY(L)+EPSY(N)
      SGAMXY(L)=SGAMXY(L)+GAMXY(N)
401   CONTINUE
400   CONTINUE
      IF(NOEL.EQ.0) GO TO 663
      GO TO 664
663   NOEL=1
C               AVERAGE VALUES BY DIVIDING BY NUMBER OF ATTACHED ELEM
664   DO 600 J=1,4
      SFORCE(L,J)=SFORCE(L,J)/NOEL
600   SSIGTO(L,J)=SSIGTO(L,J)/NOEL
      DO 601 J=1,3
      SSTR(L,J)=SSTR(L,J)/NOEL
601   SSTRTO(L,J)=SSTRTO(L,J)/NOEL
      SEPSX(L)=SEPSX(L)/NOEL
      SEPSY(L)=SEPSY(L)/NOEL
      SGAMXY(L)=SGAMXY(L)/NOEL
C               CALCULATE PRINCIPAL VALUES AND DIRECTIONS
      CALL PRIN(L,SFORCE,AVSMAX,AVSMIN,AVANG)
      CALL PRIN(L,SSIGTO,AVTMX,AVTMN,AVTANG)
      CALL PRIN(L,SSTR,AVSMX,AVSMN,AVSANG)
      CALL PRIN(L,SSTRTO,AVSTMX,AVSTMN,AVSTAN)
      E=(SEPSX(L)+SEPSY(L))/2.
      F=SQRT(((SEPSY(L)-SEPSX(L))/2.)**2+(SGAMXY(L)/2.)**2)
      AVPSI1(L)=E+F
      AVPSI2(L)=E-F
      IF(SEPSY(L).EQ.AVPSI2(L)) GO TO 307
      AVPSI(L)=57.29578*ATAN((SGAMXY(L)/2.)/(SEPSY(L)-AVPSI2(L)))
      GO TO 308
307   AVPSI(L)=90.0
308   CONTINUE
100   CONTINUE
C               WRITE CALCULATED VALUES
      IF(INDEX.EQ.0) GO TO 936
      WRITE(6,101)
      WRITE(6,102) (L,(COORD(L,J),J=1,2),(SFORCE(L,I),I=1,4),AVSMAX
     1AVSMIN(L),AVANG(L),L=1,NP)
      WRITE(6,202)
      WRITE(6,103) (L,(COORD(L,J),I=1,2),(SSTR(L,I),I=1,3),AVSMX(L),
     1 AVSMN(L),AVSANG(L),L=1,NP)
      WRITE(6,114)
      WRITE(6,306)
      WRITE(6,102) (L,(COORD(L,J),J=1,2),(SSIGTO(L,I),I=1,4),AVTMX(
     1AVTMN(L),AVTANG(L),L=1,NP)
      WRITE(6,115)
      WRITE(6,202)
```

```
      WRITE(6,103) (L,(COORD(L,J),J=1,2),(SSTRTO(L,I),I=1,3),AVSTMX(L
     1),AVSTMN(L),AVSTAN(L),L=1,NP)
      WRITE(6,5)
      WRITE(6,3)
      WRITE(6,104) (L,SEPSX(L),SEPSY(L),SGAMXY(L),AVPS11(L),AVPS12(L
     1),AVPSI(L),L=1,NP)
  101 FORMAT('1',5X,'TABLE 6 - INCREMENT STRESS AND STRAIN'//
     15X,'STRESS INCREMENT'/
     1'   NODE      X       Y      X-STRESS        Y-STRESS      XY-STRE
     2      Z-STRESS      MAX-STRESS      MIN-STRESS     ANGLE')
  202 FORMAT('0',5X,'STRAIN INCREMENT'/
     1           '   NODE      X       Y      X-STRAIN        Y-STRAIN
     1Y-STRAIN      MAX-STRAIN      MIN-STRAIN      ANGLE')
  300 FORMAT('0',5X,'TABLE 7 - TOTAL STRESS AND STRAIN'//
     1'   NODE      X       Y      X-STRESS        Y-STRESS      XY-STRES
     2      Z-STRESS      MAX-STRESS      MIN-STRESS     ANGLE')
  115 FORMAT(///,1X,'TOTAL STRAINS')
  114 FORMAT('0',1X,'TOTAL STRESSES')
    5 FORMAT('0',5X,'TABLE 13 - STRAIN RATES'//)
    3 FORMAT(1H0,'   NODE          X-STRAIN R     Y-STRAIN R
     1Y-STRAIN R      MAX-STRAIN R    MIN-STRAIN R    ANGLE')
  102 FORMAT(I5,5X,2F6.2,6F15.6,F12.3)
  103 FORMAT(I5,5X,2F6.2,5F15.6,F12.3)
  104 FORMAT(I10,5E17.4,F12.3)
  300 RETURN
      END
      SUBROUTINE PRIN(N,A,AMAXP,AMINP,ANGP)
      DIMENSION A(200,4),AMAXP(200),AMINP(200),ANGP(200)
      B=(A(N,1)+A(N,2))/2.
      C=SQRT(((A(N,2)-A(N,1))/2.)**2+A(N,3)**2)
      AMAXP(N)=B+C
      AMINP(N)=B-C
      IF(A(N,2).EQ.AMINP(N)) GO TO 701
      ANGP(N)=57.29578*ATAN(A(N,3)/(A(N,2)-AMINP(N)))
      GO TO 702
  701 ANGP(N)=90.0
  702 CONTINUE
      RETURN
      END
      SUBROUTINE NONLIN(N)
C
      COMMON/CONTR/TITLE(12),NP,NE,NB,NDF,NCN,NLD,NMAT,NSOP,LI,NT4
     1,NOPC,NCMAT,INDEX,IOUT,INCOUT(20)
      COMMON/DATA/CORD(200,2),NOP(200,4),IMAT(200),NBC(60),UA(200)
     1UY(200),IBC(10),JBC(10),PAP(10),T(200),XDEN,YDEN,GRX(200),GR
     2,PPCORD(200,2),CODE(200)
      COMMON/ANAL/NCINC,KOUNT,NTEST,LTEST,MITER,NOITER,VEL,THD,GRI
     1SOC
      COMMON/STRES/DISTO(2,200),SIGTO(200,4),SHRTO(200,3),SMAXTO(2
     1SMINTO(200),ANGTO(200),RANGTO(200),RMAXTO(200),RMINTO(200),
     2FORCE(200,4),STR(200,3),PSTGTO(200,4),PSTRTO(200,3),PDISTO(2
      COMMON/NONL/NCUR(3),CPR(3,10),NPTS(3,10),EG(30),GAM(30),
     1EY(3,10,30),GAMOC(3,10,30),PRESTR(200),PREDEV(200),CUR2RE(20
      COMMON/ELAS/E,ENEO,ENU,EE(200),EC(200),DKSIJ,DKNIJ,DKSII,DKN
```

```
      1EA(10)
C
C                     NON-LINEAR ANALYSIS
C                     NONLIN IS A ROUTINE THAT INTERPOLATES FOR
C                     STRESSES FROM KNOWN VALUES OF STRAIN
C
C                     USES (SIGMA1-SIGMA3) .VS. EPSILON1 CURVES
C
C                     COMPUTE CONFINING PRESSURE IN ELEMENT
C
      SUBTRACE
C     TRACE ON
      IF(SMAXTC(N).NE.0.) GO TO 601
      IF(SMINTC(N).EQ.0.) GO TO 392
601   CONTINUE
      IF(ABS(SMAXTC(N)).GT.ABS(SMINTC(N))) GO TO 291
      CONPRE(N)=(SMAXTC(N)+SIGTC(N,4))/2.
      GO TO 292
  291 CONPRE(N)=(SMINTC(N)+SIGTC(N,4))/2.
  292 EPRE=ER(N)
      IF(ABS(EMAXTC(N)).GT.ABS(EMINTC(N))) GO TO 351
      PRSTTC=ABS(EMINTC(N))
      GO TO 352
  351 PRSTTC=ABS(EMAXTC(N))
  352 CONTINUE
C
C                     DETERMINE TWO ADJOINING CONFINING PRESSURE DEPE
C                     CURVES DEPENDING ON THE CONFINEMENT OF THE ELEM
C
      I=IMAT(N)
      NCURV=NCUR(I)
      IF(NCURV-1) 359,300,310
  300 NC=1
      GO TO 325
  310 DO 340 NC=1,NCURV
      IF(CPR(I,NC)-ABS(CONPRE(N))) 340,325,325
  340 CONTINUE
  325 NPT=NPTS(I,NC)
C
C                     DETERMINE TWO ADJOINING STRAIN COORDINATES DEPE
C                     ON THE MAJOR PRINCIPAL STRAIN OF THE ELEMENT
C
      DO 355 LP=1,NPT
      IF(GAMOC(I,NC,LP)-ABS(PRSTTC)) 355,360,360
  355 CONTINUE
      EE(N)=EY(I,NC,NPT)/GAMOC(I,NC,NPT)
      IF(NITER.NE.NCITER) GO TO 392
      PRESTR(N)=PRSTTC
      PARDEV(N)=EY(I,NC,NPT)
      GO TO 392
C
C                     INTERPOLATE FOR STRESS DIFFERENCE VALUE
C                     CORRESPONDING TO EPSILON1
C
```

```
  350 DENOM=GAMOC(I,NC,LP)-GAMOC(I,NC,LP-1)
      FUMER=(GAMOC(I,NC,LP)-PRSTTO)*(EY(I,NC,LP-1)-EY(I,NC,LP))
      TOPSTR=EY(I,NC,LP)+FUMER/DENOM
C
C                     IF ONLY ONE STRESS-STRAIN CURVE IS GIVEN
C
      IF(NCURV-1)  359,360,365
  359 WRITE(6,452)
  452 FORMAT(5X,'ERROR IN NCURVE CARD')
  360 EE(N)=ABS(TOPSTR)/ABS(PRSTTO)
      IF(NITER.NE.NOITER) GO TO 392
      PRESTP(N)=PRSTTO
      PREDEV(N)=TOPSTR
      GO TO 392
C
C                     IF MORE THAN ONE STRESS-STRAIN CURVE IS GIVEN
C
  365 IF(ABS(CONPRE(N))-0.0) 375,370,375
  375 IF(ABS(CONPRE(N))-CPR(I,NC)) 380,370,385
  380 NC=NC-1
      IF(NC.LE.0)  GO TO 370
      BOTSTR=TOPSTR
      GO TO 325
  370 EE(N)=ABS(TOPSTR-PREDEV(N))/ABS(PRSTTO-PRESTP(N))
      IF(NITER.NE.NOITER) GO TO 392
      PRESTP(N)=PRSTTO
      PREDEV(N)=TOPSTR
      GO TO 392
  385 IF(ABS(CONPRE(N)).GT.CPR(I,NCURV)) GO TO 370
      STRNEW=TOPSTR+(ABS(CONPRE(N))-CPR(I,NC))/(CPR(I,NC+1)-CPR(I,
     1*(BOTSTR-TOPSTR)
      EE(N)=ABS(STRNEW-PREDEV(N))/ABS(PRSTTO-PRESTP(N))
      IF(NITER.NE.NOITER) GO TO 392
      PRESTP(N)=PRSTTO
      PREDEV(N)=STRNEW
  392 CONTINUE
C     TRACE OFF
      RETURN
      END
      SUBROUTINE JNONLN(N)
      COMMON/DATA/CORD(200,2),NOP(200,4),IMAT(200),NBC(60),UX(200)
     1UY(200),IBC(10),JBC(10),PRE(10),T(200),XDEN,YDEN,UMX(200),UR
     2,PRCORD(200,2),CODE(200)
      COMMON/JOINT/T1(8,8),BL(8,8),AI(200),ANG(200),DRS(200),DRN(2
     1SD(2,2),X(200,2),P(200,2),V(200,2),AVP(200,2),CV(200,2),
     2CAVP(200,2),ECV(200,2),PCAVP(200,2),B1(8,8)
      COMMON/JNONL/NVAI(2),CNP(2,10),AH(2,10),BT(2,10)
C
C                     JOINT NONLINEAR ANALYSIS
C                     JNONLIN IS A ROUTINE THAT INTERPOLATES FOR SHEA
C                     STIFFNESS MODULUS FROM HYPERBOLIC STRESS-STRAIN
C
C                     DETERMINE TWO ADJOINING NORMAL PRESSURE DEPENDE
C                     CURVES DEPENDING ON THE NORMAL PRESSURE ON THE
```

```
      I=IMAT(N)
      NVALUE=NVAL(I)
      IF(NVALUE-1) 359,300,311
  359 WRITE(6,452)
  452 FORMAT(5X,'ERROR IN NVALUE CARD')
  300 TOWM=1./BH(I,1)
      IF(CAVP(N,1)-TOWM) 350,350,355
  355 CONTINUE
      DKS(N)=0.35
      GO TO 392
  350 NV=1
      DKS(N)=((1.-ABS(CAVP(N,1))*BH(I,1))**2)/AH(I,1)
      GO TO 392
  311 NAV=NVALUE
      IF(CNP(I,1)-CAVP(N,2)) 312,314,314
  312 IF(CNP(I,NAV)-CAVP(N,2)) 315,315,310
  314 AHI=AH(I,1)
      BHI=BH(I,1)
      GO TO 364
  315 AHI=AH(I,NAV)
      BHI=BH(I,NAV)
      GO TO 364
  310 DO 340 NV=2,NVALUE
      IF(CNP(I,NV)-CAVP(N,2)) 340,325,325
  340 CONTINUE
C                     INTERPOLATE FOR A AND B VALUES CORRESPONDING TO
C                     PRESSURE - LINEAR INTERPOLATION
  325 AHI=AH(I,NV)-(AH(I,NV)-AH(I,NV-1))*(CNP(I,NV)-CAVP(N,2))/
     1(CNP(I,NV)-CNP(I,NV-1))
      BHI=BH(I,NV)-(BH(I,NV)-BH(I,NV-1))*(CNP(I,NV)-CAVP(N,2))/
     1(CNP(I,NV)-CNP(I,NV-1))
  364  TOWM=1./BHI
      IF(CAVP(N,1)-TOWM) 360,360,365
  365 CONTINUE
      DKS(N)=0.35
      GO TO 392
  360 DKS(N)=((1.-ABS(CAVP(N,1))*BHI)**2)/AHI
  392 CONTINUE
      RETURN
      END
```

C2 Computer Program for Data Manipulation

```
      DIMENSION XXD(11,32,4),YYD(11,32,4),XA(11,32,4)
      DIMENSION YA(11,32,4),NNN(16),N1(8),N2(8),MK(16),SFY(3,9)
      DIMENSION SFX(3,9),TIME(9),X(9),Y(9),XF(1),YF(1),WT(9)
      DIMENSION COF(6),XT(9),YT(9),XFIT(11,32,4),YFIT(11,32,4)
      DIMENSION UX(11,32,4),VY(11,32,4),ESTR(10,46,8),IBOW(40)
      DIMENSION EPSX(10,32,4),EPSY(10,32,4),EPSXY(10,32,4)
      DOUBLE PRECISION XA,YA,X,Y,XI,YI
      READ(5,*) NP,NR,NC,NR1,NR2,NC1,NC2,IN,IN1,IN2,IK
      READ(5,*) ((SFX(I,J),I=1,3),J=1,NP)
      READ(5,*) ((SFY(I,J),I=1,3),J=1,NP)
      READ(5,*) (TIME(K),K=1,NP)
      READ(5,*) (NNN(I),I=1,IN)
      READ(5,*) (N1(I),I=1,IN1)
      READ(5,*) (N2(I),I=1,IN2)
      READ(5,*) (MK(I),I=1,IK)
      READ(5,*) TT,NIR
      READ(5,*) (IBOW(I),I=1,NIR)
C
C        READS THE COORDINATES FROM THE DIGITIZER
C
      DO 13 JS=1,NP
      DO 13 J=1,NR
      DO 13 I=1,NC
      READ(5,*) XXD(I,J,JS),YYD(I,J,JS)
   13 CONTINUE
C
C       MULTIPLIES THE COORDINATES BY THE SCALE FACTORS
C
      DO 17 JP=1,NP
      DO 107 J=1,8
      DO 107 I=1,NC
      XXD(I,J,JP)=XXD(I,J,JP)*SFX(1,JP)
      YYD(I,J,JP)=YYD(I,J,JP)*SFY(1,JP)
  107 CONTINUE
      DO 108 J=9,20
      DO 108 I=1,NC
      XXD(I,J,JP)=XXD(I,J,JP)*SFX(2,JP)
      YYD(I,J,JP)=YYD(I,J,JP)*SFY(2,JP)
  108 CONTINUE
      DO 109 J=21,32
      DO 109 I=1,NC
      XXD(I,J,JP)=XXD(I,J,JP)*SFX(3,JP)
      YYD(I,J,JP)=YYD(I,J,JP)*SFY(3,JP)
  109 CONTINUE
   17 CONTINUE
      GO TO 9999
C
C       WRITES THE SCALED NODE COORDINATES
C
      DO 19 JR=1,NP
      WRITE(6,1301)
      WRITE(6,1302) JR,TIME(JR)
      WRITE(6,1303)
      DO 25 K=1,NR
```

```
      DO 999 I2=1,NIR
      IF(K.EQ.IROW(I2)) GO TO 998
  999 CONTINUE
      GO TO 25
  998 WRITE(6,1304) (XXD(I,K,JR),I=1,NC)
      WRITE(6,1305) (YYD(I1,K,JR),I1=1,NC)
   25 CONTINUE
   19 CONTINUE
 1301 FORMAT(1H1,15X,'CORRECTED COORDINATES')
 1302 FORMAT(1H ,'NO. OF PICTURE=',1X,I2,5X,'TIME AFTER START=',
     1F5.2,'DAYS')
 1303 FORMAT(1H ,' COORDINATES    X-AXIS      Y-AXIS')
 1304 FORMAT(1H ,'X=',6(F9.6,3X)/1H ,1X,6(F9.6,3X))
 1305 FORMAT(1H ,'Y=',6(F9.6,3X)/1H ,1X,6(F9.6,3X))
C
C       CREATION OF AN INITIAL UNDISTORTED GRID NETWORK
C
 9999 DO 100 L=1,13,4
      JK=MK(L)
      JK1=MK(L+1)
      JK2=MK(L+2)
      JK3=MK(L+3)
      DO 100 J=JK,JK1
      DO 100 I=JK2,JK3
      XA(I,J,1)=-6.35+(I-1)*1.27
      YA(I,J,1)=5.9868+(J-1)*1.27
  100 CONTINUE
C
C       GRID  ADJUSTMENTS. COORDINATES ON X-AXIS.
C       AREA  WITH NO BOUNDARY PROBLEMS.
C
      DO 200 L=1,13,4
      JN=NNN(L)
      JN1=NNN(L+1)
      JN2=NNN(L+2)
      JN3=NNN(L+3)
      DO 300 K=2,NI
      DO 300 J=JN,JN1
      DO 300 I=JN2,JN3
      D1=XA(I,J,1)-XXD(I,J,1)
      D2=XA(I+1,J,1)+XXD(I,J,1)-XA(I,J,1)-XXD(I+1,J,1)
      D3=XXD(I+1,J,1)-XXD(I,J,1)
      IF (D3-0.)  150,151,150
  151 D4=0.
      GO TO 152
  150 D4=D2/D3
  152 D5=(XXD(I,J,K)-XXD(I,J,1))*D4
      D6=XA(I+1,J+1,1)-XXD(I+1,J+1,1)-XA(I,J+1,1)+XXD(I,J+1,1)
      D7=XXD(I+1,J+1,1)-XXD(I,J+1,1)
      IF (D7-0.)  160,161,160
  161 D8=0.
      GO TO 162
  160 D8=D6/D7
  162 D9=(XXD(I,J+1,K)-XXD(I,J+1,1))*D8
```

```
      D10=(D9-D5)*(YYD(I,J,K)-YYD(I,J,1))
      D11=YYD(I,J+1,1)-YYD(I,J,1)
      IF(D11-0.)  170,171,170
  171 D12=0.
      GO TO 172
  170 D12=D10/D11
  172 XA(I,J,K)=XXD(I,J,K)+D1+D5+D12
  300 CONTINUE
  200 CONTINUE
C
C      GRID  ADJUSTMENTS FOR THE COORDINATES ON Y-AXIS.
C      AREA  WITH NO BOUNDARY PROBLEMS.
C
      DO 400 L=1,13,4
      JN=NNN(L)
      JN1=NNN(L+1)
      JN2=NNN(L+2)
      JN3=NNN(L+3)
      DO 500 K=2,NE
      DO 500 J=JN,JN1
      DO 500 I=JN2,JN3
      D1=YA(I,J,1)-YYD(I,J,1)
      D2=YA(I,J+1,1)+YYD(I,J,1)-YA(I,J,1)-YYD(I,J+1,1)
      D3=YYD(I,J+1,1)-YYD(I,J,1)
      IF(D3-0.)  180,181,180
  181 D4=0.
      GO TO 182
  180 D4=D2/D3
  182 D5=(YYD(I,J,K)-YYD(I,J,1))*D4
      D6=YA(I+1,J+1,1)-YYD(I+1,J+1,1)-YA(I+1,J,1)+YYD(I+1,J,1)
      D7=YYD(I+1,J+1,1)-YYD(I+1,J,1)
      IF(D7-0.)  190,191,190
  191 D8=0.
      GO TO 192
  190 D8=D6/D7
  192 D9=(YYD(I+1,J,K)-YYD(I+1,J,1))*D8
      D10=(D9-D5)*(XXD(I,J,K)-XXD(I,J,1))
      D11=XXD(I+1,J,1)-XXD(I,J,1)
      IF(D11-0.)  210,211,210
  211 D12=0.
      GO TO 212
  210 D12=D10/D11
  212 YA(I,J,K)=YYD(I,J,K)+D1+D5+D12
  500 CONTINUE
  400 CONTINUE
C
C      GRID ADJUSTMENTS FOR THE COORDINATES ON X-AXIS.
C      IN THAT AREA INSTEAD OF 'I+1' THE 'I-1' IS USED.
C
      DO 600 L=1,5,4
      JNN=N1(L)
      JNN1=N1(L+1)
      JNN2=N1(L+2)
      JNN3=N1(L+3)
```

```
      DO 700 K=2,NE
      DO 700 J=JNN,JNN1
      DO 700 I=JNN2,JNN3
      D1=XA(I,J,1)-XXD(I,J,1)
      D2=XA(I-1,J,1)+XXD(I,J,1)-XA(I,J,1)-XXD(I-1,J,1)
      D3=XXD(I-1,J,1)-XXD(I,J,1)
      IF(D3-0.) 220,221,220
  221 D4=0.
      GO TO 222
  220 D4=D2/D3
  222 D5=(XXD(I,J,K)-XXD(I,J,1))*D4
      D6=XA(I-1,J+1,1)-XXD(I-1,J+1,1)-XA(I,J+1,1)+XXD(I,J+1,1)
      D7=XXD(I-1,J+1,1)-XXD(I,J+1,1)
      IF(D7-0.) 230,231,230
  231 D8=0.
      GO TO 232
  230 D8=D6/D7
  232 D9=(XXD(I,J+1,K)-XXD(I,J+1,1))*D8
      D10=(D9-D5)*(YYD(I,J,K)-YYD(I,J,1))
      D11=YYD(I,J+1,1)-YYD(I,J,1)
      IF(D11-0.) 240,241,240
  241 D12=0.
      GO TO 242
  240 D12=D10/D11
  242 XA(I,J,K)=XXD(I,J,K)+D1+D5+D12
  700 CONTINUE
  600 CONTINUE
C
C      GRID  ADJUSTMENTS FOR THE COORDINATES ON Y-AXIS.
C      IN THAT AREA INSTEAD OF 'I+1' THE 'I-1' IS USED.
C
      DO 800 L=1,5,4
      JNN=N1(L)
      JNN1=N1(L+1)
      JNN2=N1(L+2)
      JNN3=N1(L+3)
      DO 900 K=2,NE
      DO 900 J=JNN,JNN1
      DO 900 I=JNN2,JNN3
      D1=YA(I,J,1)-YYD(I,J,1)
      D2=YA(I,J+1,1)+YYD(I,J,1)-YA(I,J,1)-YYD(I,J+1,1)
      D3=YYD(I,J+1,1)-YYD(I,J,1)
      IF(D3-0.) 250,251,250
  251 D4=0.
      GO TO 252
  250 D4=D2/D3
  252 D5=(YYD(I,J,K)-YYD(I,J,1))*D4
      D6=YA(I-1,J+1,1)-YYD(I-1,J+1,1)-YA(I-1,J,1)+YYD(I-1,J,1)
      D7=YYD(I-1,J+1,1)-YYD(I-1,J,1)
      IF(D7-0.) 260,261,260
  261 D8=0.
      GO TO 262
  260 D8=D6/D7
  262 D9=(YYD(I-1,J,K)-YYD(I-1,J,1))*D8
```

```
      D10=(D9-D5)*(XXD(I,J,K)-XXD(I,J,1))
      D11=XXD(I-1,J,1)-XXD(I,J,1)
      IF(D11-0.) 270,271,270
  271 D12=0.
      GO TO 272
  270 D12=D10/D11
  272 YA(I,J,K)=YYD(I,J,K)+D1+D5+D12
  900 CONTINUE
  800 CONTINUE
C
C     GRID ADJUSTMENTS. COORDINATES ON X-AXIS.
C     IN THAT AREA INSTEAD OF 'J+1' THE 'J-1' IS USED.
C
      DO 1000 L=1,5,4
      NJN=N2(L)
      NJN1=N2(L+1)
      NJN2=N2(L+2)
      NJN3=N2(L+3)
      DO 1100 K=2,NP
      DO 1100 J=NJN,NJN1
      DO 1100 I=NJN2,NJN3
      D1=XA(I,J,1)-XXD(I,J,1)
      III=I+1
      IF(J.EQ.32 .AND. I.EQ.11) III=I-1
      D2=XA(III,J,1)+XXD(I,J,1)-XA(I,J,1)-XXD(III,J,1)
      D3=XXD(III,J,1)-XXD(I,J,1)
      IF(D3-0.) 280,281,280
  281 D4=0.
      GO TO 282
  280 D4=D2/D3
  282 D5=(XXD(I,J,K)-XXD(I,J,1))*D8
      III=I+1
      IF(J.EQ.32 .AND. I.EQ.11) III=I-1
      D6=XA(III,J-1,1)-XXD(III,J-1,1)-XA(I,J-1,1)+XXD(I,J-1,1)
      D7=XXD(III,J-1,1)-XXD(I,J-1,1)
      IF(D7-0.) 290,291,290
  291 D8=0.
      GO TO 292
  290 D8=D6/D7
  292 D9=(XXD(I,J-1,K)-XXD(I,J-1,1))*D8
      D10=(D9-D5)*(YYD(I,J,K)-YYD(I,J,1))
      D11=YYD(I,J-1,1)-YYD(I,J,1)
      IF(D11-0.) 310,311,310
  311 D12=0.
      GO TO 312
  310 D12=D10/D11
  312 XA(I,J,K)=XXD(I,J,K)+D1+D5+D12
 1100 CONTINUE
 1000 CONTINUE
C
C     GRID ADJUSTMENTS.COORDINATES ON Y-AXIS.
C     IN THAT AREA INSTEAD OF 'J+1' THE 'J-1' IS USED.
C
      DO 1200 L=1,5,4
```

```
      NJN=N2(L)
      NJN1=N2(L+1)
      NJN2=N2(L+2)
      NJN3=N2(L+3)
      DO 1300 K=2,NP
      DO 1300 J=NJN,NJN1
      DO 1300 I=NJN2,NJN3
      D1=YA(I,J,1)-YYD(I,J,1)
      D2=YA(I,J-1,1)+YYD(I,J,1)-YA(I,J,1)-YYD(I,J-1,1)
      D3=YYD(I,J-1,1)-YYD(I,J,1)
      IF(D3-0.) 320,321,320
  321 D4=0.
      GO TO 322
  320 D4=D2/D3
  322 D5=(YYD(I,J,K)-YYD(I,J,1))*D4
      III=I+1
      IF(J.EQ.32 .AND. I.EQ.11) III=I-1
      D6=YA(III-1,J,1)-YYD(III-1,J,1)-YA(I-1,J,1)+YYD(I-1,J,1)
      D7=YYD(III-1,J,1)-YYD(I-1,J,1)
      IF(D7-0.) 330,331,330
  331 D8=0.
      GO TO 332
  330 D8=D6/D7
  332 D9=(YYD(I-1,J,K)-YYD(I-1,J,1))*D8
      D10=(D9-D5)*(XXD(I,J,K)-XXD(I,J,1))
      D11=XXD(I-1,J,1)-XXD(I,J,1)
      IF(D11-0.) 340,341,340
  341 D12=0.
      GO TO 342
  340 D12=D10/D11
  342 YA(I,J,K)=YYD(I,J,K)+D1+D5+D12
 1300 CONTINUE
 1200 CONTINUE
      DO 1400 J=1,NP
      WRITE(6,1306)
      WRITE(6,1302) J,TIME(J)
      WRITE(6,1303)
      DO 1450 I10=1,13,4
      JK=MK(I10)
      JK1=MK(I10+1)
      JK2=MK(I10+2)
      JK3=MK(I10+3)
      DO 1450 K=JK,JK1
      DO 997 I2=1,NIP
      IF(K.EQ.IROW(I2)) GO TO 996
  997 CONTINUE
      GO TO 1450
  996 WRITE(6,1304) (XA(I,K,J),I=JK2,JK3)
      WRITE(6,1305) (YA(I1,K,J),I1=JK2,JK3)
 1450 CONTINUE
 1400 CONTINUE
 1306 FORMAT(1H1,'COORDINATES ADJUSTED AFTER DATA REDUCTION',
     1'  TECHNIQUE IS APPLIED')
      GO TO 9992
```

```
C
C   CURVE-FIT  ROUTINE
C
      DO 1500 I9=1,13,4
      JK=MK(I9)
      JK1=MK(I9+1)
      JK2=MK(I9+2)
      JK3=MK(I9+3)
      DO 1500 JC=JK,JK1
      DO 1500 I=JK2,JK3
      DO 1550 JS=1,NP
      X(JS)=YA(I,JC,JS)
      Y(JS)=XA(I,JC,JS)
      WT(JS)=1.
 1550 CONTINUE
      XF(1)=0.
      YF(1)=0.
      N=4
      ISCAL=1
      MXDG=2
      IPRINT=-1
      NF=0
      CALL CURVFT(X,Y,WT,N,ISCAL,MXDG,COF,NCOF,IPRINT,NF,XF,YF)
      DO 1600 K=1,NP
      XT(K)=X(K)
      DO 1600 J=1,NCOF
      IF(NCOF.EQ.1) GO TO 351
      IF(XT(K).EQ.0) GO TO 351
      IF(J.EQ.1) GO TO 351
      YT(K)=YT(K)+COF(J)*XT(K)**(J-1)
      GO TO 1600
  351 YT(K)=COF(1)
      GO TO 1600
 1600 CONTINUE
      DO 352 L=1,NP
      PER=(Y(L)-YT(L))*100./Y(L)
      IF(ABS(PER)-5.) 361,361,362
  362 YT(L)=Y(L)
  361 XFIT(I,JC,L)=YT(L)
      YFIT(I,JC,L)=XT(L)
  352 CONTINUE
 1500 CONTINUE
      WRITE(6,1308)
 1308 FORMAT(1H1,'FITTED COORDINATES')
      DO 1650 JS=1,NP
      IF(JS-1) 371,372,371
  372 WRITE(6,1309) JS
 1309 FORMAT(1H0,'PICTURE',I3/)
      GO TO 381
  371 WRITE(6,1310) JS
 1310 FORMAT(1H1,'PICTURE',I3/)
  381 DO 1650 I11=1,13,4
      JK=MK(I11)
      JK1=MK(I11+1)
```

```
      JK2=MK(I11+2)
      JK3=MK(I11+3)
      DO 1650 JC=JK,JK1
      DO 995 I2=1,NIR
      IF(JC.EQ.IROW(I2)) GO TO 994
  995 CONTINUE
      GO TO 1650
  994 WRITE(6,1311) JC,(XFIT(I,JC,JS),I=JK2,JK3)
      WRITE(6,1323) (YFIT(I,JC,JS),I=JK2,JK3)
 1311 FORMAT(1H ,'ROW',I3,2X,'XFIT',10F7.3)
 1323 FORMAT(1H ,8X,'YFIT',10F7.3)
 1650 CONTINUE
C
C
C   COMPUTATION  OF  VELOCITY COMPONENTS.
C
 9992 WRITE(6,1312)
 1312 FORMAT(1H1,'VELOCITY COMPONENTS CALCULATED FROM FITTED',
     1' COORDINATES.')
      NPO1=NP-1
      DO 1700 JS=1,NPO1
      JS1=JS+1
      IF(JS-1) 411,421,411
  421 WRITE(6,1313) JS,JS1
 1313 FORMAT(1H0,'PICTURE',I2,'-',I2)
      GO TO 422
  411 WRITE(6,1314) JS,JS1
 1314 FORMAT(1H1,'PICTURE',I2,'-',I2//)
  422 DO 1700 JC1=1,13,4
      JK=MK(JC1)
      JK1=MK(JC1+1)
      JK2=MK(JC1+2)
      JK3=MK(JC1+3)
      DO 1700 JC=JK,JK1
      DO 1750 I=JK2,JK3
      UX(I,JC,JS)=(XA(I,JC,JS1)-XA(I,JC,JS))/TT
      VY(I,JC,JS)=(YA(I,JC,JS1)-YA(I,JC,JS))/TT
 1750 CONTINUE
      DO 993 I2=1,NIR
      IF(JC.EQ.IROW(I2)) GO TO 992
  993 CONTINUE
      GO TO 1700
  992 WRITE(6,1315) JC,(UX(I,JC,JS),I=JK2,JK3)
      WRITE(6,1351) (VY(I,JC,JS),I=JK2,JK3)
 1315 FORMAT(1H ,'ROW',I3,5X,'UX',3X,11E8.2)
 1351 FORMAT(1H ,11X,'VY',3X,11E8.2)
 1700 CONTINUE
C
C  COMPUTATION OF STRAIN RATES AND DIRECTION OF PRINCIPAL
C  STRAIN RATE.
C
      WRITE(6,1316)
 1316 FORMAT(1H1,'STRAIN RATES AND DIRECTION OF PRINCIPAL',
     1' STRAIN RATE.')
```

```
      DO 1800 JS=1,NPO1
      IF(JS-1) 511,512,511
  512 WRITE(6,1317) JS
 1317 FORMAT(1HO,'SET',I2,/1H ,9X,'XN',18X,'YN',17X,'EPSX',16X,
     1'EPSY',15X,'EPSXY',17X,'PSI',11X,'ESTR'/1H ,9X,'--',15X,'--'
     117X,'----',16X,'----',15X,'----',14X,'----',9X,'----')
      GO TO 513
  511 WRITE(6,1318) JS
 1318 FORMAT(1H1,'SET',I2,/1H ,9X,'XN',18X,'YN',17X,'EPSX',16X,
     1'EPSY',15X,'EPSXY',17X,'PSI',11X,'ESTR'/1H ,9X,'--',18X,'--'
     117X,'----',16X,'----',15X,'----',14X,'----',9X,'----')
  513 JS1=JS+1
      DO 1800 L=1,13,4
      JK=MK(L)
      IF(L.NE.9 .AND. I.NE.13) GO TO 9896
      JK=JK-1
 9896 JK1=MK(L+1)
      IF(L.NE.1 .AND. I.NE.5) GO TO 9898
      JK1=JK1-1
 9898 JK2=MK(L+2)
      JK3=MK(L+3)-1
      DO 1850 J=JK,JK1
      J1=J+1
      DO 1850 K=JK2,JK3
      K1=K+1
      EPSX(K,J,JS)=0.5*((UX(K1,J,JS)-UX(K,J,JS))/(XA(K1,J,JS)-
     1XA(K,J,JS))+(UX(K1,J1,JS)-UX(K,J1,JS))/(XA(K1,J1,JS)-
     1XA(K,J1,JS)))
      EPSY(K,J,JS)=0.5*((VY(K,J1,JS)-VY(K,J,JS))/(YA(K,J1,JS)-
     1YA(K,J,JS))+(VY(K1,J1,JS)-VY(K1,J,JS))/(YA(K1,J1,JS)-
     1YA(K1,J,JS)))
      EPSXY(K,J,JS)=0.25*((UX(K,J1,JS)-UX(K,J,JS))/(YA(K,J1,JS)-
     1YA(K,J,JS))+(UX(K1,J1,JS)-UX(K1,J,JS))/(YA(K1,J1,JS)-
     1YA(K1,J,JS))+(VY(K1,J,JS)-VY(K,J,JS))/(XA(K1,J,JS)-
     1XA(K,J,JS))+(VY(K1,J1,JS)-VY(K,J1,JS))/(XA(K1,J1,JS)-
     1XA(K,J1,JS)))
      XN=(XA(K,J,JS)+XA(K,J1,JS)+XA(K1,J1,JS)+XA(K1,J,JS))
     1/4.
      YN=(YA(K,J,JS)+YA(K,J1,JS)+YA(K1,J1,JS)+YA(K1,J,JS))
     1/4.
      IF(ABS(EPSX(K,J,JS)-EPSY(K,J,JS)).LE.0.0000001) GO TO 521
      F=2.*EPSXY(K,J,JS)/(EPSX(K,J,JS)-EPSY(K,J,JS))
      PSI=0.5*ATAN(F)
      PSI=(PSI*360.)/(2.*3.14159)
      GO TO 522
  521 IF(EPSXY(K,J,JS)-0.0) 531,532,533
  531 PSI=135.
      GO TO 522
  532 PSI=0.
      GO TO 522
  533 PSI=45.
  522 AI3=(ABS(EPSX(K,J,JS))**2.+ABS(EPSY(K,J,JS))**2.
     1+2.*(ABS(EPSXY(K,J,JS))**2.))
      ESTR(K,J,JS)=SQRT(0.66667)*SQRT(AI3)
```

```
      DO 991 I2=1,NIR
      IF(J.EQ.IROW(I2)) GO TO 990
  991 CONTINUE
      GO TO 1850
  990 WRITE(6,1320) XN,YN,EPSX(K,J,JS),EPSY(K,J,JS),
     1EPSXY(K,J,JS),PSI,ESTR(K,J,JS)
 1320 FORMAT(1H ,E14.3,4E20.3,10X,E10.2,2X,E11.2)
 1850 CONTINUE
 1800 CONTINUE
C
C   COMPUTATION  OF FINAL EFFECTIVE STRAINS AT (XN,YN)
C
      WRITE(6,1321)
 1321 FORMAT(1H1,5X,'EFFECTIVE   STRAINS.')
      JS=1
      JS2=2
      JS3=3
      DO 1900 L=1,13,4
      JK=MK(L)
      IF(L.NE.9 .AND. I.NE.13) GO TO 9897
      JK=JK-1
 9897 JK1=MK(L+1)
      IF(L.NE.1 .AND. I.NE.5) GO TO 9899
      JK1=JK1-1
 9899 JK2=MK(L+2)
      JK3=MK(L+3)-1
      DO 1950 J=JK,JK1
      DO 1950 I=JK2,JK3
      ESPX=(TT/2.)*(EPSX(I,J,JS)+EPSX(I,J,JS2)*2.+
     1EPSX(I,J,JS3)*2.)
      ESPY=(TT/2.)*(EPSY(I,J,JS)+EPSY(I,J,JS2)*2.+
     1EPSY(I,J,JS3)*2.)
      ESPXY=(TT/2.)*(EPSXY(I,J,JS)+EPSXY(I,J,JS2)*2.+
     1EPSXY(I,J,JS3)*2.)
      BI3=(ABS(ESPX)**2.+ABS(ESPY)**2.+2.*(ABS(ESPXY)**2.))
      EST=SQRT(0.666667)*SQRT(BI3)
      DO 989 I2=1,NIR
      IF(J.EQ.IROW(I2)) GO TO 988
  989 CONTINUE
      GO TO 1950
  988 WRITE(6,1322) J,I,EST
 1322 FORMAT(1H ,'ROW',I3,'NODE',I3,E10.3)
 1950 CONTINUE
 1900 CONTINUE
      STOP
      END
```